SYNTHESIS OF NOVEL FLUORESCENCE CATIONIC GOLD(I) COMPLEXES AS POTENT ANTI CANCER AGENT

A Thesis Submitted for the Degree of

Doctor of Philosophy

By

Fatai Afolabi

University of Sussex

Department of Chemistry

October 2018

Dedicated to the Almighty God and to my Parents

Abstract

Novel acridine ligands were synthesized and converted to the corresponding cationic gold(I) complexes to provide new fluorescent tools for the study of their mechanism of action using confocal microscopy. These complexes were characterized by X-ray crystallography and their activity was evaluated against liver hepatocellular carcinoma HepG2 cells. A new series of cationic gold(I) pyrazole complexes were also prepared in excellent yields as their perchlorate salts. Results of cell viability assays show that these novel complexes have good cytotoxic properties against the human HepG2 cancer cell line. These complexes showed promising anti-cancer activities and pyrazoles have never been tested against this cell line in prior art. The regioselectivity of the complexation is also discussed in regards to the substitution pattern of the pyrazoles. The investigation of the reactivity of gold(I) with triphenyl phosphine and trihexyl phosphine provided an insight into the behaviour of cationic gold(I) in solution. The exchange of ligands could be observed at low temperature (-80 ^{o}C) with higher coordination numbers. The photophysical properties of substituted acridine ligands and their complexes have also been investigated. The substituted acridine functionalised by small electronically active groups showed a hypsochromic shift to shorter wavelengths when the conjugated π-system is electron deficient and bathochromic shift to longer wavelengths when the delocalised ring bore electron donating group and electron withdrawing group. Investigations into the effect of halogen substituents indicated a similar trend in the excitation and emission wavelengths. The position of the substitution and the nature of the substituent(s) has been shown to have a great impact on the Stokes shift and the quantum yield of the compounds. For instance, the addition of one or more methoxy groups lead to bathochromic shift which also reflects in the Stokes shift of the acridine derivatives.

Acknowledgements

First and foremost, I will like to thank my main supervisor, Dr Eddy Viseux for his guidance, support and encouragement through the rocky waters of modern research. I would also like to thank my co-supervisors Professor Ali Nockochi for his helpful advice and Dr Shane Lo Fan Hin for his invaluable support and encouragement. I also give great thanks to Daniel Guest for his generosity and assistance in the laboratories. I thank Dr Iain Day for the NMR service, Dr Alaa Abdul-Sada for the Mass Spectrometry Service and Dr Mark Roe for the x-ray crystallography. I would like to thank Dr Crickmore, Wided Souissi and Mojtaba Nasiri for the bioassay.

I wish to thank all the project students I have worked with in the Viseux laboratory, notably Tess Livingstone, Guillaume Riviere, Clement Lemaitre, Edward Cross, Ewan Hamilton and Lise Desquien for their support and understanding.

My special thanks to Verity Holmes, Chris Davis, Alex Burns and Jonathan Paul Andrews for helping me with any technical difficulties I encountered in the laboratories. I also thank Alethea Wimble for helping me with office works.

I would like to thank my mentors- His Royal majesty Oba Adedokun Abolarin, the Orangun of Oke Ila Orangun, Papa Prince G.A.Oyinlola, Prince Yemi Adeoye and Alhaji Prince Jimon Akande for their moral supports and words of encouragements.

Special Thanks goes to Tertiary Education Trust fund (TETFund) of Nigeria for funding my PhD programme. I also give great thanks to the management of Osun State Polytechnic Iree and members of Council of Osun State Polytechnic Iree for their invaluable support throughout the programme.

Finally, and most importantly, I would especially like to thank my wife and my children for their love, support and continued encouragement. I would also like to thank my closest friends, parents, brothers and sisters for their love and support during this journey.

Table of Contents

List of Figures

List of Tables

List of Schemes

List of Abbreviations

(br)	Broad signal
(d)	Doublet
(dd)	Doublet of Doublet
(s)	Singlet
(t)	Triplet
ADP	Adenosine Triphosphate
$CDCl_3$	Deuterated chloroform
DCM	Dichloromethane
DLC	Delocalised Liphophilic Cation
DNA	Deoxyribonucleic acid
Et	Ethyl
EtOAc	Ethyl acetate
EtOH	Ethanol
HepG2	Liver hepatocellular Carcinoma
HOMO	Highest Occupied Molecular Orbital
HRMS	High Resolution Mass Spectroscopy
IR	Infrared

LUMO	Lowest Unoccupied Molecular Orbital
Me	Methyl
MeOD	Deuterated methanol
MeOH	Methanol
MS	Mass spectroscopy
NMR	Nuclear Magnetic Resonance
Ph	Phenyl
R.T	Room temperature
SA	Silylating agent
SAR	Structure Activity Relationship
Sat.	Saturated
St	(IR) stretch
TBDMS	*tert*-butyldimethysilyl
TBDMSCl	*tert*- butydimethysilychloride
THF	Tetrahydrofuran
TLC	Thin Layer Chromatography
TrxR	Thioredoxin Reductase
UV-Vis	Ultraviolet visible spectroscopy

CHAPTER I. INTRODUCTION

I.1 Metals in Medicine

Herbal medicine and traditional remedies have been used for the treatment of various ailments throughout the generations.[1,2] However, treatment of a disease requires deeper knowledge of effect of a drug on its target as well as origin of a disease. The use of bioactive drugs from the basic component of pharmaceutical development, through modern scientific discovery have allowed for deeper knowledge of drug administration and their efficacies. It is reported that metals have been used in a modern way in tackling the various medicinal problems.[3,4] Although the use of metals in medicine could be dated back to antiquity.[5]

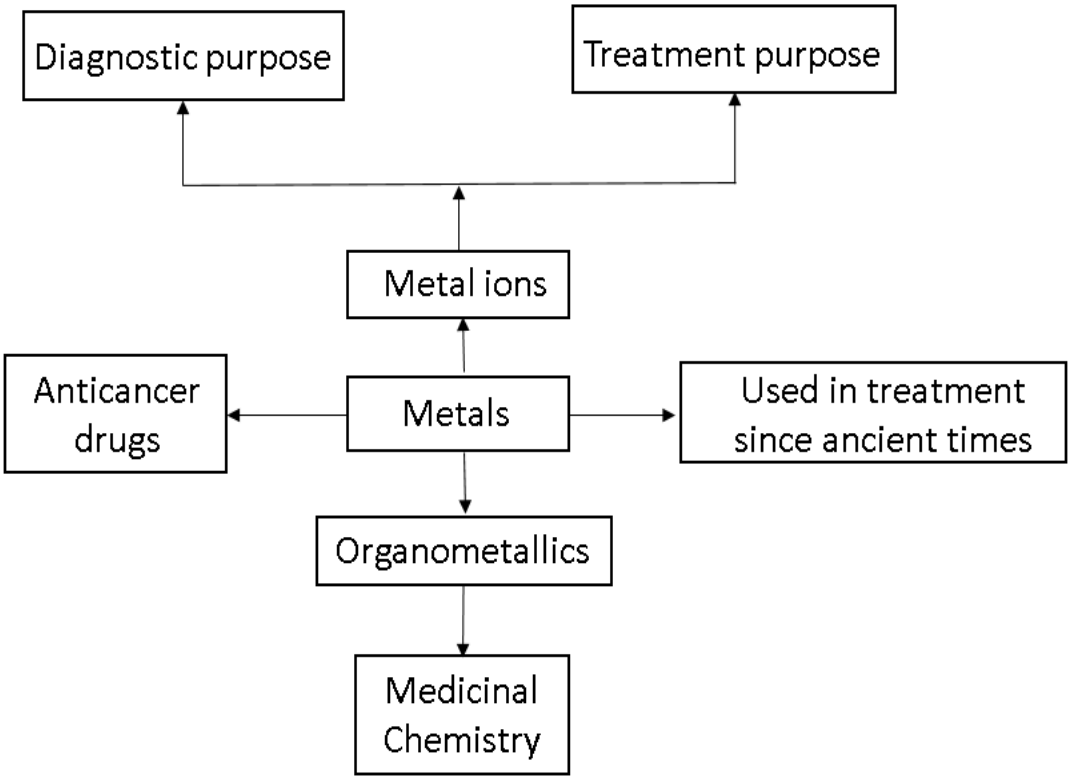

Figure 1: Schematic diagram of the basic applications of metals in medicine

For the past few decades, the synthesis of different organometallic complexes has recorded great advancement due to their wide applications in many areas such as materials

and medicinal chemistry, as well as their potential usage as reaction intermediates or as catalysts in many catalysed reactions.[3,4] Soft metal ions and their complexes are highly demanded for the design of anti-cancer drugs which specifically target proteins or enzymes with SH or SeH moieties.[6] The importance of metal complexes in the field of medicine is enormous as it can be seen in the use of antimony (Sb), bismuth (Bi), gold (Au), iron (Fe) and silver (Ag) as anti-protozoa, anti-ulcer, anti-arthritic, anti-malaria and anti-microbial respectively.[7] The ten most active metals usually used in medicine are: antimony, arsenic, bismuth, gallium, gold, iron, platinum, rhodium, titanium and vanadium.[7] Arsenic compounds such as realgar (a compound of arsenic sulfide) has been applied as a therapeutic agent by Chinese for more than twenty centuries.[8] Recently, it was reported that arsenic compounds especially, white arsenic (AS_2O_3) induced apoptosis in blood and other cancer cells with minimal side effects.[8] Arsenic trioxide was known to be an effective agent against acute Promyelocytic leukemia (APL)[9,10] It was also used for the treatment of other ailments such as diabetes, malaria rheumatism and tuberculosis.[11]Trivalent antimonial induces apoptosis on APL cells in a manner that resembled that of arsenic oxide.[12] Antimony has proved to be a good candidate as antileishmania drug.[13]The efficacies of antimony is evident in the management of patients with deadly diseases that has no cure.[14] Bismuth derivative has been demonstrated to be effective in the treatment of gastrointestinal ailment.[15] It also exhibits significant toxicity against microbial,[16] leishmanial[17] and cancer agents.[18] Certain properties of gallium have made it a potential candidate as therapeutic agent especially in the field of bone diseases,[19] infectious diseases[20] and cancer treatment.[21] Iron oxide plays a significant role in medical processes. It acts as a source of iron for animals and human cells.[22] It also useful in the treatment of anemia in cancer patients.[23] It is very important in metabolic processes such as respiration and DNA synthesis.[7] Furthermore, it plays a significant role in the citric

acid cycle and oxidative phosphorylation.[24] The physico-chemical properties of platinum made it suitable as a therapeutic agent.[25,26] Its usage as anticancer agent began with cisplatin.[27] The efficacy of cisplatin encourages the synthesis and testing of more platinum compounds on cancer cells. However, out of about 30 compounds that reached the clinical stage, only 4 are currently on the market today. These are cisplatin,[28] oxaliplatin, carboplatin[29] and nedaplatin.[30]

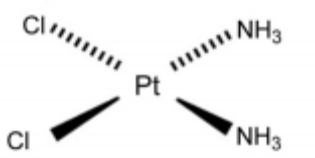

Figure 2: Structure of cisplatin

Rhodium derivatives have recently attracted interest due to their inhibitory properties against various mammalian tumour cells.[31,32] It was suggested that the inhibitory property of dirhodium(II) carboxylates may have similar structural analogy to cisplatin by binding to DNA.[33] Rhodium(III) complex was reported to be a potential candidate for the treatment of inflammatory bowel disease.[34] It was also the first metal based inhibitor of lysine-specific demethylase 1 (LSD1) with a promising antitumour activity against human prostate cancer cells.[35] Titanium alloys are one of the most useful materials for biomedical applications. They found applications in various implant devices such as artificial knee and hip joints, artificial hearts bone plates etc.[36] Titanium derivatives have been reported as a potential candidate against platinum-resistant antitumour drugs.[37]Titanocene dichloride was reported as an effective anticancer agent.[38] Vanadium derivatives have been suggested as useful probes in many biological processes.[39] It has been reported to behave in a similar way to insulin in many target tissues.[40] Vanadyl(IV) sulfate showed an interesting toxicity against mammary gland neoplasia.[41] The use of

organometallic complexes in medicine is rapidly developing and novel metallic complexes with special emphasis on targeting and biotransformation are now having great impact in modern medicine. The importance of specificity and targeting cannot be over emphasized, as most metallic complexes are usually associated with toxicity. Therefore, if they can be delivered directly to the desired receptors and tissues, then, the toxic side effects may be greatly reduced. Also, understanding of the process of deligation and ligand substitution reaction may lead to the effective use of metallic complexes in pharmaceutical and medicinal applications.[42] Essential metals could be delivered into its target in the body system while toxic metals could also be removed from the body by chelation therapy. Chelating agents usually binds to metal in the body's tissue forming a chelate complex which is then eliminated from the body by the kidney through excretory system.[43] Many drugs on the market today are basically derived from organic compounds. This is due to the fact that synthetic compounds are believed to have toxic side effect or bio-compatibility problem. In spite of this perception, the use of organo-transition metals in medicine has improved tremendously over the years because they exhibit different oxidation states which enable them to interact with negatively charged radicals. Based on this property, organo-transition metals have been utilized by many researchers to treat various human ailments.[44] Transition metals offers a great diversity in their actions: they are important in catalysis, synthesis of new materials, supramolecular, cosmetic, photochemistry and biological systems.[45,46] Medicinal applications and commercial values of organometallic complexes are increasing tremendously over the years. The study of organometallic chemistry could be divided into two major classes. These are toxic ligands that are specific on certain metals ions either free or protein bound and when the main feature of the reaction mechanism is centred on metal ions. Organo- transition metals have an array of coordination spheres, varying oxidation states versatile ligand

design and appropriate redox potential which are employing in altering the kinetic and thermodynamic parameters of the complexes in relation to prospective receptors.[47] Literature has it that about 30% of all human enzymes contained transition metal ion in their core protein.[48] Metal nanoparticles have been exploited in bio diagnostic, biophysical studies and in other field of medicine. Because of small size, metal nanoparticles are usually conjugated with target analyte in order to achieve molecular specificity. Unlike photoabsorbing and fluorescent dyes, metal nanoparticles are photo stable and allow longer probing times thereby increase sensitivity.[49] Metallotherapy has grown constantly over the past six decades; however, despite the landmark achievement of a few metallodrugs, the field is still less fully developed as compared to the traditional medicinal chemistry.[50]The introduction of metal ions into the body is for a dual purpose. It may be for diagnostic or for therapeutic purpose.[50] Metal ions are essential for the proper functioning of human body. Deficiency of some metals in the body can lead to diseases. Typical examples include anaemia which is caused by deficiency of iron and retardation growth caused by zinc deficiency.[51] Metals have wide applications in material science, catalysis and biochemistry. Transition and main group metals in cyclic phosphanes and phosphazenes have proved to be useful candidates in medicine, catalysis and precursors for synthesis of new materials such as polymers and semiconductors.[52] Transition metals with η-cyclopentaldienyl, an η-arene as ligands have proven to be useful in catalysis, new materials, biological and medical sciences.[53] Many diseases have been identified to occur as a result of imbalance of metals in the body. Typical examples include Alzheimer's and Parkinson's diseases that involved abnormal build-up of metals in brain tissues.[54,55]

I.2. Gold Complexes

Gold is a soft bright yellow metallic element. It is found in nature as a free metal or in combined state. It usually exhibit unusual physical and chemical properties compared to lighter members of group 11 elements because of relativistic effect.[56] Atomic gold has the electronic configuration [Xe]$4f^{14}\ 5d^{10}\ 6s^{1}$. The 6s orbital is contracted and stabilised and giving gold several properties. Gold is potentially more interesting than other metals due to its stable oxidation state during a reaction. Gold is a Lewis acid and usually exhibits two principal oxidation states (I) and (III). The (II) oxidation state usually forms polynuclear compounds or transforms into (I) or (III). The first oxidation state has been the major interest of study in which the complex has a linear structure: L-Au-X. Gold(I) and gold(III) complexes have different reactivity and do not always react with the same compound. Gold(III) possesses similar d^8 electronic structure with platinum(II) complexes thus exhibits geometrical configuration analogy to that of platinum(II).[57] It was believed that the square planar geometry of platinum(II) in solution influences its anticancer properties.[58] Therefore, this similar features made gold(III) a potential candidate as antitumour agents with little or no side effect.[59] The first oxidation state is preferred because the complexes are more stable and a comparative study has been reported between the complex gold(I) and gold(III).[60] This complex can be neutral, cationic and anionic. The L-ligands are usually phosphines while the X-ligands can be alkyls, aryls or halides.[61,62]Arabic and Chinese physicians of old used gold for the treatment of various diseases. Over the past two decades, interest has increased in the organogold complexes for their high medicinal activities. Their structural design with simple and potent ligands are key aspects of medicinal inorganic chemistry with uses targeting varied afflictions such as asthma, malaria, rheumatoid arthritis, HIV[63] and cancer.[64,65] Furthermore, gold complexes are excellent prototypes for the rational design

and development of novel and effective anti-cancer agents.[66] Recently, auranofin was reported to be effective in the treatment of rheumatoid arthritis by oral administration therefore, it relieves the patient of pain through injection and nitritoid reaction usually associated with injectable gold drugs.[67,68]

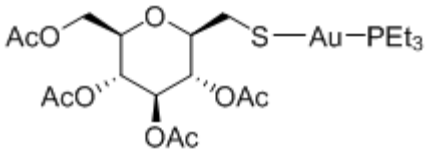

Figure 3: Structure of auranofin

Mirabelli reported that an array of phosphine gold(I) complexes showed significant *in vivo* and *in vitro* cytotoxicity against spectrum of human and mouse tumour models.[69] However, the increased interest for the gold complexes is due to the anti-bacterial properties of $[Au(CN)_2]^-$ and other compounds with various structure like linear or polymeric.[70] We have reported the potential for gold(I) complexes to serve either as vectors for specific drug delivery into hyperpolarized cancer cells or as orthogonal drugs when bearing biologically active ligands.[71] We have also provided further proof that gold(I) complexes inhibit thioredoxin reductase (TrxR), an enzyme that catalyses the reduction of thioredoxin which is responsible for cell growth,[72] due to complexation with a selenocysteine residue.[73] The inhibition of this enzyme which is over-expressed in cancerous cells further leads to cell apoptosis.[74] Though gold complexes appear to specifically target hyperpolarized cancer cells without affecting the healthy cells,[75] little is known about the mechanism of action of the cell permeation and the ligative equilibria involved. The lack of fundamental understanding of the complex interactions within the coordination sphere of gold(I) in catalysis[76,77] is mirrored in its use in the biological environment, as the dynamic ligation/deligation processes around the gold nucleus remain very unclear during cell permeation and uptake by cancer cells.[72,78] Providing

visual tools to understand the distribution of gold(I) and its ligated or free ligands will help understand its role as a chemotherapeutic agent, as well as a homogenous catalyst.[79] Gold complexes were used also as a catalyst in reaction of hydroamination and hydroalkylation of alkynes for example. But in this case the mechanism has not been ascertained to this date.[80,81] Over the last few decades, application of gold(I) complexes as catalyst for transformation of different organic synthetic reactions has atract interest.[82] An array of transformations has been reported. Gold(I) complexes have shown to be useful as catalysts for selective organic hydro amination of unactivated alkenes, alkynes, allenes and 1,3-dienes.[83] Cyclization of enynes using highly alkynophilic gold(I) complexes with biphenyl phosphine ligands.[84] as well as the use of gold(I) complexes as highly efficient tools in catalysing acid addition to alkynes with huge amount of turnover.[85]

I.3.Behaviour of Gold(I) Complexes in Solution

It is evident that the capability of gold to form stable complexes is crucial in determining its behaviour in solution. The stability of the complexes depends on the type of atom in the ligand, which is directly bonded to gold (that is the ligand donor atom). For gold(I) and gold(III) the stability of their complexes decreases with increasing electronegativity of the ligand donor atom.[86] Triphenylphosphine usually forms stable complexes with gold(I) because of the stronger π-bonding of phosphine to gold(I).[87] It is apparent that gold(I) complexes undergo disproportionation in aqueous medium but are stable in organic solutions.[88] X-ray crystallographic structures have shown that gold(I) complexes with nearly tetrahedral species in solution exist at -80 ^{o}C.[89] Mixed ligand clusters were analysed in order to understand how the number of methyl and cyclohexyl groups in the ligands and the size of the gold clusters influences the extent and stability reaction and found that the ligand loss fragmentation is correlated with the relative electron donating

ability of the ligands.[90] It has been established that Ph_3PAu^+ reacts with Ph_3P to generate higher coordinate complexes.[91] The ligand exchange reaction of gold in solution and formation as well as transformation of different oxonium and sulfonium moieties were investigated by NMR spectroscopy in solution. Detection and characterisation of the intermediate and mechanism of process involved in multiple reactive species were achieved.[13] Studies have shown that electronegativity of the substituents and angles between them were the two key factors influencing the ^{31}P NMR chemical shifts of gold(I) complexes with tertiary phosphine sulphide ligands.[92] X-ray structures of four coordinate gold(I) complexes (tetrakis (triphenylphosphine) gold(I) have been reported in which the steric bulk of PPh_3 plays a key role thus none of the three modifications shows the expected geometry.[93] The never-ending search for new variant of phosphorous-based ligands is due to their ability to adjust readily in coordination behaviour with transition metals and because of their use in new domain of synthetic applications. Essentially, they provide stupendous flexibility in the interaction of a wide array of steric and electronic properties at phosphorous atom which in turn facilitate the development of necessary metal complexes that can enhance the homogeneous catalytic properties under mild conditions.[94,95] In recent years, various complexes containing tricyclohexylphosphine and triphenylphosphine ligands have attracted increasing interest due to their wide applications as useful catalysts. [95] ^{31}P is an elegant spectroscopic tool for its long chemical shift range with high sensitivity of the shift to quick adjustment relating to slight changes in structures and reactions. The ^{31}P spin coupling values often give additional information with respect to the structures that arise.[96] ^{31}P NMR is an important analytical tool for structural elucidation and equilibrium studies of complexes containing phosphine ligands in solution. It gives evidence that two or more coordinate gold(I) compounds composed of phosphine are synthesised in solution.[97] ^{31}PNMR study

of tertiary phosphine gold(I) complexes has revealed that stoichiometry and ligand exchange properties depends on the electronic and steric behaviour of the ligands. It also reveals the higher coordination of gold(I) particularly four coordinate species.[98] Albeit the affinity of soft gold(I) π-Lewes acids for alkynes has been investigated by Widenhoefer[99] very little is known about the behaviour of cationic gold with triaryl and trialkyl phosphines, and the ability of triphenylphosphine to deligate and form more complexes species that may in turn alternates the mechanism that is usually acknowledge in the literature. The existence of polyligated gold is rarely mentioned, yet evidence for precomplexation of gold amide with alkynes prior to deligation of the amide ligand has been reported.[100]

I.4. Silver

Silver can be found in nature in pure elemental form [101] but is usually associated with lead and copper ore.[102]Pure metallic silver is malleable, ductile and usually harder than gold.[101] Silver exhibits the following oxidation state. Ag(0), Ag(I), Ag(II) and Ag(III). Ag(I) is the most stable while Ag(II) and Ag(III) are very reactive and usually unstable.[101] Silver compounds readily ionize in water and body fluids to release (Ag^{+}).[103]silver ion is very reactive and readily interact with macromolecule in the blood.[103] It also exhibits greater affinity for hard donor atoms like oxygen and nitrogen.[104] It is usually regarded as a soft cation[105] thus it forms most of its stable complexes with polarisable ligands.[106] Its usage was at par with gold and copper.[107] It has been used extensively for currency, jewellery, food preservatives and recently as consumer products.[102] It was the most effective antimicrobial before the advent of the antibiotics. [107] In the ancient times, silver coins is usually drop in fluid vessel to prevent spoilage without knowing that it was the prevention of bacterial that caused the effect.[107] Silver(I) has been used extensively in the treatment of skin diseases, recent wounds and burns.[108]Though, antibiotics still remain

very important but the rise in bacteria resistance has made the use of silver the major therapy in the healing of wounds and burns.[108] Recently attention has been shifted to the use of silver(I) as therapeutic agent because it has no side effect at moderate concentration.[109] One of silver derivatives (Silver(I) sulfadiazine) has been reported to be so effective against catheter infections.[110]

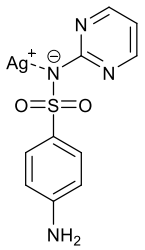

Figure 4: Structure of silver sulfadiazine

In an attempt to produce novel complexes of silver with higher antibacterial and antifungal properties, silver complexes of norfloxacin were synthesised and screened for their anti-fungal and antibacterial properties using gram positive and gram negative bacteria. They were reported to show promising result .[111] Most silver derivatives act by absorbing fluid from the wound which then lead to ionisation and release of biologically active Ag cations into the wound bed.[112] Then, the positively charged Ag^+ ions usually react with the negatively charged protein, DNA and RNA in bacterial and fungal cells.[112]

I.4.1.Silver-Organic Complexes

Bis(acridine-N)(nitrato-O,O')silver(I) was the first complex of acridine and silver to be reported.[113] The nitrate ion coordinated to silver as an asymmetrically chelating bidentate ligand.[113] A spectrum of mono, di and polynuclear silver(I) containing 2-pyrazole substituted 1,10-phenanthroline complexes have been synthesised and their photoluminescence properties have been extensively studied.[114] Heteroleptic coordination of Ag(I) with spectrum of phenanthroline ligands and various bi-phosphine have been reported.[115] Silver coordinated to different organic ligands including but not

limited to phosphine, N-heterocyclic carbenes, N-heterocycles having spectrum of properties such as antibacterial antifungi, antiseptic and anticancer have been reported.[116] The coordination chemistry of Ag(I) and its design of coordination network, as well as polymer made from nitrogen-donor ligands has been reported.[117] The coordination of AgX salts (where X is F^-, Cl^-, Br^-, I^-, $BF4^-$, PF_6^-,NO_3^-) and ligands in group 15 with particular interest in monodentate and bidentate tertiary phosphine derivatives was reviewed.[118] It was observed that the reaction condition and stoichiometry of the reaction influence the structure formed.[118] Metallic nature influences the architecture of a supramolecular assembly. To this end, Ag(I) ion usually act as a building block due to its spectrum of coordination mode.[104] In attempt to investigate the binding mode of Ag(I) ion, 1,2,3-triazole linked crown ether with coordination to Ag(I) ions were examined.[119] Different modes of coordination were observed based on the stoichiometry of the formation of the complexes.[119] It was reported that sulfur atoms were more favoured than the nitrogen atoms[119] Application of nanoparticles in the field of medicine and industry has increased tremendously over the years[120] due to incorporation of spectrum of novel products. Silver nanoparticles showed interesting physicochemical properties and high antimicrobial properties that made them to stand aloof as a better alternative to the antibiotic resistant strains.[121] Ag(I) ions have been reported to showed greater antibacterial toxicity than AgNPs(I) and AgNPs(II).[122] Though, the mode of action of the three silver drugs were similar therefore they have potential to be used as antibacterial drugs.[122] Supramolecular polymer chemistry is an emerging field of study in which polymer chemistry is combined with supramolecular chemistry.[117] Recently, attention has been shifted to coordination polymers based on Ag(I).[117] This due to the fact that they are readily available, highly labile and generally reversible.[117]Ag(I) coordination sphere is

flexible and usually exhibit various coordination number from two to six and adopt a spectrum of geometries.[117]

I.4.2.Silver as Anticancer Agent

Anticancer activity of Ag(I) derivatives of mixed nitrogen and sulfur containing ligands has been reported. It was observed that these complexes displayed an interesting antitoxicity against *Ehrlich's ascites* tumour cells.[109] Silver bearing 2,6-disubstituted pyridine ligands were synthesised[123] and tested on different human cancer cell lines including hepatocellular carcinoma (HePG2), breast adenocarcinoma (MCF7), colon carcinoma (HT29) and lung adenocarcinoma (A549).[123] They were found to exhibit significant activity against all tested cancer cell lines even more than the reference drugs.[123] Anticancer activity of silver derivatives stem from their unique mechanism of action, which differ from other metal complexes.[116] Silver has the capability of killing bacteria in different ways.[124] It may kill the bacterial by damaging the cell wall in a similar manner to the way penicillin works.[125] It may also kill the bacteria by damaging the major enzymes[126] and metabolic pathways in the cells.[125] Another way it may do so is by impairing with the respiratory process by destroying the electron transport system of the cell, since Ag^{+} readily oxidises ATP giving rise to the formation of Ag(0).[125] Furthermore, it may kill bacterial by binding to the DNA and RNA impairing the protein encoding and replication of bacterial just like the way cisplatin works.[127] However, in spite of catalogue of investigative research on the mechanism of action of silver complexes, the exact mechanism and mode of action is not yet understood[128] until date. Meanwhile it was generally believed that the nature of atom coordinated to silver with the resultant bond formed and neither the charge, chirality, solubility nor the polymerisation degree influences the efficacy of the silver derivatives.[129]

I.5.Acridine Derivatives

Naturally occurring acridone alkaloid are plant metabolites which were first extracted from rain forest plant in Australia in 1948.[130] Series of natural acridine/acridone derivatives were extracted from plants and pyridoacridine alkaloids derived from various marine organisms.[131] Recent years have seen a resurgence of interest in the synthesis of novel compounds that has high cytotoxic activity, among which acridine derivatives play a significant role.[132] Synthetic acridine and their naturally occurring alkaloids have been reported to exhibit an array of biological activities.[133] They were among the earliest useful bioactive agents. Their usage was dated back to 1940s when 9-aminoacridine was used as an antibacterial.[132] Since then, acridine derivatives have also found wide application as antimalarial, antiprotozoal and anticancer agents.[134] Different chloro-1,3-dihydroxyacridone derivatives has been reported to be promising candidate as antiviral drugs.[133,135] Reasons for their usage as bioactive agents include: biological stability, ability to be readily synthesise and their intercalative properties with DNA in mammalian cells. These compounds are found to contain a planar chromophore in form of a tri- or tetra-cyclic ring system (Figure 1) usually combined with one or two flexible substituent groups,[136]that was believed to be sufficient size to intercalate with DNA base pair and exert its pharmacological effect which generated reactive species that could initiate free radical chain reactions.[137] Intriguingly, the mode of action of acridone/acridine derivatives were not really understood for many centuries, but it was presumed that the inhibition of DNA topoisomerase II/Protein Kinase C enzymes were involved.[133]They were believed to intercalate with DNA and inhibit topoisomerase/telomerase enzymes in the protein of their target.[131,138]The cytotoxicity activity of these compounds were attributed to the planarity of their aromatic structure which allowed them to intercalate

within the DNA double stranded structure thus impairing the cellular machinery of the biological organism.[138,139]

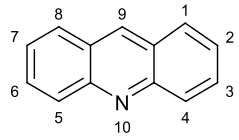

Figure 5: Structure of acridine

I.5.1.Acridine as Drugs

Acridine derivatives have been used to locate malignant cells in tumour tissues.[140–143] They were also used as fluorescent markers for detecting and inhibiting tumours *in vivo*.[140] They have greater capability to play a dual role: target-specific drug and vector to carry other drugs and monitor their movement. Acridine scaffold is an interesting phamacophore for the design of structural activity relationship of a novel anticancer drug targeting DNA.[137] Acronycine (the first acridine derivative isolated from Australian plant in 1948) was reported to exhibited significant activity over wide range of tumour cells but failed clinical trials due to solubility problem and its moderate potency. [144]It was reported that in order to observe a significant cytotoxic activity in acronycine the 1,2 double bond is an important structural requirement.[144,145] For their antitumour activity over wide range of tumour cells, two different compounds of 9-anilinoacridine derivatives were synthesized and tested against mouse tumour cell L1210 and human tumour cell HL60, and found out that both exhibited interesting cytotoxic activity.[146] Literature had it that cytotoxicity of 9-anilinoacridine derivatives could be enhanced by the addition of a strong electron-donating group on the position 4 of the ring substituent.[147] Spectrum of 9-dialkyaminoalkylaminoacridine has been reported to show significant activity against different tumour cells.[147] A wide range of fluoro substituted acridone derivatives were investigated for their cytotoxic activity against spectrum of drug sensitive and drug

resistant cancer cells, and they were found to be promising anticancer agents.[148]Recently, Szymański screened 32 acridine based compounds for their anticancer activity and found out that tetrahydroacridine and cyclopnetaquinoline derivatives with 4-fluorobenzoic were the most effective and that they induced apoptosis in lung cancer cells by activation of DNA damage signaling.[149]

I.5.2.Acridine as Fluorescent Probe

Fluorescent compounds have found useful applications in physiological monitoring, cell visualisation and sensing. Acridine derivatives are found useful as biological fluorescence probes.[132]Among them, acridine containing cyanide dyes have been given more attention because of their relative chemical stability, high molar absorptivity and fluorescence quantum yield.[150]Fluorescent probes for transition metals have been described because of their applications in a range of chemical, biological and environmental processes. Acridine based pH sensor fluorogenic properties as well as its G-quadruplex binding ligands have been reported.[151] However, acridine dyes are usually used for development probes for DNA conformational determination and structures because of their high quantum yield and binding affinity.[151–153] Microscopic observations of subcellular study on binding in hepatocyte cells indicated that acridine derivatives are more specific for mitochondria subcellular investigations.[154] It was observed that acridine orange accumulated easily in pure lysosomal particles *in vivo* and there was a good correlation between the quenching of its fluorescence and change in the pH across the lysosomal membrane. Therefore, the change in pH across lysosomal membrane could be studied by measuring the fluorescence of acridine orange.[155]Acridine based probe was reported to exhibit excellent selectivity and sensitivity to Cr^{3+} and PO_4^{3-}.[156] The probe has potential application in biological and environmental studies.[156]A robust acridine based fluorescent probe was developed as an indicator for protein analysis with high sensitivity, short

reaction time and excellent reproducibility.[157]Fluorescent probes can be used to investigate lymphocyte stimulation at cellular level.[158] It could also be applied in the study of acidic organells and autophagy.[159] Acridine orange derivatives have been reported to bind cardiolipin in vitro thus used as a stain to assay cardiolipin in order to study the mitochondria content.[160] In this research work however, acridine derivatives were chosen to serve as ligands because they present many advantages. First of all, they are highly fluorescent due to their conjugated ring system. In view of this, they can be useful to provide a method to understand the mechanism of gold(I) complexes either as a catalyst or as a drug Moreover, they can bind as an L-ligand through the nitrogen lone pair forming a fluorescent neutral gold complex, or as an X-ligand which would form a cationic gold Complex

I.6. Pyrazole

Pyrazole is a five-membered ring compound consisting of three carbon atoms and two nitrogen atoms in adjacent positions with molecular formula $C_3H_4N_2$.[161](Figure 2) One of the two hydrogen is neutral while the other one is basic.[162]They were classified as alkaloids because of their basic composition and unique therapeutic effect on human.[161] The first pyrazole derivative to be isolated naturally was 1-pyrazolyl-alanine which was obtained from watermelon in 1959.[161]Recent increase in utilization of pyrazole as a core motif in several drugs stimulate the development of novel and robust method for their synthesis.[163]

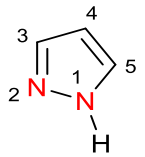

Figure 6: Structure of pyrazole

Pyrazole was investigated because of its high medicinal value.[164] They are important building blocks used in pharmaceutical and agrochemical industries.[165,166,167] Pyrazole is a special class of heterocyclic compounds that can not only coordinate to enzymes (through van der Waals interactions) but also to metals, making them useful template for the design of novel drugs.[164,168] Their motif is also present in many biologically active compounds.[169] The structural activity relationship (SAR) of pyrazoles alone has been extensively investigated and they were found to bind to a variety of receptors, enhancing the activity of many anti-angiogenesis agents.[170]

I.6.1.Applications of Pyrazole

Most of successes achieved in the field of drug discovery process is being guided by careful choice of design of new therapeutic agents.[171] Thus privileged small organic molecules have proved to be useful scaffolds for the design of novel drugs.[172]In this context, pyrazole has proven to be small molecule modulators of several targets.[171] Pyrazoles have also shown great pro-apoptotic potential against lung cancer cell lines[173] as well as excellent cytotoxicity against p53 cancer mutant Y220C, but their gold complexes have never been tested against HepG2 hitherto to the best of our knowledge.[174] Pyrazolates and imidazolates substituted with deactivating groups were used to synthesise neutral azolate gold(I) phosphane complexes and were found to act as anti-cancer agents.[175] The inhibitory properties of neutral gold(I) triphenylphosphine complexes on *E. coli* dihydrofolate reductase was found to be toxic against different human cancer cell lines.[176] It was reported that pyrazole derivatives displayed an interesting anti-

inflammatory and antimicrobial[177] activities better than standard drug (Diclofenac sodium).[178]Pyrazole derivatives have also shown to exhibit antitubercular, antibacterial and antifungal activities.[179]Furthermore they have been reported to have antidepressant,[180] antiepileptic,[181] antipyretic,[182] anti-ulcer, anticonvulsant,[180] antidiabetic[183] and anticancer[184] activities. In attempt to develop novel potential antiviral agents, a series of pyrazole derivatives bearing acetyl or thiocarbamoyl moieties were synthesised and tested on various viruses in different cell cultures and found out that they showed an interesting cytotoxicity against vesicular stomatitis virus relative to the used drugs.[185]Furthermore, Pyrazole are usually used as the basic moiety in several compounds for many applications such as catalysis, agro-chemicals and core motif of other compounds and in medicine.[186] The versatility of pyrazole and its derivatives make them attractive for the synthesis of a large number of analogues with different scaffold in them thus enhance the properties of the resultant compounds.[186] A spectrum of novel nickel(II), iron(II), and cobalt(II) complexes based on (pyrazolyl)-(phosphinoyl) pyridine ligands were synthesised and activated with $EtAlCl_2$ to form an active catalyst which afford 1-butene as the main product.[187] Recently, oligomerisation of ethylene has attracted a lot of attention due to the fact that it is one of the major application of homogeneous metal catalyst.[188] Some of the products obtained by oligomerisation process are essential commodities for industrial and household applications.[188] These include, detergents, synthetic lubricants, plasticisers[189] and monomeric unit for low density polyethylene.[188] Pyrazole derivatives has been incorporated into several transition metals such as iron cobalt nickel zinc, palladium etc as nitrogen donor ligands for olefin oligomerisation and polymerisation catalyst.[190–192]Pyrazole based complexes has also been reported to be used in epoxidation of olefins.[193]In our search for dual action orthogonal drugs, we investigated

in this research, the role of delocalised cationic gold(I) pyrazole complexes and pyrazole based silver(I) complex against HepG2 human liver cancer cell lines.

I.7.Delocalised Lipophilic Cations (DLCs)

Delocalised lipophilic cations are positively charged molecules that can penetrate through lipid membranes. They are a group of compounds that selectively accumulate in mitochondria guided by the negative transmembrane potential.[194]Members of this group are structurally diverse and selectively target the mitochondrial.[194] Studies have revealed the significant of lipophilicity and positive charge in molecules that accumulate in mitochondria. Mitochondria have been generally recognised as the powerhouse of a cell. They provide ATP for almost all cellular activities. Beside their role as energy provider, they are also recognised as integrators of a plethora of intrinsic and extrinsic pathways to cell death.[195] These dual role of energy production and cell apoptosis makes the organelle a major target in cancer treatment. Most especially, the permeability of their outer membrane becomes a major point during apoptosis. Thus, several designs usually aimed at targeting this event by preventing the activity of antiapoptotic or by interfering in the major functions of mitochondrial may help to overcome the phenomenon of drug resistance.[194]DLCs are attracted by the negatively charged mitochondria matrix and thus been used as probes for imagining mitochondria.[196] DLCs selectively accumulate in cancer cell mitochondria and thus elicit apoptosis of cancer cells. Because of their affinity to mitochondria, DLCs have been used for numerous applications such as visualisation of tumour cells, drug deliveries, photosensitizers and therapeutic agents. As a target to mitochondria, two conjugates of acridine orange and rhodamine were designed and synthesized as photosensitizer.[197] Each conjugate contained a single delocalized lipophilic cation and their photodynamic activities were evaluated.[197] It was observed that both conjugates showed higher phototoxicity which made them potential candidates for

effective photosensitisers.[197]DLC could also be embedded into peptides to enhance drug delivery into the mitochondria.[198] Though this require a balance between a charge distribution and lipophilicity in order to ensure localization within mitochondria.[198]Highly water soluble rhodacyanine dye as DLC was reported to exhibit interesting toxicity activity against spectrum of model system.[199] Based on its impressive antitumour activities in preclinical studies it has been chosen for further clinical studies.[199] Several DLC have been reported to show significant antitumour activities due to their selective uptake and retention in mitochondria of cancerous cells.[200] Many researchers have used DLCs to improve the effect and efficacy of existing antitumour modalities.[200] For instance, it was reported that selective retention of rhodamine-123 by human glioma cells with its associated photoactivated cytotoxicity shows that rhodamine-123 could be a potential candidate for photosensitising drugs for the treatment of tumour glioma cells.[201]Intramitochondrial dyes allowed selective damaged of carcinoma cells.[202]It was also shown that human ovarian carcinoma cells has elevated mitochondria membrane potential that made them more sensitive to DLC.[203] Thus one can chose cells with low mitochondrial membrane potential using DLC.[203] It has been reported that dequalinium exhibited excellent anticarcinoma activity than several established anticancer drugs in mice with intraperitoneally implanted mouse bladder tumour cells and human subcutaneous implanted colon tumour cells.[204] Therefore, this could be exploited for anticancer treatment by DLC since it was established that DLC selectively accumulated in the mitochondrial leading to death of carcinoma cells.[204]Literature stated that 'the relationship between the structure of chemical compounds and their specific effects on cancer cells are not well understood'.[205]However, in attempt to understand the structural determinants of selective phototoxic activity of selected DLC towards tumour cells, a study of the relationship between molecular structure and selectivity on tumour

cells using a spectrum of DLC dyes of the group of triarylmethane as mitochondrial photosensitizers model.[205]In view of this it was observed that the lipophilic/ hydrophilic properties of these DLC dyes influence tumour selectivity.[205] Also, a model which identified processes and molecular properties that usually lead to selective accumulation of drugs in tumour cells in the mitochondrial has been reported.[206]Increase in mitochondrial membrane potential usually induce the DLC to be selectively accumulated on the tumour cells in the mitochondrial,[207] the general mechanisms by which they accumulate in the mitochondrial[208] have been discussed but the way and manner by which each DLC exhibits it toxicity on the tumour cells in the mitochondrial varies and based on structural differences.[209,210] It has been reported that D112, one of the promising DLCs selectively bonded to transformed cells impaired the DNA in mitochondrial and induce reactive oxygen species (ROS).[150] ROS production is necessary for Bax activation and subsequently leads to cell apoptosis.[150] Interestingly, it was observed that the positive charge on DLCs is vital to their unexpected similar role in cancer cells and cardiac muscle cells.[211] Both cancer and cardiac muscle cells displayed high negative plasma membrane potential which induced the uptake of DLCs.[211] The positive charge and the lipophilicity of DLC are central to their toxicity in these two different types of cells.[211]

I.8. Fluorescence

I.8.1.Fluorescence and Phosphorescence

Fluorescence and phosphorescence are two phenomena that involve emission of photons during molecular relaxation from exited states.[212] Fluorescence is 'radiative decay between state of the same multiplicity while phosphorescence is radiative decay between state of different multiplicity and persists after the exciting radiation is removed'[213] When emission of light occurs simultaneously with absorption of the excitation light as a result of short time delay between absorption of photon and emission usually in a period of less

than microsecond. The phenomenon is called fluorescence. Phosphorescence exists or occurs when emission persist longer after the excitation light has been extinguished. In fluorescence, the compound is excited by absorbing a photon from its ground electronic state to one of different vibrational states in the excited electronic state.[214] Collisions with other molecules results in a loss of vibrational energy of the molecule until it reaches the vibratory state lower than the excited electronic state. In the ground state, the electrons are all spin paired when excited the electron maintains its orientation, if the energy gap between the first excited state is small the electron can relax, emitting a photon, this phenomenon is known as fluorescence.[214]The Jablonski diagram (figure 3) offers a convenient representation of the excited states structure and the relevant transitions. The molecule absorbed light given rise to a singlet-excited state (S_1, S2, S_3, etc.). The main characteristics used to describe the process include absorption maxima (λ_{max}) which corresponds to the absorption wavelength for which there is a maximum absorption on the spectrum and the extinction coefficient at λ_{max} (ε).[215] Following excitation to the first excited state, there is loss of energy due to rapid relaxation to the first singlet excited state (S_1). Fluorescence occurs when this excited state relaxes to the ground state (S_0) through emission of photons. Alternatively, the excited molecule may relax by splitting into radiative and non-radiative. Non-radiative emission usually occur due to interaction with the solvent or other molecule in the surrounding. Thereby leading to dissipation of energy in form of kinetic energy. Furthermore, intersystem crossing to the triplet state may occur. The fluorescence lifetime is the average time the molecule remains in the excited state before emitting a photon.

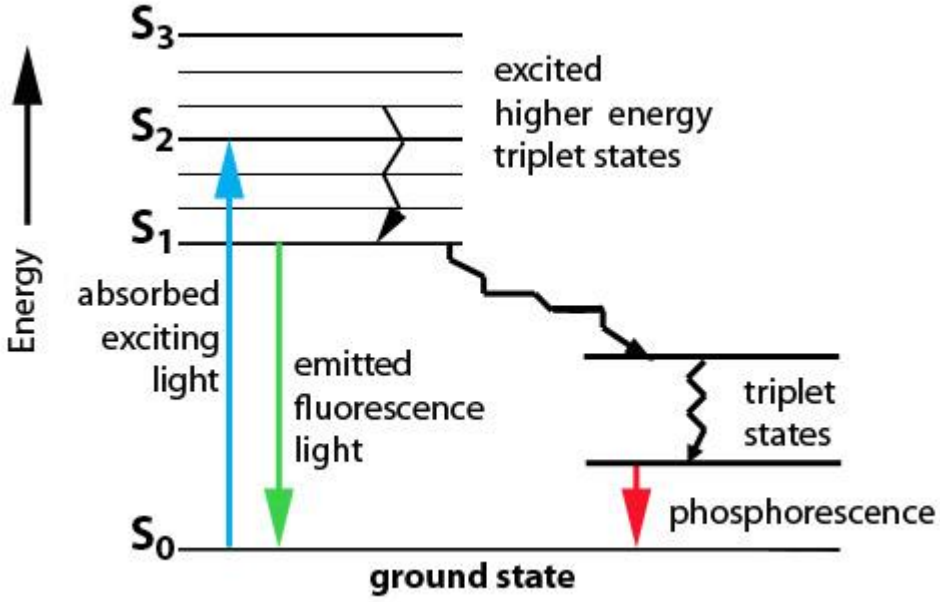

Figure 7: Jablonski diagram

The fluorescence Quantum yield (ϕ) gives the efficiency of the fluorescence process. It is the ratio of photon emitted to photon absorbed:

Φ = emitted photons/ absorbed photons

Every photon absorbed results in a photon emitted. The maximum fluorescence quantum yield is 1.0 and compounds with quantum yield of 0.10 are still considered fluorescent. Vibrational energy is lost when electrons relax from the excited state back to the ground state as a result of the energy loss; the emission spectrum of an excited fluorophore is usually shifted to longer wavelengths when compared to absorption or excitation spectrum. This is known as Stokes shift. At wavelength higher than 200 nm, two lowest energy transition are usually obtained due to the energy available from photons. The available transition are n→π*and π →π*.[216] When compounds are radiated by light, having the same energy with possible electronic transition within the molecule, part of the energy would be absorbed and the electron would be promoted to the higher energy orbital. That is from Highest Occupied Molecular Orbital (HOMO) to the lowest

unoccupied molecular orbital.[213] Therefore, the energy difference between the lowest vibrational energy level (the singlet ground state S_0) and the excited vibrational level (the singlet excited state S_1) is the excitation energy.[216] Fluorescence usually occurred in aromatic systems because of the presence of mobile electrons, which arise from delocalisation in the ring system. These mobile electrons are easily excited because they are loosely bonded to the atoms.[217] The observed excitation and emission spectra are usually mirror images of each other due to the similarities in the vibrational transition between the ground and excited states. Typical fluorophores include fluorescein, rhodamine B, quinine and acridine orange. Emission from polycyclic aromatic such as anthracene and perylene are usually used for environmental monitoring of oil pollution. Pyridine 1 and rhodamine are often used in dye laser. Acridine orange is usually used as DNA stain.[217]The use of acridine dyes as reagents for the selective luminescence determination of polycylic aromatic hydrocarbons has been reported.[218] Phosphorescence is not prominent in fluid substances at room temperature due to different deactivation processes that compete with emission, such as quenching and non-radioactive decay processes.[217] There are many factors that influence the excitation energy of a compound. These include level of aromaticity or conjugated double bond. The incremental in conjugated double bond implies that incremental addition of π bonds in a compound gives rise to decrease in energy gap between the HOMO and LUMO, allowing for excitation by lower energy UV light.[219]Interaction of solvent with the molecule may lead to an asymmetric emission spectrum due to the redistribution of solvent molecules around the chromophore in order to account for the electronically induced dipole of the excited state.[213] The freedom of the π electron in polyaromatic compounds can be enhanced by substituent group and heteroatoms leading to increase in fluorescent properties.[220] Other

factors affecting the intensity of fluorescence include concentration, pH, temperature and stability of compound in light.[220]

I.8.2.Fluorescence Quenching

Fluorescence quenching is a process that decreases the intensity of the fluorescence emission.[221]This may occur from the following factors, dynamic or collisional quenching, where noninteractive random collision of a small molecule deactivates the excited state of the fluorophore[221]and when a small molecule makes a ground state complex with the fluorophore thus becomes nonfluorescent.[221]It can also occur by other factors such as attenuation of the incident light by the fluorophore itself or other absorbing species.[217]

I.8.3.Fluorescence Microscopy

Fluorescence microscopic technique is an integral part of biomedical sciences and material sciences due to attributes that are not readily available in traditional optical microscopy. This is a powerful technique for sensing changes in the environment of the fluorophore. Thus it could help in providing clues to the de-ligation processes.[222] It is also one of the main techniques used to obtain the images of organometallic compounds in biological environment. Fluorescence is also useful in a number of safety applications as a scientific research tool, and in investigative medicine. Fluorescence microscopy is in a state of rapid evolution with novel techniques, probes and equipment emerging almost on a daily basis.[214]There are several factors that affect the quality of fluorescence image.[214] These include choice of fluorophore, concentration of fluorophore, wavelength of the exciting light, magnification, quenching, bleaching, background fluorescence, degradation of fluorophore, detector sensitivity[214] etc. Confocal microscopy was used to study Au(III) complexes that were effectively ‘switch on’ fluorescence thiol probes and also act as anticancer agents.[6] In that study, it was reported that only the ligand released on thiol mediated Au(III) to Au(I) reduction was fluorescence hence its description as a

thiol probe.[6]Incoporation of fluorescence through aurophilic (Au-Au) interaction in dinuclear Au(I) carbine has been reported.[223] In this study, confocal microscopy revealed that the complexes accumulated in the lysosome though they possessed anti mitochondrial activities.[223] In this research, attempts were made to develop novel fluorescent anticancer agents based on gold(I) in other to understand the deligation process. Therefore acridine derivatives were chosen to serve as ligands due to their biocompatibility and liphopholicity. The potential mechanism of action of gold(I) complexes are described in figure 4

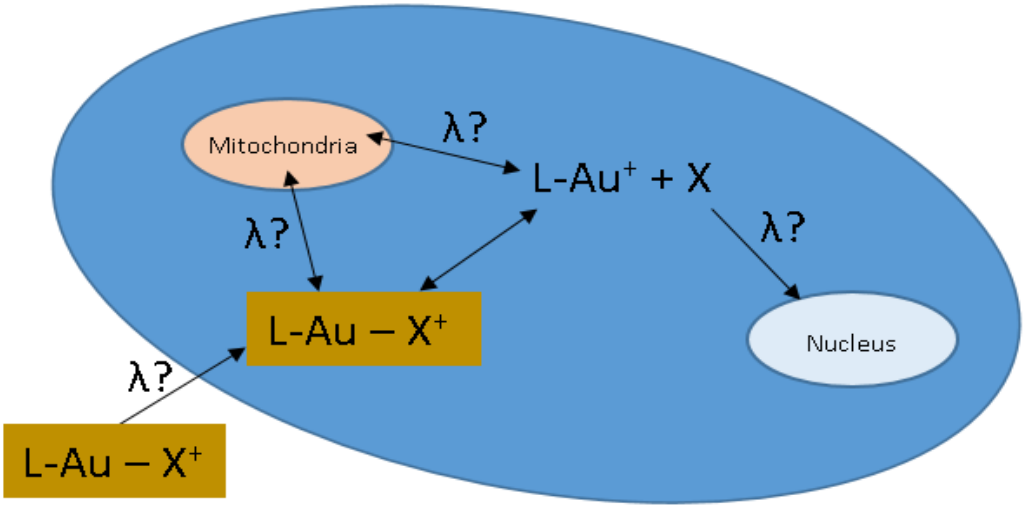

Figure 8: Ligation and cell permeation

I.9.Human Cancer

Cancer are diseases caused by cells which are unable to form stable functional structure which multiply sporadically and invade the organism.[224] They involve dynamic changes in the genome.[225] The hallmark of cancer consists of six biological capabilities acquired at different stages of human tumour development. These include sustaining proliferative signalling, evading growth suppressors, resisting cell death, enabling replicative immortality, inducing angiogenesis and activating invasion and metastasis.[226] Literature has established that cancer is in essence a genetic disease.[227,228] Viruses caused about 15

percent of human cancer in the world. Viruses accounted for about 80 percent of cervix and hepatocellular carcinoma.[229] Cancer is one of the major public health concern worldwide and is the second leading source of death in the United States.[230] Over the past two decades, the cancer incidence rate remained stable in women but decline by about 2% annually in men.[230] However, the combined cancer death rate decline by about 26% for the past two decades[230]due to advance in the fight against cancer and wider application of cancer control knowledge, including reduction in the rate of smoking, cancer screening and HPV vaccination.[230] Cancer treatment with extensive surgery, radiation therapy and toxic multiagent chemotherapy were all given hope that by adopting new strategy of multidisciplinary treatment teams using collaboration to build new and sustaining treatment, the war against cancer could be won in not too distant future.[231]

I.9.1. Liver Cancer

Hepatocellular carcinoma (HCC) is the major primary liver cancer and the most dreaded complication of chronic liver disease.[232] It is the fifth worldwide most common cancer and the third most common cause of cancer-related death.[233]In spite of wide scope of research on systemic chemotherapy for HCC, it has been so ineffective due to low response rate and no survival benefit.[233] However, studies are ongoing on the molecular pathways involved in hepatocarcinogenesis as potential therapeutic target.[233] It is widely established that HCC is one of the cancer cells with poor chemosensitivity to drugs.[234] Factors such as lower flow capability of blood in the solid tumour and lower permeability to drugs are part of the obstacles to HCC chemotherapy.[234] Furthermore, both intrinsic drug resistance and acquired drug resistance are also known obstacles in this regard.[234]It has been reported that SUMOylation –activating enzyme UBA2[235] and activation of Nrf2 by microcystin-LR[236] involved in proliferation of liver tumour cells.[235] Many of the liver cancer are diagnosed at a later stage when just a few therapeutic options are available.[237]

However, cancer specific aptamers were generated as molecular probes for early cancer diagnosis and basic mechanism studies.[237] It has been reported that three triterpenic acids, oleanolic acid, ursolic acid and maslinic are potent antiangiogenic agents to reduce and invasion and migration in liver cancer cell lines.[238]Sorafenib, an orally-available kinase inhibitor has been reported to exhibit excellent cytotoxicity against HCC.[239]The effect of anticin A, anticin C and methyl anticinate A (MAA) derived from *Antrodia camphorata* were studied on the proliferation of human liver cancer cell lines HepG2 and normal cell. It was observed that all the compounds selectively exhibit high toxicity against tumour cells living the normal cell.[240]

I.10. Aims and Objectives

This research work is therefore aimed at providing insights and understanding into the cytotoxic activity of Au(I) complexes so as to facilitate their development and potency maximization via the following objectives:

(1) To synthesise an array of fluorescent Au(I) complexes bearing acridine derivatives.

(2) To characterise the complexes synthesised in (1) above using NMR, IR, MS, UV-vis and X-ray crystallographic studies

(3) To test/assay the cytotoxicity of these fluorescent Au (I) complexes against human liver cancer, cell lines.

(4) To modify the complexes synthesised in aim (1) above using a variety of functional moieties.

(5) To perform aim (3) above with the modified moieties.

(6) To perform aim (1) above with pyrazole derivatives.

(7) To study the behaviour of fluorescent gold(I) complexes in solution.

(8) To investigate the photophysical properties of acridine bearing diverse substitution motifs

(9) To investigate the photophsical properties of fluorescent gold(I) complexes.

(10) To synthesis a spectrum of Ag(I) bearing acridine derivatives

(11) To synthesis an array of Ag(I) bearing pyrazole derivatives.

CHAPTER II. RESULTS AND DISCUSSION

II.1. Literature Background

Davis and Pizzini in 1960 reported that *p*-substituted nitrobenzenes condense with arylacetonitriles in methanolic potassium hydroxide solution to give anthranil, which rearranged under the right conditions to produce acridine (Scheme 1).[241] Wróbel modified this in 2007 and found out that under appropriate reaction conditions, efficient formation of the σ^H-adduct of substituted nitrobenzene and aryacetonitrile followed by reductive transformation of the nitro group in the presence of silylating agents usually led to the production of the corresponding acridine.[242]

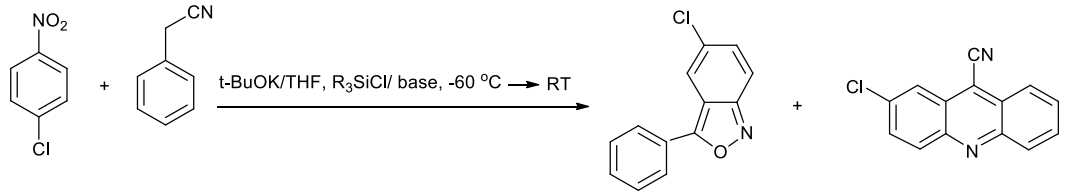

Scheme 1: Reaction scheme for Davis acridine synthesis as modified by Wróbel[243]

An array of acridines were synthesised by reacting the corresponding nitrobenzene and arylacetonitrile with TBDMSCl and *t*-BuOK as Lewis acid and base respectively in anhydrous THF, as aprotic solvent. The reaction conditions were adapted from Wróbel . However, discrepancies on the reaction conditions were noted. For example, they stated in 2007[242] that the yield was improved for 2-chloroacridine carbonitrile with 2.2 equivalent of the base, *t*-BuOK being added in the second addition and in 2015[243] indicated that an increase of the base from 1.1 to 2.0 equivalent was detrimental to the yield (from 85 % to 50 % respectively). Intriguingly, further increase to 2.5 equivalent partially recovered the yield to 74 %. It is acknowledged that conversion to acridines goes via benzisoxazoles, which are converted, to acridones and finaly acridines under markedly different conditions. The dilute concentration of the released cyanide ions makes their involvement unlikely and the 3-position (where attack would need to occur)

is sterically hindered. More probable is a variety of ring opening and degradation reactions; these reaction mixtures contain a variety of reactive species, making side reactions likely. The target of their 2015 publication was benzisoxazoles not acridines, consequently the discussion were not focussed on acridines. Certainly some aspects of their results went without discussion: the time difference between the formation of benzisoxazoles (1-2 hours) and acridines (~48 hours), the bulkier silylating agent (SA) favouring acridine formation, DBU giving solely benzisoxazole formation and perhaps most puzzlingly the ability to control the resulting motif purely by ratio of reagents using TBDMSCl and t-BuOK. Interestingly, the benzisoxazole was not observed as a side product at any point during the project described herein.

II.2. Synthesis of Novel Acridine Ligands

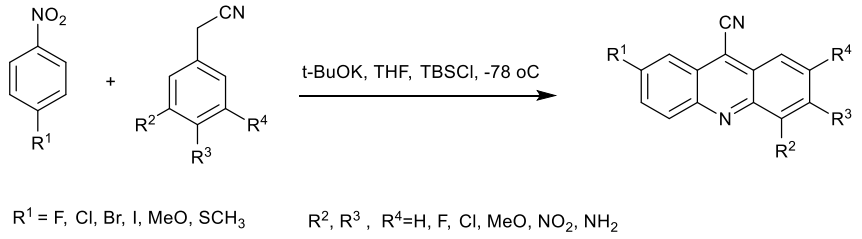

Scheme 2: General synthetic pathway for acridine derivatives.

We modified the method and synthesised an array of acridine ligands using a modification method outlined by Wróbel according to the reaction in scheme 2. It required 4-halonitrobenzene and benzyl cyanide as the starting materials and proceeded via the formation of a σ^H-adduct. The reaction was carried out under inert atmosphere and started at low temperature (-78 ^oC) until the second equivalent of the base was added. The reaction was monitored by thin-layer chromatography (TLC), and a fluorescent product can be observed and confirmed that the reaction proceeded. Indeed, the first step of the reaction is the formation of the σ^H-adduct which is blue fluorescent. Then, the reaction

was maintained at room temperature until it is subsequently quenched and work up carried out to isolate the product.

II.2.1 Mechanism of the Reaction

The mechanism involves a vicarious nucleophilic substitution of hydrogen (VNS) [244] (scheme 3). It provides a suitable method for the introduction of a specific substituent or moiety into heterocyclic ring systems.[245,246] The first step is the use of first equivalent of the base to de-protonate the α-H of cyano group ready for the first addition of the benzyl cyanide **1** onto the nitrobenzene **2** and subsequent conversion to σ^H-adduct **3.** Blue fluorescent under UV-light confirmed this. Next was the addition/elimination reaction of TBSCl leading to transformation of σ^H-adduct into nitroso carbanion[242] **4** which gave orange colour in solution. The carbanion deprotonated and transformed into oxime **5** which undergoes pi-electrocyclisation to afford the desired product **6**.

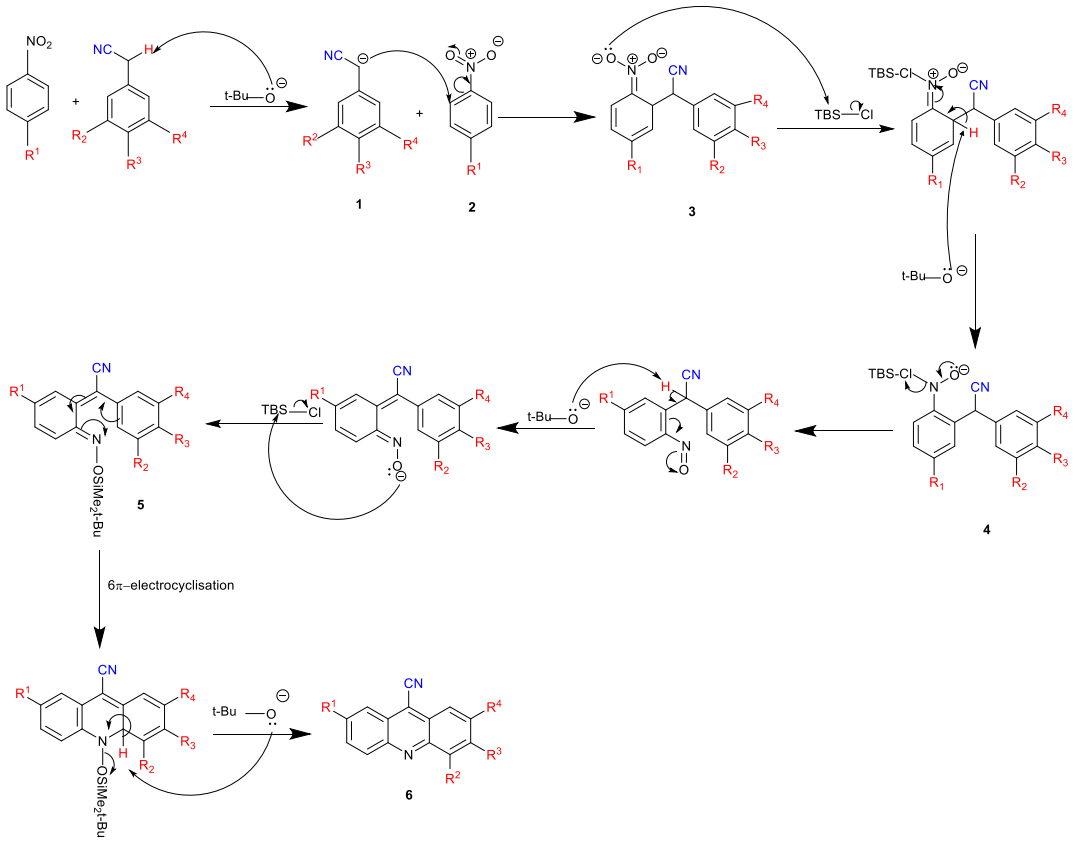

Scheme 3: Proposed mechanism of reaction

Table 1: Substituted Acridines synthesised based on scheme 2

Entry	R^1	R^2	R^3	R^4	product	Yield (%)
1	Cl	H	H	H	**7**	79
2	Br	H	H	H	**8**	75
3	Cl	H	OCH_3	H	**9**	73
4	Cl	H	F	H	**10**	68
5	Br	H	OCH_3	H	**11**	82
6	Br	H	F	H	**12**	87
7	Cl	H	Cl	H	**13**	84
8	I	H	H	H	**14**	75
9	Cl	OCH_3	OCH_3	OCH_3	**15**	92
10	I	OCH_3	OCH_3	OCH_3	**16**	78
11	I	H	OCH_3	H	**17**	85
12	I	H	F	H	**18**	90
13	Br	OCH_3	OCH_3	OCH_3	**19**	91
14	I	H	OCH_3	OCH_3	**20**	77
15	Cl	H	OCH_3	OCH_3	**21**	78
16	Cl	H	Br	H	**22**	82
17	Br	H	OCH_3	OCH_3	**23**	80
18	SCH_3	H	OCH_3	H	**24**	84
19	SCH_3	H	F	H	**25**	82

Entry	R^1	R^2	R^3	R^4	product	Yield (%)
20	SCH_3	H	Cl	H	**26**	78
21	SCH_3	OCH_3	OCH_3	OCH_3	**27**	79
22	OCH_3	H	F	H	**28**	87
23	OCH_3	H	Cl	H	**29**	90
24	OCH_3	H	OCH_3	OCH_3	**30**	88
25	OCH_3	H	Br	H	**31**	88
26	SCH_3	H	OCH_3	OCH_3	**32**	86
27	SCH_3	H	Br	H	**33**	81
28	H	H	H	H	**34**	83
29	H	H	OCH_3	H	**35**	86
30	H	H	F	H	**36**	83
31	H	**H**	Cl	H	**37**	79

II.2.2. Synthesised Product Characterisation

The structure of the product was confirmed by ^{1}H NMR, ^{13}C NMR, IR, melting point analysis and mass spectrometry. The acridine derivatives in table 1 were chosen to investigate the impact of the substituents on their fluorescent properties and their cytotoxicity. Since acridines can intercalate with DNA[247,248] we believe they could play a role in the drug mechanism. In the synthesis of these derivatives, we intended to have a cyano group at position 9 and a halogen group at position 2 and then modify other positions. The cyano group is key to design a potential drug because it is a functional group which can be easily modified, for example, an alkyl chain can be added to increase liphophilicity or the cyano group can be replaced by many other functional groups such as acids, amines, amides, etc. which can increase drug potency. The initial procedure reported by Wróbel was not successful: it required extensive reaction times and we observed significant decomposition of the intermediates during the work-up phase, leading to problematic flash chromatography purification to separate the desired compound from the crude. Modification of the procedure to a two-step recrystallisation in methanol and ethyl acetate. This required 4-halonitrobenzene and benzyl cyanide as the starting materials and proceeded via the formation of a fluorescent σ^H-adduct intermediate. The reactions were performed under inert atmosphere and started at low

temperature (-78 ^{o}C) until further equivalents of the base were added. The progress of the reaction was monitored by thin-layer chromatography and a fluorescent product confirmed that the reaction proceeded smoothly. However, the work-up outlined by Wróbel was removed and also the purification procedure was changed which improved the purity of the products as well as the yields from about 20% to 92%. The reaction periods were also reduced from 6 days to 42 hours.

II.2.3. Process Optimisation

Initially, we found out that the aqueous work up proposed by Wróbel was detrimental to purity and yield. We therefore replaced this process by concentrating the reaction mixture on the rotary evaporator followed by acetone recrystallisation. Recrystallisation is an attractive purification method in this case because of the longer period of time (3 days) required to achieve satisfactory separation through column chromatography. In addition, it is comparatively environmentally friendly, cheap and scalable. The use of silica and large volumes of organic solvents pose unnecessary risks to human health and the environment. However, we later found out that the acetone recrystallisation used previously reduced reproducibility. On standing, in a minimal amount of acetone, multiple new spots appeared in TLC, including one faint fluorescent spot. The pH of this was found to be zero; it therefore seems likely that the residual water in acetone caused quenching of the TBDMSCl releasing HCl. Another result of acetone recrystallisation from a concentrated reaction mixture was the significant amount of inorganic impurities left in the product, giving misleading yields. Nitrobenzene, one of the starting materials, is partially soluble in acetone and having a basic centre it would follow that this solubility was increased at lower pH values. Then, a solvent that would either solubilise the reactant without solubilising the product or vice versa was proposed. Methanol was effective in precipitating the product; however, heating did not solubilise it. Nevertheless, methanol

trituration followed by dissolution in CH_2Cl_2 and filtering to remove any inorganic contaminants, then a final recrystallisation in either methanol or ethyl acetate was found to give highly pure acridine in moderate to good yields.

II.2.4.Substituent Effects

The nature and position of the substituent on the nitroarene and phenylacetonitrile usually determined the degree of formation of the σ^H-adduct and consequently dictated the feasibility of the process for a particular derivative. The reason being that each substituent is expected to exert its electronic effects on the ring system of the nitroarene. Whilst the substituent on the phenylacetonitile are also expected to affect the rate of reaction to certain degree. For optimum yield of chloronitroarene, 2.9 equivalents of base and 5.0 equivalents of silylating agent is required. For the bromonitroarene, 2.9 equivalents of base and 6.1 equivalents of silylating agent gave the best yields. However, 3.5 equivalent of base and 7.5 equivalents of silylating agent is required to obtain optimum yield for the iodonitroarene. The halogen groups (F, Cl, Br, I) are electron withdrawing through inductive effect (- I) in the order of F >Cl >Br >I while the methoxy groups are electron donating through mesomeric effect (+M).[249] The position of the substituents on the ring system influences the yield. When the halogen and methoxy groups were positioned in such a way that their effects cancelled out, thus higher percentage yields were expected. This proposition was in tandem with our experimental observations as excellent yields were obtained when we have both on either side of the reaction. For example, the yield for 2, 3, 4-trimethoxy-7-cholroacridine-9-carbonitrile **15** was 92% which was greater than 91% obtained for **19** 2, 3, 4-trimethoxy-7-bromoacridine-9-carbonitrile (Figure 9).

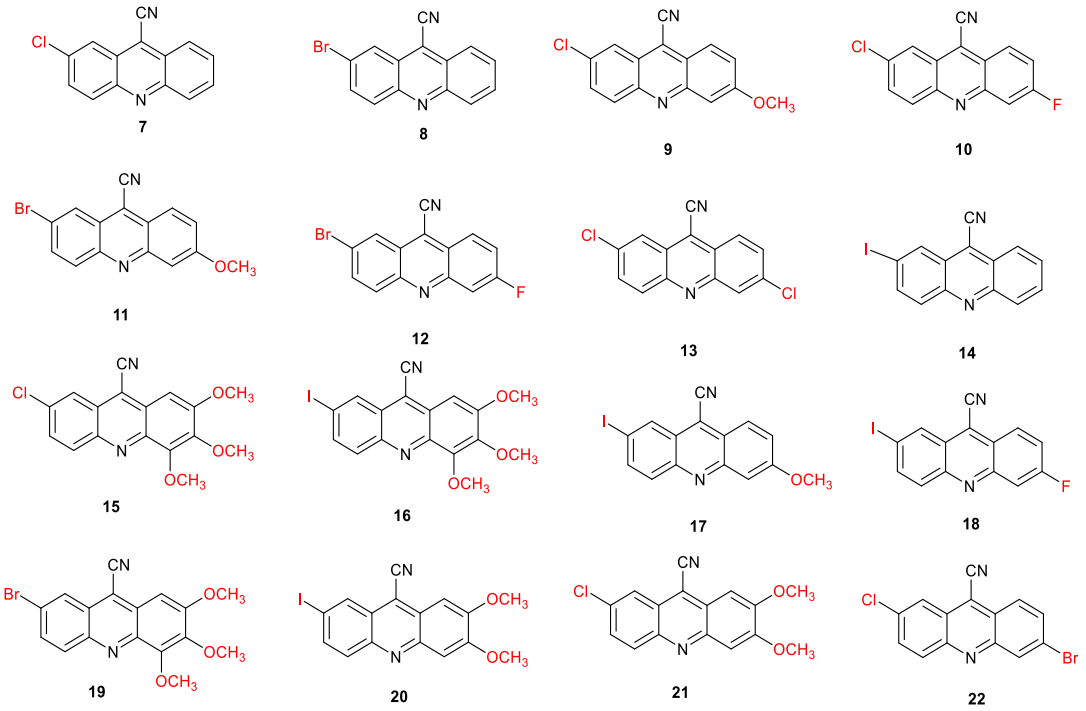

Figure 9: Structures of compounds **7-22**

This was also greater than 78% yield obtained for **16** 2,3,4-trimethoxy-7-iodoacridine-9-carbonitrile. When there was no substituent on the phenylacetonitrile, the chloro substituted acridine synthesised **7** gave the highest yield of 79 % compared with bromo substituted **8** and iodo substituted **14** that have equal percentage yield of 75 %. When there was a fluoro substituent on the phenylacetonitrile, the iodo substituted acridine **18** gave the best yield followed by bromoacridine **12** with chloroacridine **10** substituted having the least in order of 90 % > 87 % >68 %. Experimental observation on the synthesis of only one methoxy substituted on the acridine are in the order of Cl< Br< I (that is **9** with 73 % < **11** with 82 % < **17** with 85 %). Our experimental conditions and work up procedures met improvements on the previous acridine synthetic procedures as the yield were considerably increased and various substituted acridines not readily synthesised by one pot methodology could be readily synthesised. Our procedure gave better yield compared with almost all the similar acridine synthesised in the literature. For

example, while the yield in non-substituted acridine in the literature was 20 % acridine-9 carbonitrile[242] our procedure gave 83 % (**34**) (Figure 10).

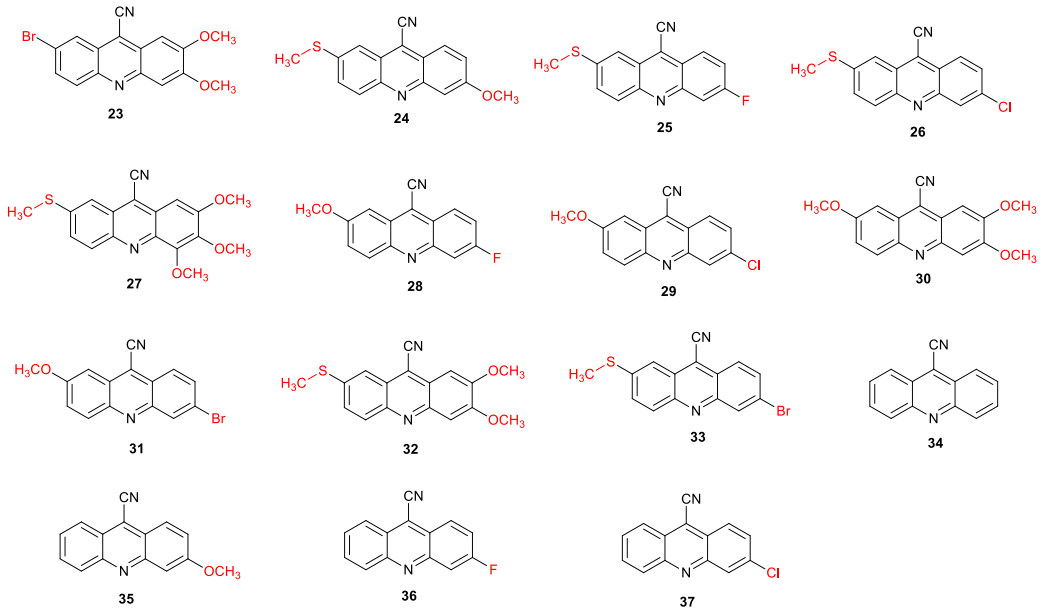

Figure 10: Structures of compounds **23-37**

The synthesised 7-chloro-2,3-dimethoxyacridine-9-carbonitrile **21** was 78 % while it was 66 % in the literature.[242] Also, our 2-bromoacridine-9-carbonitrile **8** was 75 % against 74 % in the literature.[242] It is worth mentioning that there was no data in the literature for the reaction of arylacetonitriles with *p*-fluorobenzene forming a desired product through σ^{H}-adducts intermediate. We assumed that this may be due to the tendency of fluorine to dissociate from the system or it may undergo displacement reactions with other substituents due to high reactivity of fluorine. In other word, it may lead to formation of 4-nitrodiphenylacetonitrile instead of the σ^{H}-adducts intermediate. However, it should be noted that not all acridine attempted to synthesised were successful. These include: 4-nitrophenylacetonitrile, 4-aminobenzylcyanide, 2,4-dimethoxyl-1-nitrobenzene, 4-hydroxylphenylacetonitrile, 4-isocyanatobenzylcyanide and benzyl phenyl sulfone. The reason for unsuccessful results for these reagents could be due to the reactivity of their functional group with TBDMSCl leading to production of unwanted products. In

addition, the no observable product obtained in 4-nitrophenylacetonitrile, 4-isocyanatobenzylcyanide and 4-aminobencylcyanide may be due to the role of nitro group in the proposed mechanism. For 4-hydroxylphenylacetonitrile, oxygen in a hydroxyl group (OH) is electron withdrawing by induction (-I) because the oxygen atom is relatively electronegative and is uncharged in that bonding arrangement. Therefore, the OH group may ionized (loss of proton) prior to deprotonation of the α-H of the nitroarene. In order words, there could be a competitive formation of para σ^H –adducts which cannot be transformed into a desired product. Then, for 2,4-dimethoxy-1-nitrobenzene, this can be explained also by competitive formation of the σ^H –adducts as one of the ortho position of the nitro arene has been blocked.

II.3. Alternative Routes

II.3.1. First Alternative Route

In an attempt to propose a simple way for the synthesis of acridine derivatives with varying substituents, we explored a one pot process proposed by Pordel.[250,251] as shown in the scheme 4 below:

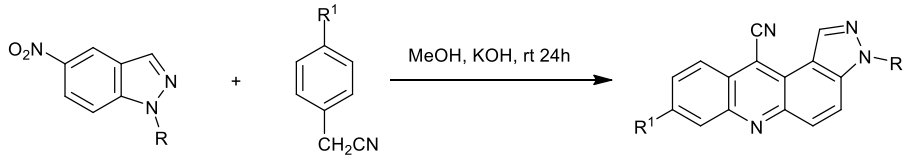

R. R1 = Me, Et, OMe

a : Pordel reaction for the synthesis of acridine derivatives

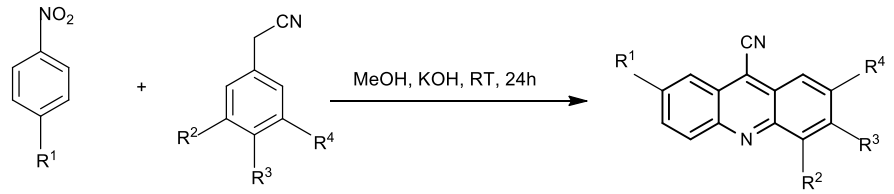

R^1 = F, Cl, Br, I, MeO, SCH_3 R^2, R^3, R^4=H, F, Cl, MeO, NO_2, NH_2

b : Proposed Pordel reaction for the synthesis of acridine derivatives

Scheme 4: Proposed reaction for Pordel acridine synthesis[252]

The reaction is initiated by nucleophilic substitution of the α-hydrogen of the nitrobenzene with benzyl cyanide in basic methanol solution followed by intramolecular electrophilic aromatic substitution which afforded the products in a low yields.[252] This method shows some advantages over the previous method, notably, it is a single reaction step and has shorter reaction time (24 h) compared with our modification of the Wróbel reaction (42 h). In addition, it requires simple reagents and conditions compared with low temperature condition. Some of the acridine derivatives were prepared using a modified method proposed by Pordel. However, the major setback of this method is that it gave low yield of product (36% for 2-chloro-9-acridinecarbonitrile) compared with the modified Wróbel method (79% for the same compound).

II.3.2. Modification of the Pordel work up

Initially, the synthesis of a series of acridine was carried out without a single success by following the step by step in their report. A simple work up was proposed in their paper: procedure removed methanol on a rotary evaporator followed by washing the precipitate

with water and with ethanol, and then air dried to afford the desired product. The work-up proved to be unsuccessful. We then modified the work up by washing the precipitate in water and ethanol after concentrating on the rotary evaporator and then dissolving the precipitate in CH_2Cl_2. Filtration was performed to remove the residual inorganic impurities while the yellow filtrate was concentrated on a rotary evaporator to remove the solvent, then dissolved in small amount of ethyl acetate and filtered. The yellow residue were dried under reduced pressure to give the desired compounds.

II.3.2.1 Modification of the Reaction Conditions

Further attempts were made to improve the yield by increasing the reaction temperature from room temperature to 50 ^oC (Scheme 5) and increase the reaction time from 24 h to 42 h. The Reactions were monitored by TLC. These conditions slightly improve the yield (from 36 % to 54 % for **7** and from 31 % to 47 % for **8**)

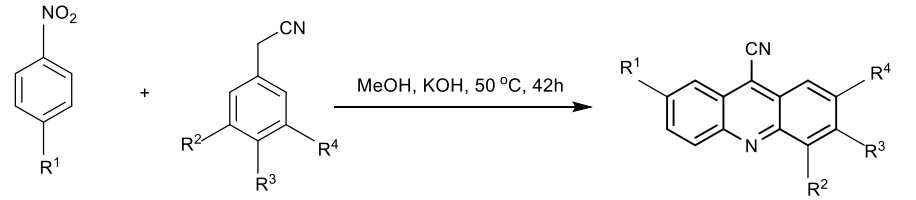

R^1 = F, Cl, Br, I, MeO, SCH_3 R^2, R^3, R^4=H, F, Cl, MeO, NO_2, NH_2

Scheme 5: Modification reaction conditions of the Pordel acridine synthesis

It should be noted that some substrates do not work with either methods. These include 4-nitrophenylacetonitrile, 4-aminobenzylcyanide, 2, 4-dimethoxyl-1-nitrobenzene, 4-hydroxylphenylacetonitrile, 4-isocyanatobenzylcyanide and benzyl phenyl sulfone.

II.3.3. Second Alternative Route

Alternatively, we used a rearrangement of heterocyclic system[253–257] leading to a desired product as proposed by Elliot *et al (*Scheme 6).[253]

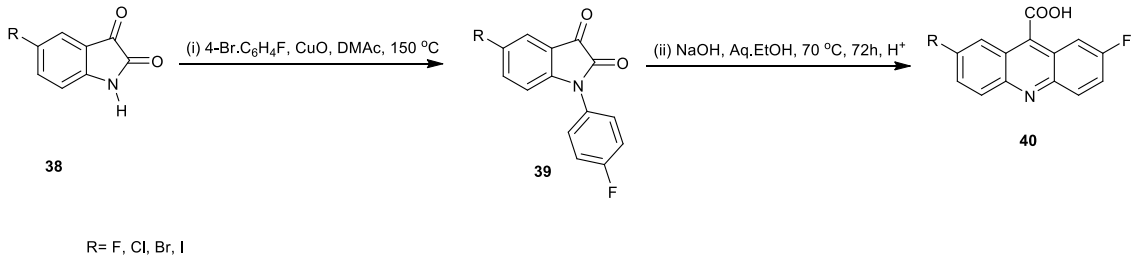

Scheme 6: Alternative reaction for acridine synthesis by Elliot

In an attempt to synthesise **39 (**R=Cl**),** Chloroisatin and copper oxide were suspended in dimethyacetamide (DMAc). 1-bromo-4-fluorobenzene was subsequently added dropwise over 1 h. The reaction mixture was heated to 150 ^{o}C for 24 h. The product was filtered through celite R 521 and the filtrate poured into an ice-water slurry and then stirred for 30 minutes. The resulting red/ brown precipitate was isolated by filtration and dried. It was then re-dissolved in acetone and filtered for a second time through celite R 521 to remove any insoluble materials. The filtrate was concentrated on the rotary evaporator to remove the solvent. Then, purified by column chromatography using CH_2Cl_2 as eluent. The result was not the desired product. However, several attempts were made to synthesise fluorinated acridine derivatives using the above stated methods but were not successful.

II.4. Preparation of Monodentate Cationic Gold

In order to generate active cationic gold(I) species as potential candidate for the complexation reaction a monodentate cationic gold(I) was prepared. It has been established that monodentate cationic gold PPh_3Au^+ with non-coordinating or weakly coordinated anions react with PPh_3 to produce mixtures of higher coordinated complexes of the type $(Ph_3P)_2Au^+$, $(Ph_3P)_3Au^+$ or $(Ph_3P)_4Au^+$. However, it was also stated that $(Ph_3P)_3Au^+$ and $(Ph_3P)_4Au^+$ (equations 3 and 4 below) could not be observed at room temperature by NMR because of fast exchange of ligands,[258–260] which we also observed

at room temperature. Since it has been established that three or four coordinated species of triphenylphosphine gold(I) may not be observed by ^{31}P NMR at room temperature, we then focused on very low temperature (-80 ^{o}C).

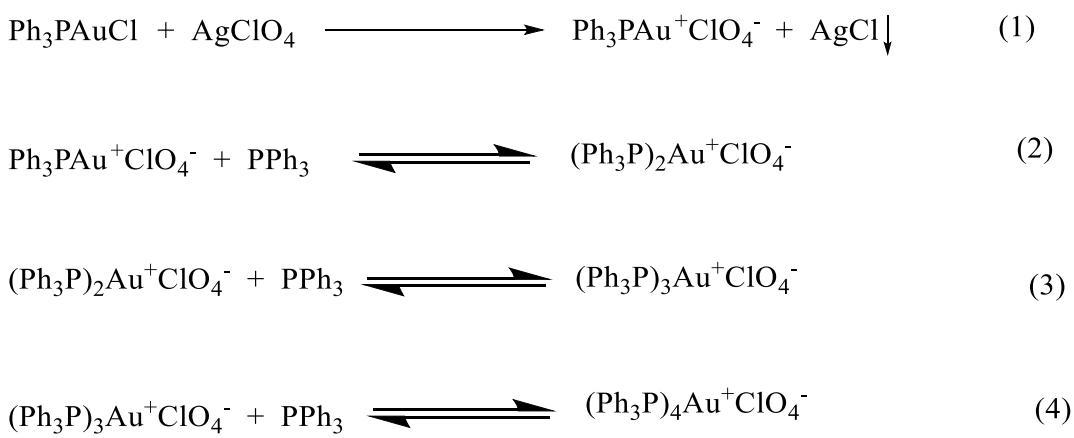

Scheme 7: Step by step reactions for formation of higher gold(I) complexes

The solution of cationic gold [Ph_3PAu^+,ClO_4^-], was prepared from Ph_3PAuCl and a solution of $AgClO_4$. Due to solubility problems, the reaction was performed in two different solvents. While the solution of gold(I) was prepared in deuterated chloroform, the solution of silver perchlorate was prepared in dry THF. Then, the solution of silver(I) was added to the solution of gold(I). The silver solution was protected from light because of the sensitivity of silver(I) salts. The silver solution was added to the gold solution and the mixture was protected from light by covering the reaction vessel with black cover and stirred. A white precipitate of silver chloride was formed immediately. Then the mixture was filtered on glass microfiber filter into an NMR tube placed in an NMR Schlenk. ^{31}P NMR was done to check the presence of the intermediate. The peak shifted from 33 ppm (which was the peak for the starting material that is Ph_3PAuCl) to between 27 and 29 ppm depending on the concentration. Thereafter, solutions of the ligand were prepared and added directly to the NMR tube using Schlenk conditions in order to prevent air oxidation of the analyte. In order to prove that the filtration of the AgCl precipitate does not affect

the reaction, we ran the ^{31}P NMR of the mixture before and after filtration. The shift was the same in both cases (28.3 ppm). Therefore, the solution was filtered for all the reactions presented to obtain the cleanest solutions as much as possible.

II.5. Reactivity of Gold(I) with Triphenylphosphine

Gold(I) usually coordinates with two ligands to give a linear structure but sometimes undergo advance in coordination numbers. Studies of some ligands such as PEt_3, $P(C_6H_4Me\text{-}p)_3$, $P(C_6H_{11})_3$ and PPh_3 with two, three and four coordinate fashion has been reported.[260,261] In addition, X-ray data of the solid state structure of some complexes such as the three co-ordinate $[(PPh_3)_2AuX]$ (X = C1 or I) and four-co-ordinate $[Au(PPh_3)_3\text{-}(SnCl_3)]$ has been established.[262] However, ^{31}P NMR study of tertiary phosphine complexes of gold(I) revealed that the maximum coordination number depends on the type of the ligand and the steric and electronic properties of the ligand.[258] For proper understanding of the ligation of phosphorous ligands on cationic gold(I) species, the reactivity of gold(I) in complexation reaction was studied. On many occasions, a peak around 44 ppm was observed by ^{31}P NMR for the reaction of complexation and has been proven to be a peak for the bis[triphenylphosphinegold(I)], $[Au(PPh_3)_2]^+$.[263,264] Therefore, many experiments were carried out to understand and confirmed the possible side products of the complexation reaction as well as the dynamic exchange around gold to identify species and to determine the different structures of gold(I).

II.5.1. Impact of the Sequential Addition on the Shifts

The first experiment was to determine whether free PPh_3 could be observed in solution. To this end, PPh_3 was added until the peak of free PPh_3 could be visible in ^{31}P NMR. The reaction was performed in an NMR tube in dry tetrahydrofuran (THF) A few drops of deuterated chloroform ($CDCl_3$) were added for deuterium lock. THF was used for this reaction because PPh_3 was readily soluble in it. THF was also used in order to

easily compared, the results with the VT-NMR results. The concentration in PPh_3 was modified accordingly to keep the concentration in gold constant in the NMR sample. Practically, the same volume of PPh_3 at the same concentration was added before the tube was concentrated to return to the original concentration in gold between each NMR recorded. The results are summarised in table 2 and were acquired with a minimum of 1 h between each addition

Table 2: Sequential addition of PPh_3

Equiv. of PPh_3 added	δ1 (ppm)	δ2 (ppm)	Ratio
1	44.0	32.6	85:15
2	31.6	24.0	96:4
3	26.4	21.4	2:98
4	27.0	14.0	1:99
5	27.1	7.0	<1:99
6	27.1	6.3	<1:99
7	27.5	2.9	1:99
8	27.5	0.0	<1:99
9	27.6	-0.2	1:99
10	27.8	-0.9	1:99
11	27.8	-1.2	1:99
12	28.4	-1.3	2:98

Broad peak are in red indicating fast exchange of ligands

The first interesting point was that the peak of free PPh_3 was never observed, even after 12 equivalents were added. The ^{31}P NMR spectrum of PPh_3 was recorded in THF and the peak was found at –5.9 ppm. The experiment was stopped after the addition of 12 equivalent because there were only limited changes observed after 8 equivalents. Addition of one equivalent of PPh_3 gave two sharp ^{31}P NMR resonance at 44.0 and 32.6

ppm in the ratio 85:15 .The peak at 44 ppm was confirmed to be that of complex $[Au(PPh_3)_2]^+$. It is important to note that after the addition of the second equivalent, a white precipitate of AgCl was observed. The peak by ^{31}P NMR was broad probably due to partial suspension or to a fast ligand exchange. Then, the suspension was filtered with glass micro fibre filter paper and the supernatant was then collected and ^{31}P NMR of it was recorded but the result was found to be the same. However, the addition of further equivalents were continued once it was established that the precipitate did not interfere with the result. On addition of the third equivalent, two peaks were observed, one sharp minor peak at 26.4 ppm and one broad major peak at 21.4 ppm. Presumably, the broad peak was an indication that $[Au(PPh_3)_2]^+$ undergoes rapid exchange with PPh_3. On further addition of the fourth equivalent, the minor peak shifted downfield to 27.0 ppm while the major peak shifted upfield to 14 ppm. It should be noted that after the addition of a third equivalent and with subsequent addition of further equivalents, two peaks were always observed in approximately ratio 1:99 except for the addition of 12 equivalent, with the one downfield shifted downward progressively as the concentration increases while the upfield peak also shifted progressively upfield. The minimum of shift reached was at –1.3 ppm.

II.5.2. Thermodynamic Aspects: Equilibrium Between the Ligands and Gld(I)

With two equivalents added, the peak at 44 ppm shifted and with five equivalents, the amplitude of the shift started to decrease. This is the reason why the experiment was repeated only with these two and five equivalents but separately. The results were presented in table 3.

Table 3: Addition of 2 and 5 equivalents of PPh_3 separately

Equiv. of PPh_3 added	δ1 (ppm)	δ2 (ppm)	Ratio
2	44.1	25.6	93:7
5	25.7	23.8	5:95

Broad peak

The results obtained were not the same with that previously obtained. The peak at 44 ppm was present with two equivalents and the shifts were different without logical reason for the moment. The results observed in the sequential addition and in the direct addition of two and five equivalents differed. This observation required confirmation to ensure whether the repeatability of the reactions was not at stake. An apparent loss of sensitivity was observed as well as a broad peak at 23.82 ppm between the addition of two equivalent and the addition of five equivalent. The same experiment was therefore repeated but the addition was performed in the same NMR tube (Table 4). Thus, two equivalent wad added first and then three equivalent was added into the same NMR tube and the tube was concentrated until it reached the initial volume.

Table 4: Sequential addition of 2 equivalents followed by 3 equivalents of PPh_3

Equiv. of PPh_3 added	**δ1 (ppm)**	**δ2 (ppm)**	**Ratio**
2	39.9	24.2	97:3
2 + 3	24.3	20.3	3:97

Broad peak

The results were again different, it was impossible to say if there was a problem of reproducibility or if the results depend on the mode of addition (direct or sequential addition). There is one sharp peak and one broad peak, the hypothesis was that the clean peak corresponds to the complex and the other one correspond to an exchange of the free ligand. In addition, the sharp peak stays always at the same shift and the other change with the number of equivalent of PPh_3.

II.5.3. Kinetic Aspects: Dynamic Ligand Exchange in the Complexes

For better results and to reduce the number of scans, the concentration of gold(I) reagent was increased from 0.012 mmol to 0.020 mmol. This change established that the NMR shift is dependent on the concentration of the sample and on the solvent used. This is the reason why it was necessary to ensure that the concentration of gold was the same in each reaction but with different equivalent numbers. First time with the new conditions, the precipitate before filtration was dark purple and not white as previously observed. It was first thought that the colour was due to the increase of the concentration but later found out that it was due to the sensitivity of silver salt to light. The same reaction was repeated with different equivalents of PPh_3 in a mixture of $CDCl_3$ and dry THF and every time a VT-NMR was performed at different temperatures. The main goal was to inhibit the possible ligand exchange that it is not possible to see at 30 °C (30 °C is the temperature of NMR acquisition in normal conditions). At low temperatures, the exchange is much slower and we postulated that the various species could be observed at low temperature without freezing the solvent in which the reaction is performed. The effect of temperature was not investigated by Maier *et al.*[265] We were also interested to see whether it was possible for the gold(I) to coordinate to multiple ligands. The experiment was performed with 1-5 equivalents of PPh_3 added onto Ph_3PAu^+, ClO_4^-, and the results of the study were summarised in Table 5 below. Each VT-NMR experiment was performed during a single session and the addition of PPh_3 was achieved at least 1h before recording the acquisition.

II.5.4. VT-NMR Study

Table 5: VT-NMR study of gold(I) complexation with PPh_3

Equiv. of PPh_3 added	30 °C δ (ppm)	Ratio	δ (ppm)	Ratio	δ2 (ppm)	Ratio	δ (ppm) ^2J (Hz)	Ratio	δ (ppm)	Ratio
	44.7		44.7		44.4		43.9		44.7	
2	36.4	99.0	39.6	98.0	42.2	99.0	43.1		36.7	99.0
	28.1	1.0	28.7	2.0	30.1	1.0	42.2		28.1	1.0
							32.2			
							31.0			
							3.5 (21.6)	50.0		
							1.6 (21.5)	50.0		
3	29.7	60.2	31.0	92.0	34.1	89.2	34.1		29.2	97.1
	28.2	39.8	28.8	8.0	30.2	3.6	31.1		28.2	2.9
					3.5	3.6	5.5 (18.0)	22.4		
					1.6	3.6	4.0 (17.0)	22.4		
							3.5 (21.7)	27.6		
							1.7 (21.6)	27.6		
4	28.1	1.5	28.8	1.5	30.2	2.2	31.1		28.1	1.4
	18.2	43.2	17.6	98.5	18.9	97.8	17.6		18.0	98.6
	17.5	55.3					5.5 (17.1)	35.7		
							4.0 (17.2)	35.1		
							3.5 (21.9)	14.3		
							1.7 (21.6)	14.9		
5	28.0	1.0	28.6	0.9	29.8	1.3	30.7		28.0	0.8
	20.1	99.0	20.2	99.1	21.0	91.7	18.7		20.3	99.2
					5.6	3.3	5.4 (17.5)	50.8		
					4.1	3.7	3.9 (17.2)	49.2		

Sharp peak Broad peak doublet

On addition of one equivalent, which indicated that there are two ligands in solution (that is, one from singly complexed cationic gold and the added PPh_3), there is no change in the spectrum. There was only one sharp peak at around 44 ppm regardless of the temperature. This result seems reasonable and indicated that there is no exchange between singly complexed cationic gold and a gold with two ligands. This result validated the experimental method. On the addition of two equivalent of PPh_3 , the peak around 44.0 ppm disappeared completely while a broad singlet peak appeared at 36.4 ppm with a sharp small singlet peak high field of it at 28.1 ppm (suspected to be a peak for Ph_3PO) in the ratio 99:1. Reduction of temperature to 0 ^oC caused the shifting of the broad peak downfield to 39.6 ppm and the sharp singlet peak to 28.7 ppm. (See figure 11) showing the broad peak obtained for different equivalent. Presumably, the broad peak was an indication of multiple gold(I) species in dynamic equilibration. Then, a further decrease

of temperature to -80 ºC brought about the growth of new peaks upfield of the NMR spectrum. Of particular interest were the two sets of doublet peaks at 3.5 ppm and 1.6 ppm.

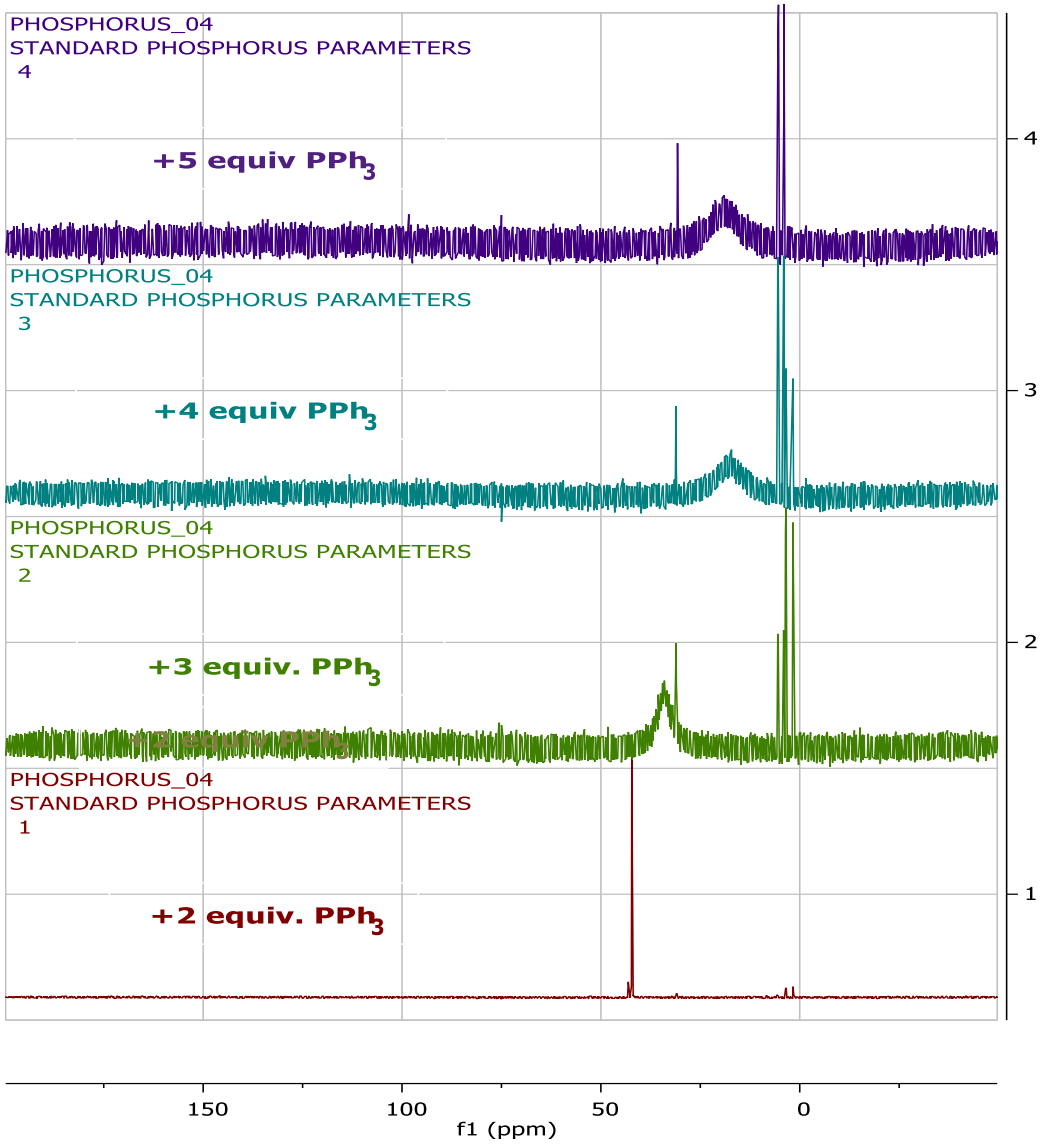

Figure 11: Showing broad peaks with different equivalent, which is an indication of fast ligand exchange between Ph3PAu+ and PPh3 in solution

Addition of three equivalent resulted in the diminution of the intensity of the broad peak, which appeared up field at 29.7 ppm with concomitant increase in the intensity of the singlet resonance at 28.2 ppm at room temperature. When the temperature was reduced to 0 ºC, the two peaks shifted downfield with the broad peak moved to 31.0

ppm while the sharp peak appeared at 28.8 ppm at -50 ^{o}C, the broad peak had shifted downfield to 34.1 ppm and the sharp peak appeared at 30.2 ppm. This also resulted in the growth of two new peaks at high field, one at 3.5 ppm and the other one at 1.6 ppm. On further decrease of temperature to -80 ^{o}C, the broad peak remained unchanged in its position but the sharp singlet peak shifted a bit downfield to 31.1 ppm. Then, four new sets of doublet peaks appeared upfield of the spectrum. They were at 5.5, 4.0, 3.5, and 1.7 ppm respectively (See figures 12 and 13 for the new appearance of doublet peaks up field of the spectrum).

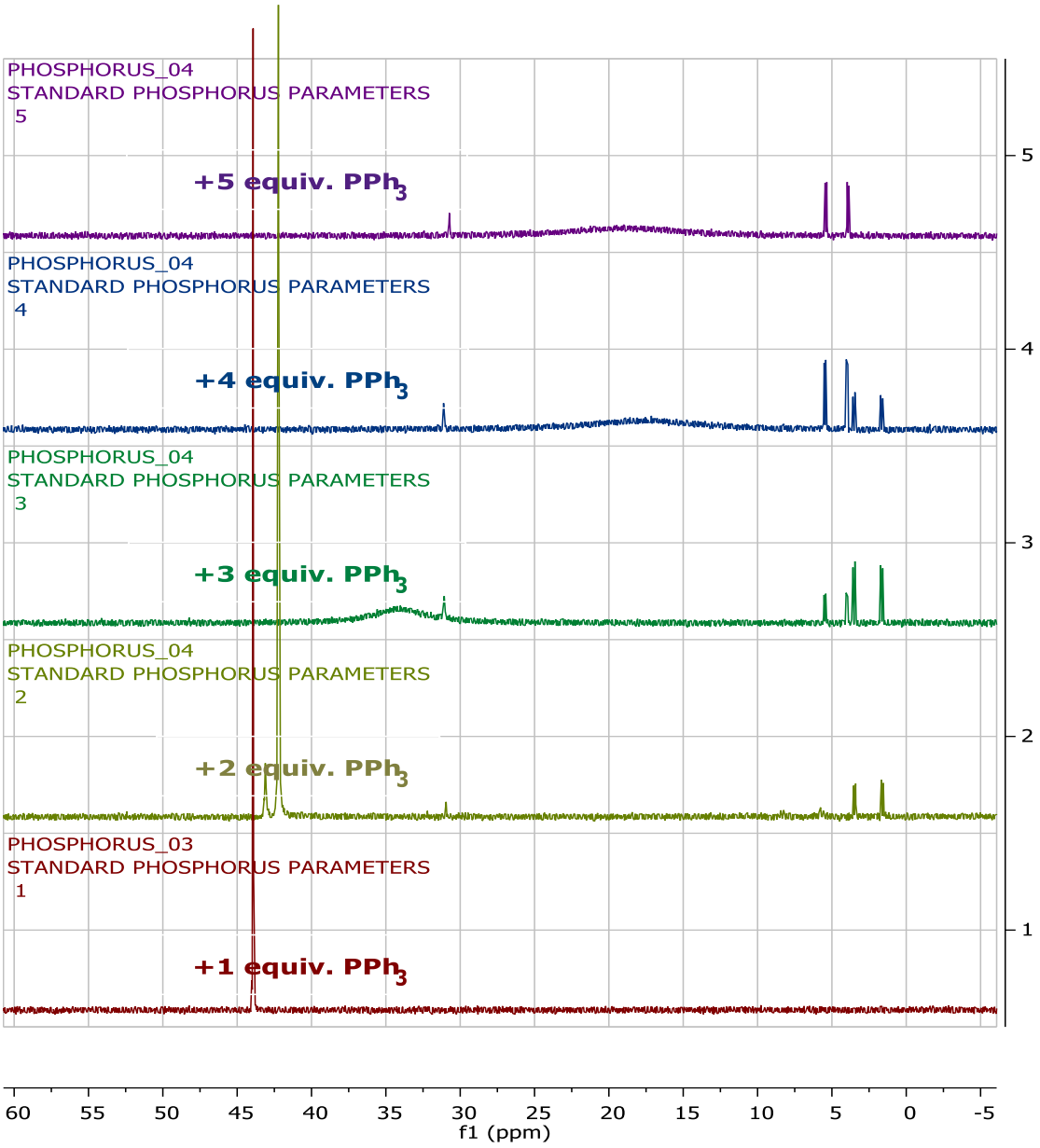

Figure 12: Appearance of new peaks up field bellow 10.0 ppm at -80 ºC

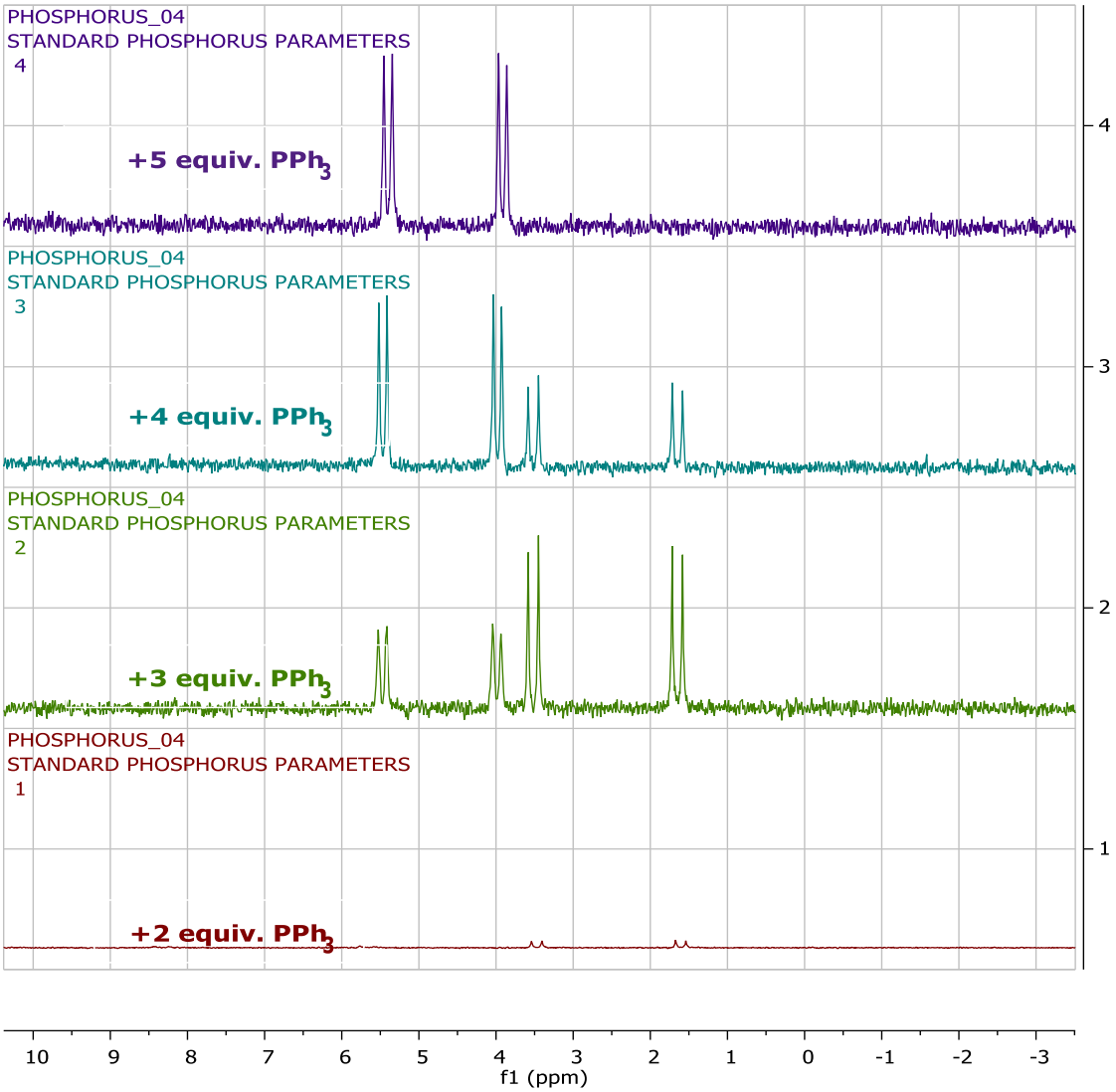

Figure 13: Expansion of doublet peaks emerged below 10.0 ppm in solution at very low temperature of -80 ^{o}C.

The doublets peaks were attributed to a ^{31}P-^{31}P coupling between the phosphorus of the coordinated PPh_3. On addition of four equivalent of PPh_3, the ^{31}P NMR study of the solution at room temperature (that is 30 ^{o}C) showed that there was a small sharp peak at 28.1 ppm and two broad peaks at 18.2 ppm and 17.5 ppm. When the temperature was reduced to -80 ^{o}C, the sharp peak had shifted downfield to 31.1 ppm while the broad peak shifted up field to 17.6 ppm with appearance of four new doublet peaks up field of the spectrum. The new peaks were at 5.5 ppm, 4.0 ppm, 3.5 ppm and 1.7 ppm. It was proposed that each doublet corresponds to one phosphorous and then, four doublets were equivalent

to the four maximum coordination number of gold. However, when the ^{31}P NMR of five equivalents was studied at room temperature, it revealed that there was a small sharp peak at 28.0 ppm and one broad peak at 20.1 ppm. When the temperature was reduced to -80 ^{o}C the sharp peak had shifted downfield to 30.7 ppm while the broad peak also shifted up field to 18.7 ppm. Interestingly, two new doublet peaks also emerged upfield of the spectrum at 5.4 ppm and 3.9 ppm. It should be noted that with three or more ligands in solution, there is in general one fine peak and one broad peak regardless of the temperature (even after repeating the experiment). However, addition of three equivalent at 30 ^{o}C was one of the exception. The peak at 28.2 ppm was broad peak containing a sharp peak. The second exception was the addition of four equivalent, at 30 °C; both peaks at 18.2 and 17.5 ppm were broad and much closed to each other. It should be noted that as the concentration of PPh_3 increases in the solution, the chemical shift tend to shift from downfield to up field of the spectrum irrespective of the temperature. In addition, 31P NMR exhibit increasingly larger differences in chemical shifts when the temperature decreases from 30 ^{o}C to -80 ^{o}C. However, when the temperature was increased back to the initial temperature, (that is room temperature of 30 ^{o}C) the spectrum was similar to the initial one at 30 °C. This result proved that there was no modification or degradation during the VT-NMR, and that the thermodynamic equilibrium was reached when the spectrum was initially recorded. The temperature dependence can be elucidated by hindered rotation around the Au-PPh_3 bond, which may be too fast to observe at room temperature. Following the same reasoning with the previous sequential addition of PPh_3. The peak of free PPh_3 was never appeared. Also, it is possible for the gold(I) to coordinate to multiple ligands and the shift of the complex decrease with the number of ligand. The shift of the complex could be the broad peak. Thus, possible structures of gold were described in Figure 14.

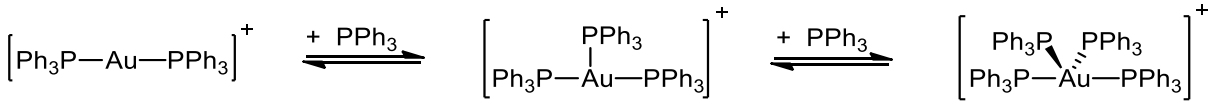

Figure 14: Putative equilibria of gold(I) complex with PPh_3

It is evident that phosphines were non-equivalent in cationic gold complexes under investigation due to the ^{31}P-^{31}P 2J couplings observed at low temperature. The coupling cannot be tetravalent gold with four P as would be triplet instead. In addition, it cannot be silver or ^{13}C-^{31}P because of the natural abundance of isotopes. It cannot be 2D-^{31}P coupling because of splitting. Gold is a quadrupolar nucleus therefore, it would not couple with P. It has been reported that zero quadrupole splitting of $[Au(PPh_3)_4]ClO_4$ substantiates its tetrahedral four coordinate for the cation.[266] Distorted gold(I) or C-H insertion was also suggested.

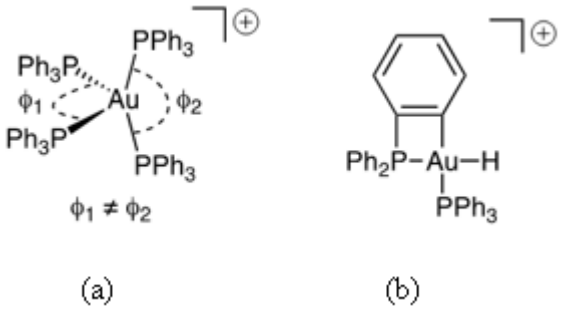

Figure 15: Showing hypothetical structure of (a) distorted tetrahedral Au(I) and (b) C-H insertion

Elder et al (1981)[89] reported that there was no problem for methyldiphenylphosphine to attain tetrahedral coordination in the solid state but this was not possible for a larger triphenylphosphine due to steric factors which force P-Au bond to be elongated. If it were tetrahedral, ϕ_1 would be equal to ϕ_2. Then, only one signal should be observed but more than one signal was observed, which implies that it is not tetrahedral at low temperature. It was proposed that it is most likely to be hydrogen insertion.

II.5.5. Importance of Perchlorate

The perchlorate ion is negatively charged. It consists of one chlorine atom and four oxygen atoms. It is usually weakly coordinated and can be replaced by a good and useful functionality. It can play the role of anionic terminal ligands or act as an anionic moiety for the stabilisation of coordination geometry and resulting structure. It is usually present in applications where energetic oxidant is required. Some compounds containing perchlorate include: oxidants in airbags, flares, fireworks etc. Ammonium perchlorate is among the most important oxidizers in industries.[267,268]

II.5.6. Validation of Findings

In an attempt to validate our findings, the complexation reaction was completed with triphenylphosphine oxide ($OPPh_3$) to see whether one of the species observed in our test is due to the oxidation of PPh_3 in air or by residual gold(III). The results of the ^{31}P NMR were summarised in table 6.

Table 6: ^{31}P NMR of addition of $OPPh_3$

Equivalent of $OPPh_3$ added	δ1 (ppm)	δ2 (ppm)	δ3 (ppm)	Ratio
1	41.6	27.2	27.0	53.5 : 5.9 : 40.6
2	37.3	27.3		71.9 : 28.1

Sharp peak Broad peak

A broad and a sharp peak were again observed. These values were not observed in our experiments with PPh_3, which suggests that $OPPh_3$ did not previously complex with gold via the oxygen and that the reaction with PPh_3 was clean. The hypothetical structures to explain the values from Table 6 were shown in figure 16.

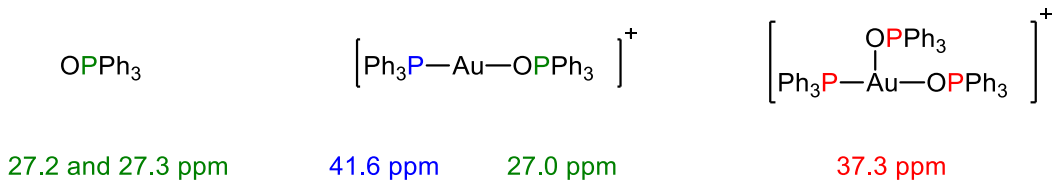

Figure 16: Possible structures for the complexation of $OPPh_3$ with gold(I)

First, the peak of free $OPPh_3$ appeared at 28.9 ppm in $CDCl_3$. In the Table 6, in both cases, there was a sharp peak at 27.2 ppm. This peak could be attributed to the $OPPh_3$. Then, the sharp peak at 41.6 ppm which corresponds to the peak of $[Au(PPh_3)_2]^+$. Thus, this peak could be the phosphorus from complexed PPh_3. In addition, this value is different because the second ligand is an $OPPh_3$ and not a PPh_3. The reason, which support this hypothesis was that the peak was sharp and PPh_3 is a stable ligand because there is no peak of free PPh_3. The broad peak at 37.3 ppm represents an average of the three phosphorus with a fast ligand exchange. Furthermore, the ratios could confirm these hypotheses. With one $OPPh_3$ in solution is approximatively 1:1 for one phosphorus from complexed PPh_3 and another one from $OPPh_3$ for one gold(I). The ratio with two $OPPh_3$ in solution is approximatively 3:1 for two phosphorus from $OPPh_3$ and one from complexed PPh_3 for one gold(I). PPh_3 was chosen as L-ligand for VT- NMR study instead of $OPPh_3$ because $OPPh_3$ is less stable as was revealed by NMR spectroscopy with a broad signal. ^{31}P NMR spectroscopy of the PPh_3 was completed and seems to be contaminated by $OPPh_3$. Furthermore, the ratio between PPh_3 and $OPPh_3$ was 99:1 and very close to the ratio obtained during all the experiments. Furthermore, complexation with tricyclohexylphosphine $P(Cy)_3$ was also carried out to establish these findings. The results were as stated in the table 7 below.

Table 7: ^{31}P NMR of addition of $P(Cy)_3$

Equiv. of $P(Cy)_3$ added	30 °C δ (ppm)	Ratio	-80 °C δ (ppm) ^2J (Hz)	Ratio	Back to 30 °C δ (ppm)	Ratio
1	10.31	98.0	9.61	96.3	10.31	98.0
	-5.95	2.0	-8.86	3.7	-5.95	2.0
2	9.84	99.1	8.51	96.8	9.84	99.1
	-5.95	0.9	-8.62	3.2	-5.95	0.9
3	10.8	99.3	8.27	95.4	10.08	99.3
	-6.18	0.7	-9.09	4.6	-6.18	0.7
5	9.61	99.8	8.27	96.6	9.61	99.8
	-6.58	0.2	-9.09	3.4	-6.58	0.2

Major peak bellow 20ppm minor peak bellow 20ppm

It should be noted that two peaks were observed in all cases irrespective of the concentration and the temperature. These peaks were for the [Au $\{P(Cy)_3\}$]$^+$ and free phosphine in tandem with the literature.[258] ^{31}PNMR study of additional phosphine in solution revealed that the maximum coordination of $P(Cy)_3$ was 2.[266]

II.5.6.1. More Validation Studies

Addition of 5 equivalents of water had no immediate impact on the shift of PPh_3Au^+ and $(PPh_3)_2Au^+$, but a black residue were deposited on the wall of the NMR tube after 24 hours. Two peaks were observed at 44.9 and 27.7 ppm with a ratio 17: 83. A mixture of THF (mp = -108.4 °C) and $CDCl_3$ (mp = -64 °C) in ratio 1:1 was initially used to lower the freezing point of chloroform. CH_2Cl_2 has a melting point (mp) at -96.7 ˚C and was therefore also attempted for VT-NMR. The reaction did not proceed under the usual experimental conditions (where both solutions of gold and silver were prepared separately). The conditions were therefore modified and the reagents were added directly to a flask as solids and CH_2Cl_2 was subsequently added. The ^{31}P NMR with 1 equivalent of PPh_3 added were similar to the one previously observed in a mixture of THF and $CDCl_3$ with a peak at 44 ppm. The reaction was tried with another salt, sodium tetrafluoroborate

($NaBF_4$) to avoid any potential interference of unreacted silver(I) salts. Reaction in DCM showed a peak between 41 and 37 ppm.

II.6. Synthesis of Acridine Based Gold(I) Complexes

II.6.1. Protocol Optimisation

It should be recalled that one of the objectives of this research work is to synthesise an array of gold(I) complexes with fluorescent X-ligands, while keeping the triphenylphosphine as an L-ligand. The synthetic procedure used was a modification of the method outline by Munakata et al.[269]It involved the addition of gold precursor (Ph_3PAuCl), and another reagent. The reagent used here was silver perchlorate, which play a dual role. The first role was ligand methathesis. That is abstraction of the chloride X-ligand with concomitant formation of active gold species. The second role was to stabilise the cationic product formed by acting as a counter anion. The reaction was carried out under inert atmosphere. The reaction is as stated in scheme 8 below.

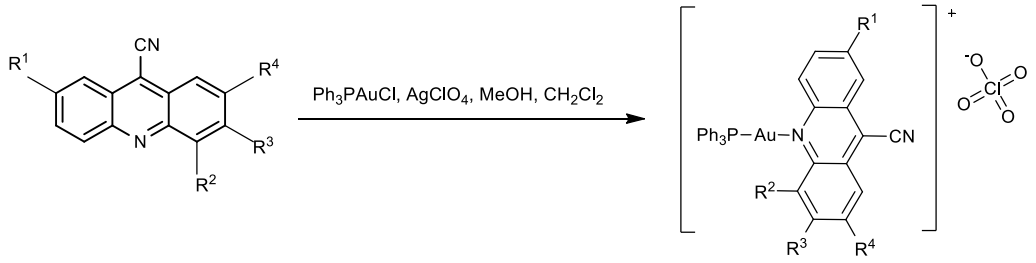

R^1 = F, Cl, Br, I, MeO, SCH_3 R^2, R^3, R^4=H, F, Cl, MeO, NO_2, NH_2

Scheme 8: Synthesis of acridine(triphenylphosphine)gold (I) perchlorate

$AgClO_4$ and Ph_3PAuCl were dissolved in methanol with constant stirring for thirty minutes in the dark (using black felt) because of the sensitivity of silver salt to light. A white precipitate of silver chloride appeared. Then, acridine ligands were added in DCM with vigorous stirring for thirty minutes. The mixture was filtered under nitrogen, with a glass microfiber filter into an NMR tube for analysis. The solvent was concentrated under vacuum and replaced by deuterated chloroform. ^{31}P NMR, and a single peak between 27

and 29 ppm systematically assessed the successful synthesis of the intermediary cationic triphenylphosphinegold(I) perchlorate, depending on the concentration. All complexes were characterised by ^{1}H, ^{13}C and ^{31}P NMR and their positive-ion ESI-MS displayed the $[M]^{+}$ peaks in agreement with the calculated isotopic pattern. The synthesis of these complexes is commonly hampered by long reaction times (two days and more)[269] and so our procedure was optimised to give rapid, facile and reproducible results within one hour.

Table 8: Synthesis of acridine gold(I) complexes based on the scheme 8

Entry	**R^1**	**R^2**	**R^3**	**R^4**	**product**	**Yield (%)**
1	Cl	H	H	H	**41**	70
2	Br	H	H	H	**42**	72
3	Cl	H	OCH_3	H	**43**	68
4	Br	H	OCH_3	H	**44**	66
5	Br	H	F	H	**45**	70
6	Cl	H	Cl	H	**46**	72
7	I	H	H	H	**47**	69
8	Cl	OCH_3	OCH_3	OCH_3	**48**	72
9	I	OCH_3	OCH_3	OCH_3	**49**	75
10	I	H	OCH_3	H	**50**	71
11	Br	OCH_3	OCH_3	OCH_3	**51**	74
12	I	H	OCH_3	OCH_3	**52**	78
13	Cl	H	OCH_3	OCH_3	**53**	78
14	Br	H	OCH_3	OCH_3	**54**	80

Entry	R^1	R^2	R^3	R^4	product	Yield (%)
15	SCH_3	H	OCH_3	H	**55**	78
16	SCH_3	H	F	H	**56**	75
17	SCH_3	OCH_3	OCH_3	OCH_3	**57**	71
18	OCH_3	H	OCH_3	OCH_3	**58**	83
19	SCH_3	H	OCH_3	OCH_3	**59**	72
20	H	H	OCH_3	H	**60**	71
21	H	H	F	H	**61**	74

II.6.2. Analysis of the Yield of the Complexes

Complex **58** gave the highest yield with 83 % followed by complex **54** with 80 %. While complex **44** produced the lowest yield with 66 %. It should be noted that the yield for chloro substituted acridine ligand **41** gave a slightly lower yield (70 %) compares with the bromo substituted acridine ligands **42** (72 %) but greater than iodo substituted acridine ligands **47** (69 %). Chloro substituted ligand without the electron donating group **41** has a higher yield than chloro substituted ligands with a single electron donating group **43** but less than chloro substituted with trimethoxy **48** (72 %) and dimethoxy **53** (78 %) in that order. Bromo acridine ligand without an electron-donating group **42** gave a higher yield (72 %) than than the bromo acridine with a monosubstituted methoxy **44** (66 %) but less than bromo acridine with trimethoxy **51** (74 %) and dimethoxy **54** (80 %**)** in that order. While, iodo acridine without an electron-donating group **47** (69 %) gave a lower yield than iodo acridine ligand with monomethoxy **50**, (71 %), trimethoxy **49** (75 %) and dimethoxy **52** (78 %) in that order. It should be noted that in the three halogen substitution bearing mono, di and tri methoxy, the di methoxy has the highest yield. Interestingly, the

highest yield (83 %) was obtained when we have electron-donating group (methoxy) on both side of the acridine ligand **58.** In a nut shell, good to excellent yield were obtained in all the reactions.

II.6.2.1. ^{31}P NMR of the Novel Acridine Gold(I) Complexes

Table 9: ^{31}P NMR data of acridine gold(I) complexes

Entry	Compound	δ (ppm)	Ratio
1	**41**	33.00	
2	**42**	29.96	
3	**43**	31.29	98.8
		49.12	1.2
4	**44**	32.39	
5	**45**	31.29	
6	**46**	31.92	
7	**47**	31.76	
8	**48**	31.29	
9	**49**	31.53	
10	**50**	33.10	
11	**51**	31.76	
12	**52**	31.50	
13	**53**	30.82	97.7
		45.04	2.3
14	**54**	31.06	99.7
		75.21	0.3
15	**55**	30.00	
16	**56**	32.86	
17	**57**	30.58	
18	**58**	32.08	
19	**59**	32.39	
20	**60**	30.11	98.2
		44.57	1.8
21	**61**	29.72	

Sharp major peak sharp minor peak

The ^{31}P NMR spectra of the complexes **41** to **61** were measured at room temperature in deuterated chloroform. They all showed only one sharp resonance except for **43**, **53, 54** and **60** as shown in the table 9. The major sharp peak in all the novel complexed synthesised ranges from δ 29.72 to 33.00 (Table 9). These chemical shifts were in the region usually observed for the triphenylphosphine ligands coordinated to gold(I).[270–272]

This is also in the same region with the PPh_3 coordinated to silver(I) complexes.[273] The minor peak showed by complex **43**, **53** and **60** were proposed to be $[Au(PPh_3)_2]^+$. It should be noted that the minor peaks were less than 2.5 % in all cases of where they appeared. In addition, the absence of broad peak in the entire spectrum suggested that the ligand exchange did not show at the room temperature. Thus, a single major sharp peak suggests that the dissociation equilibrium of the PPh_3 ligands takes place very rapidly in the NMR time scale.

II.7. Synthesis of Novel Pyrazole based Gold(I) Complexes[274]

II.7.1 Rational for the Synthesis

In our search for dual action orthogonal drug and based on our previous observations of the reactivity of gold amide complexes on cancer cells,[79] we decided to investigate a different class of amide ligands that is known to be active against cancer cells, yet with a different pathway to that of gold(I) alone, to further the applicability of anticancer drug candidates based on a gold-nitrogen bond. We investigated the design flexibility provided by anti-cancer agents based on gold(I) and found that gold with an amide linkage exhibit substantial activity against mammalian breast cancer cells.[79] This discovery on the nature of the linkage to gold to retain substantial anti-cancer activity regardless of the structure of the ligands is crucial to outsmart cancer resistance and improve potency. Ligand design has since been focused on features that are complementing the gold apoptotic pathways against cancerous cells. The choice of the substitution pattern was based on previous observations whereby substitution at the 4-position (scheme 1) seemed to stabilise binding to p53-Y220C through London interactions in a lipophilic pocket.[275] A closer look at the X-ray diffraction of the protein shows further possible interactions, notably Debye and Keesom dipolar interactions with the carbonyl at P153 and P152. We decided to include a range of substitutive functional

groups (pyridine, bromo-phenyl, nitrile and bromine) to verify any impacts of such interactions on the activity of our complexes.

II.7.2. Synthesis of the Complexes

The complexation of pyrazole ligands (entry 1-5) to form an array of pyrazole gold(I) complexes **62-66** (Scheme 9, Table 10) were herein reported.

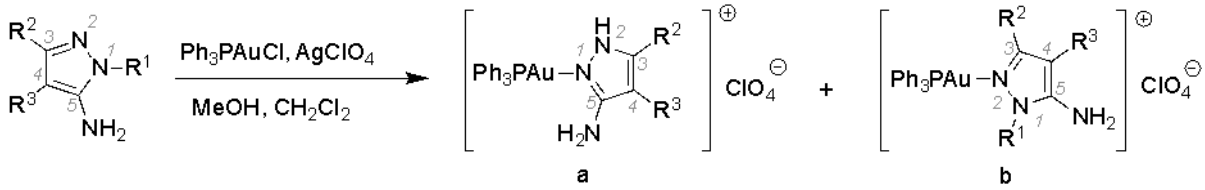

Scheme 9: Regioselective synthesis of pyrazole triphenylphosphinegold(I) perchlorates **62-66.**

The synthesis of these complexes were carried out following a modification of the procedure used by Munakata *et al*[269] as described earlier. The successful synthesis of the intermediary cationic triphenylphosphinegold perchlorate was systematically assessed by ^{31}P NMR, and a single peak between 27 and 29 ppm, depending on the concentration, was observed. All complexes were characterised by ^{1}H, ^{13}C and ^{31}P NMR and their positive-ion ESI-MS displayed the $[M]^+$ peaks in agreement with the calculated isotopic pattern. Minor partial disproportionation to homoleptic complexes and to $[Au(PPh_3)_2]^+$ was observed for complex **62** (less than 0.1%) and for complex **65** (5%). The results are collated in table 10

Table 10: Synthesis of gold(I) pyrazole complexes.

Entry	R^1	R^2	R^3	Complex	Yield
1	H	H	Py	**62**	83%
2	H	H	Br-Ph	**63a**	94%
3	H	Methyl	Br-Ph	**64a**	88%
4	C_2H_4OH	H	CN	**65b**	95%
5	Methyl	H	Br	**66b**	87%

II.7.2.1 ^{31}P NMR of the Novel Pyrazole Gold(I) Complexes

The ^{31}P NMR spectra of the novel pyrazole gold(I) complexes **62-66** were measured at room temperature in deuterated chloroform. While complexes **63**, **64** and **66** gave only one sharp peak at δ 31.00, 31.50 and 30.00 respectively (see table 11). Complex **62** gave an intense sharp peak at δ 30.00 and a small sharp peak at δ 45.04 in the ratio 99.9: 0.1. Then complex **65** gave three sharp resonances at δ 29.70, 44.80 and 75.05 in the ratio 91.9:4.4:3.7. It should be noted that the small sharp peaks observed at δ 45.04 for complex **62** and the small sharp peak observed for **65** at δ 44.80 were attributed to the ^{31}P chemical shift of the coordinated $[Au(PPh_3)_2]^+$. While the peak at δ 75.05 is due to ligand exchange.

Table 11: ^{31}P NMR of novel pyrazole gold(I) complexes synthesised

Entry	Compound	δ (ppm)	Ratio
1	**62**	30.00	99.9
		45.04	0.1
2	**63**	31.00	
3	**64**	31.50	
4	**65**	29.70	91.9
		44.80	4.4
		75.05	3.7
5	**66**	30.00	

Major sharp peak Minor sharp peak

II.8. Synthesis of Silver(I) Complexes

II.8.1 Synthesis of Acridine Silver(I) complexes

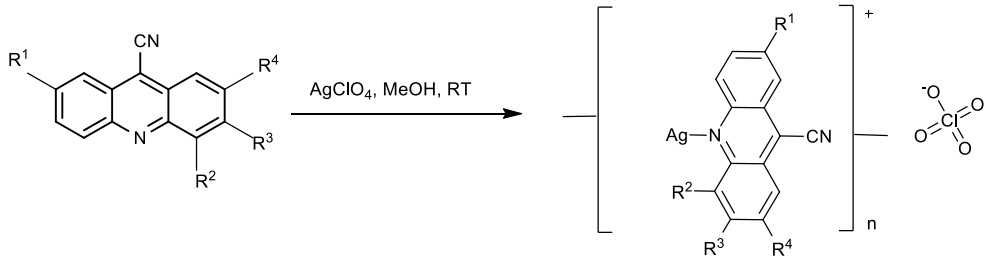

Scheme 10: Reaction conditions for the synthesis of acridine silver(I) perchlorates **67-71.**

$AgClO_4$ was dissolved in methanol and solution of acridine in CH_2Cl_2 was added with constant stirring for thirty minutes under black protection because of the sensitivity of silver salt to light. The mixture was filtered under nitrogen, with a glass microfiber filter into an NMR tube. CH_2Cl_2 was removed under reduced pressure. Then deuterated chloroform was added for the NMR analysis. The yield obtained are shown in the table 12 below. All silver complexes were characterised by ^{1}H, ^{13}C and IR and their positive-ion ESI-MS displayed the $[M]^+$ peaks in agreement with the calculated isotopic pattern. However, only one acridine ligand was expected to coordinate with silver(I) through the

nitrogen atom considering the fact that an equimolar quantity of silver perchlorate and acridine solution were used in the reaction but silver(I) formed bis-cordinate complex with acridine as revealed by the x-ray of complexes **70** and **71**.

Table 12: Acridine silver(I) perchlorate synthesised from scheme 10

Entry	R^1	R^2	R^3	R^4	product	Yield (%)
1	Cl	H	H	H	**67**	78
2	Br	H	H	H	**68**	75
3	Cl	H	OCH_3	H	**69**	72
4	Cl	OCH_3	OCH_3	OCH_3	**70**	86
5	Br	OCH_3	OCH_3	OCH_3	**71**	83

II.8.2. Synthesis of pyrazole based silver(I) complexes

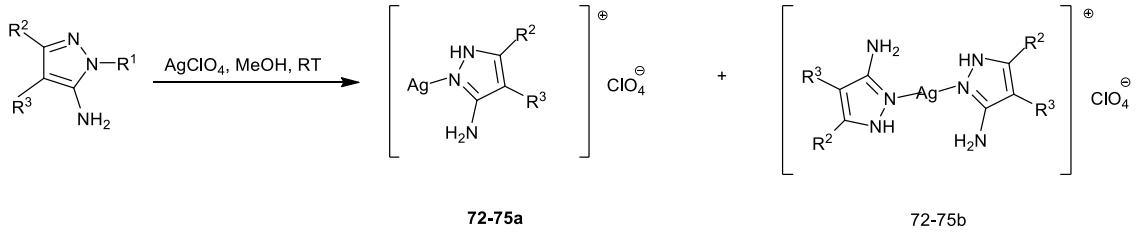

Scheme 11: Reaction conditions for the synthesis of pyrazole silver(I) perchlorates **72a-75b.**

$AgClO_4$ was dissolved in methanol and solution of pyrazole was prepared in CH_2Cl_2 and then added to the solution of silver previously prepared. The mixture was stirred for thirty minutes under black protection because of the sensitivity of silver salt to light. Then, the mixture was filtered under nitrogen, with a glass microfiber filter into an NMR tube. The solvent were vacuum off under reduced pressure. Then deuterated chlroform was added for the NMR analysis. Table 13 below shows the product obtained. All the complexes were characterised by ^1H, ^{13}C and IR and their positive-ion ESI-MS displayed the $[M]^+$ peaks in agreement with the calculated isotopic pattern.

Table 13: Pyrazole silver(I) perchlorate synthesise from scheme 11

Entry	R^1	R^2	R^3	Complex	Yield (%)
1	H	H	Py	**72a**	88
2	H	H	Br-Ph	**73b**	93
3	H	Methyl	Br-Ph	**74b**	91
4	Methyl	H	Br	**75b**	90

II.9. X-Ray Cystallography

II.9.1. X-Ray of Acridine gold(I) Complexes

Single crystals of the complexes**: 41,42,45,46,47,48,49,50,51,53,55,56,57** and **58** were grown by slow diffusion of $CDCl_3$ or CH_2Cl_2 1:1 n-Hexane. The main results of the crystal structure determinations and list of some selected bond lengths and angles are reported in Tables 14 -21. Figures 18 and 19 shows the structures in ORTEP format with the selected numbering scheme. Selected crystalline specimens of the complexes: **41, 42, 45, 46, 47, 48, 49, 50, 51, 53, 55, 56, 57** and **58** were mounted on Mitegen loops and centered on the goniometer head of a Rigaku Oxford Diffraction Gemini E diffractometer equipped with an EOS CCD area detector, data collection was performed at 173 K. Complexes **44** and **49** were collected with monochromated MoKα radiation, by means of ω-scans, all other complexes were collected with monochromated CuKα radiation. The diffraction intensities were corrected with respect to Lorentz and polarization effects. Empirical multi-scan absorption corrections, using equivalent reflections, were also performed with the scaling algorithm SCALE3 ABSPACK. Raw data collection, data reduction and refinalization were carried out with the CrysAlisPro software. All complexes were solved by means of the intrinsic phasing method in SHELXT[276] and

refined by full-matrix least squares methods based on F_o^2 with SHELXL[277] in the framework of the OLEX2[278] software. In the last cycles of refinement all non-hydrogen atoms were refined anisotropically; hydrogen atoms were placed and refined as riding atoms with their isotropic displacement parameters set to 1.2 times the U_{eq} of the parent atom. In all cases the gold centre is coordinated to P and N with expected Au-P (2.2- 2.4 Å) and Au-N (2.0-2.2 Å) distances.[279,280,281] See figure 17 below.

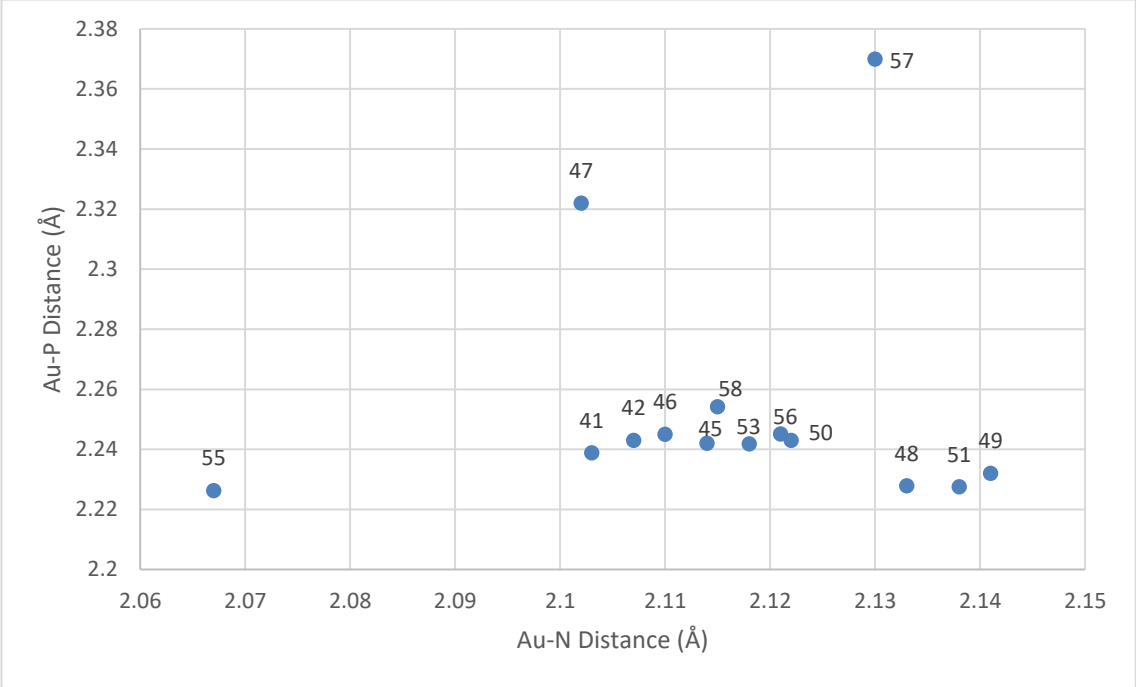

Figure 17: Comparative graph between distances around the gold(I) centre.

The solvent perchlorate molecule from the reaction steps and chloroform molecule used in growing the crystals were included in the crystal lattice of the complexes: **41, 42, 45, 46** and **48** but did not show any interaction with the complexes. While Perchlorate and dichloromethane used in growing the crystals were included in the crystal lattice of the complexes **56** and **57**.Whereas, only perchlorate molecule were included in the crystal lattice of the complexes **47, 48, 50, 51, 53, 55** and **58** Meanwhile, complex **49** is the only regioisomer in all the complexes as shown by their x-ray analysis. ^{31}P NMR indicated a

single point of attachment to gold (I) due to the presence of only one major peak in each case.

Table 14: Crystal Data for complexes **41, 42, 45** and **46**

Compound	**41**	**42**	**45**	**46**
Empirical formula	$C_{32}H_{22}N_2ClPAu$, ClO_4, $CHCl_3$	$C_{32}H_{22}N_2PBrAu$, ClO_4, $CHCl_3$	$C_{32}H_{21}N_2FPBrAu$, ClO_4, $CHCl_3$	$C_{32}H_{21}N_2PCl_2Au$, ClO_4, $CHCl_3$
Formula weight	916.72	961.18	979.17	951.16
Temperature/K	173.0(1)	173.0(1)	173.0(1)	173.0(1)
Crystal system	Triclinic	Triclinic	Triclinic	Triclinic
Space group	P-1	P-1	P-1	P-1
a/Å	9.6910(4)	9.8586(4)	9.8356(12)	9.6949(9)
b/Å	12.7037(5)	12.6661(5)	12.9246(11)	13.25819)
c/Å	14.3404(5)	14.3922(5)	14.0878(13)	14.1094(10)
α/°	79.393(3)	79.316(3)	80.059(8)	81.745(6)
β/°	72.537(3)	72.083(4)	72.326(9)	71.422(8)
γ/°	79.981(3)	79.646(4)	81.182(8)	82.452(7)
Volume/$Å^3$	1642.00(11)	1665.82(12)	1671.0(3)	1694.1(2)
Z	2	2	2	2
$\rho_{calc}/Mg/m^{-3}$	1.854	1.916	1.946	1.865
μ/mm^{-1}	4.977	13.457	13.475	4.904
F(000)	892.0	928.0	944.0	924.0
Crystal size/mm	0.20x0.20x0.15	0.22x0.18x0.15	0.12x0.08x0.06	0.32x0.11x0.08
Reflections collected	15382	18375	8378	21396

Compound	**41**	**42**	**45**	**46**
Data/restraints/ parameters	6661/0/415	6321/0/415	5801/497/424	7349/449/424
Goodness-of-fit[a] on F^2	1.064	1.037	1.110	1.032
Final R indexes [I>2σ(I)]	R_1[b] = 0.0362, wR_2[c] = 0.0755	R_1[b] = 0.0336, wR_2[c] = 0.0854	R_1[b] = 0.0806, wR_2[c] = 0.2224	R_1[b] = 0.0579, wR_2[c] = 0.1163
Largest diff. peak/hole/e $Å^{-3}$	1.21/-1.01	1.58/-1.13	2.57/-1.69	3.00/-2.74

[a] Goodness-of-fit = $[\Sigma(w(F_o^2 - F_c^2)^2]/(N_{obsevns} - N_{params})]^{1/2}$, based on all data.

[b] $R_1 = \Sigma(|F_o| - |F_c|)/\Sigma(|F_o|$, [c] $wR_2 = [\Sigma[w(F_o^2 - F_c^2)^2]/\Sigma[w(F_o^2)^2]]^{1/2}$.

Table 15: Selected bond lengths (Å) and angles (°) for complexes **41, 42, 45** and **46**

	41	**42**	**45**	**46**
Au – P	2.2388(12)	2.2430(10)	2.242(4)	2.245(2)
Au – N1	2.103(4)	2.107(4)	2.114(14)	2.110(6)
N1 – C1	1.356(6)	1.366(6)	1.38(2)	1.374(10)
N1 – C13	1.351(6)	1.356(6)	1.36(2)	1.361(9)
P – C31	1.818(5)	1.820(5)	1.810(19)	1.827(8)
P – C41	1.803(5)	1.809(4)	1.795(18)	1.812(8)
P – C51	1.808(5)	1.817(5)	1.798(19)	1.823(8)
N1 – Au – P	172.66(12)	176.16(11)	171.8(5)	174.71(17)
Au – N1 – C1	121.2(3)	117.3(3)	120.0(11)	118.9(5)
Au – N1 – C13	117.6(3)	121.6(3)	117.5(11)	121.1(5)
C1 – N1 – C13	121.0(4)3	120.7(4)	122.2(14)	119.9(6)
Au – P – C31	109.39(16)	109.74(16)	115.9(5)	114.8(3)
Au – P – C41	111.29(15)	111.26(14)	111.7(6)	110.8(3)
Au – P – C51	116.14(14)	116.8(15)	109.3(6)	112.0(2)
C31 – P – C41	104.9(2)	105.4(2)	106.9(8)	106.4(3)
C41 – P – C51	107.7(2)	107.1(2)	104.9(8)	104.9(4)
C31 – P – C51	106.8(2)	106.6(2)	107.5(9)	107.3(4)

Table 16: Crystal Data for complexes **47, 48, 49,** and **50**

Compound	**47**	**48**	**49**	**50**
Empirical formula	$C_{32}H_{22}N_2PIAu, ClO_4$	$C_{35}H_{28}N_2O_3PClAu, ClO_4$	$C_{35}H_{28}N_2O_3PIAu, ClO_4, CHCl_3$	$C_{33}H_{24}N_2OPIAu, ClO_4$
Formula weight	888.84	887.43	1098.25	918.83
Temperature/K	173.0(1)	173.0(1)	173.0(1)	100.0(1)
Crystal system	Monoclinic	Monoclinic	Triclinic	Triclinic
Space group	P2/n	$P2_1/c$	P-1	P-1
a/Å	17.2159(3)	15.5071(4)	12.0780(8)	8.9239(8)
b/Å	10.0287(1)	10.9932(3)	18.1594(12)	10.1339(9)
c/Å	17.5695(3)	21.3096(6)	18.7739(11)	17.2630(12)
α/°	90	90	77.914(5)	88.576(7)
β/°	96.448(1)	104.334(3)	87.941(5)	80.748(7)
γ/°	90	90	71.754(6)	88.500(7)
Volume/$Å^3$	3014.2(1)	3519.6(2)	3822.0(4)	1540.0(2)
Z	4	4	4	2
$\rho_{calc}/Mg/m^{-3}$	1.9595	1.675	1.909	1.981
μ/mm^{-1}	18.867	10.103	16.972	18.515
F(000)	1696.0	1744.0	2120.0	880.0
Crystal size/mm	0.32x0.09x0.02	0.23x0.20x0.18	0.08x0.03x0.02	0.09x0.046x0.046
Reflections collected	13536	12596	20633	12526
Independent reflections/R(int)	5717/0.0286	6684/0.0270	14159/0.0833	6429/0.0287

Compound	**47**	**48**	**49**	**50**
Data/restraints/parameters	5717/24/380	6684/48/436	14159/798/943	5335/48/398
Goodness-of-fit[a] on F^2	1.075	1.032	0.954	0.886
Final R indexes [I>2σ(I)]	R_1[b] = 0.0437, wR_2[c] = 0.1247	R_1[b] = 0.0377, wR_2[c] = 0.0975	R_1[b] = 0.0833, wR_2[c] = 0.1907	R_1[b] = 0.0638, wR_2[c] = 0.1292
Largest diff. peak/hole/e $Å^{-3}$	2.44/-1.18	0.86/-3.89	5.95/-2.84	2.37/-2.83

[a] Goodness-of-fit = $[\Sigma(w(F_o^2 - F_c^2)^2]/(N_{obsevns} - N_{params})]^{1/2}$, based on all data.

[b] $R_1 = \Sigma(|F_o| - |F_c|)/\Sigma(|F_o|$, [c] $wR_2 = [\Sigma[w(F_o^2 - F_c^2)^2]/\Sigma[w(F_o^2)^2]]^{1/2}$.

Table 17: Selected bond lengths (Å) and angles (°) for complexes **51, 53,55,56,57** and **58.**

	47	**48**	**49**	**50**
Au – P	2.322(18)	2.2279(7)	2.232(4), 2.239(4)	2.243(4)
Au – N1	2.102(6)	2.133(2)	2.141(10), 2.161(10)	2.122(12)
N1 – C1	1.357(9)	1.353(4)	1.338(18), 1.358(18)	1.354(18)
N1 – C13	1.362(9)	1.363(5)	1.367(18), 1.353(18)	1.318(18)
P – C31	1.813(7)	1.813(4)	1.816(17), 1.826(17)	1.832(15)
P – C41	1.821(8)	1.802(4)	1.814(17), 1.792(17)	1.813(14)
P – C51	1.816(7)	1.824(4)	1.814(15), 1.873(18)	1.794(14)
N1 – Au – P	178.98(17)	172.29(8)	171.9(3), 173.8(3)	176.4(4)
Au – N1 – C1	119.9(5)	123.8(2)	121.1(10), 115.4(9)	118.8(10)
Au – N1 – C13	119.5(4)	116.1(2)	115.6(9), 121.3(9)	118.9(10)
C1 – N1 – C13	120.0(6)	119.9(3)	122.7(12), 122.3(11)	122.2(13)
Au – P – C31	112.0(2)	114.36(14)	116.9(6), 116.9(5)	115.0(5)
Au – P – C41	113.1(3)	110.93(10)	110.4(5), 115.3(5)	111.3(5)
Au – P – C51	113.2(2)	111.55(11)	109.5(5), 108.0(5)	110.2(4)
C31 – P – C41	105.4(4)	107.10(17)	107.6(8), 105.9(8)	107.0(6)
C41 – P – C51	106.4(3)	109.24(18)	106.2(8), 105.2(8)	106.0(7)
C31 – P – C51	106.2(3)	103.27(17)	105.6(7), 104.4(8)	106.8(7)

Table 18: Crystal data for complexes **51, 53** and **55**

	51	**53**	**55**
Empirical formula	$C_{35}H_{28}N_2O_3PBrAu$, ClO_4.	$C_{34}H_{26}N_2O_2PClAu$, ClO_4.	$C_{34}H_{27}N_2OPSAu$, ClO_4,
Formula weight	931.89	957.40	839.02
Temperature/K	173.0(1)	100.0(1)	100.0(1)
Crystal system	Orthorhombic	Triclinic	Triclinic
Space group	Pbca	P-1	P-1
a/Å	10.5709(2)	9.3637(3)	9.0096(3)
b/Å	21.2934(3)	10.3983(3)	10.0468(4)
c/Å	30.0455(5)	16.9732(5)	17.3820(5)
α/°	90	107.749(3)	88.295(3)
β/°	90	99.704(3)	80.028(3)
γ/°	90	96.082(3)	87.509(3)
Volume/Å^3	6763.0(2)	1529.49(9)	1547.75(9)
Z	8	2	2
ρ_{calc}/Mg/m^{-3}	1.830	1.862	1.800
μ/mm^{-1}	11.174	11.573	11.233
F(000)	3632.0	840.0	824.0
Crystal size/mm	0.21x0.13x0.05	0.579x0.296x0.05	0.03x0.02x0.005
Reflections collected	15115	15515	14909
Independent reflections/R(int)	6429/0.0287	5361/0.0500	5374/0.0898
Data/restraints/parameters	6429/381/436	5361/0/417	5374/0/409
Goodness-of-fit[a] on F^2	1.049	1.095	1.072
Final R indexes [I>2σ(I)]	R_1[b] = 0.0375, wR_2[c] = 0.0989	R_1[b] = 0.0531, wR_2[c] = 0.1344	R_1[b] = 0.0551, wR_2[c] = 0.1364
Largest diff. peak/hole/e Å^{-3}	2.60/-1.01	3.65/-1.68	2.57/-1.69

[a] Goodness-of-fit = $[\Sigma(w(F_o^2 - F_c^2)^2]/(N_{obsevns} - N_{params})]^{1/2}$, based on all data.

[b] $R_1 = \Sigma(|F_o| - |F_c|)/\Sigma(|F_o|$, [c] $wR_2 = [\Sigma[w(F_o^2 - F_c^2)^2]/\Sigma[w(F_o^2)^2]]^{1/2}$.

Table 19: Selected bond lengths (Å) and angles (°) for complexes **51, 53,** and **55**

	51	**53**	**55**
Au – P	2.2275(11)	2.2418(15)	2.2263(16)
Au – N1	2.138(4)	2.118(5)	2.067(5)
N1 – C1	1.365(6)	1.376(8)	1.382(9)
N1 – C13	1.347(6)	1.339(8)	1.156(9)
P – C31	1.805(5)	1.814(6)	1.808(7)
P – C41	1.811(6)	1.813(6)	1.826(7)
P – C51	1.834(5)	1.810(6)	1.816(6)
N1 – Au – P	171.21(11)	176.06(13)	178.64(14)
Au – N1 – C1	115.3(3)	117.5 (4)	119.5(4)
Au – N1 – C13	124.4(3)	121.4(4)	121.0(4)
C1 – N1 – C13	120.2(4)	120.9(5)	119.4(6)
Au – P – C31	114.66(16)	113.5(2)	112.3(2)
Au – P – C41	112.9(2)	113.14(19)	113.3(2)
Au – P – C51	109.41(15)	109.85(19)	111.3(2)
C31 – P – C41	108.1(2)	104.5(3)	106.8(3)
C41 – P – C51	112.9(2)	107.6(3)	106.5(3)
C31 – P – C51	103.2(2)	107.9(3)	106.2(3)

Table 20: Crystal Data for complexes **56, 57,** and **58**

	56	**57**	**58**
Empirical formula	$C_{33}H_{24}N_2FPSAu$, ClO_4, CH_2Cl_2	$C_{36}H_{31}N_2O_3PSAu$, ClO_4, CH_2Cl_2	$C_{35}H_{29}N_2O_3PAu$, ClO_4
Formula weight	911.91	984.00	852.99
Temperature/K	100.0(1)	100.0(1)	173.0(1)
Crystal system	Monoclinic	Triclinic	Triclinic
Space group	$P2_1/n$	P-1	P-1
a/Å	8.9446(3)	8.4589(2)	9.9443(5)
b/Å	20.3425(6)	12.4577(3)	10.0794(4)
c/Å	18.2243(5)	18.4284(4)	16.7111(8)
α/°	90	80.508(2)	84.071(4)
β/°	97.325(3)	86.565(2)	77.381(4)
γ/°	90	75.184(2)	83.931(4)
Volume/$Å^3$	3288.95(17)	1851.37(8)	1619.81(13)
Z	4	2	2
$\rho_{calc}/Mg/m^{-3}$	1.842	1.765	1.749
μ/mm^{-1}	12.114	10.834	10.206
F(000)	1784.0	972.0	840.0
Crystal size/mm	0.25x0.02x0.015	0.467x0.099x0.05	0.22x0.12x0.03
Reflections collected	27463	38192	10012
Independent reflections/R(int)	5921/0.0661	6462/0.0754	6028/0.0446
Data/restraints/parameters	5921/0/425	6462/0/473	6028/0/427
Goodness-of-fit[a] on F^2	1.047	1.042	1.018

	56	**57**	**58**
Final R indexes [I>2σ(I)]	R_1[b] = 0.0524, wR_2[c] = 0.1394	R_1[b] = 0.0356, wR_2[c] = 0.0828	R_1[b] = 0.0363, wR_2[c] = 0.0884
Largest diff. peak/hole/e Å^{-3}	2.41/-1.76	1.64/-1.11	1.95/-1.18

[a] Goodness-of-fit = $[\Sigma(w(F_o^2 - F_c^2)^2]/(N_{obsevns} - N_{params})]^{1/2}$, based on all data.

[b] $R_1 = \Sigma(|F_o| - |F_c|)/\Sigma(|F_o|$, [c] $wR_2 = [\Sigma[w(F_o^2 - F_c^2)^2]/\Sigma[w(F_o^2)^2]]^{1/2}$.

Table 21: Selected bond lengths (Å) and angles (°) for complexes **56, 57,** and **58**

	56	**57**	**58**
Au – P	2.2451(16)	2.370(11)	2.2542(11)
Au – N1	2.121(6)	2.130(3)	2.115(4)
N1 – C1	1.345(9)	1.361(6)	1.355(6)
N1 – C13	1.350(9)	1.370(5)	1.358(6)
P – C31	1.798(7)	1.809(4)	1.816(6)
P – C41	1.798(7)	1.805(4)	1.810(6)
P – C51	1.822(7)	1.819(5)	1.814(5)
N1 – Au – P	174.34(16)	178.30(10)	176.29(11)
Au – N1 – C1	118.5(4)	123.0(3)	117.9(3)
Au – N1 – C13	119.9(4)	116.6(3)	120.0(3)
C1 – N1 – C13	121.6(6)	120.3(4)	121.6(4)
Au – P – C31	113.9(2)	108.34(15)	113.66(19)
Au – P – C41	114.4(2)	114.49(14)	109.70(17)
Au – P – C51	109.6(2)	113.99(14)	110.97(17)

	56	**57**	**58**
C31 – P – C41	105.7(3)	105.2(2)	106.9(3)
C41 – P – C51	106.5(3)	107.0(2)	108.5(3)
C31 – P – C51	106.1(3)	107.4(2)	106.9(2)

Figures 18 and 19: ORTEP views of complexes **41** as a representative of the complexes with perchlorate and chloroform. **47** as a representative of the complexes with perchlorate only while **56** represent the complexes with perchlorate and dichloromethane in their crystal lattice. In addition complex **48** is shown as the only complex with regioisomer. It also shows the numbering scheme used. Thermal ellipsoids have been drawn at the 40% probability level and hydrogen atoms were included for clarity.

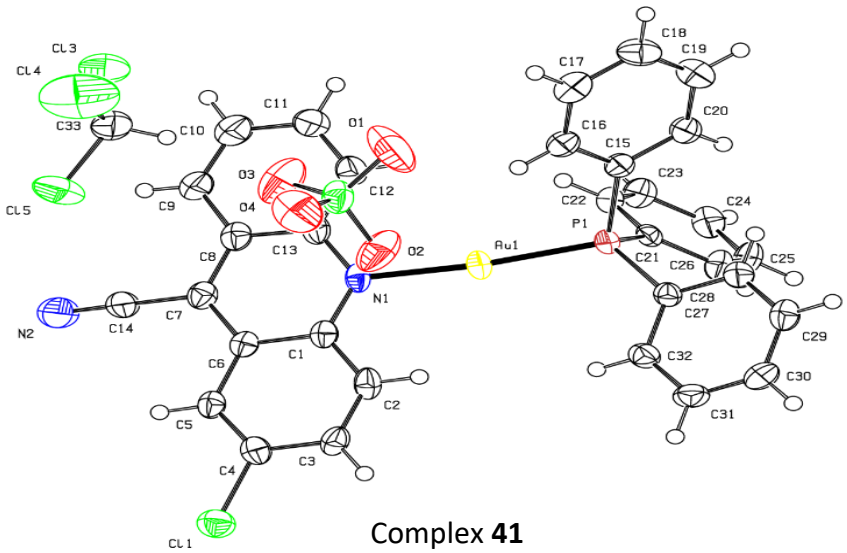

Complex **41**

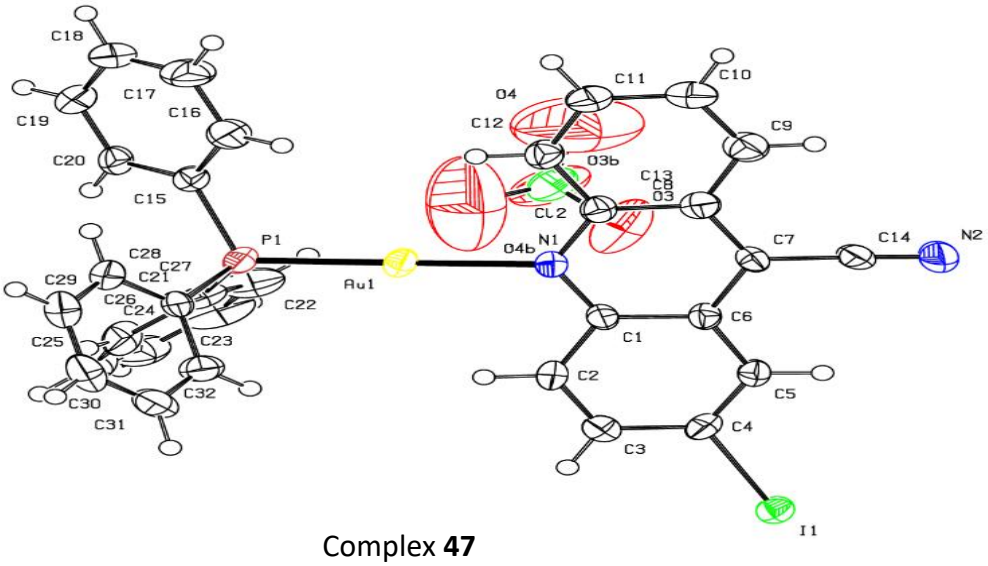

Complex **47**

Figure 18: ORTEP views of complexes **41** and **47**

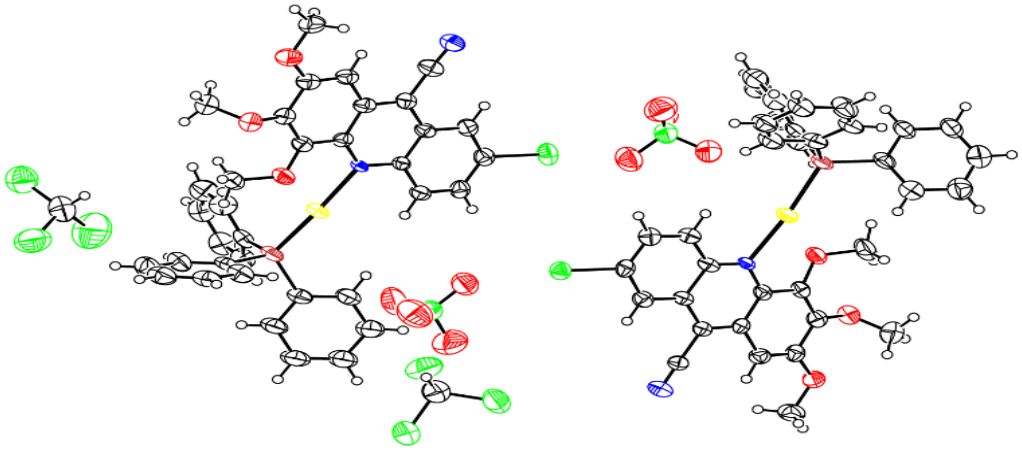

Complex **48**

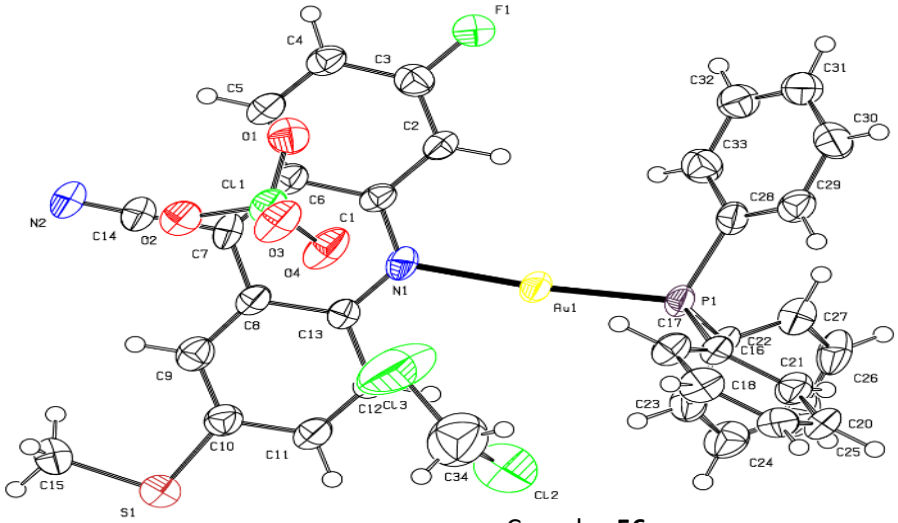

Complex **56**

Figure 19: ORTEP views of complexes **48** and **56**

I.9.2. X-Ray Crystallography of Pyrazole gold(I) Complexes

Suitable crystals for x-ray crystallography of complexes **63-66** were obtained by slow evaporation of dichloromethane and n-hexane in a [1:1] ratio although the crystals for complex **62** were too small for x-ray diffraction. The crystals were characterised by X-ray crystallography to confirm the atom connectivity and molecular geometry. The main results of the crystal structure determinations are reported in Table 22. Table 23 lists some selected bond lengths and angles of the four complexes.

Table 22: Crystal Data for complexes **63a, 64a, 65b** and **66b**

	63a	**64a**	**65b**	**66b**
Empirical formula	$C_{28}H_{25}N_3PBr$ Au, ClO_4	$C_{27}H_{23}N_3PBr$ Au, ClO_4	$C_{24}H_{23}N_4OP$ Au, ClO_4	$C_{22}H_{21}N_3PBr$ Au, ClO_4, CH_2Cl_2
Formula weight	810.80	796.78	710.85	819.64
Temperature/K	100.0(1)	173.0(1)	173.0(1)	173.0(1)
Crystal system	Triclinic	Orthorhombic	Triclinic	Monoclinic
Space group	P-1	Pbcn	P-1	$P2_1/c$
a/Å	12.7645(4)	18.9094(6)	13.2511(11)	13.8129(4)
b/Å	15.6061(5)	16.3880(5)	14.8189(13)	6.9184(2)
c/Å	16.4732(4)	17.9115(5)	15.7353(12)	29.6985(9)
α/°	105.959(2)	90	66.312(8)	90
β/°	93.268(2)	90	74.845(7)	103.268(3)
γ/°	112.402(3)	90	66.970(8)	90
Volume/$Å^3$	2868.22(16)	5550.6(3)	2584.0(4)	2762.33(14)
Z	4	8	4	4

	63a	64a	65b	66b
ρ_{calc}/Mg/m^{-3}	1.878	1.907	1.827	1.971
μ/mm^{-1}	12.982	13.404	12.601	15.222
F(000)	1568.0	3072.0	1384.0	1576.0
Reflections collected	31051	10573	15895	16828
Independent reflections/R(int)	10158/0.0544	5023/0.0393	9215/0.0310	5048/0.0394
Data/restraints/parameters	10158/60/707	5023/331/343	9215/8/671	5048/39/327
Goodness-of-fit[a] on F^2	1.093	1.057	1.022	1.151
Final R indexes [I>2σ(I)]	R_1[b] = 0.0612, wR_2[c] = 0.1639	R_1[b] = 0.0755, wR_2[c] = 0.2012	R_1[b] = 0.0338, wR_2[c] = 0.0906	R_1[b] = 0.0497, wR_2[c] = 0.1424
Largest diff. peak/hole/e Å^{-3}	5.17/-2.72	2.10/-1.10	1.25/-1.83	3.26/-1.29

a Goodness-of-fit = $[\Sigma(w(F_o^2 - F_c^2)^2]/(N_{obsevns} - N_{params})]^{1/2}$, based on all data.

b $R_1 = \Sigma(|F_o| - |F_c|)/\Sigma(|F_o|$, [c] $wR_2 = [\Sigma[w(F_o^2 - F_c^2)^2]/\Sigma[w(F_o^2)^2]]^{1/2}$.

Table 23: Selected bond lengths (Å) and angles (°) for complexes **63a, 64a, 65b** and **66b**

	63a	**64a**	**65b**	**66b**
Au – N1	2.048(7)		2.075(3), 2.055(4)	2.056(7)
Au – N2	2.042(6)	2.068(10)		
Au – P	2.238(2), 2.233(2)	2.241(3)	2.234(1), 2.223(1)	2.234(2)
N1 – N2	1.368(9), 1.374(8)	1.341(15)	1.368(5), 1.374(5)	1.367(11)
N1 – C5	1.337(10), 1.330(10)	1.317(16)	1.325(6), 1.333(6)	1.317(12)
N2 – C3	1.338(10), 1.355(9)	1.354(15)	1.351(6), 1.343(6)	1.357(12)
C3 – C4	1.393(11), 1.405(10)	1.382(16)	1.402(6), 1.407(6)	1.398(13)
C4 – C5	1.412(11), 1.396(11)	1.379(16)	1.384(6), 1.383(6)	1.395(13)
C3 – N6	1.393(10), 1.410(10)	1.327(17)	1.342(6), 1.337(6)	1.340(13)
C4 – C7	1.477(10), 1.470(11)	1.484(16)	1.419(6), 1.418(6)	
C4 – Br7				1.859(9)
P – C9	1.815(8), 1.817(7)	1.803(12)	1.812(4), 1.814(4)	1.812(9)
P – C10	1.818(8), 1.811(7)	1.805(12)	1.813(5), 1.801(5)	1.816(9)

	63a	**64a**	**65b**	**66b**
P – C11	1.808(7), 1.816(7)	1.795(15)	1.819(4), 1.805(4)	1.813(9)
N1 – Au – P	176.68(19)		176.01(11), 176.98(11)	175.3(2)
N2 – Au – P	178.56(17)	175.3(3)		
Au – N1 – N2	123.3(5)		125.7(3), 125.1(3)	124.4(6)
Au – N2 – N1	123.4(5)	119.9(8)		
Au – N1 – C5	131.1(5)		125.7(3), 127.6(3)	125.5(6)
Au – N2 – C3	130.3(5)	133.0(9)		
Au – P – C9	116.4(3), 111.3(2)	109.8(4)	113.42(14), 109.91(14)	113.4(3)
Au – P – C10	112.7(2), 111.8(2)	114.5(4)	111.98(14), 113.82(16)	112.1(3)
Au – P – C11	109.3(2), 112.8(2)	113.1(4)	113.86(14), 113.15(14)	112.2(3)
N1 – N2 – C3	111.6(6), 105.6(6)	106.5(10)	110.4(3), 110.4(3)	110.3(8)
N2 – C3 – C4	107.5(7), 110.1(6)	109.3(10)	106.5(4), 106.4(3)	106.1(8)
C3 – C4 – C5	104.6(7), 104.9(6)	104.9(10)	105.8(4), 106.3(4)	106.2(8)
C4 – C5 – N1	110.7(7), 108.2(6)	108.8(11)	110.5(4), 109.8(4)	109.9(8)

	63a	**64a**	**65b**	**66b**
C5 – N1 – N2	105.5(6), 111.1(6)	110.5(10)	106.8(3), 107.0(3)	107.4(8)
N2 – C3 – N6	120.8(7), 121.2(6)	120.7(12)	124.5(4), 124.0(4)	125.3(9)
N6 – C3 – C4	131.6(7), 128.7(7)	129.9(12)	128.9(4), 129.4(4)	128.3(9)
C3 – C4 – C7	129.2(7), 128.2(7)	126.2(10)	126.5(4), 126.6(4)	
C7 – C4 – C5	126.2(7), 126.9(7)	128.8(11)	127.6(4), 127.0(4)	
C3 – C4 – Br7				125.6(7)
Br7 – C4 – C5				128.2(7)
C4 – C5 – C8	129.6(7), 131.3(7)			
C8 – C5 – N1	119.6(7), 120.5(7)			

Figures 20 and 21 show ORTEP views of complexes **63a, 64a, 65b** and **66b**, with the numbering scheme used. Thermal ellipsoids have been drawn at the 40% probability level and hydrogen atoms have been omitted for clarity. Figure 22 and 23 show ORTEP view and 1D polymer structure of complex **71**

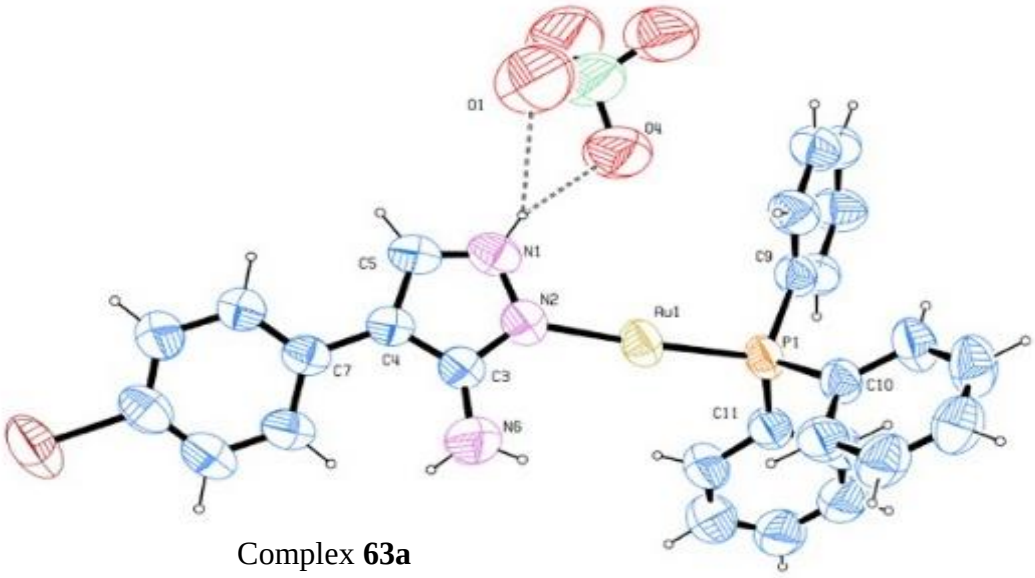

Complex **63a**

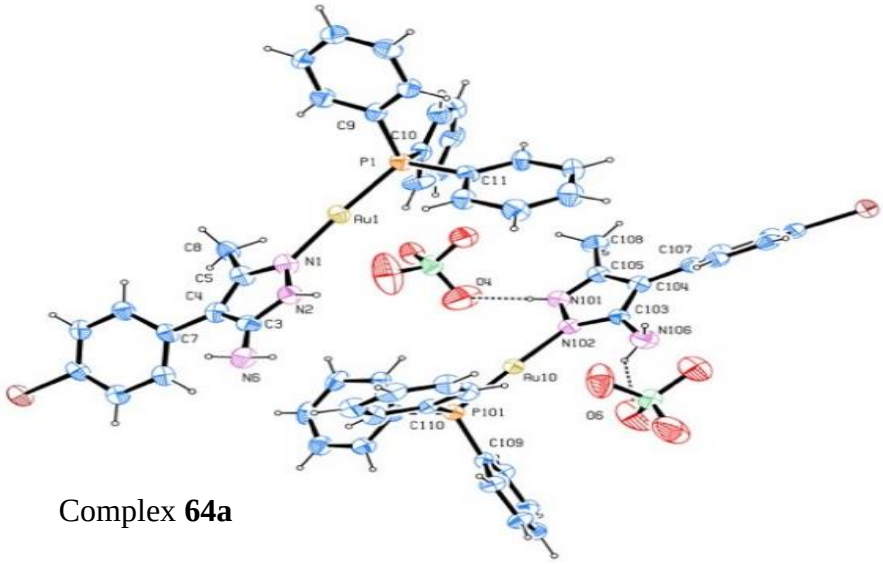

Complex **64a**

Figure 20: ORTEP view of complexes **63a** and **64a**

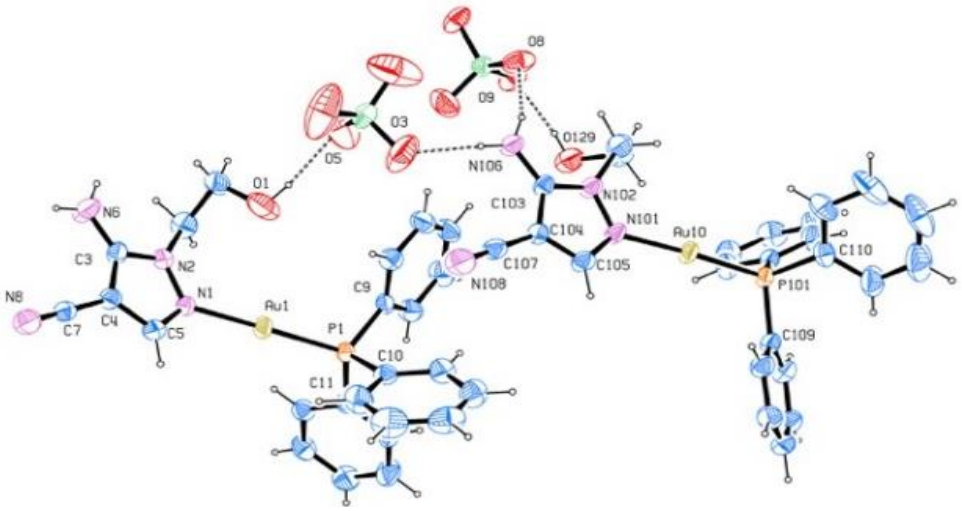

Complex **65b**

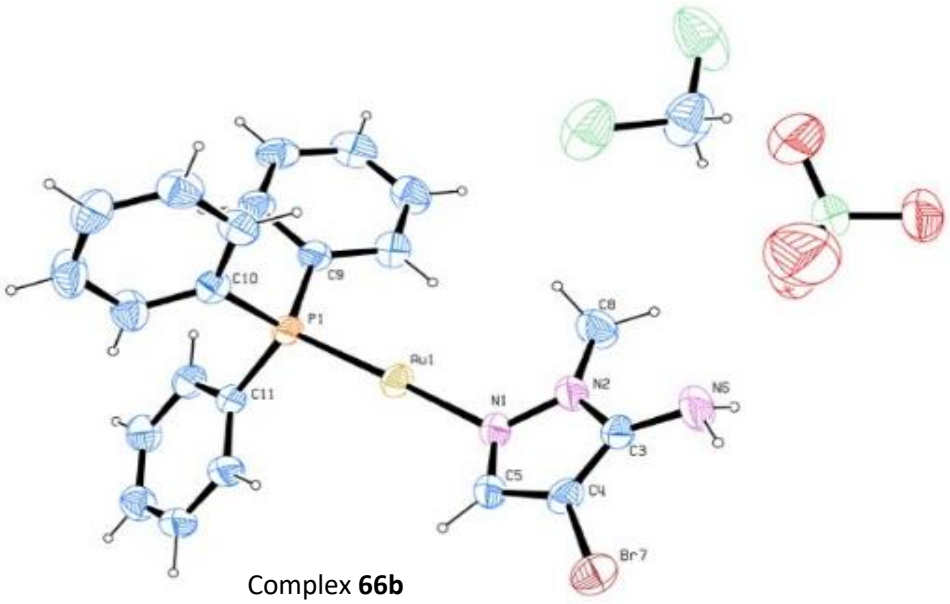

Complex **66b**

Figure 21: ORTEP view of complexes **65b** and **66b**

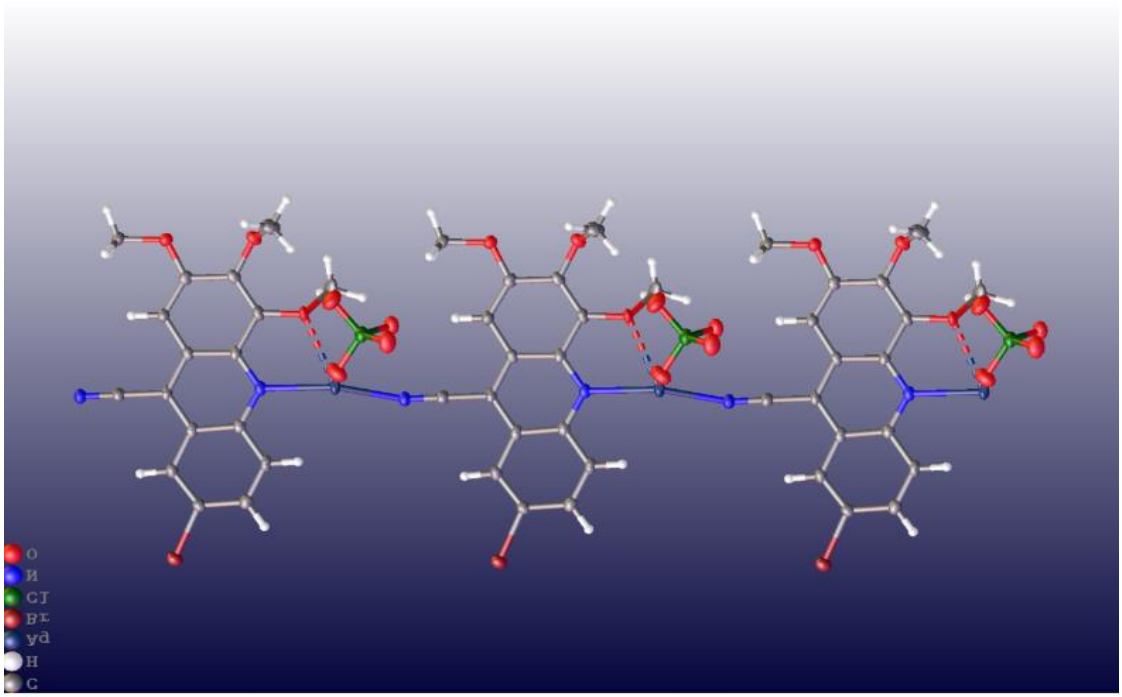

Figure 22: ORTEP view of complex **71**

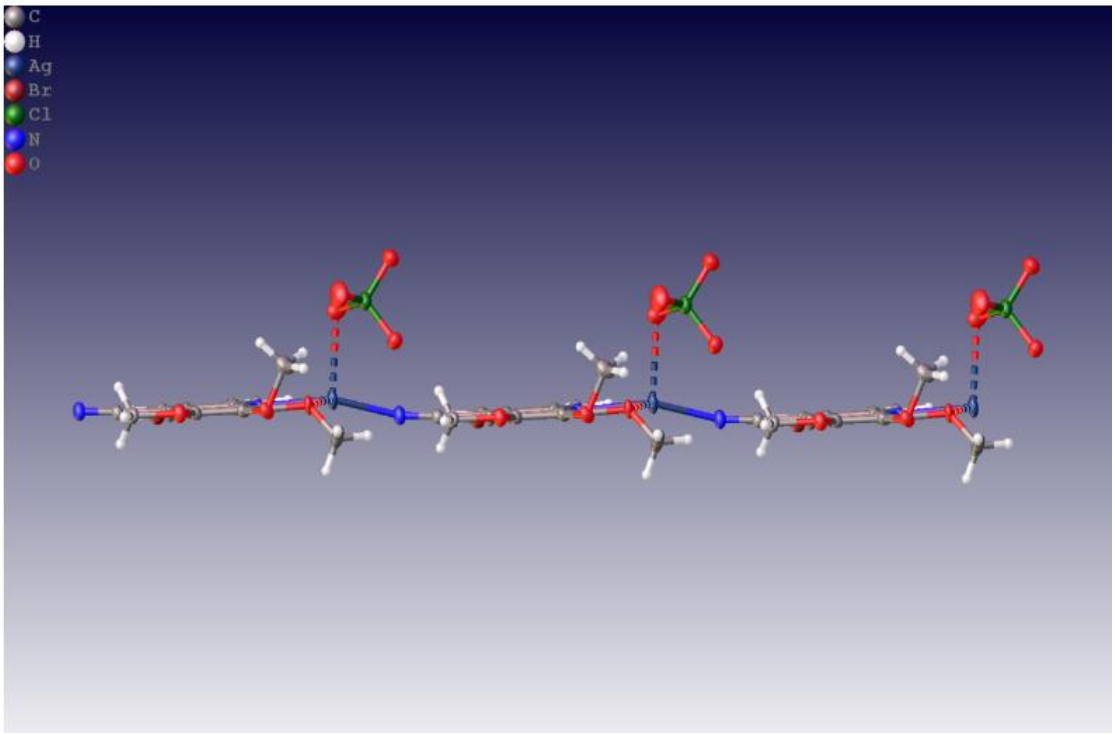

Figure 23: 1D polymer structure of complex **71**

Selected crystalline specimens of the complexes **64a, 65b** and **66b** were mounted on Mitegen loops and centered on the goniometer head of a Rigaku Oxford Diffraction Gemini E diffractometer equipped with an EOS CCD area detector, data collection was performed at 173K. Complex **63a** was collected on a Rigaku Oxford Diffraction 007HFM/AFC11 diffractometer equipped with a Saturn 944+ CCD area detector at 100K. All complexes were collected with monochromated CuKα radiation, by means of ω-scans. The diffraction intensities were corrected with respect to Lorentz and polarization effects. Empirical multi-scan absorption corrections, using equivalent reflections, were also performed with the scaling algorithm SCALE3 ABSPACK. Raw data collection, data reduction and refinalisation were carried out with the CrysAlisPro software. All complexes were solved by means of the intrinsic phasing method in SHELXT[276176]and refined by full-matrix least squares methods based on F_o^2 with SHELXL[277]in the framework of the OLEX2[278]software. In the last cycles of refinement all non-hydrogen atoms were refined anisotropically; hydrogen atoms were placed and refined as riding atoms with their isotropic displacement parameters set to 1.2 times the U_{eq} of the parent atom. The best crystal of complex **63a** necessitated the collection on the Rigaku 007HFM due to its small size. In complex **64a**, there is a small amount of disorder relating to the ligand binding through N2 or N1. The amount of disorder was too low to model satisfactorily, so this has been left unmodelled. The molecular structures of all complexes contained a two- coordinate Au centre with expected Au-P (2.2-2.4Å) and Au- N (2.0-2.2Å) distances and linear coordination irrespective of the state of molecularity in the crystal (Table 19).[279] The Au-P were in very good agreement with 2.25 Å reported by Keter et al[282] and 2.26 Å results of Cambridge Structural Database (CSD).[282] The perchlorate molecule was included in the lattice of the complexes **63-66** and CH_2Cl_2 was present only in the lattice of complex **66b**. These do not show chemical interactions with

the complexes. Ligand in entry**1** has a pyridine at the fourth position, which provides another possible point of attachment compared to others. There is four possibilities for the point of attachment to gold (I). Therefore, four peaks were expected by ^{31}P NMR but only one peak at 30.0 ppm was observed indicating that there is only one possible linkage. Ligand in entry **2** is a pyrazole with a bromophenyl at position 4 with three possible points of attachment but only one peak at 31.0 ppm was observed. X-ray crystallography also confirmed one linkage. The point of attachment was the nitrogen at the position one replacing the proton in that position but leaving a positive charge on the nitrogen ligand in entry **3** has a similar structure to ligand in entry **2** but with a methyl group at position three. Three points of attachment were also possible but the ^{31}PNMR indicated a single attachment point to gold (I) by given only one peak at 31.50 ppm. X-ray result also confirmed the single point of attachment but indicated that complex **64a** is a regioisomer with a positive charge on the nitrogen in position 1. Ligand in entry **4** has a cyano group at position four and an ethyl alcohol at position two given different likely point of attachment. However, ^{31}P NMR of the complex gave a single peak at 29.7ppm indicating a single point of attachment to gold (I). X-ray diffraction indicated that complex **65b** is a regioisomer with only one point of attachment to gold (I). Ligand in entry **5** has a bromo substituent at position 4 and a methyl group at position one. ^{31}P NMR indicated only one point of attachment with a single peak at 30.0 ppm and attested to by the x-ray diffraction study. The point of attachment was at position 2. Complex **66b** is non regioisomeric.

II.10. Fluorescence Properties

II.10.1.UV-VIS and Fluorescence

To evaluate the fluorescence properties of this new class of compounds, an array of fluorescent cationic gold(I) complexes were prepared. The photo physical properties of these complexes and their constituent free ligands were determined at room temperature.

The solvent selected for these measurements was ethanol, as larger stoke shifts are usually obtained when polar solvents are used.[250]As stated in the literature the fluorescence absorption and emission maxima in polar solvent exhibit solvatochromic red shift with increasing polarity.[250] Fluorometry measurements of these novel gold (I) catalysts revealed all the tested complexes were fluorescence active. The UV-Vis spectra of most of the acridine ligands and their complexes showed an absorption maximum at two different wavelengths. The first excitations were between 360-456 nm and the second within the range of 265-270 nm. It was observed that the second excitation deviated from expected results, as the compounds' concentration at different dilution measured against UV-Vis absorption did not obey Beer Lambert law and their emission bands were not mirror symmetrical to their absorption band. It was hypothesised that the first excitation was the fluorescence from $S_1 \rightarrow S_0$ as against the fluorescence from the second excitation $S_2 \rightarrow S_0$ (Figure 24) which usually occurred with loss of energy from internal conversion or photobleaching which may lead to decrease in fluorescence intensity.[283] Attention was then shifted to the first excited state for the fluorescence analysis of the compounds where each compound shows the emission band, which is mirror symmetrical to its maximum absorption band.

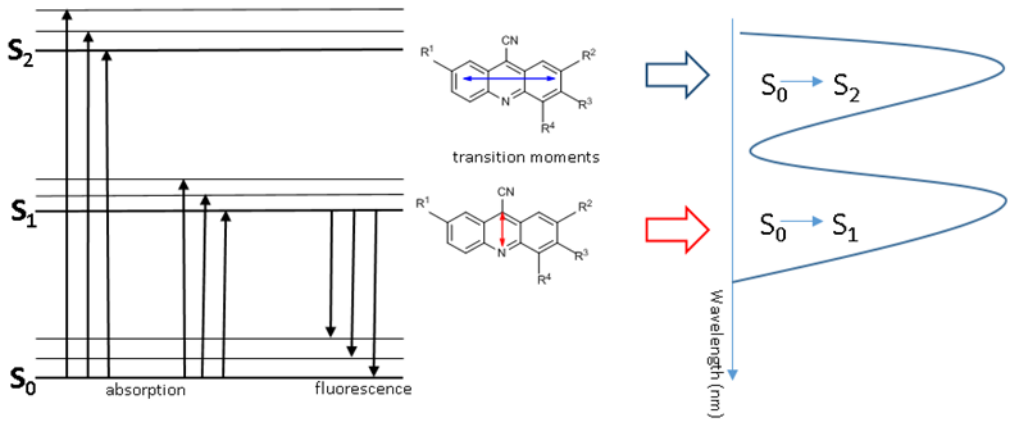

Figure 24: Transition moments for acridine derivatives.[286] The blue arrow represented π→π* transition ($S_0 \rightarrow S_2$) while the red arrow represented n→π* transition ($S_0 \rightarrow S_1$)

UV-Vis spectroscopy was used to identify an appropriate excitation wavelength. The results showed that 365 nm would be the most viable, as it yielded high absorption values for both the target compounds and the selected standard.[284] There should be a linear relationship between the analyte concentration and absorbance, which is usually achieved when the absorbance values lie between 0.05 and 0.04.[284] When emission intensity is above0.05 values tend to deviate from the linear dependence on the concertation because most instruments lacks precision in this range.[284] linear dependence between the absorbance and the concentration is very important because it shows that only the monomeric units are present in the solution. It should obey the Beer-Lambert law (equation below).

$$A = \varepsilon cl$$

Where A is the absorbance at a given wavelength, ε is the molar absorptivity, C is the concentration of the sample and l is the path length.[285] The typical linear relationship obtained for acridine derivatives and their complexes in ethanol for concentration ranging from $1x10^{-9}$ M to $1x10^{-5}$ M are shown in figure 25. This shows that only monomer units are in solution.

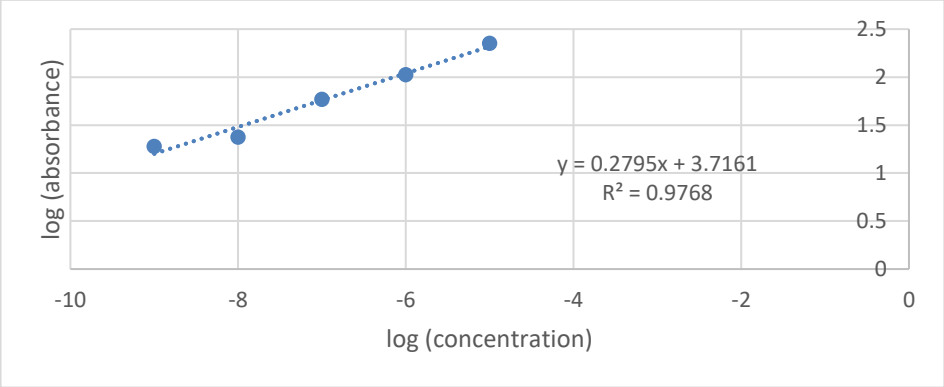

Figure 25: The linear relationship between emission intensity and concentration of 9 showing that Beer-Lambert law is obeyed.

The wavelengths of emission maxima ranges from 385.0 nm to 526.0 nm indicating that by proper selection of the appropriate acridine ligand the emission could easily be used to achieve a variety of visible colours.

Figure 26: Selected acridine ligands under UV light (λ=365nm) L-R **7, 9, 11, 12, 13, 14, 15** and **16.**

II.10.1.1.Possibility of Excimer or dual Excitation

Excimer formation implies that more than a single unit of monomer is in solution but dual excitation usually occurs because of isomerization dynamics of the compound. A monomer may have resonance hybrid which may excite at different wavelength.[286–288] It was reported that alkyl ester of 9-anthrilic acid isomerised in solution when photoexcited but the reason for the formation of stereoisomer by this compound has not been proved.[289] The photochemical isomerization of anthracene derivatives has been studied extensively.[290] It has been reported that 2-methoxy-substituted anthracene exhibited dual emission wavelengths, which originate from two different interconvertible species in solution.[288]Though, it was reported that 9-amino acridine belong to the class of compounds that dimerises easily at higher concentrations[291] but it only dimerises in the excited state.[292] It was observed that some of the spectra, particularly the methoxy substituted derivatives gave more than one emission maxixma. In an attempt to identify whether excimer formation or dual excitation was responsible for this phenomenon a concentration dependence study on 2-iodo-6-methoxy-9-acridinecarbonitrile was undertaken (Figure 27).

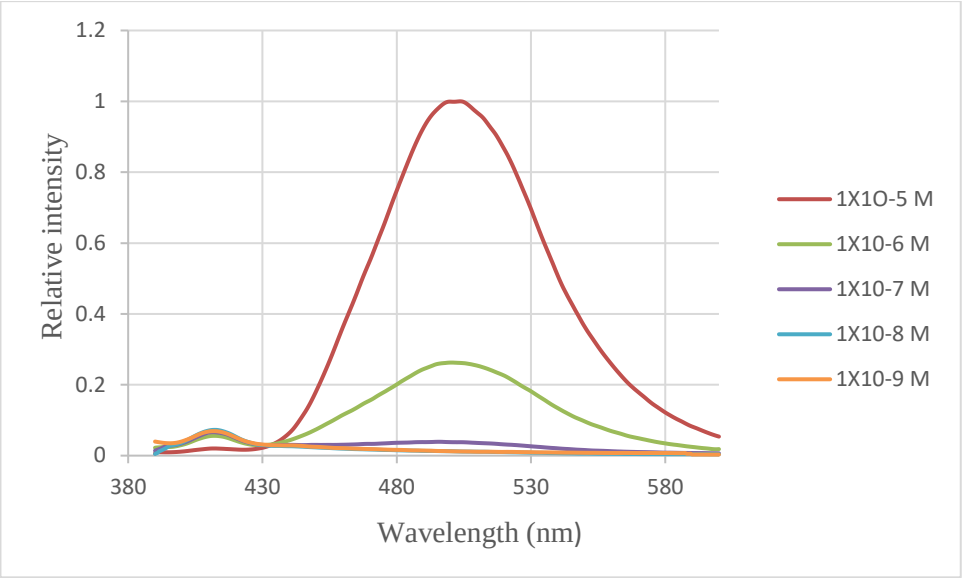

Figure 27*:* Concentration dependence studied of 2-iodo- 6-methoxyacridine-9-carbonitrile **17**

If it were to be an excimer, at low concentration the dimer would not form therefore a pure fluorescence spectrum was expected to be observed and as the concentration increases the dimer should be more probable and the excimer peak should be more pronounced. In other words, the occurrence of a new peak at higher concentration confirm the formation of excimer. Surprisingly, the higher the concentration, the purer the spectra. Therefore, the absence of a new peak at higher concentration rules out the possibility of dimerization.[292] It was then proposed that this could be due to dual excitation as the compound may isomerised in solution when photoexcited (figure 28) thereby emitting at different wavelength.

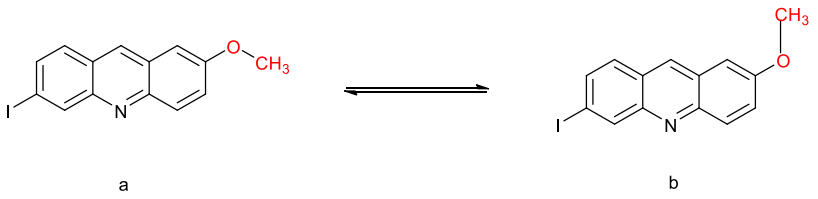

Figure 28*:* Geometrical isomerisation of compound a to compound b when photoexcited or vice versa

II.10.2.Sustituent Effect on Photophysical Properties of Acridine

II.10.2.1.Substituent Effect on the Absorption and Emission of Acridine

The term substituent was defined by Exner in 1996,[293] as structural entity that fulfils at least one of the following criteria:

(i) The substituent is a smaller part of a molecule which can be introduced by a (simple) chemical operation, particularly when it can directly replace a hydrogen atom.

(ii) The substituent is a smaller and less important part of a molecule which influences the properties of the molecule in a quantitative sense but does not alter its general character; the latter is controlled by another group present: the functional group (or the reaction site).”[293] In other word, substituent is a fractional part of a molecule that can replace a hydrogen atom thereby influences the quantitative properties of the molecule but has no effect on its general character.[293,294] Substituent effect is one of the major concept of structural effect that determines the photo physical and chemical properties of a compound.[295] Literature revealed that addition of substituent on polycyclic aromatic compound influences the photophysical properties such as fluorescence intensity, absorption and emission maxima, Stokes shift and quantum yield etc. Substituents can affect the fluorescence properties in many ways depending on a number of factors. These include nature of the substituents i.e. whether it is electron donating or electron withdrawing group, the position and number of the substituents, on both side of the polycyclic aromatic hydrocarbons and the dipole moment of the molecule. In this

research, it was attempted to study the influence of electron donating group (EDG) and electron-withdrawing group (EWG) on the fluorescence properties of acridine. In this regard, mono, di, tri and tetra substituted acridine-9-carbonitrile were synthesised to determine the influence of substituent position. Furthermore, the combined effect of simultaneous multiple addition of substituent group such as double, triple and tetra substitution are also investigated. Monosubstituted acridine derivatives were synthesized with different halogens at position 2 and methoxy, methythiophene and halogens were alternated at position 2, 3, 4, 5 and 7 for poly substitutions.

II.10.2.2. Effect of halogen Substituents on Absorption and Emission wavelength of Acridine

A number of acridine-9-carbonitrile analogues were prepared (**7**, **8,** and **14**) with different halogens substituted at position 2. The order of absorbance intensity observed was Cl >Br >I (Figure 29). The order of maximum absorbance was Cl < Br < I, this was expected heavy atom such as bromine and iodine substituent on a fluorescent compound are believed to disturb and quench the fluorescence state by increasing the spin-orbit coupling thereby creating a charge-transfer complex.[296] They also induce intramolecular intersystem crossing. Their effect on aromatic molecule usually leads to a decrease in fluorescence intensity and fluorescence lifetime. [297,298] The excitation wavelength in halogenated aromatic compounds are assumed to be influenced by balance between two major interactions: (a) Resonance effect which takes place due to interaction between nonbonding orbital of the halogen and the C=C π orbital of the chromophore. (b) The second type of interaction is due to the inductive electron withdrawing effect of the halogens.[299] The higher bathochromic shift observed in the absorbance maxima for iodine relative to that of chlorine and bromine is assumed to be due to the difference in the electronegativity of the halogens. Electronegativity decreases down the group, thus iodine

is less electronegative than chlorine and bromine, and as a result, it is less inductivity withdrawing on the adjacent ring system. In other words, the electrons on the iodine atom are more loosely held because of its lower electronegativity compared with chlorine and bromine thus it exhibit higher resonance effect.

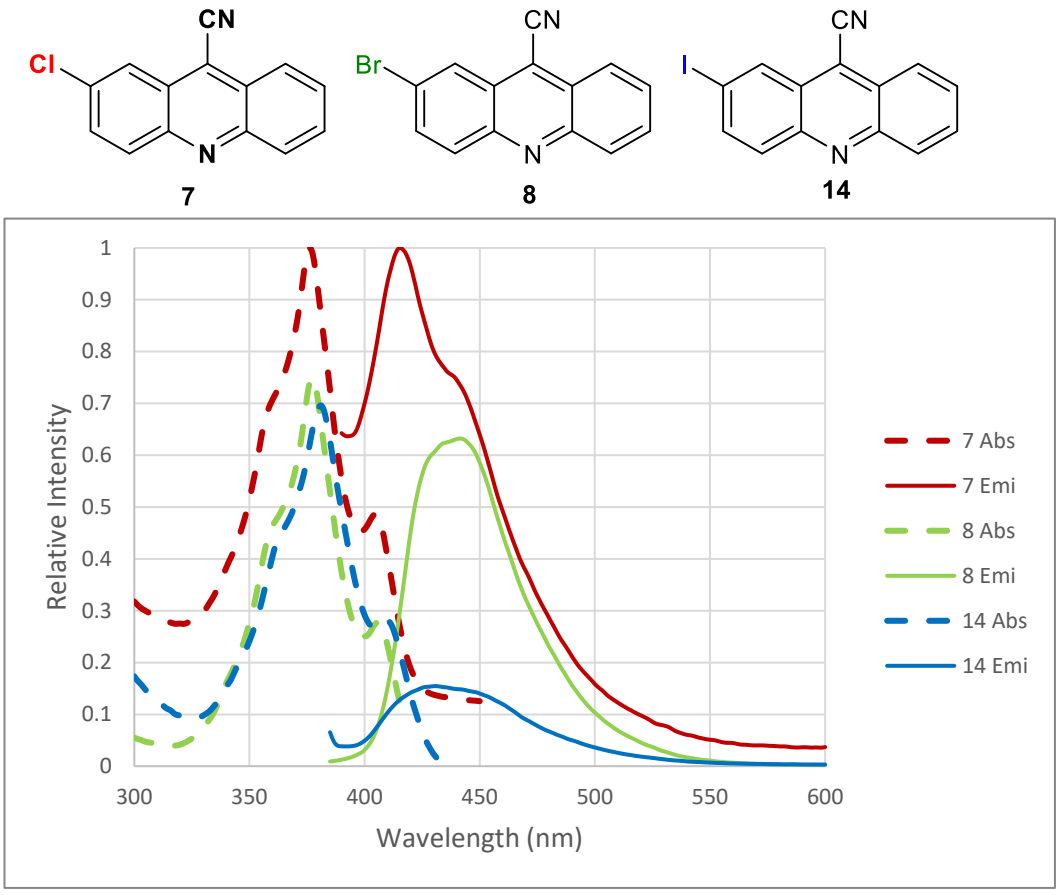

Figure 29: Normalised absorption (dashed line) and emission (solid line) spectra of **7. 8** and **14. 7** in red line, **8** in green line and **14** in blue line at identical concentrations

This implies that resonance effect influences the absorbance maxima more when considering the electron withdrawing cum electron donating capacities of a halogen on aromatic ring system.[300]. In addition, it was observed that both emission intensity and emission wavelength maxima for **7, 8** and **14** followed the same trend as that of the absorption (Figures 30 and 31). That is, **7**> **8** > **14** in terms of emission intensity while the emission maxima increases as the electronegativity of the halogen decreases. It was proposed that the absorbance and emission maxima of halogenated acridine derivatives was depend on the electron density of the π system.

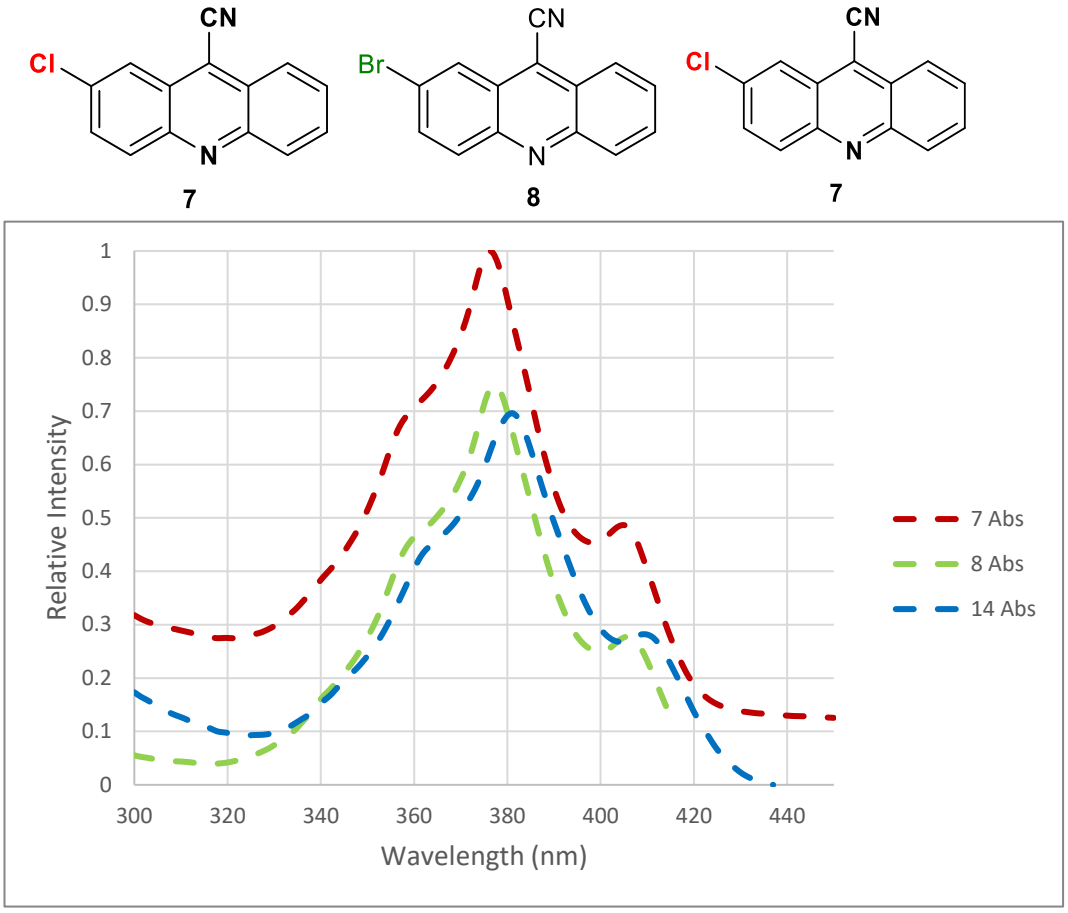

Figure 30: Normalised absorption intensities and wavelength for **7**(red), **8** (green) and **14** (blue) at the same concentrations.

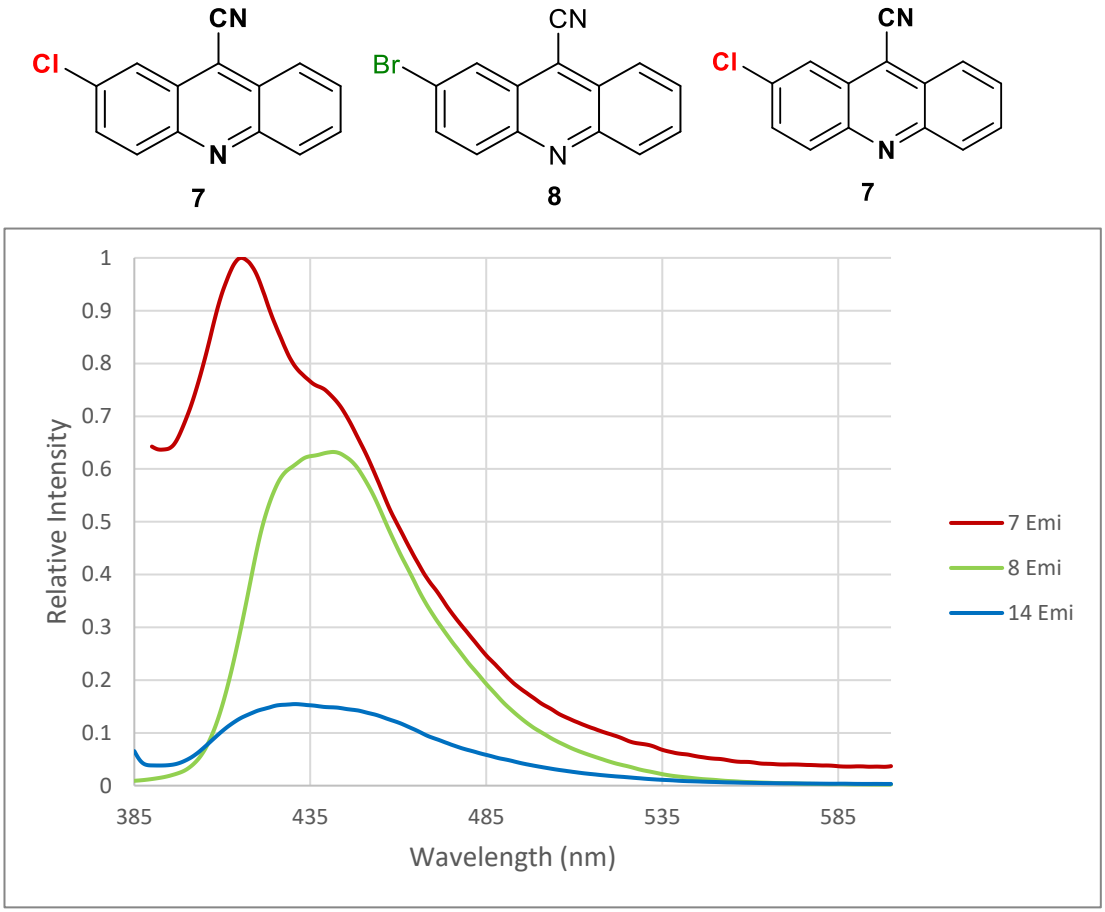

Figure 31: Normalised emission intensities and wavelength for **7 (red), 8** (green) and **14** (blue).

II.10.2.3.Effect of Electron Donating Group on the Absorption and Emission wavelength of Acridine

The effect of double substitutions was also considered. In the first set of acridine derivatives, the electron-donating group (EDG) methoxy was placed on position 6 and varied the halogen substituent on position 2**.** These compounds were synthesised in order to ascertain whether an EDG/ EWG pair on acridine could have a stronger effect on the intensity and wavelength of absorbance as well as that of the emission. Interestingly, the observed trend in absorbance intensity is quite different from that of the emission intensity (Figures 32, 33 and 34). While the absorbance intensity was highest in compound **11**, followed by compound **9** then compound **17**.When considering emission intensity this

trend was reversed, with compound **9** the highest and **11** the lowest**.** These results suggested that a pair of EDG (methoxy)/ EWG (halogen) has no defined trend on the intensity of the absorbance and emission of acridine derivatives. However, absorbance and emission maxima increases as the size of the halogen atom increases. Thus, the absorbance for **9**, **11** and **17** were 367.0 nm, 367.0 nm and 370.0 and the emission maxima were 481.25 nm, 493.5 nm and 500 nm respectively. Concisely, the absorption and emission maxima depends on EDG/EWG pair capabilities.

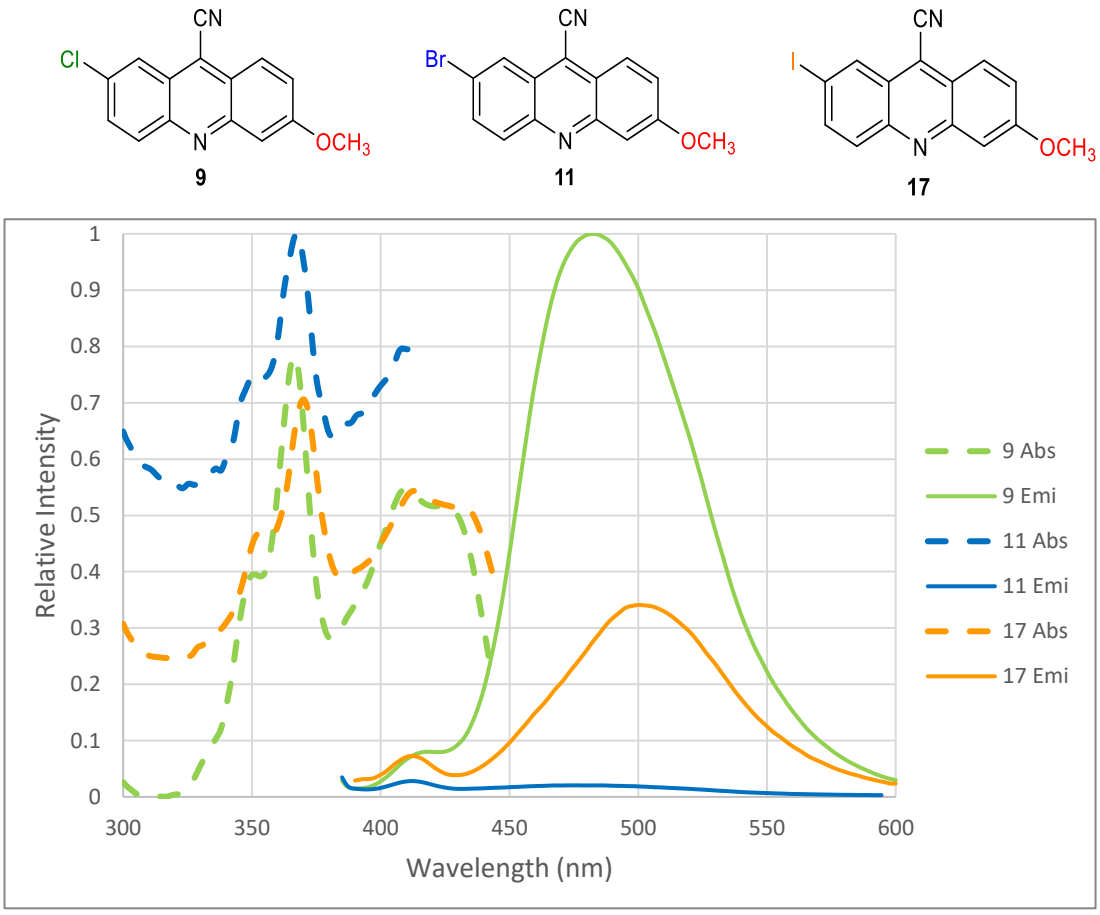

Figure 32: Normalised absorption (dashed line) and emission (solid line) spectra of **9** (green), **11** (blue) and **17** (orange) at the same concentrations

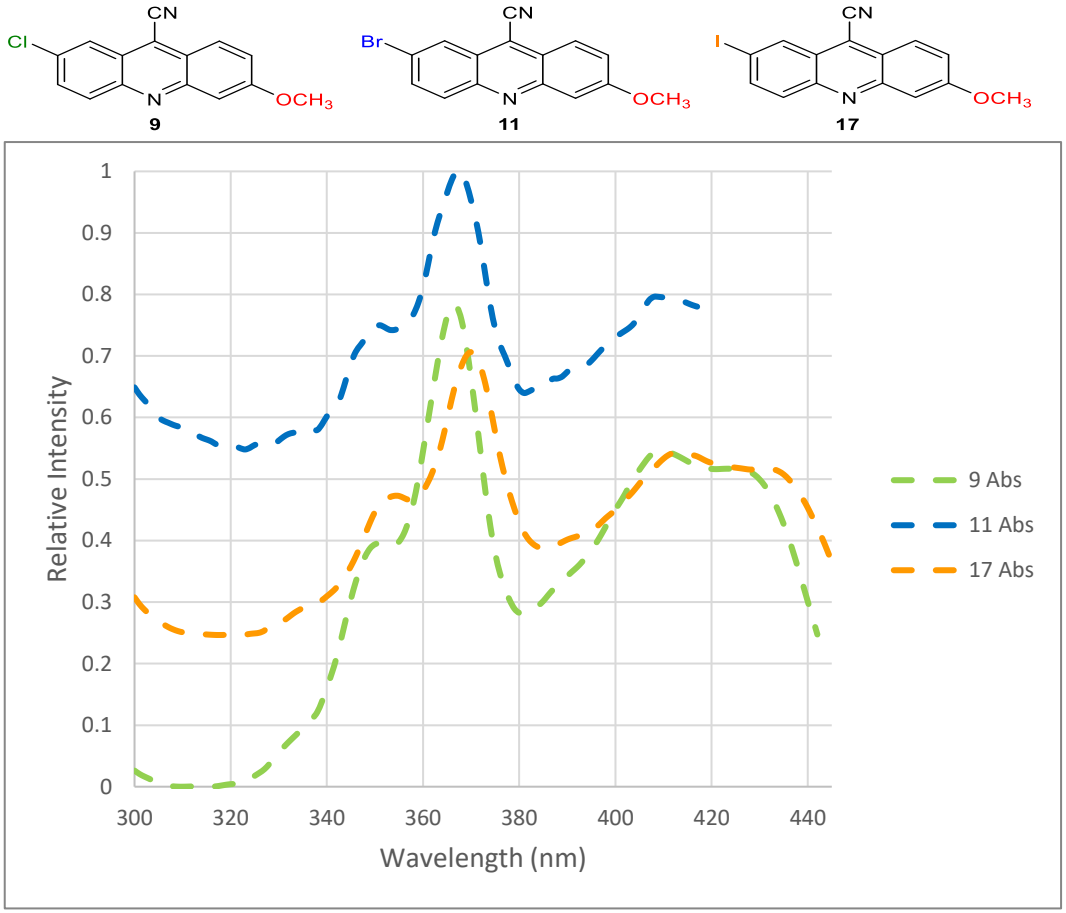

Figure 33: Normalised absorption intensities and wavelength of **9** (green), **11** (blue) and **17** (orange) at the same concentrations

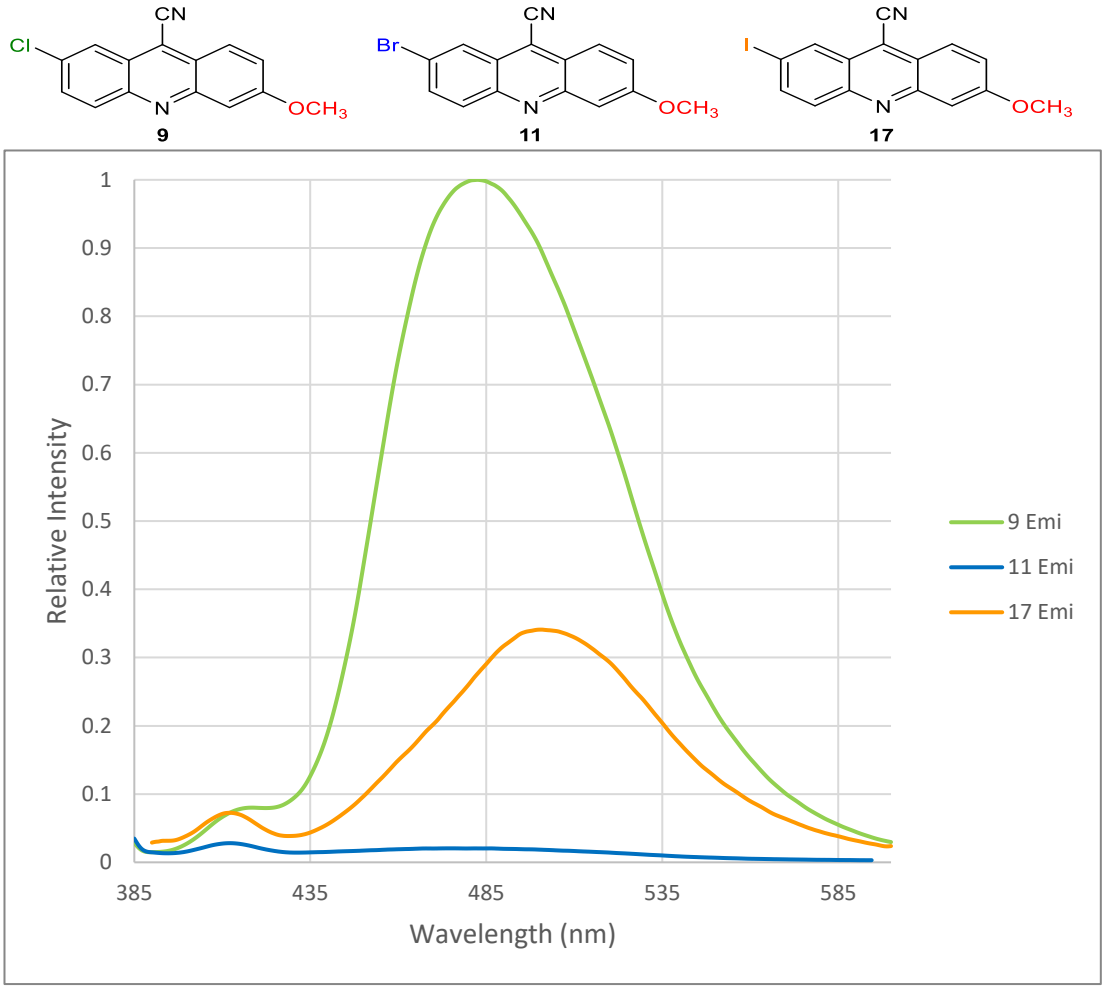

Figure 34: Normalised emission intensities and wavelength of **9** (green), **11** (blue) and **17** (orange) at the same concentrations

II.10.2.4.Effect of Increasing the Number of Methoxy Group on the Absorption and Emission Wavelength

The effect of multiple EDG (methoxy) as substituents on acridine derivatives was investigated. Firstly, the effect of di-methoxy group as substituent on acridine were studied. Halogens were varied on position 7 and added di-methoxy groups at position 2 and 3. To obtain 7-iodo-2,3-dimethoxyacridine-9-carbonitrile **20**, 7-chloro-2, 3-dimethoxyacridine-9-carbonitrile **21** and 7-bromo-2, 3-dimethoxyacridine-9-carbonitrile **23**. It was observed that the intensities for both absorbance and emission decreases down the halogen group (Figure 35). Chloro substitution has the highest followed by bromo while iodo substitution has the lowest intensity. It was proposed that both the absorbance

and emission intensity of dimethoxy halogenated acridine derivatives decreases as inductive effect of halogen decreases. However, the wavelength of absorbance and emission maxima did not follow the same trend figures (36 and 37). It was observed that bromo substitution **23** has the highest absorbance (402.0 nm) and emission (457.5 nm) maxima while iodo substitution **20** has absorbance (380.0 nm) maxima next to it but with the lowest emission (448.5 nm) maxima. The chloro substituted acridine derivative **21** has the lowest absorbance (367.0 nm) maxima but with higher emission (455.75 nm) maxima. The lowest emission wavelength observed in the iodo substituted may be due to heavy atom effect.

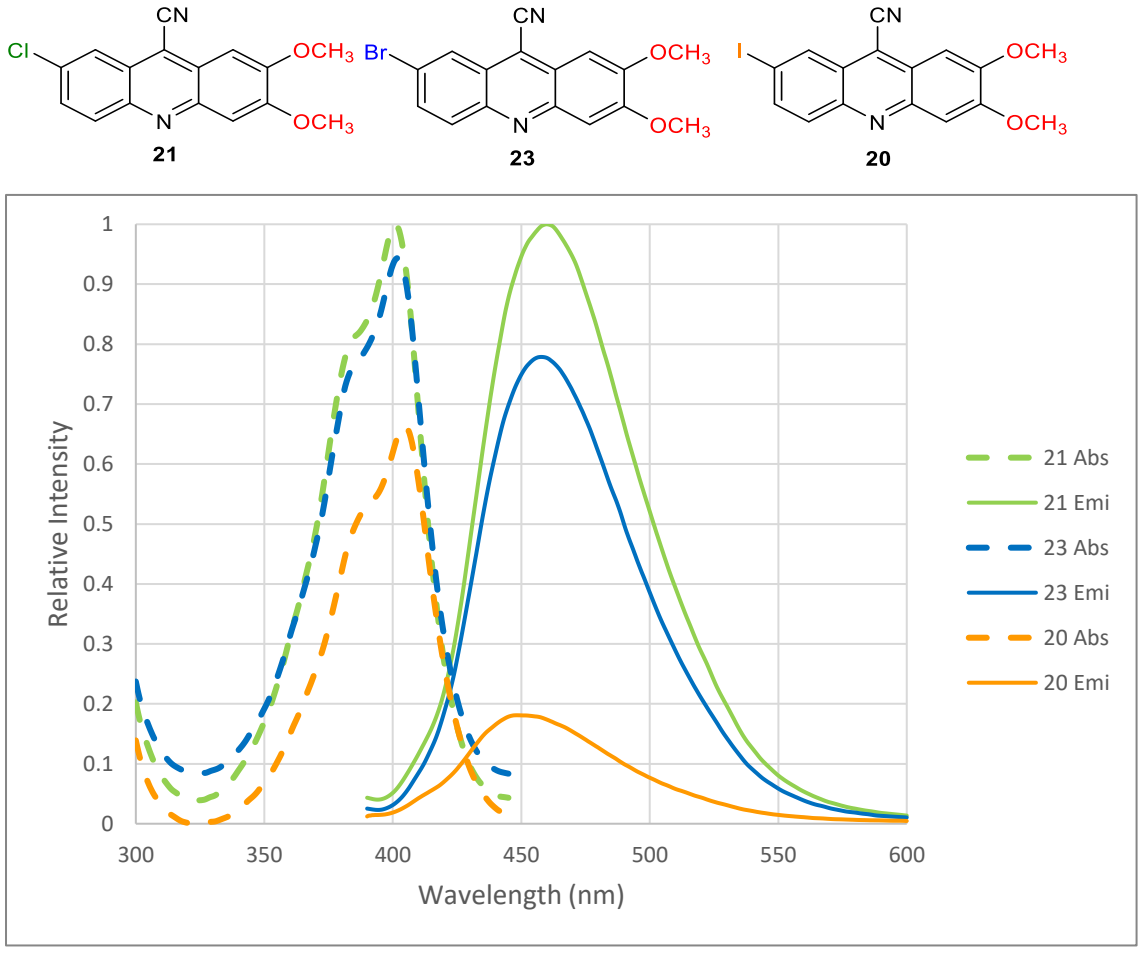

Figure 35: Normalised absorption (dashed lines) and emission (solid lines) properties of **20** (orange), **21** (green) and **23** (blue) at the same concentrations ($1x10^{-6}$ M).

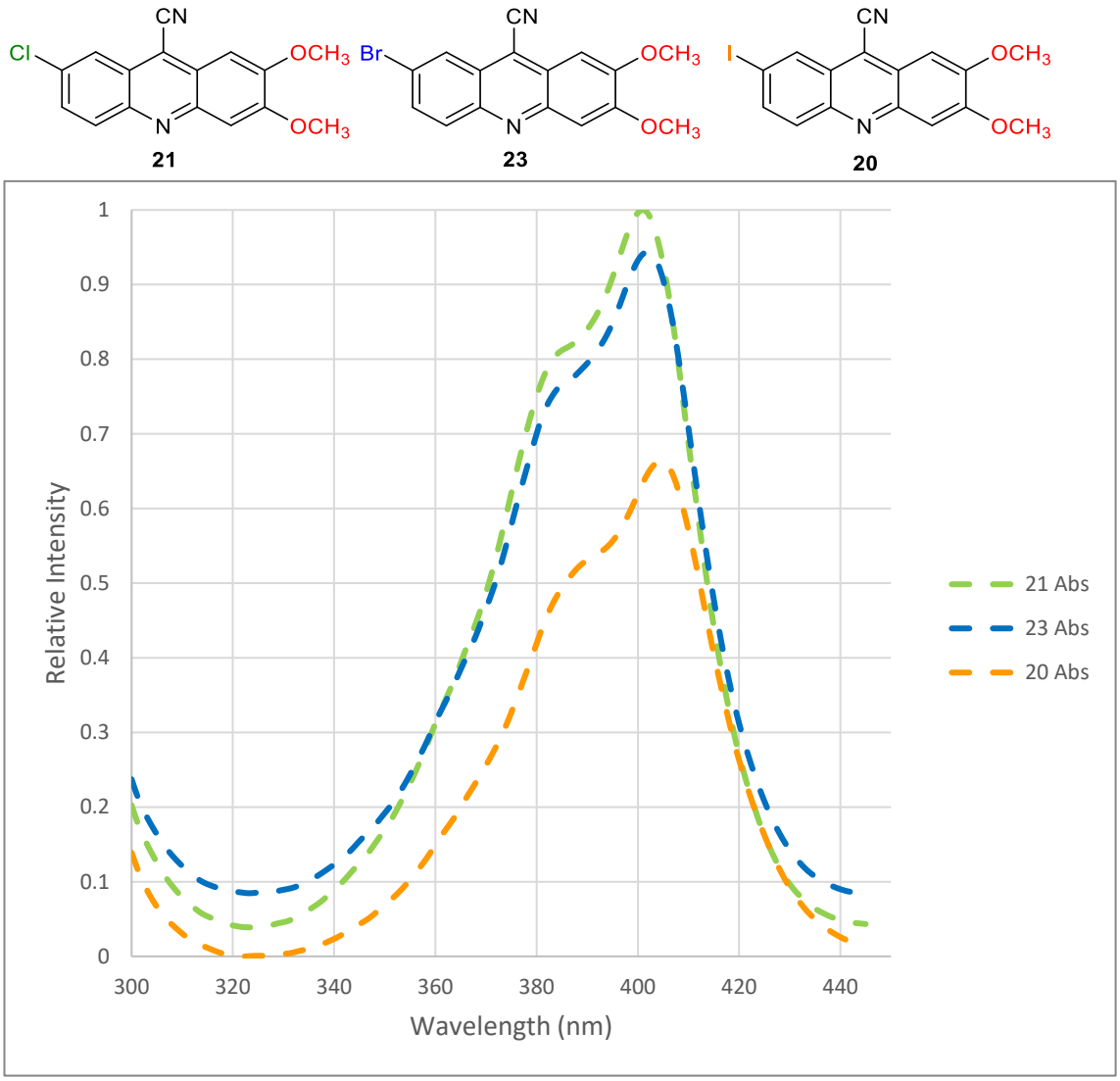

Figure 36: Normalised absorbance maxima and intensities of **20** (orange), **21** (green) and **23** (blue) at the same concentrations ($1x10^{-6}$ M)

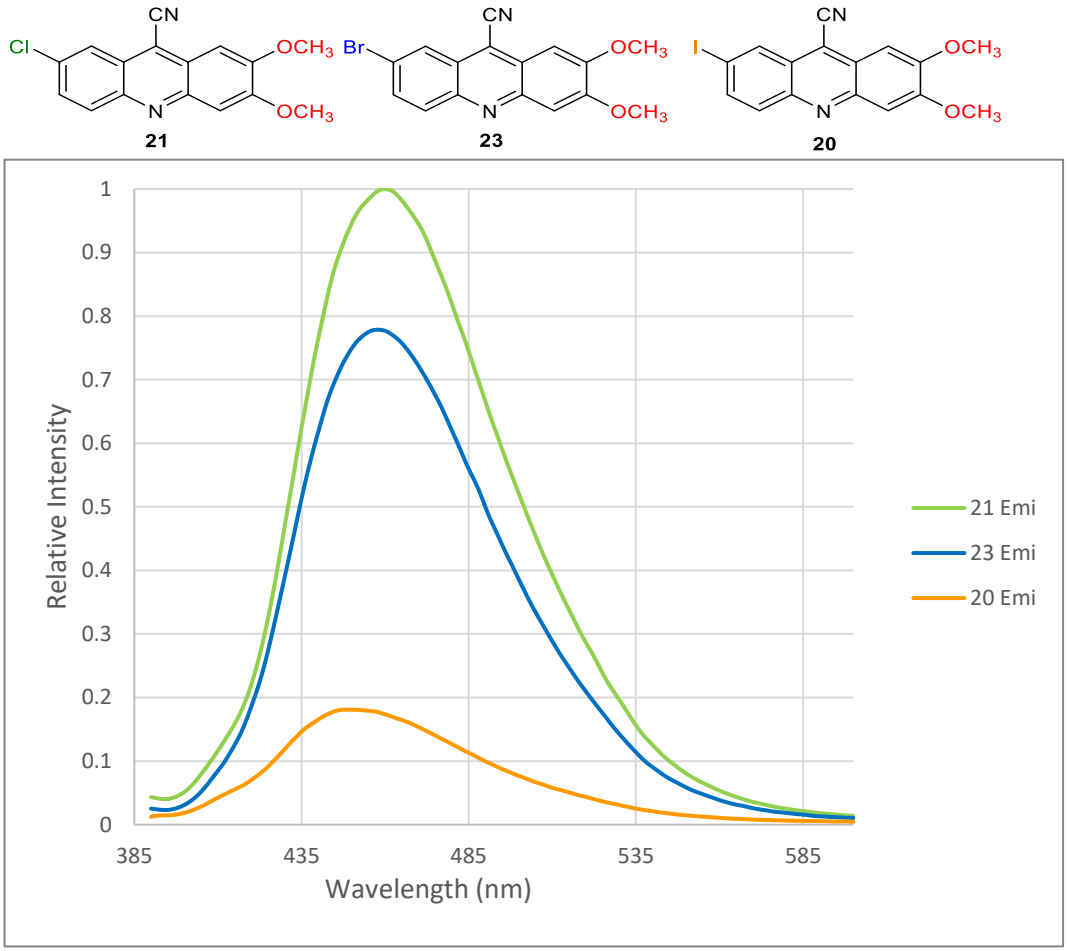

Figure 37: Normalised emission maxima and intensities of **20** (orange), **21** (green) and **23** (blue) at the same concentration

II.10.2.5. Effect of Quadruple Substitution on the Absorption and Emission Properties

The effect of four substituents on acridine-9-carbonitrile was also examined (figure 38). Here the number of methoxy groups were increased to three, resulting in a configuration with methoxy groups at position 2, 3 and 4 and varied the halogen on position 7. It was observed that there was no clear-cut correlation in the intensities of the absorbance as the bromo substituted **19** has the highest intensity followed by iodo substituted **16** while the chloro substituted **15** has the least intensity. This could be explained based on the EWG/EDG effect in which the bromo substituted has the electron density that falls in- between the iodo substituted and chloro substituted derivatives. However, the absorbance maxima increases as inductive effect of the

halogen decreases. The iodo-substituted derivative **16** has the highest absorbance maxima (398.0 nm) followed by bromo substituted 19 (396.0 nm) with chloro substituted **15** has the lowest absorbance maxima. But the chloro substituted has the highest emission maxima (480.5 nm) followed by iodo substituted (475.0 nm) with bromo substituted having the least (473.0 nm).

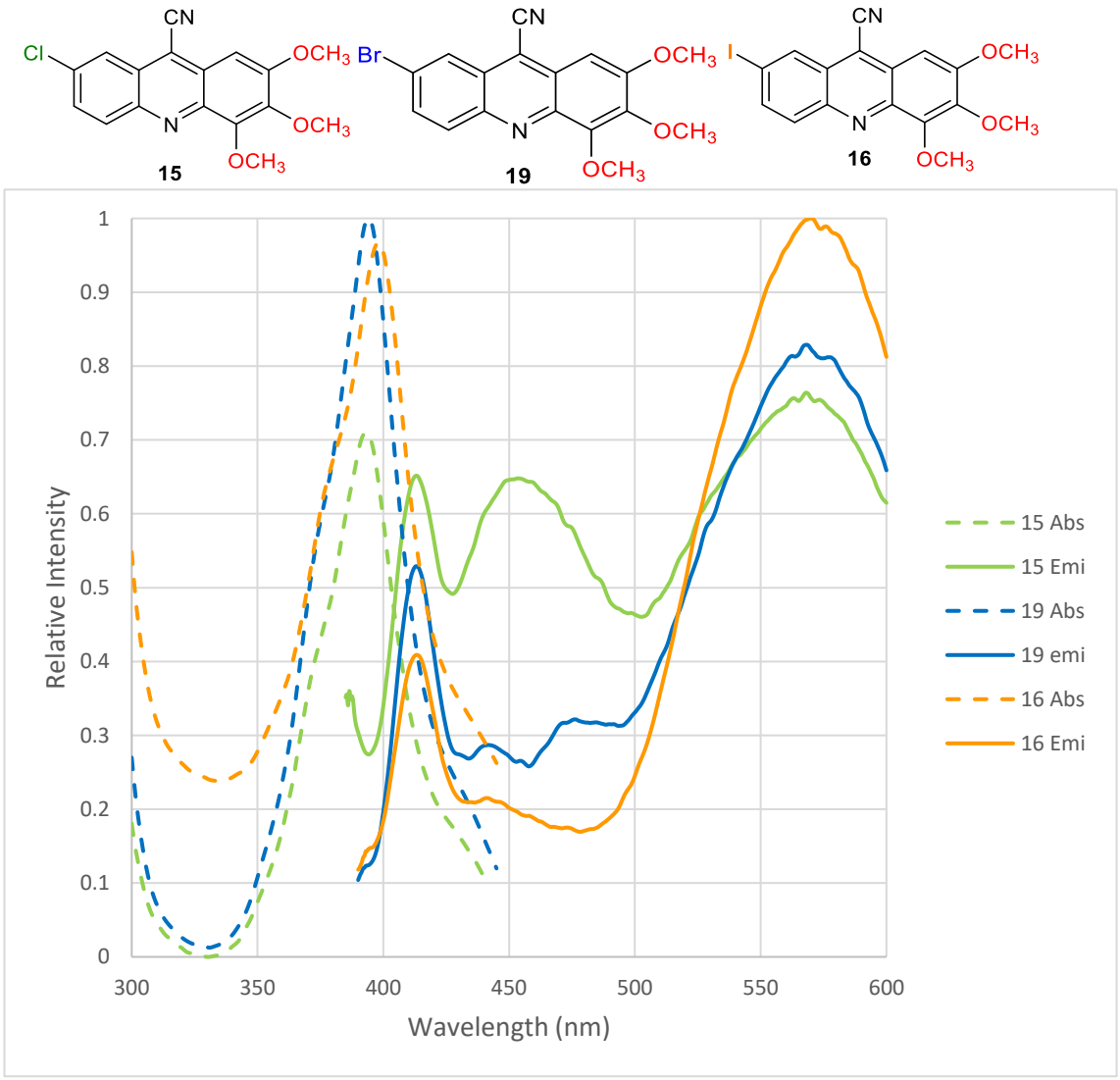

Figure 38: Normalise absorbance (dashed lines) and emission (solid lines) properties of **15** (green), **16** (orange) and **19** (blue) at the same concentrations ($1x10^{-6}$ M)

II.10.2.6.Chloro-Substitution with Increase in the Number of Methoxy Group

The effect of multiple substitution of EDG (methoxy) at position 2,3 and 4 on acridine derivatives whilst keeping the chlorine on position 7 were examined (Figures 39, 40and

41). The absorbance intensity was reduced when one methoxy was added compares to when there was no methoxy. This could be as a result of push-pull system which is usually experience when EDG/EWG are substituted across a ring system.[301–303] Contrary to our expectation, progressive addition of methoxy group did not result in a progressive red shift of the absorption maxima as observed by Griffits.[304] They observed a progressive shift into longer wavelength in arylamine as the addition of electron donating group increases. The absorbance maxima for 2-chloro-9-carbonitrile **7** (377.0 nm) was greater than absorbance maxima of 2-chloro-6-methoxyacridine-9-carbonitrile **9** (367.0 nm). Even addition of two methoxy groups **21** did not change the absorbance maxima (367.0 nm). However, on addition of three methoxy group, the λ_{max} value was displaced to longer wavelength (392.5 nm). The emission maxima followed the expected progressive increment up to the addition of two methoxy group. (i.e. 412.2 nm for **7**, 492.5 nm for **9** and 492.5 nm for **21**). Nevertheless, the value decreased on further addition of the methoxy. (**15** has 480.5 nm).

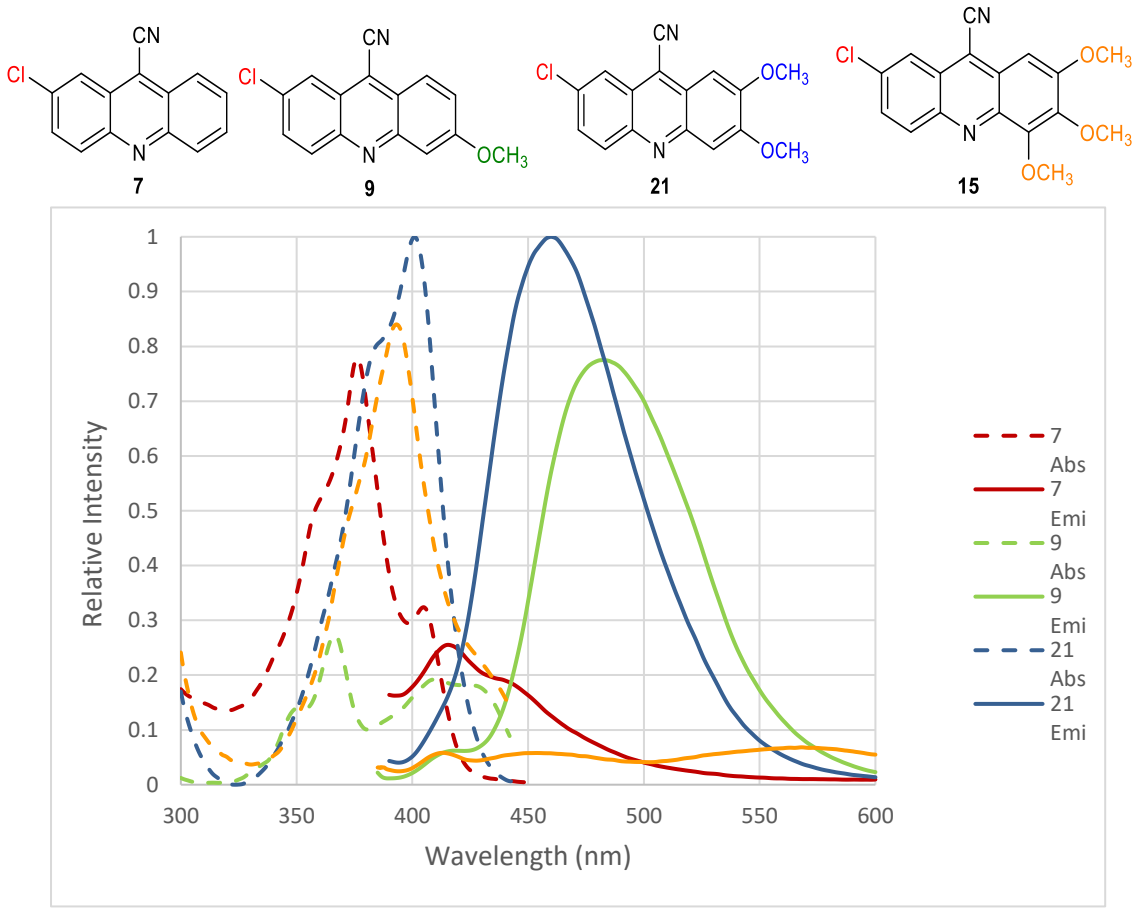

Figure 39: Normalised absorbance (dashed lines) and emission (solid lines) properties of 7 (red), **9** (green), **15** (orange) and **21** (blue) at the same concentrations.

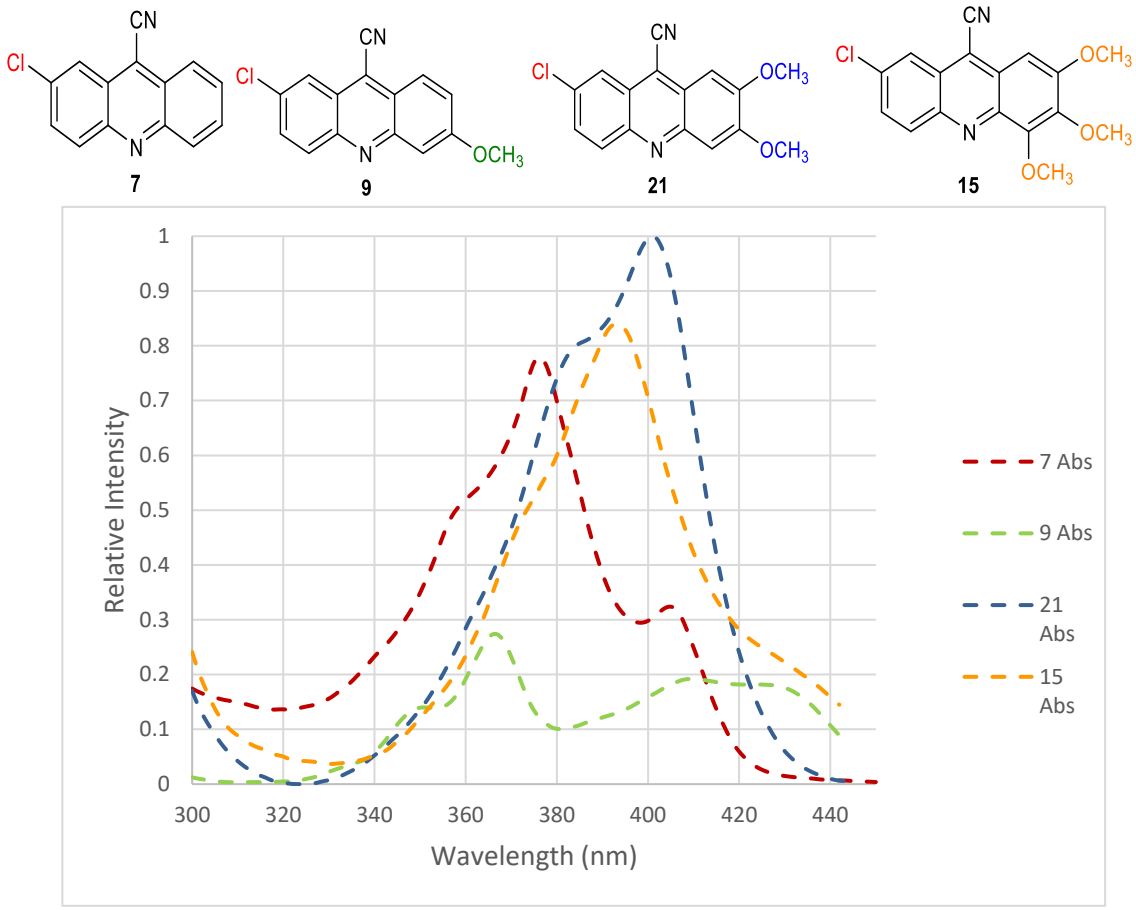

Figure 40: Normalised absorption spectra of **7** (red), **9** (green), **15** (orange) and **21** (blue) at the same concentrations.

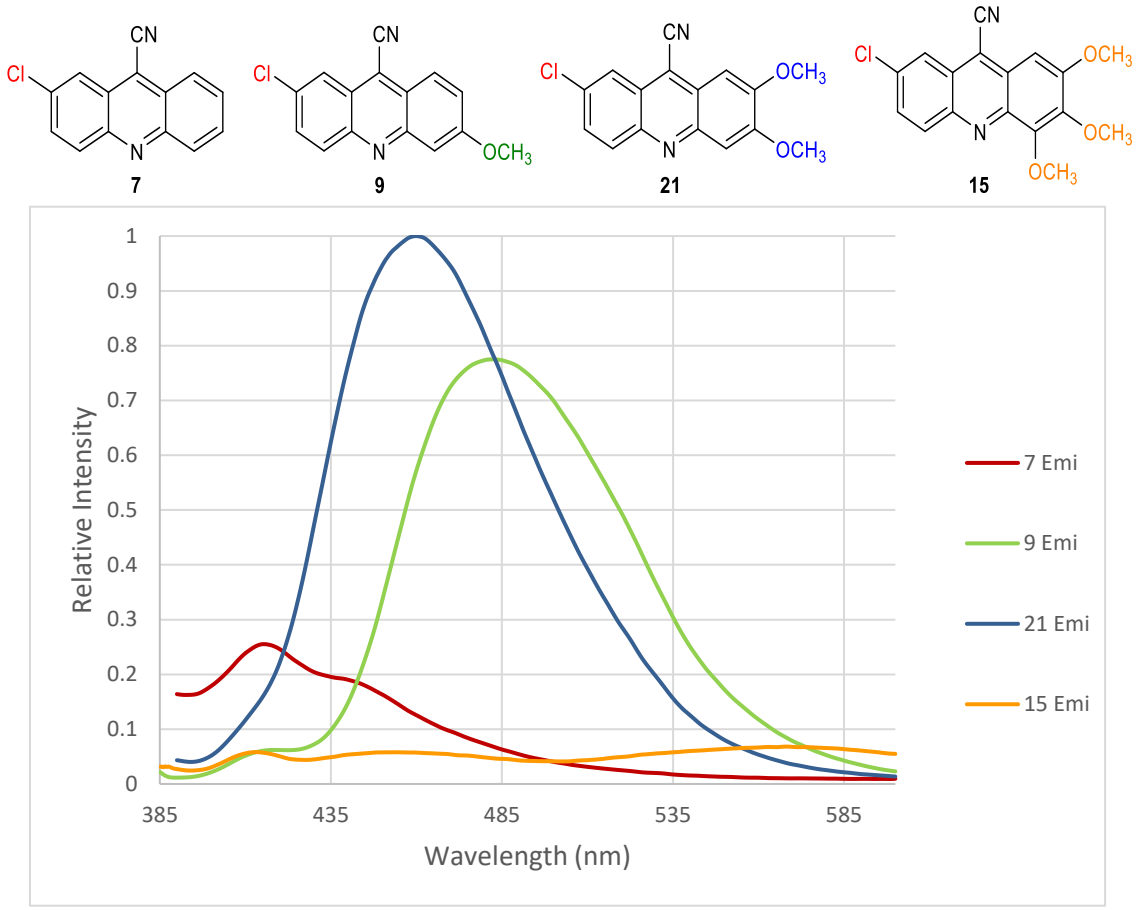

Figure 41: Normalised emission spectra of **7** (red), **9** (green), **15** (orange) and **21** (blue) at the same concentrations.

II.10.2.7.Bromo Substitution with Increase in the Number of Methoxy Group

It was observed that the absorbance intensity of mono-methoxy **11** was lower than the bromine only substituted acridine **8** (figure 42). However a progressive increase in intensity was observed (Figure 43) as the number of methoxy (EDG) increased to two **23** and three **19**. It is noteworthy to state that there was negative halochromism (i.e. reversible shift of the absorption band to shorter wavelength on further addition of the EDG)[304] between **8 (377.0 nm)** and**11** (367.0 nm) which was also present between **23 (402.0 nm)** and **19 (396.0 nm)**. There was a wide gap between the emission intensity of 7-bromo-2,

3-dimethoxyacridine-9-carbonitrile **23 (**figure 44**)** and others. It should be noted that the lowest emission intensity was observed in the mono-methoxy substituted compound **11.** However the emission maxima increases progressively as the number of methoxy substitution increases except for the mono-methoxy substituted which has the lowest. (i.e. **8** has 422-5 nm, **11** has 385.0 nm, **23** has 458.0 nm and **19** has 396.0 nm).

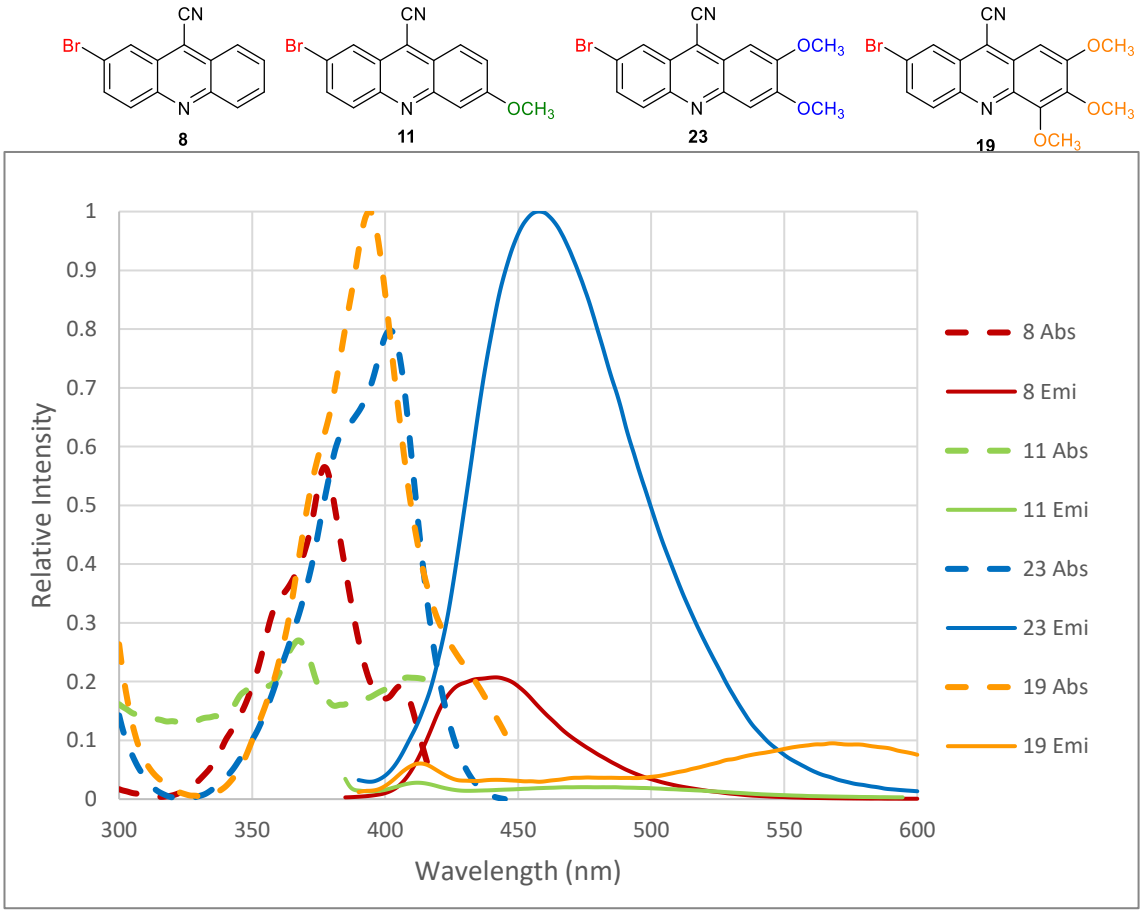

Figure 42: Normalised absorption (dashed lines) and emission (solid lines) spectra of **8** (red), **11** (green), **19** (orange) and **23** (blue) at the same concentrations.

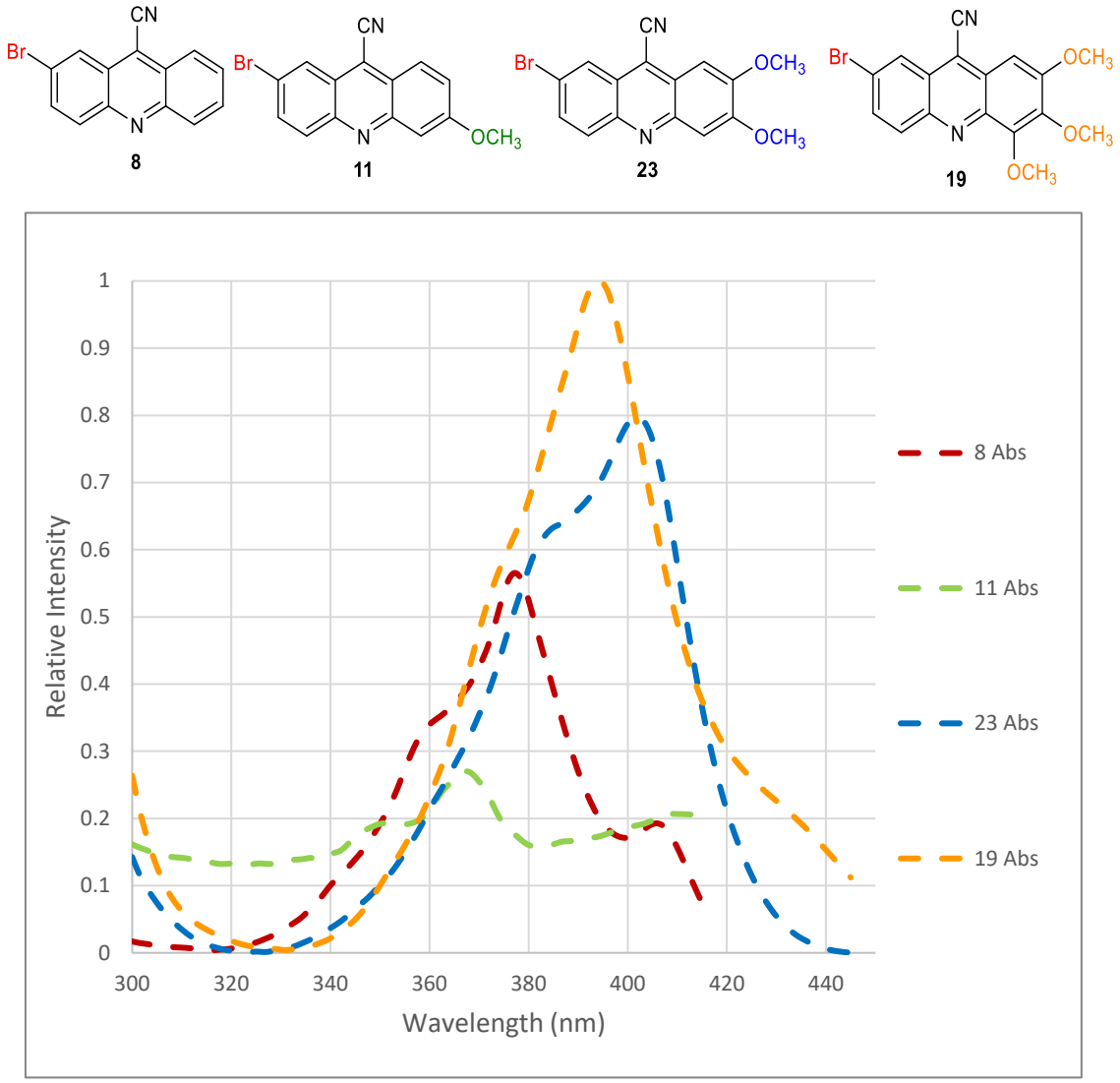

Figure 43: Normalise absorption spectra of **8** (red), **11** (green), **19** (orange) and **23** (blue) at the same concentrations.

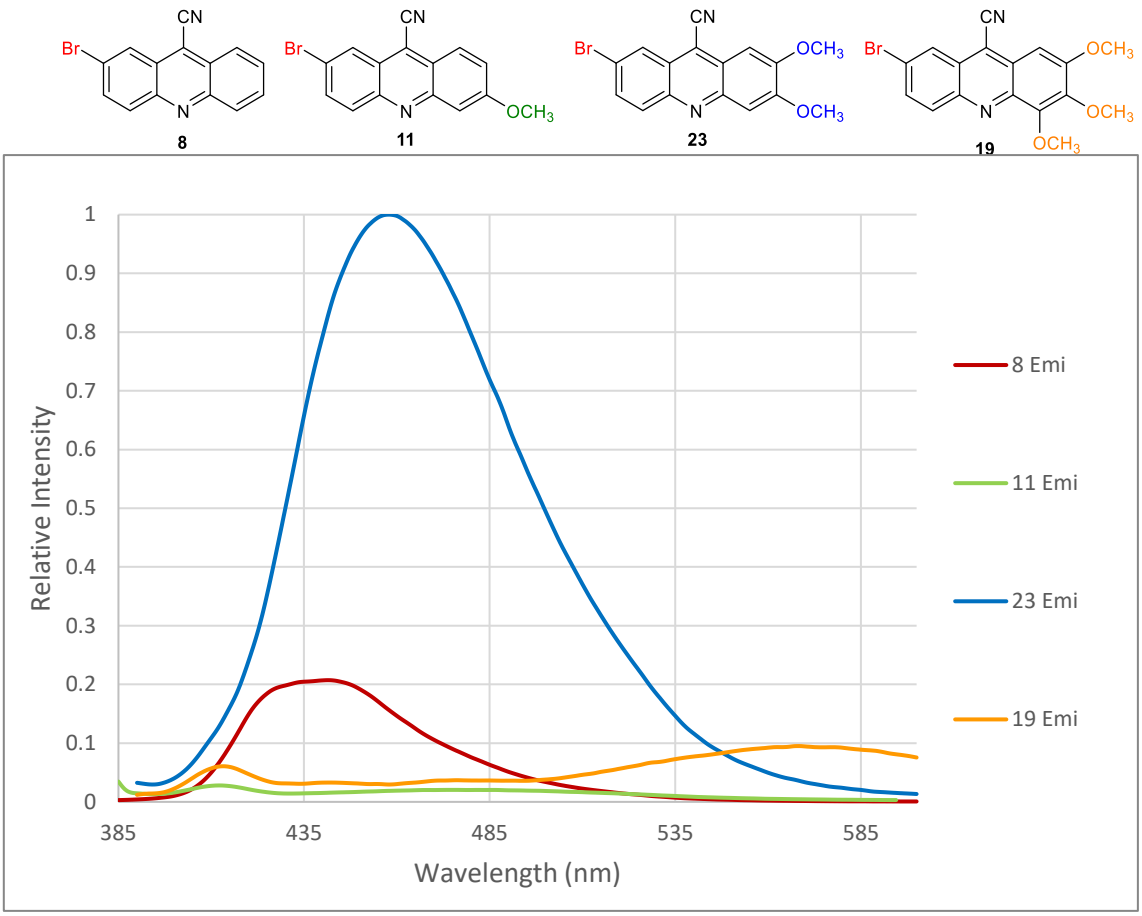

Figure 44: Normalised emission spectra of **8** (red), **11** (green), **19** (orange) and **23** (blue) at the same concentrations.

II.10.2.8.Iodo Substitution with Increase in the Number of Methoxy Group

It was observed that there was a reduction both in intensity and absorbance maxima with monosubstitution of methoxy on iodo acridine derivative **17** relative to 2-iodoacridine-9-carbonitrile **14.** Figures 45-47 elucidated all cases examined. Interestingly, there was a progressive red shift in the absorbance maxima as the number of methoxy substitution increases progressively. This was also accompanied with concomitant increase in the absorbance intensity. There was a red shift in absorbance maxima from mono-substitution **17** (370.0 nm) to di-substitution **20** (380.0 nm) and tri-substitution **16** (398.0 nm).

Surprisingly, the emission intensity for di-substitution was too high compares with others.

However, the emission maxima was in order of **20** < **14** < **16** < **17.**

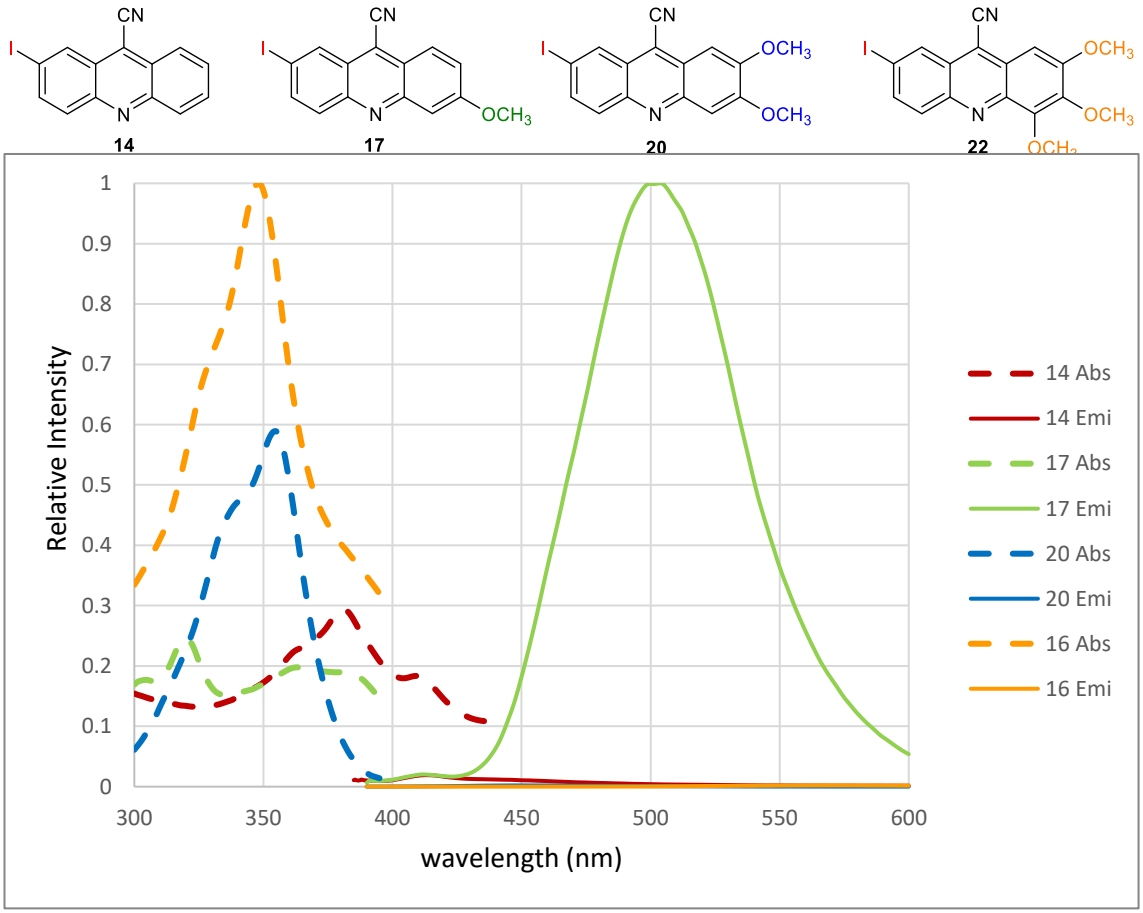

Figure 45: Normalised absorption and emission spectra of **14** (red), **16** (orange), **17** (green) and **20** (blue) at the same concentrations.

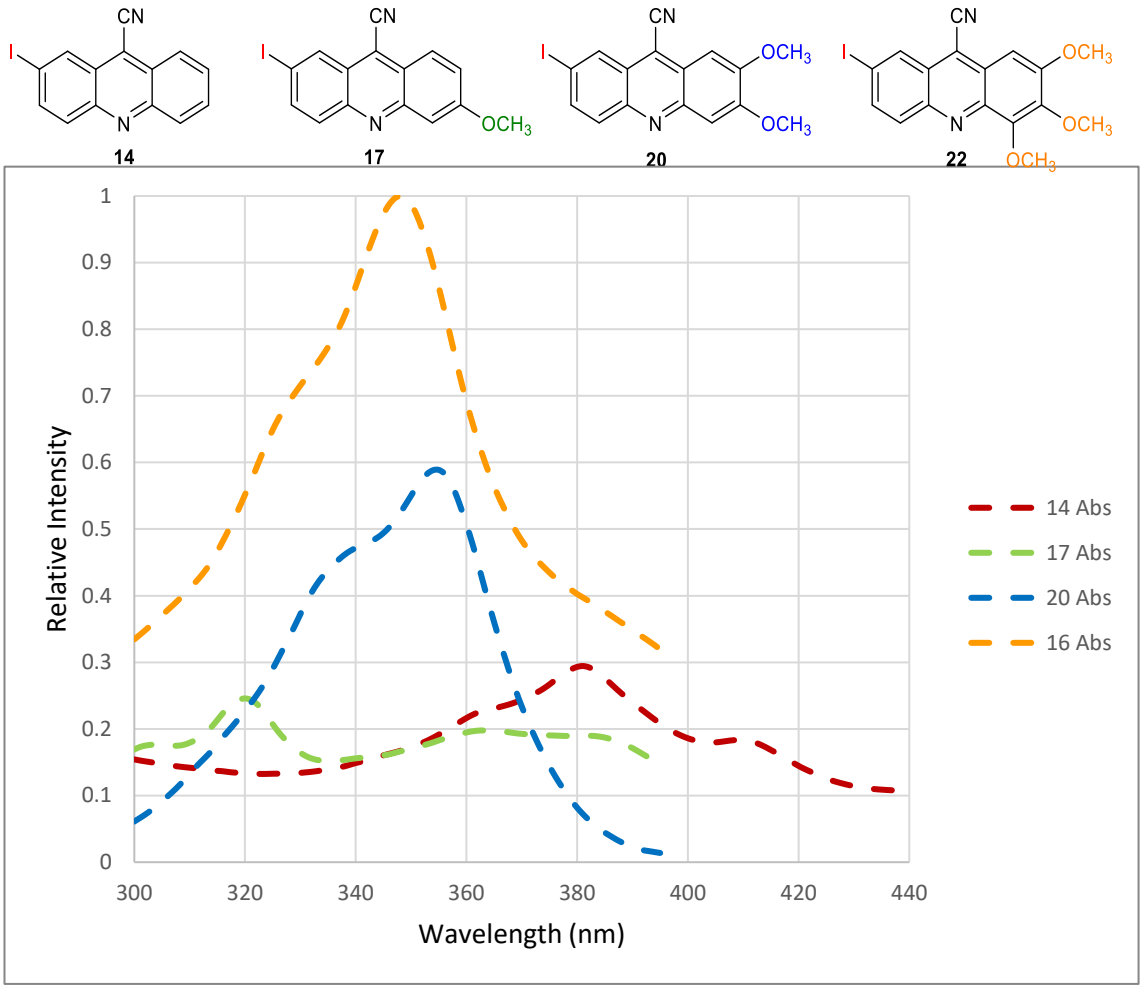

Figure 46: Normalised absorption spectra of **14** (red), **16** (orange)**, 17** (green) and **20** (blue) at the same concentrations.

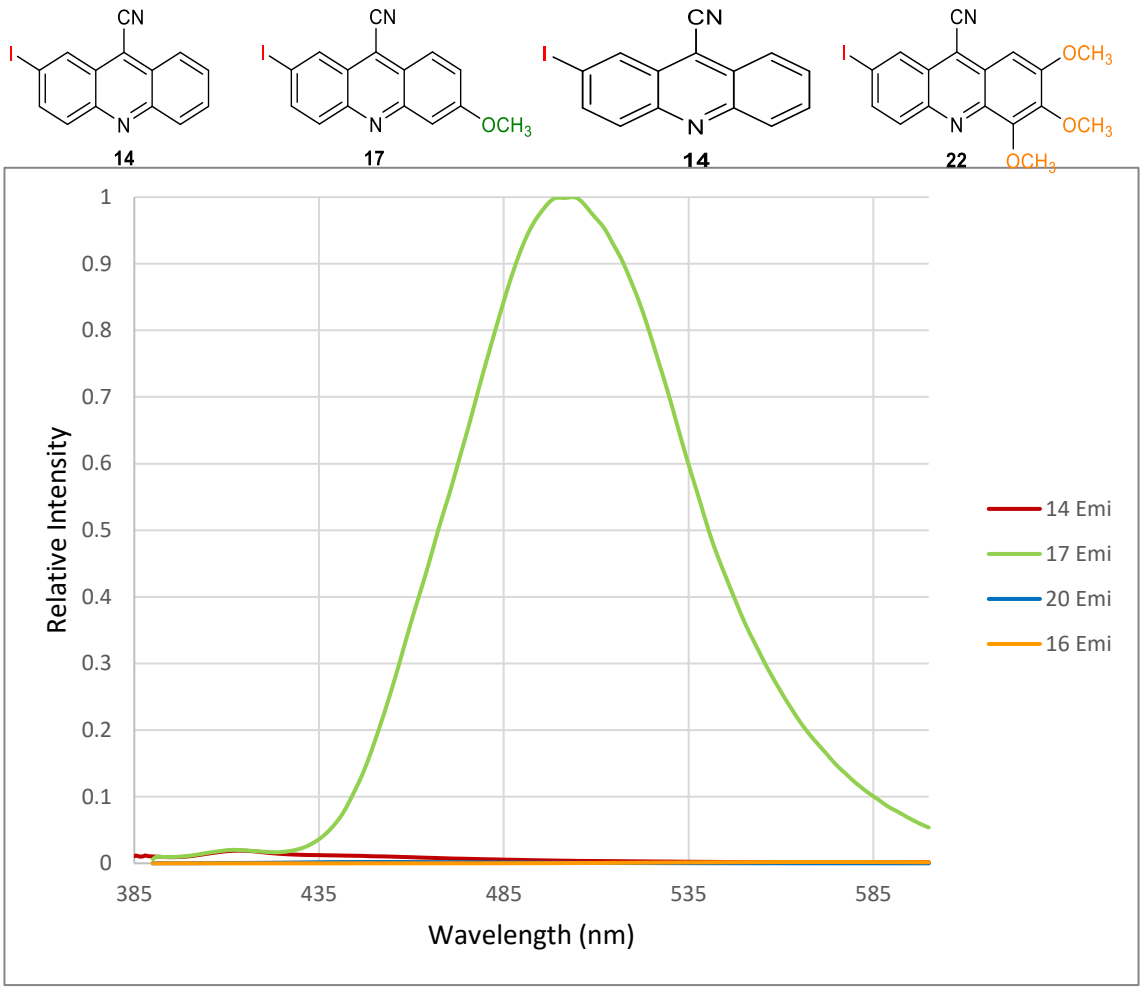

Figure 47: Normalised emission spectra of **14** (red), **16** (orange), **17** (green) and **20** (blue) at the same concentrations.

II.10.2.9.Methylsulfide Substitution with Increase in Number of Methoxy Group

In order to investigate the effect of poly substitution of EDG exclusively, without the influence of electron WDG on the photophysical properties a number of acridine derivatives were synthesised. In these compounds the halogen on one side of the ring was replaced with methyl sulphide. Our observation are presented in figures 48-50. Interestingly, both absorbance and emission intensities increased with increasing methoxy substitution. However, absorbance maxima decreased from mono-substitution **24** (455.5 nm) to di-substitution **32** (409.5 nm)**.** A red shift of 15.0 nm in absorbance maxima was observed from tri-substitution relative to di-substitution. The trend in

emission maxima indicated that the more the substitution the lower the emission maxima. That is mono-substituted **24** (with 514.5 nm) has the highest emission maxima followed by di-substituted **32** (with 494.5 nm), whilst tri-methoxy **27** (with 467.0 nm) has the lowest emission maxima

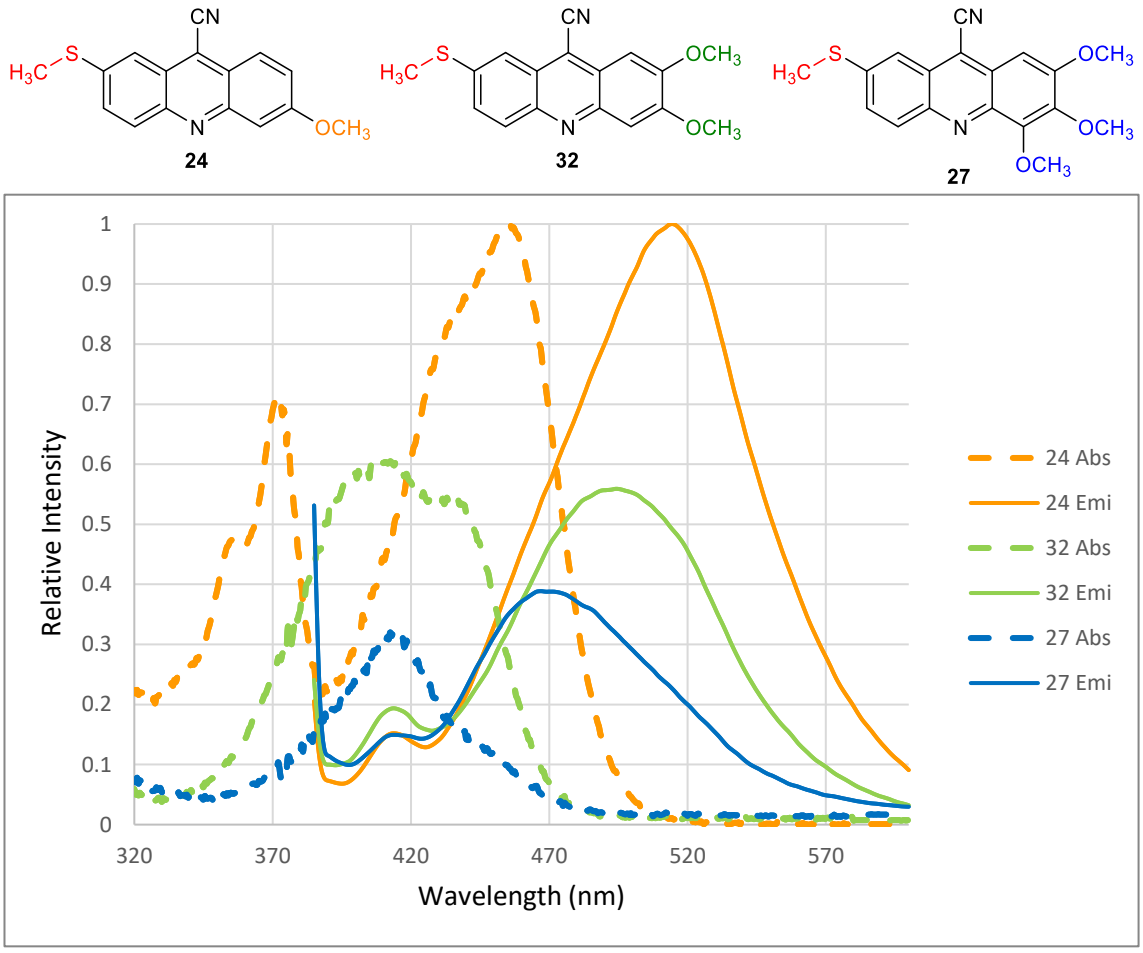

Figure 48: Normalised absorption (dashed lines) and emission (solid lines) spectra of **24** (orange), **27** (blue) and **32** (green) at the same concentrations.

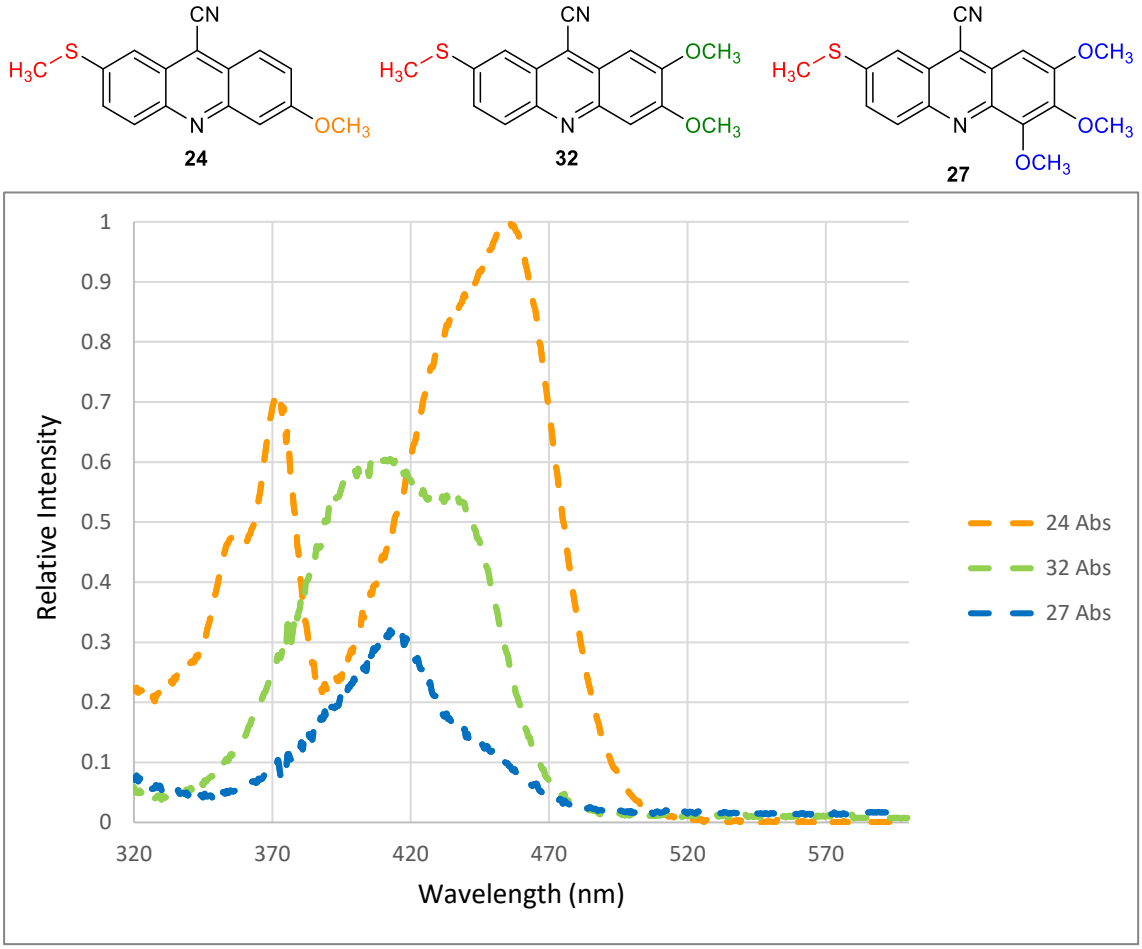

Figure 49: Normalised absorption spectra of **24** (orange), **27** (blue) and **32** (green) at the same concentrations.

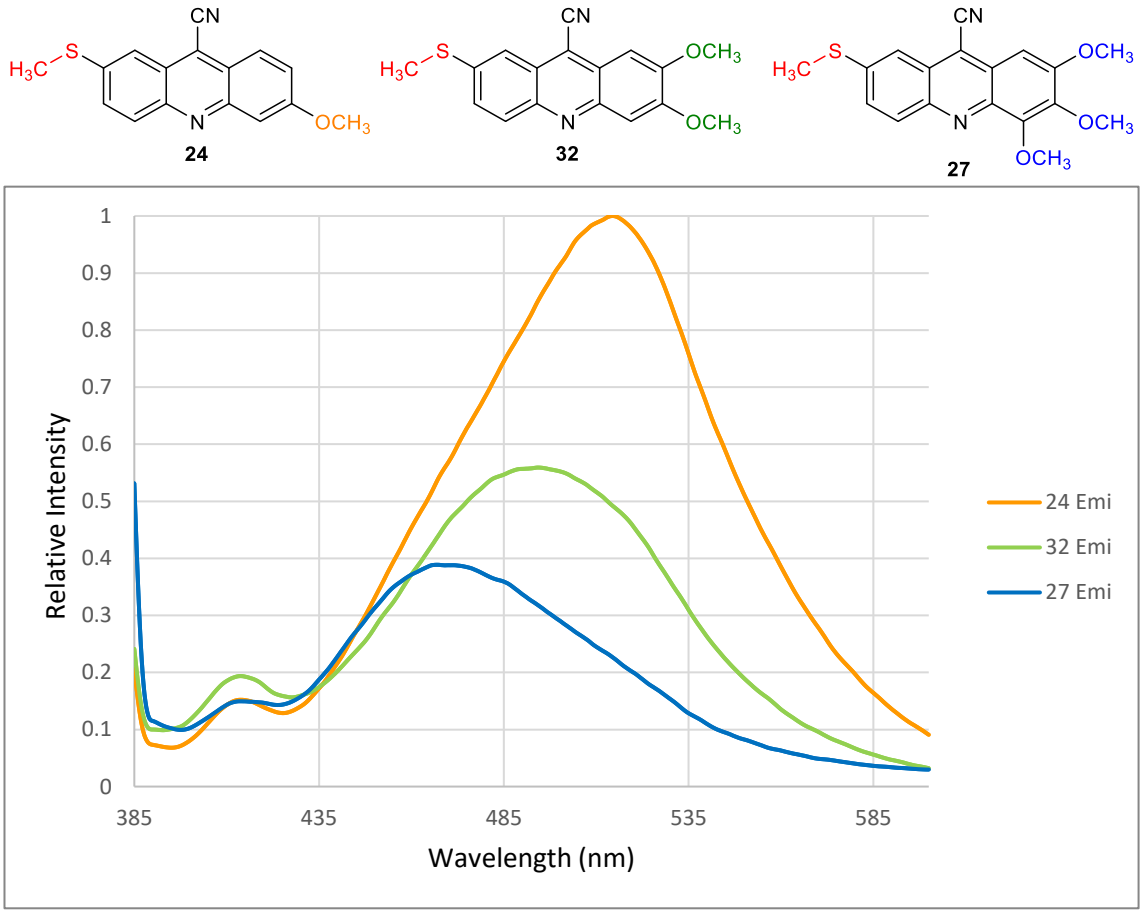

Figure 50: Normalised emission spectra of **24** (orange), **27** (blue) and **32** (green) at the same concentrations.

II.10.2.10.Comparism of Halogen Substituent on the Complexes

In order to understand the photophysical properties of acridine based gold(I) complexes so that it could be used as tools to unravel the mechanism of gold complexes, the effect of varying the halogen on position 2 of the organic ligand on the fluorescence properties of triphenyl phosphine gold(I) complexes was investigated. Figures 51-53 showed the cases examined. The fluorescence spectra of the complexes are modified significantly on changing the substituent and their position in the organic ligand.[305,306] It was observed that the absorbance intensity of mono-halogen substituted complexes followed no defined pattern. Iodo substituted **47** had the most intense absorbance followed by chloro substituted and bromo substituted was the least intense. There was a slight red shift in the absorbance of bromo substituted **42** (379.0 nm) compared with chloro substituted **41**

(377.0 nm). There was a blue shift on absorbance on the iodo substituted organic ligand of the complex. This is due to heavy atom effect. The emission intensity of the halogen substituted acridine gold(I) complexes decreased down the group. That is, the lower the inductive effect on the organic ligand of the complexes, the lower the emission intensities. However, as emission intensities decreases, there was a bathocromic shift in the emission maxima. The emission maxima increase as the atomic size increases. Thus, we have **41** with 412.5 nm, **42** with 414.5 nm and **47** with 481.25 nm.

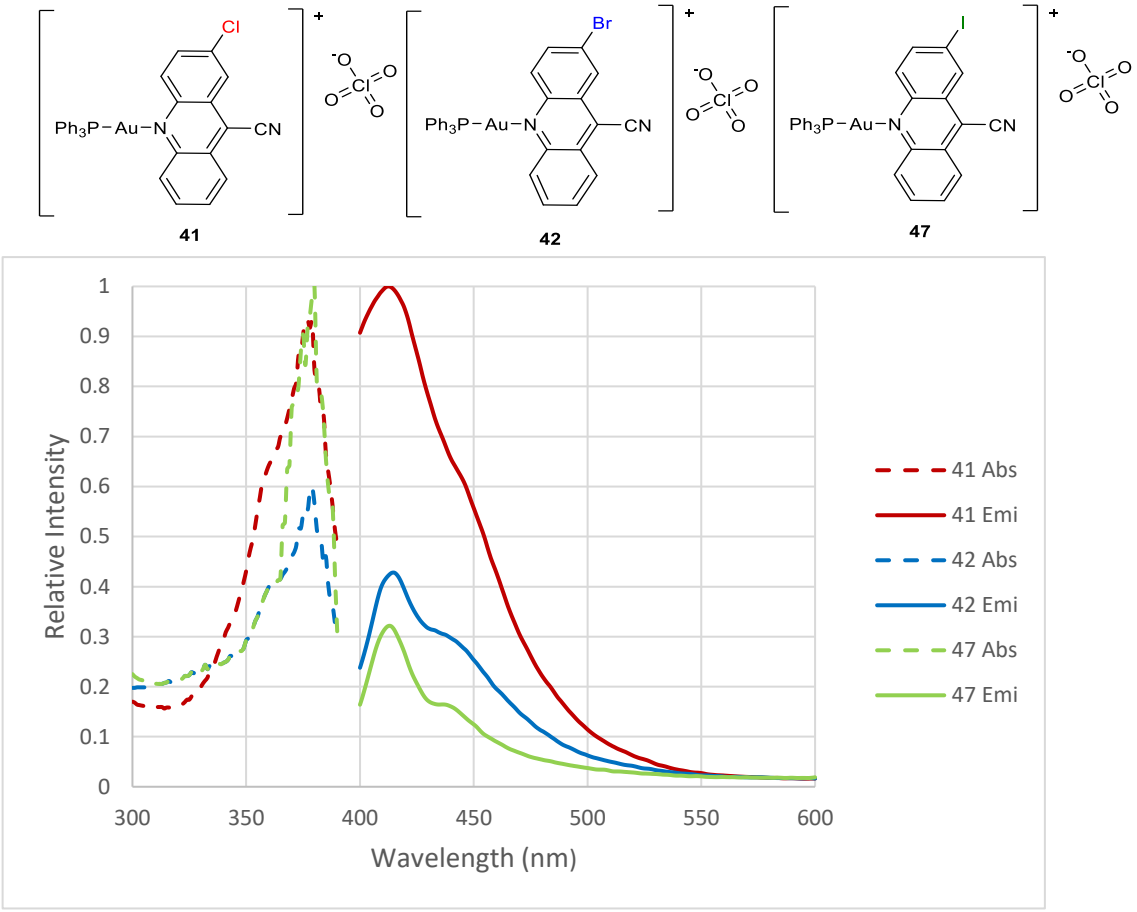

Figure 51: Normalised emission spectra of **24** (orange), **27** (blue) and **32** (green) at the same concentrations.

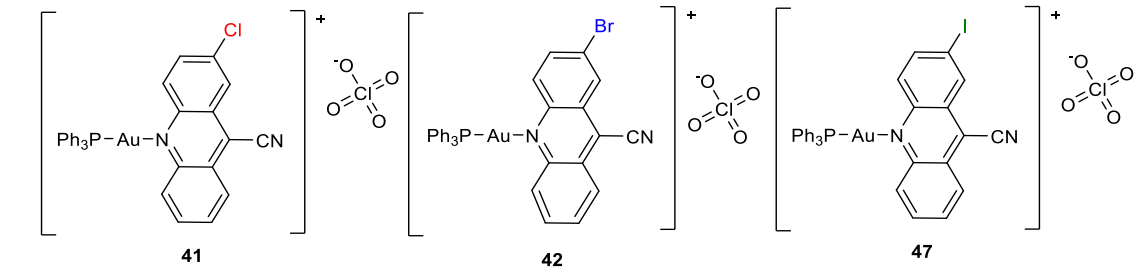

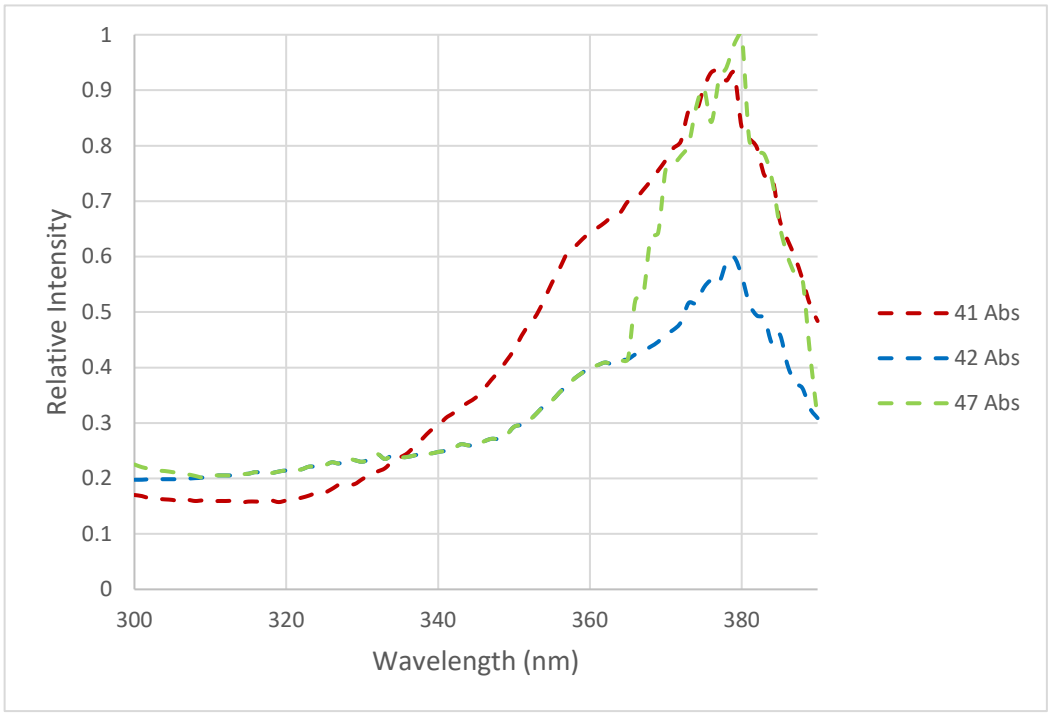

Figure 52: Normalised absorption spectra of **41** (red), **42** (blue) and **47** (green) at the same concentrations.

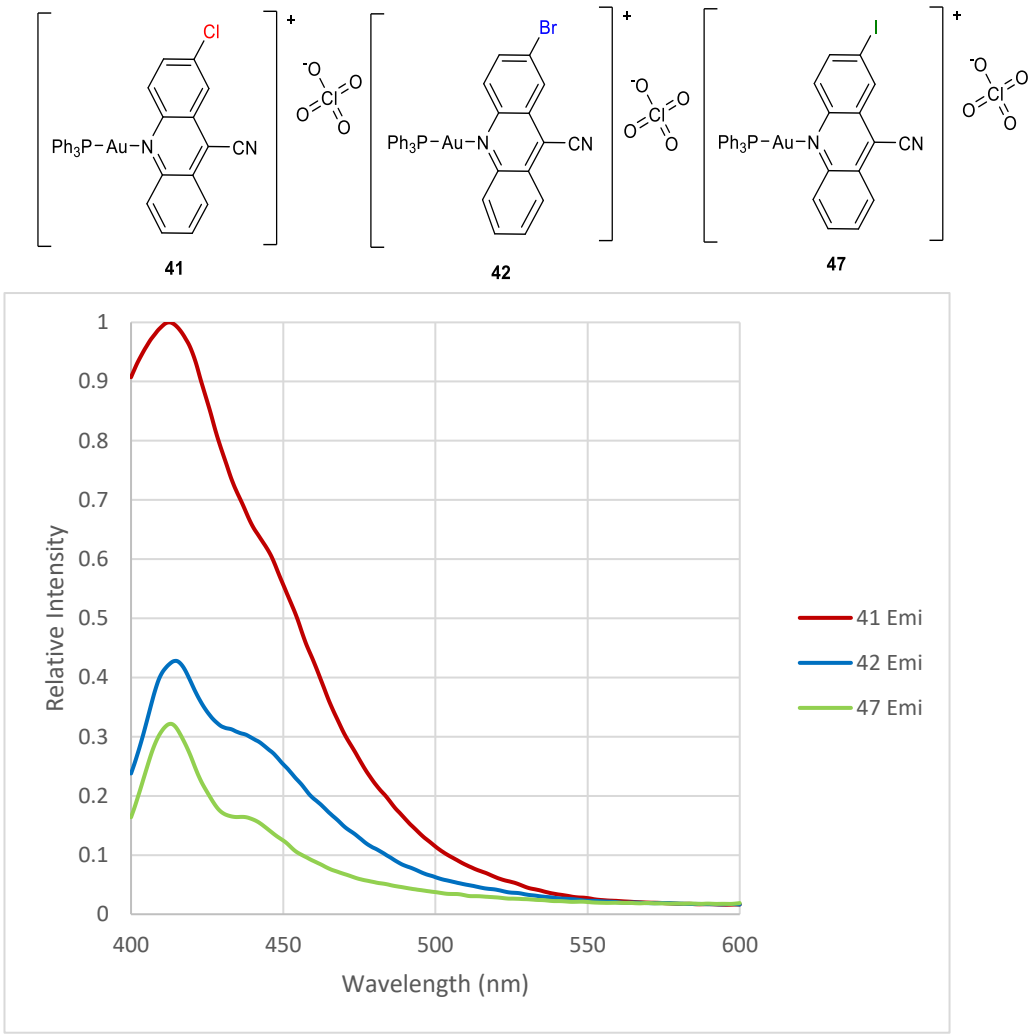

Figure 53: Normalised emission spectra of **41** (red), **42** (blue) and **47** (green) at the same concentrations.

II.10.2.11.Effect of Methoxy Group on the Complexes

Effect of EDG-EWG on acridine based triphenyl phosphine cathionic gold(I) complexes was also investigated. When the mono methoxy was substituted on the position 6 as electron donating group and halogen on position 2 as electron withdrawing group through inductive effect, it was observed that the chloro substituted had the highest intense absorbance. As expected, there was a bathocromic shift in the absorbance maxima from chloro substituted to iodo substituted. The absorbance maxima increases as the inductive effect of the EWG decreases. Thus it was observed that chloro substituted **43** (365.0 nm)

less than **44** (367.5 nm) less than **50** (371.0 nm). The emission intensities decreases (Figure 54) as the inductive effect decreases while the emission maxima increases as the inductive effect decreases. It was proposed that the absorbance and emission maxima of halogenated mono methoxy acridine triphenyl phosphine gold(I) complexes increase as the inductive effect of the halogen decreases. For the halogenated di-methoxy acridine gold(I) complexes, it was observed that the most intense absorbance was from the iodo substituted followed by chloro substituted and the bromo substituted was with the least intense absorbance. There was a red shift in the absorbance maxima of the bromo substituted **54** (402.0 nm) compares with the chloro substituted **53** (374.0 nm). A blue shift was observed for the iodo susbstituted **52** compares with the bromo substituted. The emission intensity decreases with decrease in inductive effect (figure 55). A red shift was observed for the emission maxima for bromo substituted compares with chloro substituted but there was a blue shift in iodo substituted compares with bromo substituted which could be attributed to intersystem crossing. Both the absorbance intensity and absorbance maxima increases as the inductive effect decreases for the halogenated trimethoxy acridine gold(I) derivatives (figure 56). Nevertheless, the emission intensity of bromo substituted was the highest followed by chloro substituted while iodo substituted was the least intense. Emission maxima for both chloro and bromo were the same while there was a blue shift compare with emission maxima for the iodo substituted derivative. It is noteworthy, to state that the absorption maxima showed expected progress shift to longer wavelength as the EDG increase on the ring.[304] The exception to the rule was the bromo substituted complex which showed a blue shift for trimethoxy substituted compared with the di-methoxy substituted.

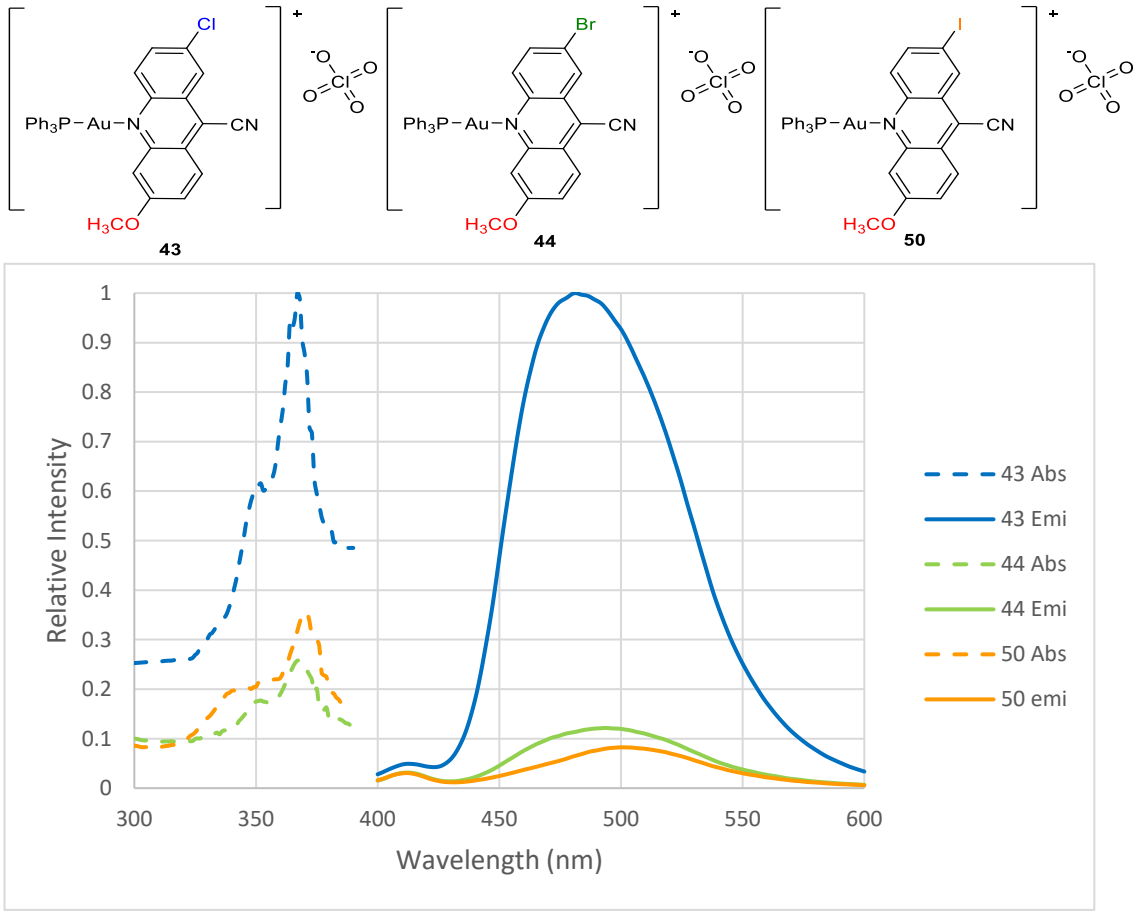

Figure 54: Normalised absorbance (dashed lines) and emission (solid lines) spectra of **43** (blue), **44** (green) and **50** (orange) at the same concentrations.

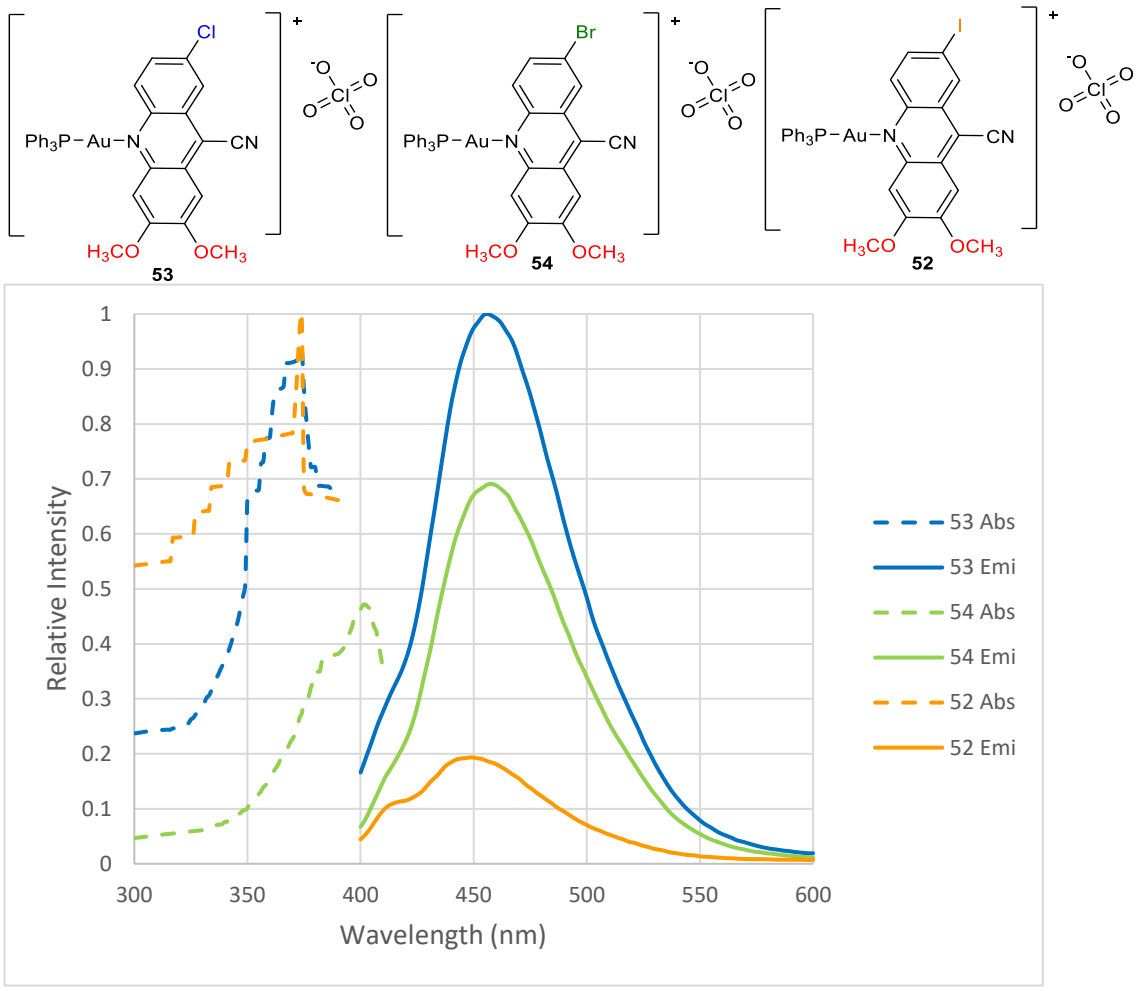

Figure 55: Normalised absorption (dashed lines) and emission (solid lines) spectra of **52** (orange), **53** (blue) and **54** (green) at the same concentrations.

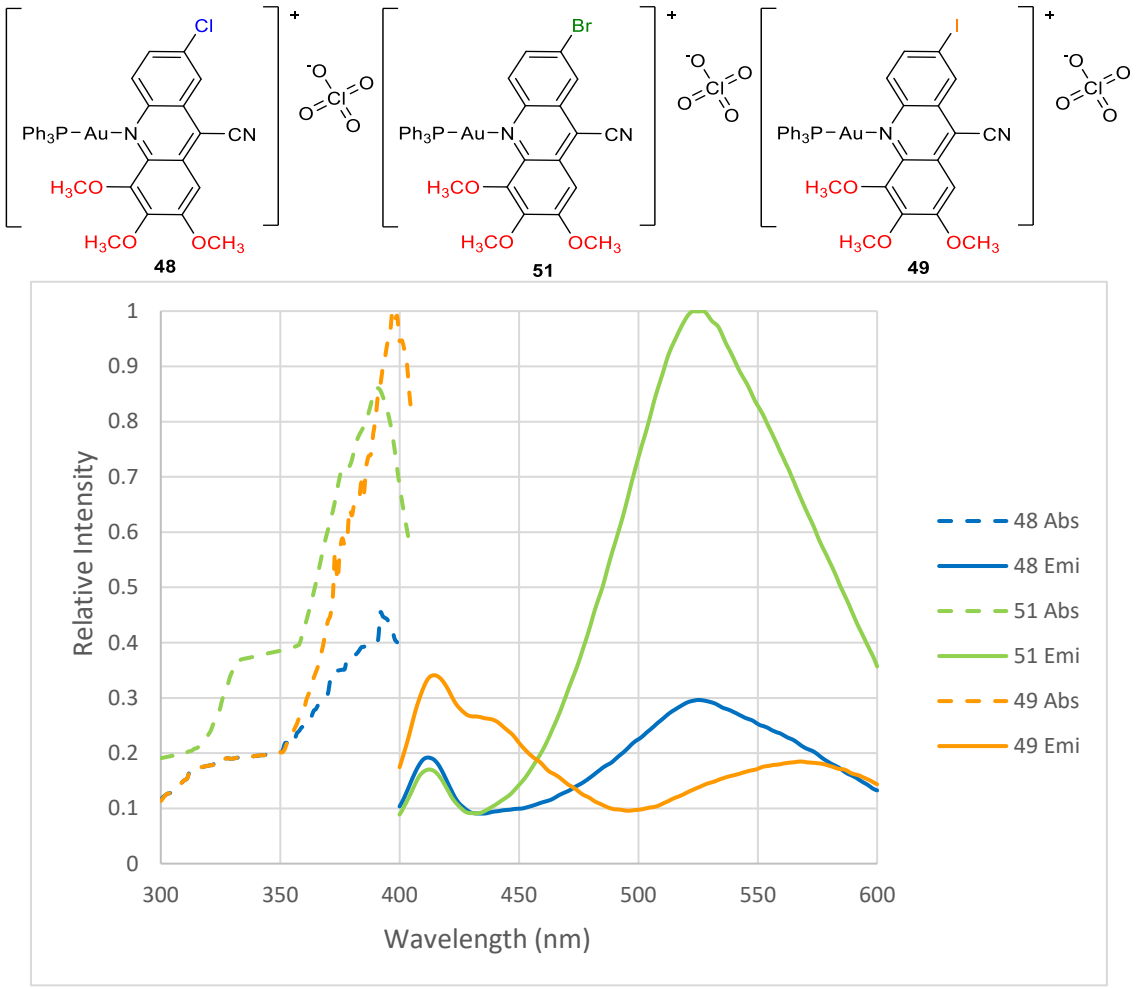

Figure 56: Normalised absorption (dashed lines) and emission (solid lines) spectra of **48** (blue), **49** (orange) and **51** (green) at the same concentrations.

II.10.2.12.Comparism of the Fluorescence Properties of the Free Ligands with the Corresponding Complex

It was observed that the absorption and emission intensities were higher in most of the complexes when compared to their corresponding free organic ligand (figures 57-61). The exceptions to this observed trend were cases when all the substituents are EDG. For instance when there is a methyl sulphide on position 7 and methoxy group were present on position 2, 3 and 4 (figures 58 and 59). The intensities of the ligands were greater than their corresponding complexes. For comparison of the absorbance and emission maxima, See Tables 24 and 25 on stokes shift.

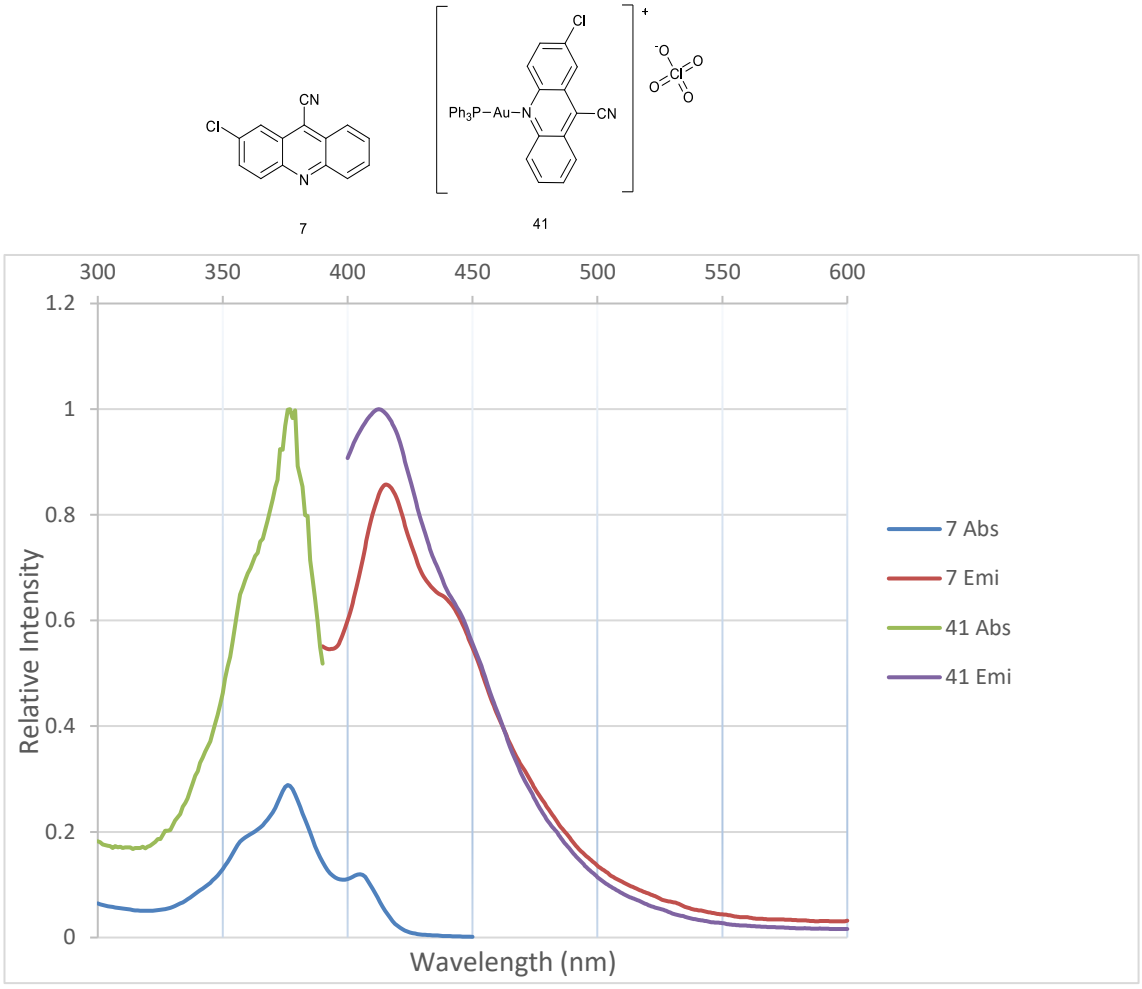

Figure 57: Normalised absorption and emission spectra of compound **7** and its corresponding complex **41** at the same concentrations.

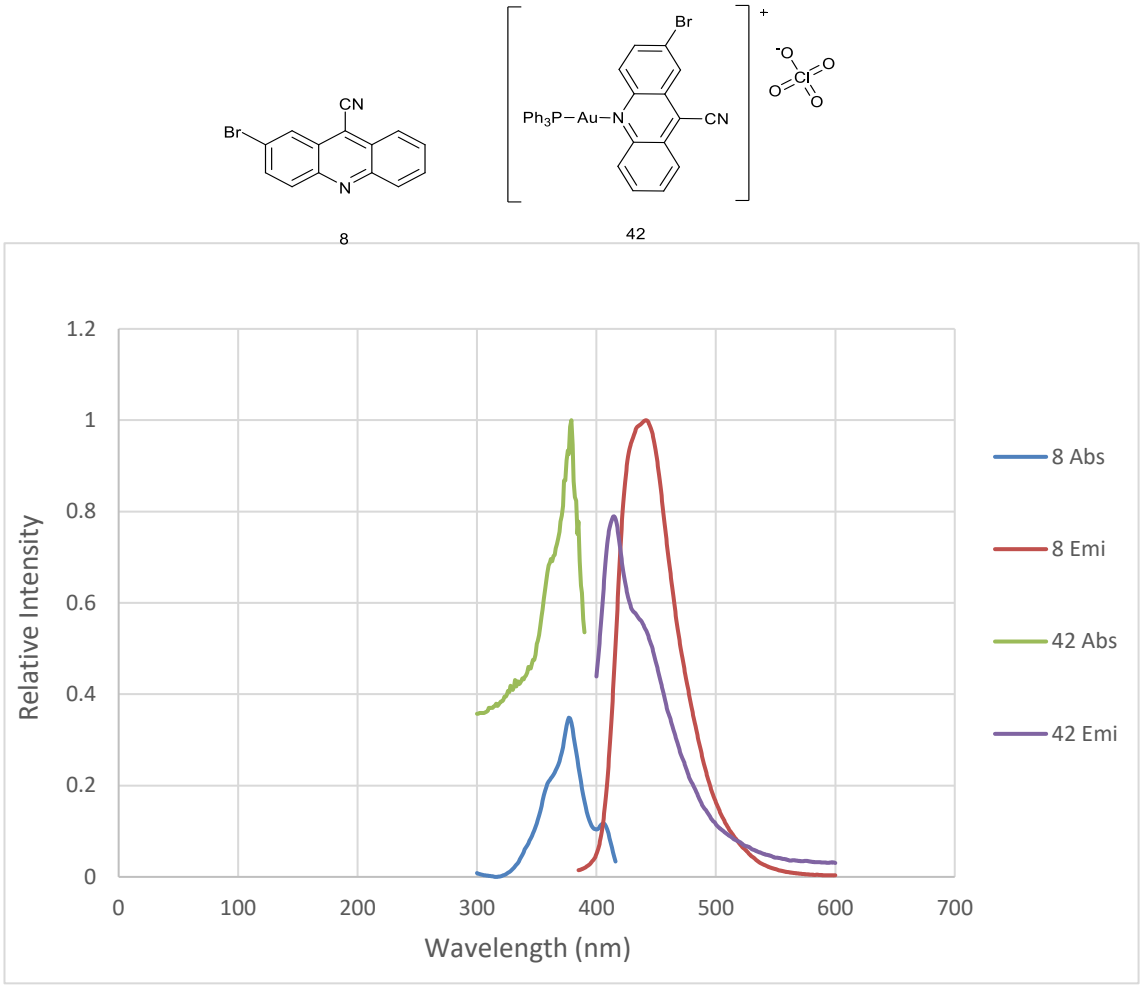

Figure 58: Normalised absorbance and emission spectra of compound **8** and its corresponding complex **42** at the same concentrations.

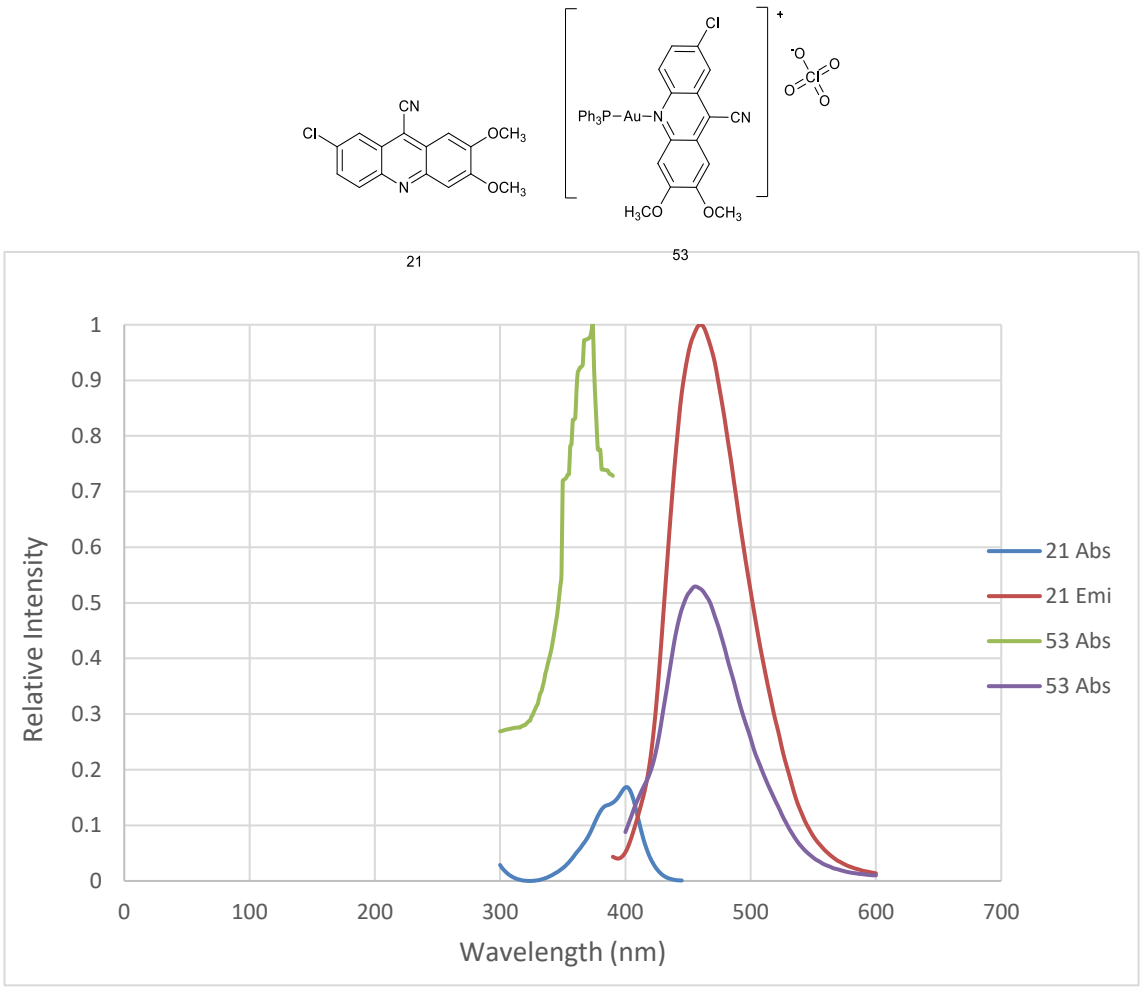

Figure 59: Normalised absorbance and emission spectra of compound **21** and its corresponding complex **53** at the same concentrations.

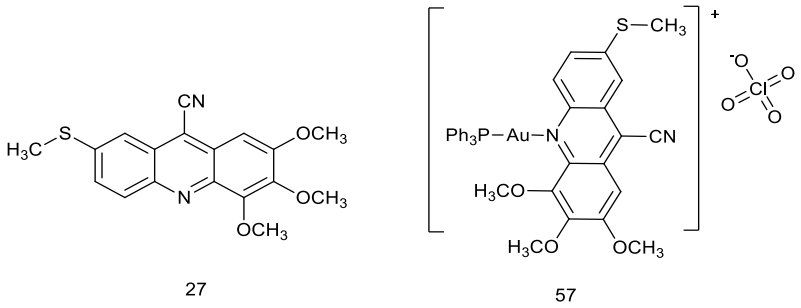

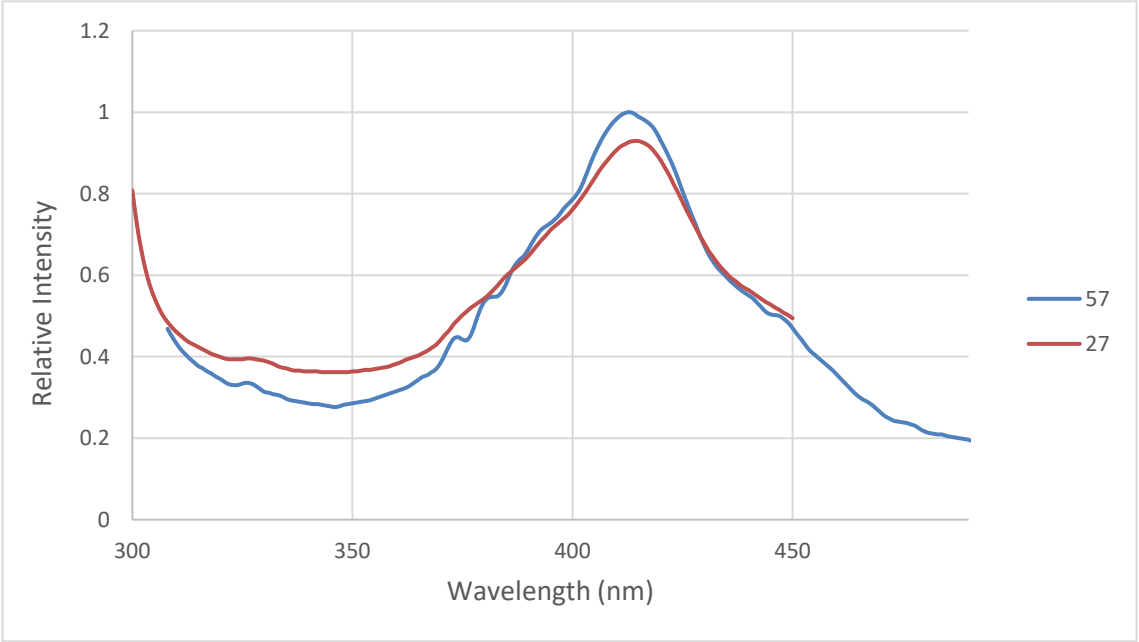

Figure 60: Normalised absorbance spectra of compound **27** and its corresponding complex **57** at the same concentrations.

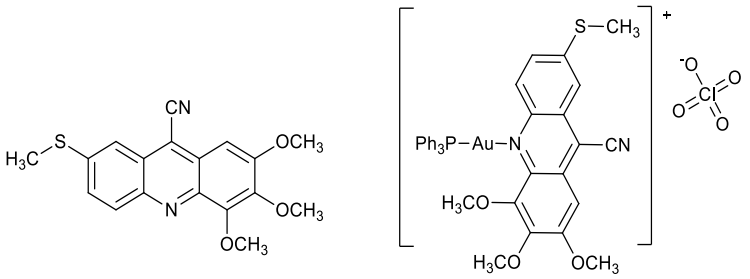

27

57

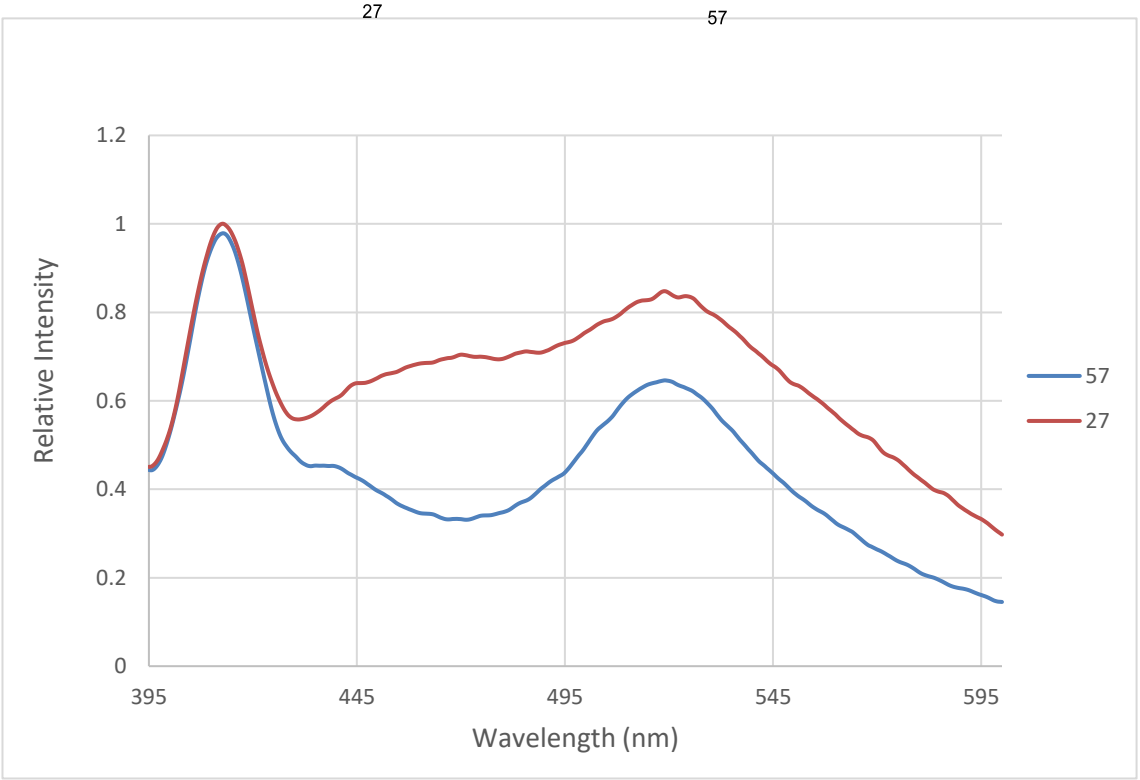

Figure 61: Normalised emission spectra of compound **27** and its corresponding complex **57** at the same concentrations.

II.10.2.13.Stoke shift for ligands and complexes

The differences in the wavelength between the position of absorption maxima and the emission maxima of the same electronic transition of a compound is called the Stokes shift. If the molecule fluoresces, the emitted photon has a lower energy than the excitation photons and that is why the emission spectra is red shifted when compared to the absorption spectrum.[307] A stoke shift of a chromophore suggests the displacement in potential surface between the ground state and excited state with a loss of vibrational energy in the excited state.[308] Fluorescent dyes with large stokes shift and good photo-stability are desirable for biological and microscopy study. [309] A fluorophore dye is

considered to exhibit small Stokes shift if its less than 80 nm and large if it is above that value. [309] Small Stoke shift proposes that the molecular structure of a compound in the ground state is the same with that in its excited state. [310] It gives rise to reabsorption of emitted photons leading to unwanted background interferences.[309]The Stokes shift values on the prepared complexes and their constituent free ligands are provided below (Table 24-26). Interestingly, there was a considerable stoke shift for both the ligands and the complexes. For the ligands, the smallest Stokes shift was observed in the compound **18** with 13.5 nm while both compounds **9** and **21** has the highest value with 125.5 nm each. It is worth to note that more than half of the free ligands under investigation have high Stokes shift values of 80.0 nm and above. For the complexes, compound **49** has the lowest observed Stokes shift with the value of 17.5 nm, while compounds **48** and 51 has the highest value of 133.0 nm. Also more than half of the complexes showed high Stokes shift of 80.0 nm and above. It should be added that considerable number of these novel acridine ligands and complexes exhibited a great differences in the Stokes shift between the ligands and their corresponding complexes as observed in table 26. Ligand **11** and its corresponding complex **44** has the highest Stokes shift difference of 81.0 nm while compound **7** and its corresponding complex **41** has the least value with 0.0 nm.

Table 24: Stokes shift for the ligands

Entry	compound	λmax Abs	λmaxEmi	Stoke's shift
1	**7**	377.0	412.5	35.5
2	**8**	377.0	422.5	45.5
3	**9**	367.0	492.5	125.5
4	**11**	367.0	385.0	18.0
5	**13**	351.1	431.5	80.4
6	**14**	381.5	453.5	72.0
7	**15**	392.5	480.5	88.0
8	**16**	398.0	475.0	77.0
9	**17**	370.5	476.5	106.0
10	**18**	371.5	385.0	13.5
11	**19**	396.0	473.0	77.0
12	**20**	380.0	413.5	33.5
13	**21**	367.0	492.5	125.5
14	**23**	402.0	458.0	56.0
15	**24**	455.5	514.5	59.0
16	**25**	443.5	523.5	80.0
17	**27**	414.5	467	52.5
18	**28**	360	473	113.0
19	**29**	365	476.5	111.5
20	**30**	398.5	462	63.5
21	**32**	409.5	494.5	85.0
22	**33**	361.5	485	123.5

Table 25: Stoke shift for the complexes

Entry	compound	λmax Abs	λmaxEmi	Stokes shift
1	**41**	377	412.5	35.5
2	**42**	379	414.5	35.5
3	**43**	365	476.25	111.25
4	**44**	367.5	493.5	126
5	**45**	369	427	58
6	**46**	371	431	60
7	**47**	380	413	33
8	**48**	392	525	133
9	**49**	397	414.5	17.5
10	**50**	371	500	129
11	**51**	392	525	133
12	**52**	374	448.5	74.5
13	**53**	374	455.75	81.75
14	**54**	402	457.5	55.5
15	**55**	455	521.5	66.5
16	**56**	445	526	81
17	**57**	385	413	28
18	**58**	378	466.5	88.5
19	**59**	409.5	502	92.5

Table 26: Ligands Stokes shift compares with their corresponding complexes

		Ligands				Complexes			Comparison		
Entry	**Compound**	λmaxab	λmax Emi	Stoke's shift	**Compound**	λmax Ab	λmaxEmis	Stoke's shift	ΔλAb	ΔλEmi	Δ Stoke's shift
1	**7**	377.0	412.5	35.5	**41**	377.0	412.5	35.5	0.0	0.0	0.0
2	**8**	377.0	422.5	45.5	**42**	379.0	414.5	35.5	2.0	8.0	10.0
3	**9**	367.0	492.5	125.5	**43**	365.0	481.25	111.25	2.0	13.3	14.3
4	**11**	367.0	412.0	45.0	**44**	367.5	493.5	126	0.5	81.5	81.0
5	**13**	351.1	431.5	80.4	**46**	371.0	430.5	59.5	19.9	1.0	20.9
6	**14**	381.5	453.5	72.0	**47**	380.0	413.0	33.0	1.5	40.5	39.0
7	**15**	392.5	480.5	88.0	**48**	392.0	525.0	133.0	0.5	44.5	45.0
8	**16**	398.0	475.0	77.0	**49**	397.0	414.5	17.5	1.0	60.5	59.5
9	**17**	370.5	476.5	106.0	**50**	371.0	500.0	129.0	0.5	23.5	23.0
10	**19**	396.0	473.0	77.0	**51**	392.0	525.0	133.0	4.0	52.0	56.0
11	**20**	380.0	413.5	33.5	**52**	374.0	448.5	74.5	6.0	35.0	41.0
12	**21**	367.0	492.5	125.5	**53**	374.0	455.8	81.75	7	36.8	43.8
13	**23**	402.0	458.0	56.0	**54**	402	457.5	55.5	0	0.5	0.5
14	**24**	455.5	514.5	59	**55**	455	521.5	66.5	0.5	12.5	7.5
15	**25**	443.5	523.5	80.0	**56**	445.0	526.0	81.0	1.5	1.5	1.0

	Ligands				Complexes				Comparison		
Entry	**Compound**	λmaxab	λmax Emi	Stoke's shift	**Compound**	λmax Ab	λmaxEmis	Stoke's shift	ΔλAb	ΔλEmi	Δ Stoke's shift
16	**27**	414.5	519.0	104.5	**57**	413.0	519.5	106.5	1.5	0.5	2.0
17	**30**	398.5	462.0	63.5	**58**	378.0	466.5	88.5	20.5	4.5	25
18	**32**	409.5	494.5	85.0	**59**	409.5	502.0	92.5	0.0	7.5	7.5

II.10.2.14.Qantum Yield for Ligands and Complexes

Fluorescence quantum yield determines the efficiency of fluorescence process.[284] It is usually denoted as the number of emitted photons divided by the number of absorbed photons.[311] In order to investigate the quantum yield of the novel acridine derivatives and their corresponding complexes, 9,10-diphenylanthracene was used as the standard. This was chosen as it absorbed and emit in a similar region to investigated compounds in ethanol solvent.[312,313] The quantum yield was calculated using the equation delineated below:

$$\phi_{F(x)} = \phi_{F(s)} \times (Fx/ Fs) \times (Ab_s/Ab_x) \times (n_x/ n_s)^2$$

Where $\phi_{F(x)}$ is the fluorescence quantum yield of unknown, $\phi_{F(s)}$ is the fluorescence quantum yield of the standard, Ab_s is the absorbance of the standard at the excitation wavelength, Ab_x is the absorbance of the unknown at the excitation wavelength and n is the refractive index of the solvent. Subscripts x and s refer to unknown and the standard. Tables 27 and 28 showed the result obtained for the acridine ligands and complexes.

Table 27: Quantum yield of the ligands

ENTRY	COMPOUND	QUANTUM YIELD
1	**7**	0.16
2	**8**	0.62
3	**9**	0.30
4	**11**	0.61
5	**13**	0.14
6	**14**	0.30
7	**15**	0.22
8	**16**	0.41
9	**17**	0.71
10	**18**	0.59
11	**19**	0.29
12	**20**	0.36
13	**21**	0.60
14	**23**	0.51
15	**24**	0.15
16	**25**	0.39
17	**27**	0.85
18	**28**	0.30
19	**29**	0.42
20	**30**	0.91
21	**32**	0.25
22	**33**	0.30

Table 28: Quantum yield for the complexes

ENTRY	COMPOUND	QUANTUM YIELD
1	**41**	0.21
2	**42**	0.37
3	**43**	0.95
4	**44**	0.23
5	**45**	0.19
6	**46**	0.23
7	**47**	0.24
8	**48**	0.30
9	**49**	0.24
10	**50**	0.17
11	**51**	0.18
12	**52**	0.13
13	**53**	0.11
14	**54**	0.17
15	**55**	0.29
16	**56**	0.55
17	**57**	0.18
18	**58**	0.74
19	**59**	0.51

Interestingly, good to excellent quantum yield were observed for both the free ligands and the complexes when compared with the literature values of similar compounds. The quantum yield of acridine derivatives varies widely in the literature depending on the substituents attached or the solvent used. For example neutral acridine orange in ethanol has quantum yield of 0.20 while cationic acridine orange in ethanol has a quantum yield of 0.46.[314] 9- amino acridine in ethanol Φ_F was 0.99 while acridone in ethanol was 0.83[315,316] The quantum yield obtained for the ligands ranges from 0.15 to 0.91 while that of the complexes ranged from 0.11 to 0.95 It was proposed that the electron donating group influences the quantum yield both in the free ligands and the complexes. This was based on the fact that the highest quantum yield (0.91) for ligands was observed in the ligand **30** with only electron donating group in both side (Figure 62) followed by **27 (**0.85) followed by **17** (0.71), followed by **21**(0.60).Also, the highest quantum yield (0.95) in complexes was observed for compound **43** followed by compound **58** (0.74). It is noteworthy to state that both of these compounds contained electron-donating group (figure 63). However, halogen may influence the rate of intersystem crossing in compounds **52, 53** and **54** leading to low quantum yield observed.[290,317]

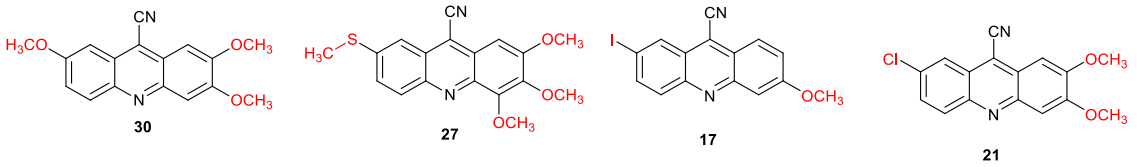

Figure 62: Structures of compounds **17, 21, 27** and **30**

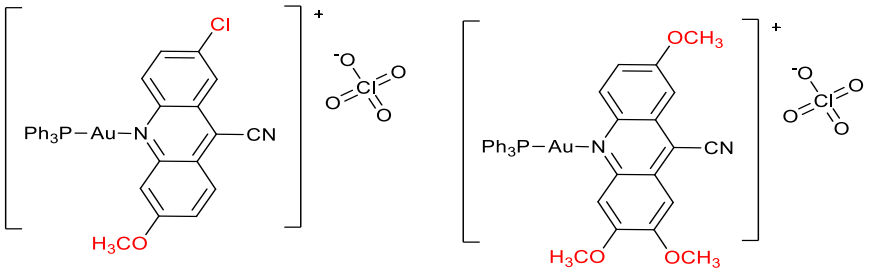

Figure 63: Structures of the compounds **43** and **58**

II.11. Cell Viability Assays

II.11.1 Cytotoxicity of The Pyrazole Gold(I) Complexes

The biological activity of the complexes were assessed after dilution in DMSO/H_2O (10% v/v) and addition to HepG2 cells. Assays were performed in 96-well plates using the Promega CellTiter-Blue assay as an endpoint method with a 2-hour incubation with the assay reagent. This assay measures cell viability and is based upon the ability of living cells to convert a redox dye (resazurin) into a fluorescent product (resorufin). Each well received 90 µL of cell suspension at a density of 22,500 cells per well and was cultured overnight (at 37 °C/5% CO_2 humidified air) before 10 µL of the test sample was added. The experiments were set up in triplicate. The mock control wells received 90 µL of cell suspension and 10 µL of the appropriate buffer (DMSO/H_2O). Wells that contained just 100 µL of cell culture medium served as background fluorescence controls. Fluorescent readings were taken using the GloMax-Multi Detection System (Promega). The five complexes shown in Table 10 all indicated that they possessed reasonable

activity against this cell line in a preliminary screen (data not shown). To confirm this activity various doses were then tested alongside their respective un-complexed ligands. Figure 64 shows that even at the lowest dose tested (20 μM) all of the complexes showed high activity. In contrast the free ligands showed no significant activity at the same concentrations (Figure 65). Due to the high level of activity observed, further dilutions were made and tested (Figure 66). These data indicate that complexes 63a, 64a, 65b and 66b remain highly toxic at 2 μM while 62 is significantly less toxic at this concentration. IC_{50} values were calculated as 1.75 μM (6), 0.19 μM (7b), 0.31 μM (8b), 0.13 μM (9a) and 0.23 μM (10a).

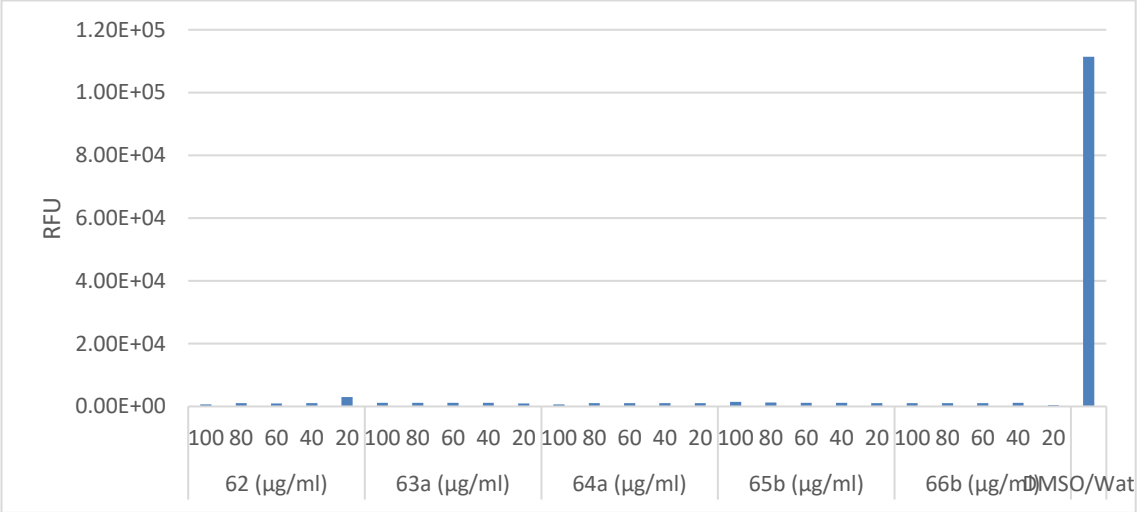

Figure 64: Toxicity data for the gold complexes **62-66b** against HepG2 cells. Five doses of each compound were tested, background fluorescence was subtracted from each reading and the resulting values are shown relative to a buffer-only control (100% viability). Controls performed under full assay conditions confirmed that none of the compounds, or the separate ligands, interfered with the readings when tested at a concentration of 18 μM in the absence of cells.

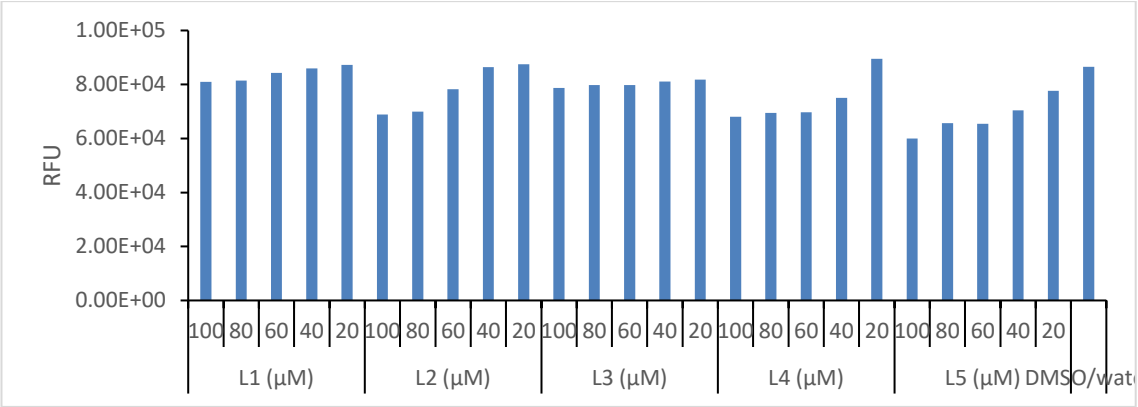

Figure 65: Toxicity data for the free pyrazole ligands indicated that there was no significant activity against HepG2 cells at the same concentration.

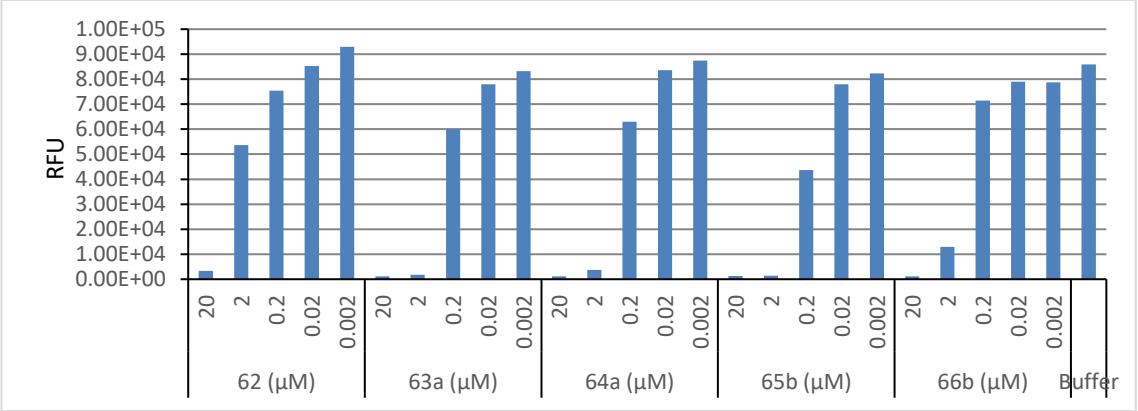

Figure 66: Dose response assay of gold complexes against HepG2 cells. Five doses of each complex were tested, background fluorescence was subtracted from each reading and the resulting values are shown relative to a buffer-only control (100% cell viability).

II.11.2. Cytotoxicity of Acridine Gold(I) Complexes

To assess their activity against the human cancer cell line HepG2 eight complexes were initially tested at a single dose of 20 µM and the results are shown in Figures 67 and 68. Complexes **48**, **49** and **51** showed little toxicity at this concentration whereas **42**, **45** and **47** were the most effective.

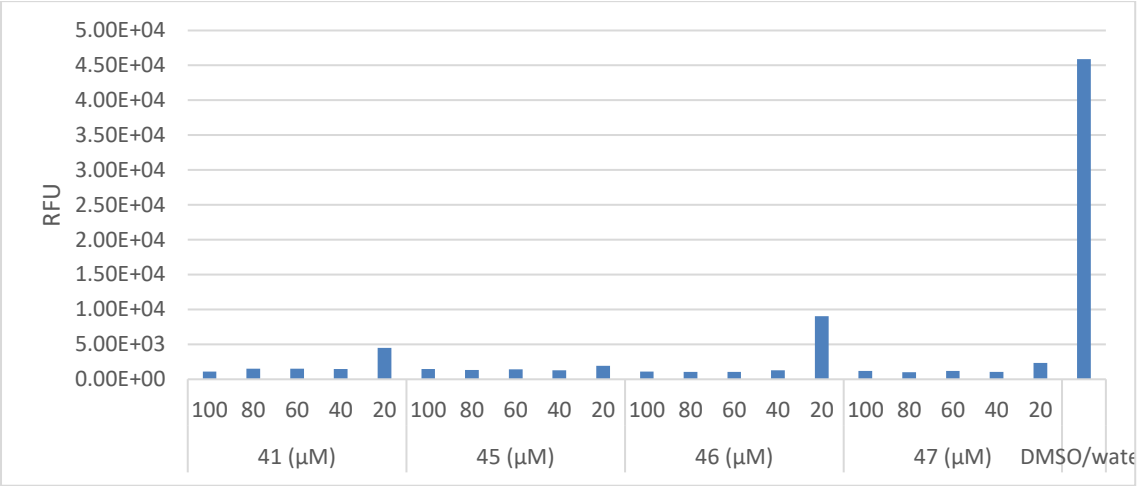

Figure 67: Toxicity of the acridine / gold (I) complexes against HepG2 cells. Background fluorescence was subtracted from each reading and the resulting values are shown relative to a buffer-only control

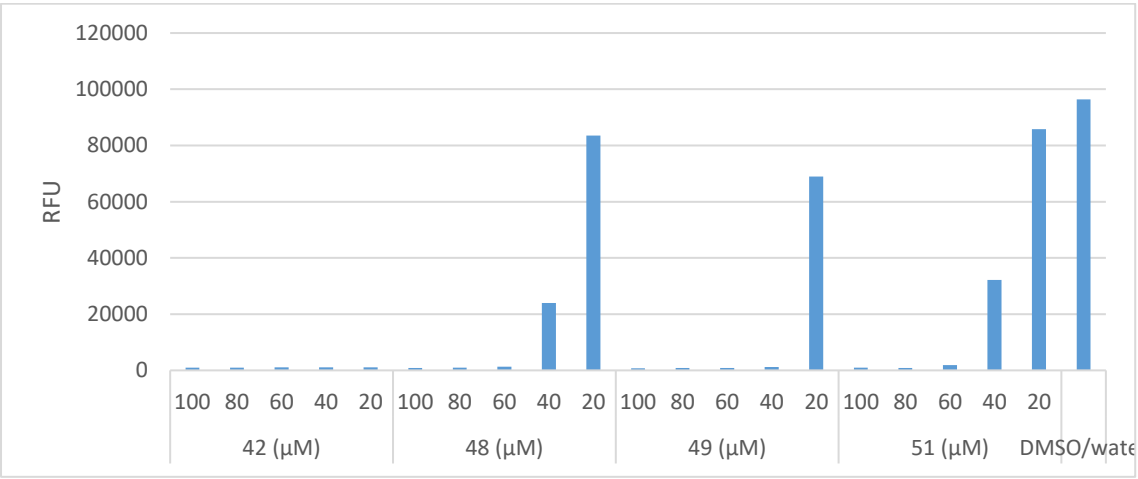

Figure 68: Toxicity of the acridine / gold (I) complexes against HepG2 cells. Background fluorescence was subtracted from each reading and the resulting values are shown relative to a buffer-only control

To confirm that the toxicity associated with the latter three complexes was not due to the ligand alone a further assay was performed just with the free ligands (Figure 69). None of these showed significant toxicity confirming that complexation with gold was required for activity. Since complexes **42**, **45** and **47** showed significant toxicity at 20µM further assays were performed using higher dilutions (Figure 70). All three complexes showed a dose-dependent toxicity and from these data IC_{50} values were calculated as 11.18µg/ml (Complex **42**), 12.32µg/ml (Complex **45**) and 5.18µg/ml (Complex **47**). The results

indicated that the activity of the complexes greatly depended on the number and chemical nature of the substituents. The complexes **41**, **42** and **47** which were the analogues of complexes **48**, **49** and **51** exerted an interesting cytotoxicity on HepG2 cancer cell lines. Comparison with the results observed for complexes **48**, **49** and **51** indicated that addition of methoxy at position 2, 3, and 4 greatly reduced the activities of the complexes. Furthermore, addition of second Chloro at position 2 (**46**) slightly reduced the cytotoxicity of the compound when compared with mono chloro compound (complex 41). Interestingly, the toxicity increases as the electronegativity of the halogen substituent decreases, I other words as the inductively withdrawing effect of the halogen substituent decreases on the acridine ring system the toxicity of the complexes increases. As indicated by complexes **41**< **42** < **47.** Surprisingly, the addition of fluoro and bromo substitution (**45**) has little or no effect on the activity of the complex. It has been reported that acridine derivatives induced p53 dependent apoptosis of tumour cells at the concentration of 20 μM [142] which was higher than the activity observed in these complexes. However, the observed activity was slightly higher than the value reported for acridine derivatives against human glioblastoma cell with IC_{50} of 176.9 nM and human colon cancer cell line with IC_{50} of 166.7 nM.[140] Furthermore, the observed activity was higher than the toxicity of pyrazole gold(I) complexes reported for the same cancer cell line with IC_{50} values ranges from 0.13μg/ml to 1.75μg/ml.[274] The choice of acridine as a ligand for the gold was based on the fact that these molecules have a natural fluorescence that alters upon complexation. This potentially provides the means to better understand the mechanism of action of these toxic complexes through detailed real-time imaging of exposed cells. As a proof-of-concept experiment cells were exposed to either buffer or complex **47** and the fluorescent signal associated with the complex observed (Figure 71). As can be seen after exposure to the complex fluorescence is seen to concentrate in the cells over time

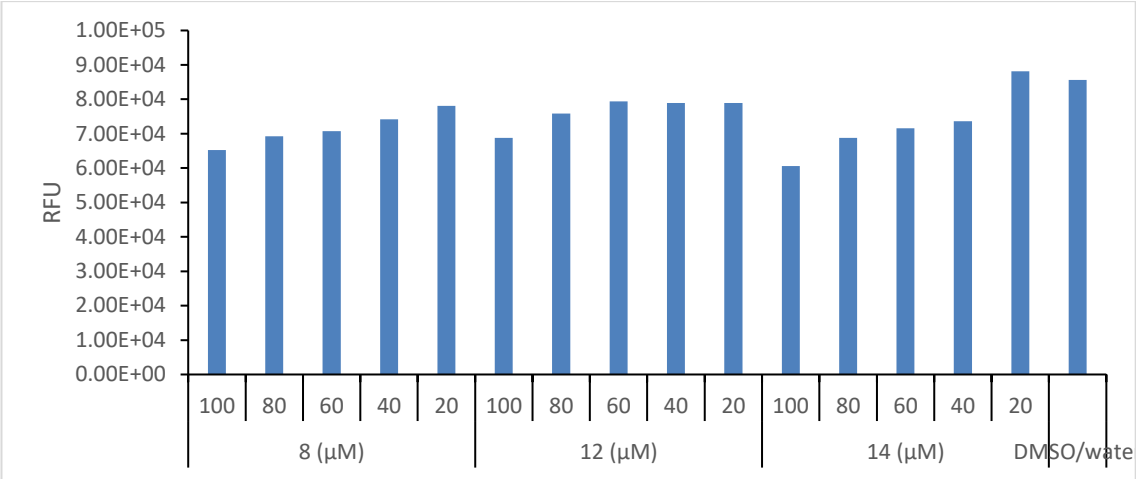

Figure 69: Toxicity of the acridine / gold (I) complexes against HepG2 cells. Background fluorescence was subtracted from each reading and the resulting values are shown relative to a buffer-only control

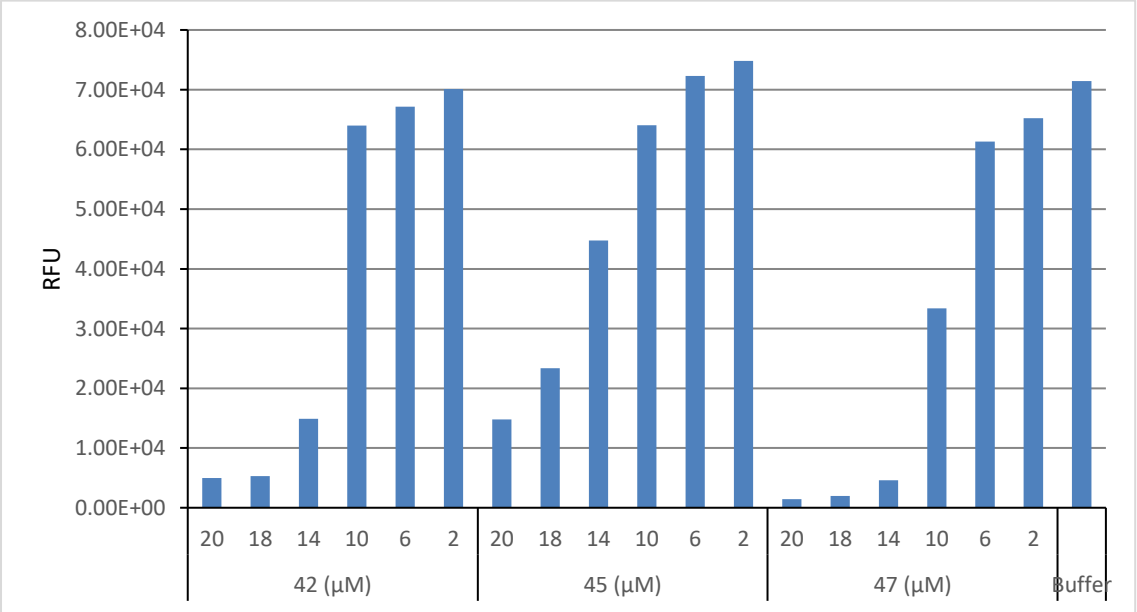

Figure 70: Toxicity of selected complexes against HepG2 cells. Background fluorescence was subtracted from each reading and the resulting values are shown relative to a buffer-only control.

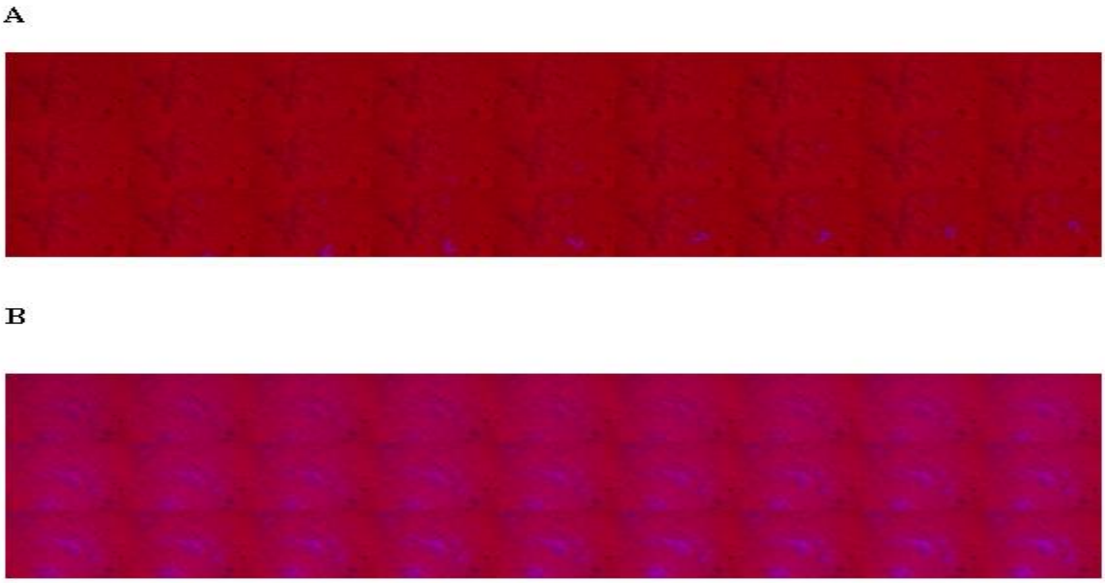

Figure 71: Imaging of HepG2 cells unexposed (A) or exposed (B) to complex 47 by fluorescence microscopy. The stills were taken over a period of 50 minutes

II.11.3. Cytotoxicity of Acridine Silver(I) Complexes

To investigate the activity of these novel Ag(I) bearing acridine complexes against human cancer cell line HepG2 five complexes synthesised were tested at a dose of 100 µM to 20 µM and the results are shown in figure 72

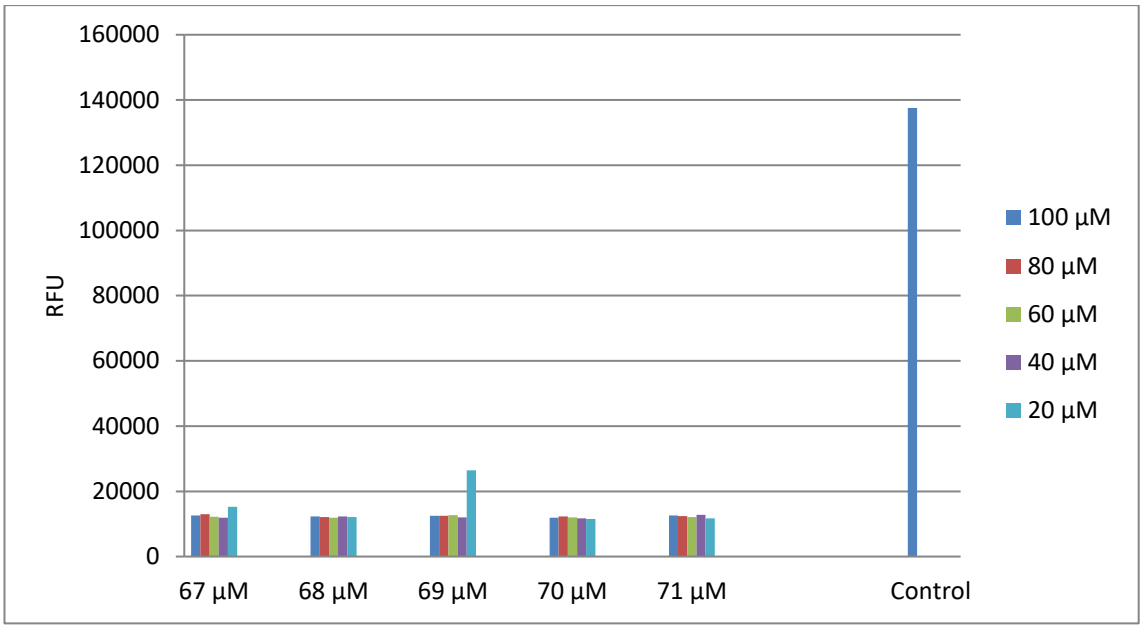

Figure 72: Toxicity of complexes **67-71** against HepG2 cells. Background fluorescence was subtracted from each reading and the resulting values are shown relative to a buffer-only control.

It was observed that all the complexes tested showed an interesting cytotoxic activity against human HepG2 cancer cell lines at these concentrations. Therefore, further test were carried out with higher dilution and the result are shown in figure 73. All these complexes showed a dose-dependent toxicity and from these data IC_{50} values were calculated as 1.66µg/ml (Complex **67**), 1.87µg/ml (Complex **68**), 1.96 (complex **69**), 1.69 µg/ml (complex **70**) and 1.68µg/ml (Complex **71**). Interestingly, they all show high toxicity at micro molar range which makes them a potential candidate as anti-cancer agent.

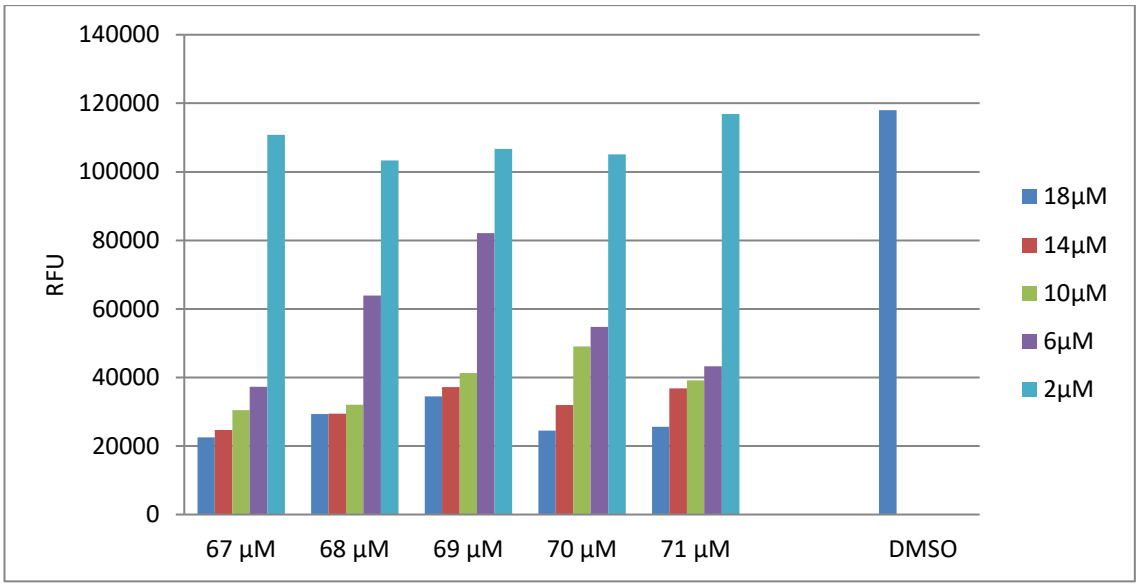

Figure 73: Toxicity of complexes 67-71 against HepG2 cells at less than 20 µM. Background fluorescence was subtracted from each reading and the resulting values are shown relative to a buffer-only control.

II.11.4. Cytotoxicity of Pyrazole Silver(I) Complexes

To study the activity of the new pyrazole Ag(I) complexes against human HepG2 cancer cell lines, the four complexes synthesised in table 11 were tested at a single dose of 2 µM and the results are shown in figure 74 below.

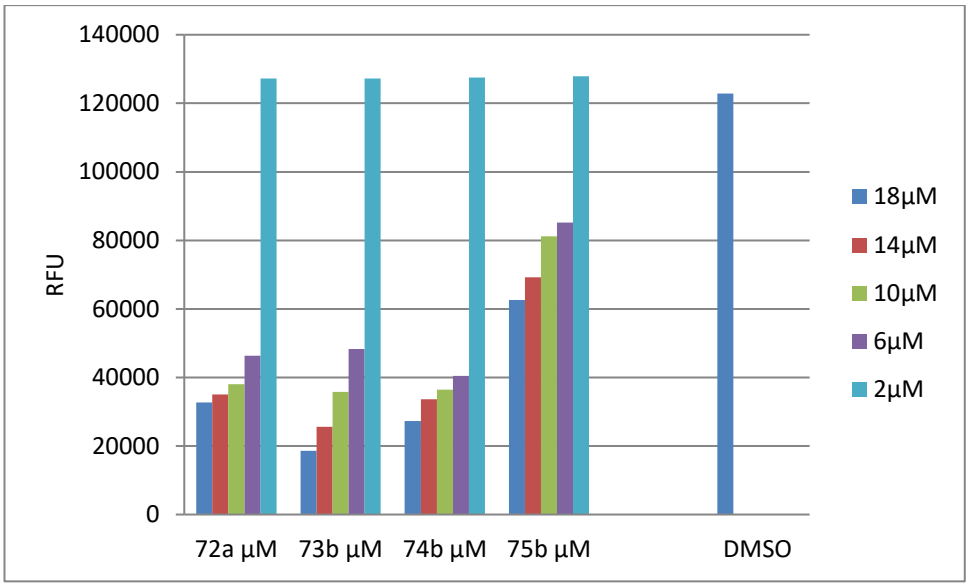

Figure 74: Toxicity of complexes 72a-75b against HepG2 cells at less than 20 µM. Background fluorescence was subtracted from each reading and the resulting values are shown relative to a buffer-only control

The four complexes indicated that they possessed interesting activity against this cell lines. IC_{50} values were calculated as 2.203µg/ml (Complex **72a**), 2.36µg/ml (Complex **73b**), 2.18 (complex **74b**), and 3.06µg/ml (Complex **75b**). The result indicated that these new complexes showed toxicities in the micro molar range against HepG2 human cancer cell lines, which implies that they could be develop as drug against this cancer cell lines.

CHAPTER III. Conclusions and Future work

III.1.Conclusions

A novel series of acridine ligands bearing different substituents were successfully synthesised by optimisation of a modified method first outlined by Wróbel. Through altering the method as well as the purification sequence, the yield was improved to 92%. The reaction time was also reduced from six days to less than 48 hours. The complexation protocol to form gold (I) cationic complexes has been optimised. Some complexes gave good crystals and were characterised by x-ray analysis to determine the coordination environment of the gold atom. X-ray studies revealed that complex **49** was the only regioisomer while the other complexes were not.

Cell viability assays demonstrated that some of the complexes showed toxicities in the micromolar range against the hepatocarcinoma cell line HepG2. The fluorescence properties will allow future studies to establish subcellular interactions between the complex and target/non-target cells.

Five new monocationic pyrazolium gold complexes were prepared in excellent yields and the substitution pattern did not seem to have a notable effect on their activity against the cancer cell line described herein. This flexibility in the design is desirable when fine-tuning structural motifs for druggable applications. The regioselectivity of the complexation was found to be dependent on the substitution pattern on the endocyclic nitrogen N1, favouring the complexation of the nitrogen proximal to the 5-amino group when R1 = H.

All compounds are highly active against HepG2 cancer cells and display activity in the submicromolar range comparable to the previous work on gold complexes and breast cancer cell lines.[79] Furthermore their efficacy compares well to other chemotherapeutic

drugs on this cell line[318] including Doxorubicin (IC50 1.1 μM) and Cisplatin (IC50 15.9 μM) Hepatocellular carcinomas readily acquire resistance to chemotherapeutic drugs – usually through the expression of a multidrug efflux pump. It is unknown whether these mechanisms would prevent the action of the gold amides or whether they have potential in treating resistant cells. This work therefore provides strategic tools to investigate such avenues of research.

Investigation of the reactivity of gold(I) with triphenyl phosphine and trihexyl phosphine provided an insight into the behaviour of cationic gold(I) in solution. It showed that the exchange of ligands could be observed at low temperature (-80 ^{o}C) with maximum coordination numbers revealed.

The photophysical properties of substituted acridine ligands and their complexes have been studied. The substituted acridine functionalised by small electronically active groups showed a hypsochromic shift to shorter wavelengths when the conjugated π system is electron deficient and bathochromic shift to longer wavelengths when the delocalised ring bore EDG and EWG.

The susbstituent effects on absorption and fluorescence properties of acridine derivatives were investigated by considering changes in the behaviour on the basis of the position of single substitution, double substitution and multiple substitution and the electron donating/ withdrawing properties of the substituted acridine.

Investigations into the effect of halogen substituents indicated a similar trend in the excitation and emission wavelengths. The addition of methoxy group lead to bathochromic shift which showed a great effect on the Stoke's shift of the acridine derivatives. The position of the substitution and the nature of the substituent has a great impact on the stoke's shift and the quantum yield of the compounds.

Novel pyrazole bearing Ag(I) and acridine bearing Ag(I) complexes were also synthesised and characterised by x-ray crystallography.

III.2.Future work

Fluorescent gold complexes as diagnostic tools for cancer and tuberculosis.

Description

The focus here would be on validation with in vitro and in vivo testing on human cancer cell lines other than liver cancer cell lines.

Role of the ligands and deligation on the activity of the complexs: Fluorescence and confocal spectroscopy.

Investigation of fluorescent shift in solution with various solvents and various aurophilic molecule

Catalytic activities of fluorescence gold complexes

Description:

Investigation into the connectivity of fluorescent gold complexes to different substrates

Investigation into their reactivity and stabilities

Study the influence of electron donating and electron withdrawing group on the reactivity and yield of reactions promoted by fluorescent gold complexes.

Exemplification of the catalytic activity on key transformations.

Catalytic activities of acridine bearing Ag(I) complexes

CHAPTER IV. Experimental

IV.1 Methods and Materials

The starting materials and solvents were used without further purification from commercially available sources unless otherwise stated. All reactions were conducted using oven-dried glassware, a nitrogen atmosphere and Schlenk techniques, unless stated otherwise. The solutions of silver(I) salts and the mixtures of silver(I) salt and gold(I) were protected/ shielded from the light until the filtration of the residual silver chloride.

The NMR were recorded on a Varian 400 (400 MHz) or Varian 600 (600 MHz). Chemical shifts were reported in parts per million (ppm) referenced to residual solvent resonances or external 85% H_3PO_4 as appropriate. The IR spectra were recorded on a Perkin Elmer Spectrum One FT-IR spectrometer, equipped with a diamond top plate. Mass spectra were obtained using VG Autospec Magnetic Sector MS and Bruker Daltonic FT-ICR-MS Apex III 4.7 Tesla instruments, using electrospray ionisation (ESI).

For the X-ray data acquisition, a selected crystal was placed on an Xcalibur, Eos, and Gemini ultra-diffractometer. The crystal was kept at 173.0 K during data collection. Using Olex2, the structure was solved with the ShelXT structure solution program using Direct Methods and refined with the ShelXL refinement package using Least Squares minimisation.

IV.2. General Procedure for the Synthesis of Acridines 7-37.

The Corresponding nitrobenzene (0.63 mmol) and benzylcyanide (0.64 mmol) were dissolved in THF (4.7 mL) and the solution cooled to −78 ˚C under nitrogen. A solution of t-BuOK (100.9 mg, 0.9 mmol) in THF (1.6 mL) was slowly added at this temperature. The solution was stirred for 10 minutes before a solution of t-BuMe_2SiCl (473.3 mg, 3.14 mmol) in THF (1.6 mL) was added. The reaction mixture was stirred for a further 20

minutes and a solution of t-BuOK (100.0 mg, 0.9 mmol) in THF (1.6 mL) was subsequently added. The dark orange solution was allowed to warm up to the room temperature and stirred for 42 hours to give a yellow orange solution which was concentrated under reduced pressure. Methanol was added and then heated to recrystallise the product. The yellow solid, which was insoluble in methanol, was filtered under vacuum to separate it from dark brown solution of impurities. CH_2Cl_2 was added to dissolve the yellow solid product. Then, the solution was filtered under vacuum to remove the white KCl impurities. The yellow filtrate solution was concentrated on the rotary evaporator. Ethyl acetate was added to recrystallize the yellow product, which was placed in a sonic bath for five minutes to obtain a yellow homogeneous suspension and it was filtered under vacuum to give the required product as a solid.

2-chloroacridine-9-carbonitrile 7

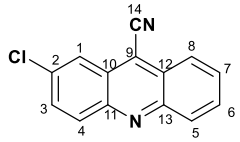

Bright yellow solid. (118.6 mg, 79 %).

MP: 209.5-211.5 ^{0}C. Lit[242] mp 208-210 ^{0}C

^{1}H NMR (500 MHz, Chloroform-*d*) δ 8.33 – 8.39 (m, 2H), 8.23 – 8.34 (m, 2H), 7.91 (ddd, *J* = 8.8, 6.6, 1.4 Hz, 1H), 7.77 – 7.84 (m, 2H).

^{13}C NMR (126 MHz, Chloroform-*d*) δ 148.4 (13-C), 146.6 (11-C), 135.7 (2-C), 132.4 (3-CH), 132.1 (12-C), 131.2 (6-CH), 130.5 (4-CH), 129.8 (5-CH), 126.4 (10-C), 126.3 (8-CH), 125.1 (7-CH), 123.6 (1-CH), 114.6 (9-C), 114.3 (14-C).

MS (EI) m/z: 238 (100), 203 (17), 176 (12).

HRMS (ESI) Calculated for $C_{14}H_8ClN_2$:239.0371. Found 239. 0372. Error: -0.75 ppm

IR (diamond, cm^{-1}):3060.32 (aromatic C-H), 2222.39 (CN), 1608.76 (C=C).

2-bromoacridine-9-carbonitrile 8

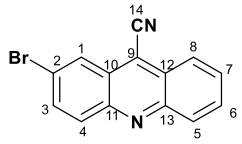

Yellow solid. (106.2 mg, 75 %).

MP: 212.6-214.8 ^{0}C. Lit[242] mp 212-214 ^{0}C

^{1}H NMR (500 MHz, Chloroform-*d*) δ 8.55 (q, *J* = 2.0 Hz, 1H), 8.33 – 8.40 (m, 1H), 8.31 (ddd, *J* = 8.5, 2.5, 1.1 Hz, 1H), 8.15 – 8.22 (m, 1H), 7.93 (ddt, *J* = 11.9, 8.2, 2.0 Hz, 2H), 7.77 – 7.85 (m, 1H).

^{13}C NMR (126 MHz, Chloroform-*d*) δ 148.4 (13-C), 146.7 (11-C), 134.8 (3-CH), 131.9 (6-CH), 131.3 (12-C), 130.5 (4-CH), 129.8 (5-CH), 127.1 (8-CH), 126.8 (7-CH), 126.3 (10-C), 125.2 (1-CH), 124.1 (2-C), 114.7 (9-C), 114.3 (14-C).

MS (EI) m/z: 284 (100), 282 (98), 203 (42) 176(37) 88 (14).

HRMS (ESI) Calculated for $C_{14}H_7BrKN_2$:320.9424. Found: 320.0938. Error: -4.33 ppm

IR (diamond, cm^{-1}): 3055.50 (aromatic C-H), 2221.37 (CN), 1604.68 (aromatic C=C).

2-chloro-6-methoxyacridine-9-carbonitrile 9

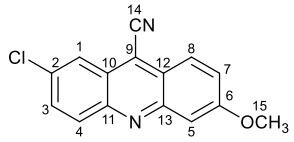

Yellow solid. (123.6 mg, 73 %).

MP: 216.1-218.1^{0}C.

^{1}H NMR (500 MHz, Chloroform-*d*) δ 8.28 (d, *J* = 2.2 Hz, 1H), 8.19 (dd, *J* = 14.9, 9.2 Hz, 2H), 7.78 (dd, *J* = 9.1, 2.2 Hz, 1H), 7.42 – 7.52 (m, 2H), 4.04 (s, 3H)

^{13}C NMR (126 MHz, Chloroform-*d*) δ 162.0 (6-C), 150.1 (13-C), 146.7 (11-C), 134.1(2-C), 132.3 (3-CH), 131.2 (12-C), 126.1 (8-CH), 125.4 (4-CH), 124.8 (10-C), 123.64 (1-CH), 122.9 (7-CH), 114.6 (9-C), 114.2 (14-C), 105.9 (5-CH), 55.9 (15-CH_3).

MS (EI) m/z: 268 (100), 270 (37), 225 (52) 227 (22).

HRMS (ESI) Calculated for $C_{15}H_{10}ClN_20$: 269.0476. Found: 269.0484.Error: -2.89 ppm.

IR (diamond, cm^{-1}):2955.07 (CH sat), 2221.31 (CN), 1626.51 (aromatic C=C), 1288.45 (C-O).

2-chloro-6-fluoroacridine-9-carbonitrile 10

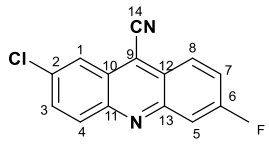

Yellow solid. (109.0 mg, 68 %).

MP: 240.1-241.1 ^{0}C.

^{1}H NMR (500 MHz, Chloroform-*d*) δ 8.34 – 8.43 (m, 2H), 8.26 (d, *J* = 9.3 Hz, 1H), 7.94 (dd, *J* = 9.6, 2.4 Hz, 1H), 7.85 (dd, *J* = 9.2, 2.2 Hz, 1H), 7.60 – 7.68 (m, 1H).

^{13}C NMR (126 MHz, Chloroform-*d*) δ 163.8 (d, *J* = 257.0 Hz,) (6-C), 149.0 (13-C), 147.2 (11-C), 135.6 (2-C), 133.1 (3-CH), 131.6 (8-CH), 127.7 (12-C), 126.0 (4-CH), 125.8 (10-C), 123.7 (1-CH), 121.9 (7-CH), 115.0 (9-C), 114.3 (14-C), 113.0(5-CH).

MS (EI) m/z: 256 (100), 221 (20), 91 (12

HRMS (ESI) Calculated for $C_{14}H_7ClFN_2$:257.0276. Found: 257.0289. Error: -4.86 ppm

IR (diamond, cm^{-1}): 2222.58 (CN), 1627.35 (aromatic C=C).

2-bromo-6-methoxyacridine-9-carbonitrile 11

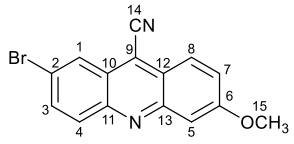

Yellow solid. (128.2 mg, 82 %).

MP: 216.9 -219 ^{0}C.

^{1}H NMR (500 MHz, Chloroform-*d*) δ 8.49 (d, *J* = 2.0 Hz, 1H), 8.22 (d, *J* = 9.3 Hz, 1H), 8.10 (d, *J* = 9.2 Hz, 1H), 7.91 (dd, *J* = 9.2, 2.0 Hz, 1H), 7.44 – 7.53 (m, 2H), 4.05 (s, 3H).

^{13}C NMR (126 MHz, Chloroform-*d*) δ 162.3 (6-C), 146.5 (13-C), 134.9 (3-C), 130.9 (8-CH), 127.2 (12-C), 127.2 (4-CH), 126.2 (10-C), 125.6 (1-CH), 125.3 (2-C), 123.0 (7-CH), 122.5 (9-C), 114.6 (14-C), 105.7 (5-CH), 55.9 (15-CH_3).

MS (EI) m/z: 312 (100), 226 (76), 190 (25), 78 (18).313 (17).

HRMS (ESI) Calculated for $C_{15}H_{10}BrN_2O$:312.9971. Found: 312.9984. Error: -4.15ppm

IR (diamond, cm^{-1}): 2956.20 (saturated CH) 2224.99 (CN), 1628.75 (aromatic C=C), 1289.47 (C-O).

2-bromo-6-fluoroacridie-9-carbonitrile 12

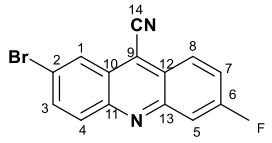

Yellow solid. (131.3 mg, 87 %).

MP: 230.9-232.9 ^{0}C.

^{1}H NMR (500 MHz, Chloroform-*d*) δ 8.55 (d, *J* = 2.1 Hz, 1H), 8.40 (dd, *J* = 9.4, 5.8 Hz, 1H), 8.16 (d, *J* = 9.2 Hz, 1H), 7.94 (dd, *J* = 9.4, 2.3 Hz, 2H), 7.64 (ddd, *J* = 9.4, 7.8, 2.5 Hz, 1H).

^{13}C NMR (126 MHz, Chloroform-*d*) δ 163.8 (d, *J* = 257.0 Hz,) (6-C), 149.2 (13-C), 147.4 (11-C), 135.4 (4-CH), 131.6 (8-CH), 127.7 (12-C), 127.6 (4-CH), 126.2 (10-C), 124.0 (1-CH), 123.6 (2-C), 121.7 (7-CH), 114.8 (9-C), 114.4 (14-C), 113.1 (5-CH).

MS (EI) m/z: 300 (100), 221 (30), 194 (18), 301 (17).

HRMS (ESI) Calculated for $C_{14}H_7N_2FBr$:300.9777. Found: 300.9772. Error: -.5 ppm

IR (diamond, cm^{-1}): 3028.15 (aromatic CH) 2224.57 (CN), 1628.12 (aromatic C=C).

2, 6-dichloroacridine-9-carbonitrile 13

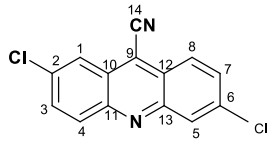

Yellow solid. (115.2 mg, 84 %).

MP: 226.4-228.4 ^{0}C

^{1}H NMR (500 MHz, Chloroform-*d*) δ 8.34 – 8.46 (m, 1H), 8.29 – 8.34 (m, 2H), 8.27 (d, *J* = 9.3 Hz, 1H), 7.85 (dd, *J* = 9.3, 2.2 Hz, 1H), 7.74 (d, *J* = 2.0 Hz, 1H).

^{13}C NMR (126 MHz, Chloroform-*d*) δ 148.2 (13-C), 147.3 (11-C), 137.7 (6-C), 136.0 (2-C), 133.1 (3-CH), 132.0 (12-C), 131.1 (8-CH), 128.9 (4-CH), 126.4 (5-CH), 126.2 (10-C), 124.79 (7-CH), 123.7 (1-CH), 114.8 9-C), 114.3 (14-C).

MS (EI) m/z: 272 (100), 274 (67), 202 (25).

HRMS (ESI): Calculated for $C_{14}H_7Cl_2N_2$:272.9986. Found: 272.9986. Error: -0ppm

IR (diamond, cm^{-1}): 3070.83 (aromatic CH), 2226.94 (CN), 1616.23 (aromatic C=C).

2-iodoacridine-9-carbonitrile 14

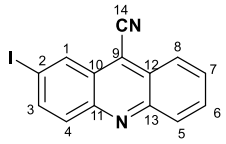

Bright yellow solid. (497.4 mg, 75 %).

MP 225.3-228.3 ^{0}C.

^{1}H NMR (600 MHz, Chloroform-*d*) δ 8.76 (d, *J* = 1.7 Hz, 1H), 8.35 (d, *J* = 8.6 Hz, 1H), 8.27 (d, *J* = 8.8 Hz, 1H), 8.08 (dt, *J* = 9.2, 1.4 Hz, 1H), 8.00 (d, *J* = 9.1 Hz, 1H), 7.91 (ddd, *J* = 8.8, 6.6, 1.2 Hz, 1H), 7.79 (ddd, *J* = 7.9, 6.7, 1.2 Hz, 1H).

^{13}C NMR (151 MHz, Chloroform-*d*) δ 148.5 (13-C), 146.6 (11-C), 139.8 (3-CH), 133.9 (1-CH), 131.6 (4-CH), 131.4 (12-C), 130.5 (10-C), 129.6 (6-CH), 127.2 (5-CH), 126.1 (8-CH), 125.2 (7-CH), 114.7 (9-C), 114.0 (14-C), 96.2 (2-C).

HRMS (ESI) Calculated for $C_{14}H_8IN_2$:330.12. Found: 330.9727. Error: 0.4 ppm

IR (diamond, cm^{-1}): 3049.06 (aromatic H), 2220.45 (CN), 1597.17cm^{-1} (aromatic C=C).

7-chloro-2, 3, 4-trimethoxyacridine-9-carbonitrile 15

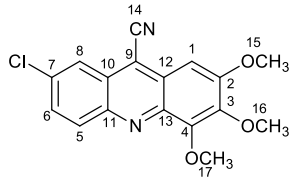

Yellow solid. **(**189.8 mg, 92 %).

MP: 210.7-212.7 ^{0}C.

^{1}H NMR (500 MHz, Chloroform-*d*) δ 8.24 – 8.33 (m, 2H), 7.69 – 7.76 (m, 1H), 7.26 (d, *J* = 6.6 Hz, 1H), 4.26 (s, 3H), 4.11 – 4.18 (m, 6H).

^{13}C NMR (126 MHz, Chloroform-*d*) δ 156.7 (2-C), 146.9 (13-C), 145.9 (4—C), 144.1 (11-C), 141.9 (7-C), 135.1 (6-CH), 132.3 (3-C), 130.9 (12-C), 125.9 (5-CH), 125.5 (10-C), 123.0 (8-CH), 115.3 (9-C), 111.2 (14-C), 96.8 (1-CH), 62.5 (17-CH_3), 61.7 (16-CH_3), 56.5 (15-CH_3).

MS (EI) m/z: 313 (100), 328 (33), 299 (27), 330 (17) 164 (12).

HRMS (ESI): Calculated for $C_{17}H_{14}ClN_2O_3$:329.0687. Found: 329.0696. Error:-2.51 ppm.

IR (diamond, cm^{-1}): 2940.08 (saturated CH) 2219.23 (CN), 1621.76 (aromatic C=C), 1289.80 (C-O).

7-iodo-2, 3, 4-trimethoxyacridine-9-carbonitrile 16

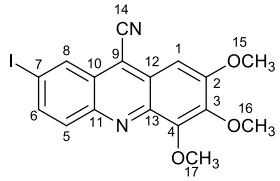

Bright yellow solid. (655.5 mg, 78 %).

MP: 232.2-233.2 ^{0}C

^{1}H NMR (600 MHz, Chloroform-*d*) δ 8.68 (d, *J* = 1.7 Hz, 1H), 8.06 (d, *J* = 9.1 Hz, 1H), 8.01 (dt, *J* = 9.1, 1.4 Hz, 1H), 7.26 (d, *J* = 2.8 Hz, 1H), 4.24 (s 3H), 4.11 – 4.17 (m, 6H).

^{13}C NMR (126 MHz, Chloroform-*d*) δ 156.6 (2-C), 146.6 (13-C), 146.3 (4-C), 144.1 (11-C), 141.7 (6-CH), 138.7 (8-CH), 133.2 (3-C), 131.6 (5-CH), 126.8 (12-C), 125.3 (10-C), 115.2 (9-C), 111.1 (14-C), 96.9 (7-C), 95.6(1-CH), 62.5 (17-CH_3), 61.7 (16-CH_3), 56.6 (15-CH_3).

HRMS (ESI): Calculated for $C_{17}H_{14}IN_20_3$:421.0044. Found: 421.0055. Error: -2.63 ppm.

IR (diamond, cm^{-1}): 2931.16 (aromatic H), 2219.38 (CN), 1619.08cm^{-1} (aromatic C=C), 1289.85 (C-O).

2-iodo-6-methoxyacridine-9-carbonitrile 17

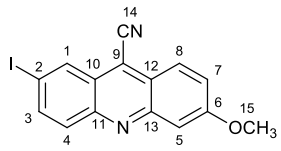

Orange solid. (615.3 mg, 85 %).

MP: 235.6-238.6 ^{0}C.

^{1}H NMR (500 MHz, Chloroform-*d*) δ 8.73 (d, *J* = 1.8 Hz, 1H), 8.23 (d, *J* = 9.3 Hz, 1H), 8.07 (dd, *J* = 9.1, 1.8 Hz, 1H), 7.94 (d, *J* = 9.1 Hz, 1H), 7.44 – 7.51 (m, 2H), 4.05 (s, 3H).

^{13}C NMR (126 MHz, Chloroform-*d*) δ 162.2 (13-C), 150.3 (6-C), 147.0 (11-C), 139.8(3-CH), 133.9 (1-CH), 130.9 (4-CH), 126.2 (12-C), 125.8 (10-C), 125.4 (8-CH), 122.7 (7-CH), 114.7 (9-C), 113.8 (14-C), 106.0 (5-CH), 94.1 (2-C), 55.9 (15-CH_3).

HRMS (ESI): Calculated for $C_{15}H_{10}IN_2O$:360.9832. Found: 360.9842. Error: -2.82 ppm.

IR (diamond, cm^{-1}): 2938.05 (saturated CH), 2222.57 (CN), 1625.33 (aromatic C=C), 1290.57 (C-O).

6-fluoro-2-iodoacridine-9-carbonitrile 18

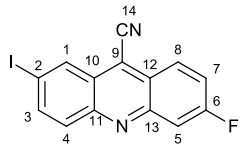

Orange solid. (627.8 mg, 90 %).

MP: 247.8-249.8 ^{0}C.

^{1}H NMR (500 MHz, Chloroform-*d*) δ 8.79 (d, *J* = 1.8 Hz, 1H), 8.40 (dd, *J* = 9.4, 5.8 Hz, 1H), 8.09 – 8.15 (m, 1H), 8.00 (d, *J* = 9.2 Hz, 1H), 7.91 (dd, *J* = 9.6, 2.5 Hz, 1H), 7.63 (ddd, *J* = 9.7, 7.9, 2.5 Hz, 1H).

^{13}C NMR (126 MHz, Chloroform-*d*) δ 149.2 (13-C), 147.6 (11-C), 140.4 (3-CH), 134.0 (1-CH), 131.3 (8-CH), 127.8 (4-CH), 126.7 (12-C), 123.4 (10-C), 121.9 (7-CH), 121.7 (9-C), 114.5 (14-C), 113.1 (5-CH), 95.9 (2-C).

HRMS (ESI): Calculated for $C_{14}H_7FIN_2$:348.9632. Found: 348.9636. Error: 1.0 ppm.

IR (diamond, cm^{-1}): 3018.45 (aromatic CH) 2221.60 (CN), 1624.41cm^{-1} (aromatic C=C).

7-bromo-2,3,4-trimethoxyacridine-9-carbonitrile 19

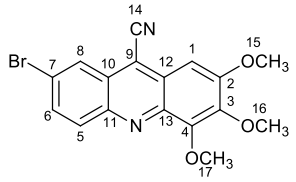

Orange yellow solid. (169.9 mg, 91 %).

MP: 223.6-225.6 ^{0}C.

^{1}H NMR (500 MHz, Chloroform-*d*) δ 8.47 (d, *J* = 2.0 Hz, 1H), 8.34 (d, *J* = 9.1 Hz, 1H), 7.88 (dd, *J* = 9.2, 2.1 Hz, 1H), 7.28 (s, 1H), 4.27 (s, 3H), 4.12-4.15 (m, 6H).

^{13}C NMR (126 MHz, Chloroform-*d*) δ 156.7 (2-C), 146.8 (13-C), 146.0 (11-C), 144.1 (4-C), 141.9 (6-CH), 133.4 (3-C), 132.1 (12-C), 126.5 (5-CH), 126.4 (10-C), 125.4 (8-CH), 123.5 (7-C), 115.2 (9-C), 111.1 (14-C), 96.8 (1-CH), 62.5 (17-CH_3), 61.7 (16-CH_3), 56.6 (15-CH_3).

MS (EI) m/z: 357 (100), 359 (97) 69 (44), 219 (35), 374 (32), 373 (22).

HRMS (ESI) Calculated for $C_{17}H_{14}BrN_2O_3$: 373.0182. Found: 373.0193. Error:-2.93 ppm.

IR (diamond, cm^{-1}): 2938.26 (aromatic H), 2219.74 (CN), 1621.66 (aromatic C=C), 1291.22 (C-O).

7-iodo-2,3-dimethoxyacridine-9-carbonitrile 20

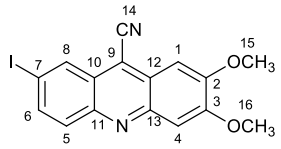

Pale yellow solid. (602.5 mg, 77 %).

Procedure 2:

MP: 231.0-233.0 ^{0}C.

^{1}H NMR (500 MHz, Chloroform-*d*) δ 8.67 (t, *J* = 1.4 Hz, 1H), 8.01 (dt, *J* = 9.0, 1.4 Hz, 1H), 7.91 (d, *J* = 9.0 Hz, 1H), 7.46 (d, *J* = 1.1 Hz, 1H), 7.40 (s, 1H), 4.16 (s, 3H), 4.11 (s, 3H).

^{13}C NMR (126 MHz, Chloroform-*d*) δ 155.1 (3-C), 153.8 (2-C), 146.9 (13-C), 145.2 (11-C), 138.6 (6-CH), 133.4 (8-CH), 130. 9 (5-CH), 126.1 (12-C), 124.5 (10-C), 115.3 (9-C), 110.4 (14-C), 107.0 (1-CH), 101.0 (4-CH), 94.19 (7-C), 56.7 (16-CH_3), 56. 6 (15-CH_3).

HRMS (ESI) Calculated for $C_{16}H_{12}IN_2O_2$:390.9938. Found: 390.9944. Error: -1.58 ppm.

IR (diamond, cm^{-1}): 3090.06 (aromatic H), 2940.05 (saturated CH), 2165.54 (CN), 1622.80 (aromatic C=C).

7-chloro-2, 3-dimethoxyacridine-9-carbonitrile 21

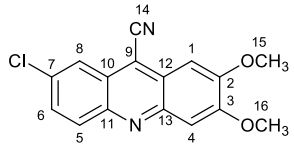

Deep yellow solid. (147.2 mg, 78 %).

MP: 263.0-265.0 ^{0}C. Lit mp 262-263 ^{0}C

^{1}H NMR (500 MHz, Chloroform-*d*) δ 8.24 – 8.31 (m, 2H), 7.77 (dt, *J* = 9.2, 1.7 Hz, 1H), 7.64 (s, 1H), 7.40 (d, *J* = 1.2 Hz, 1H), 4.11-4.15 (m, 6H).

^{13}C NMR (151 MHz, Chloroform-*d*) δ 155.7 (3-C), 153.8 (2-C), 145.5 (13-C), 143.3 (11-C), 134.4 (7-C), 131.7 (6-CH), 129.9 (12-C), 125.0 (5-CH), 124.8 (10-C), 123.3 (8-CH), 123.2 (9-C), 114.8 (14-C), 105.8 (1-CH), 100.8 (4-CH), 56.7 (16-CH_3), 56.7 (15-CH_3).

MS (EI) m/z: 298 (100), 255 (23), 212 (15)

HRMS (ESI): Calculated for $C_{16}H_{12}ClN_20_2$:299.0582. Found: 299.0582 Error: 0.05 ppm.

IR (diamond, cm^{-1}): 3009.87 (aromatic H), 2946.16 (saturated CH), 2225.90 (CN), 1625.66 (aromatic C=C).

6-bromo-2-chloroacridine-9-carbonitrile 22

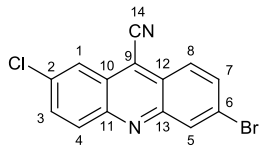

Deep yellow solid**.** (163.5 mg, 82 %).

MP: 261.0-263.0 ^{0}C. Lit[242]. mp 260.0 ^{0}C.

^{1}H NMR (500 MHz, Chloroform-*d*) δ 8.54 (t, *J* = 1.5 Hz, 1H), 8.36 (t, *J* = 1.6 Hz, 1H), 8.25 (dd, *J* = 13.7, 9.1 Hz, 2H), 7.86 (ddt, *J* = 12.6, 9.2, 1.6 Hz, 2H).

^{13}C NMR (151 MHz, Chloroform-*d*) δ 148.3 (13-C), 147.1 (11-C), 136.1 (2-C), 133.4 (3-CH), 133.2 (5-CH), 132.4 (7-H), 132.0 (8-CH), 126.3 (4-CH), 126.1 (11-C), 124.8 (6-C), 123.7 (1-CH), 114.8 (9-C), 114.3 (14-C).

MS (EI) m/z: 318 (100), 316 (75), 202 (45), 237 (20).

HRMS (ESI): Calculated for $C_{14}H_7BrClN_2$:316.9476. Found: 316.9490. Error: -2.96 ppm.

IR (diamond, cm^{-1}): 3067.79 (aromatic H), 2225.98 (CN), 1612.84 (aromatic C=C).

7-bromo-2, 3-dimethoxyacridine-9-carbonitrile 23

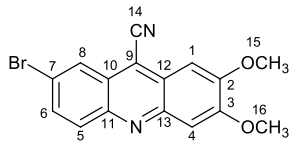

Orange yellow solid. (136.8 mg, 80 %).

MP: 217.8-219.8 ^{0}C.

^{1}H NMR (500 MHz, Chloroform-*d*) δ 8.50 (d, *J* = 2.0 Hz, 1H), 8.31 (s, 1H), 7.94 (d, *J* = 8.9 Hz, 1H), 7.77 (s, 1H), 7.44 (s, 1H),), 4.15-4.17 (m, 6H).

^{13}C NMR (151 MHz, Chloroform-*d*) δ 155.6 (3-C), 153.9 (2-C), 133.9 (6-CH), 130.2 (12-C, 5-CH), 126.7 (10-C), 125.5 (8-CH), 124.8 (7-C), 122.7 (9-C), 115.0 (14-C), 106.2 (1-CH), 100.9 (4-CH), 56.7 (16-CH_3), 56.7 (15-CH_3).

MS (EI) m/z: 344 (100), 192 (30), 299 (23), 256 (17).

HRMS (ESI) Calculated for $C_{16}H_{12}BrN_2O_2$:343.0077. Found: 343.0069. Error: 2.14 ppm.

IR (diamond, cm^{-1}): 2227.46 (CN), 1616.18 (aromatic C=C).

6-methoxy-2-(methylthio)acridine-9-carbonitrile 24

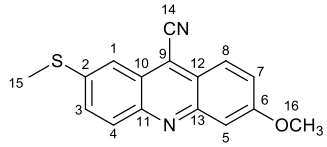

Yellow solid. (138.5 mg, 84 %).

MP: 214.7-216.7 ^{0}C.

^{1}H NMR (500 MHz, Chloroform-*d*) δ8.18 (d, *J* = 9.3 Hz, 1H), 8.06 (d, *J* = 9.1 Hz, 1H), 7.81 (d, *J* = 2.1 Hz, 1H), 7.66 (dd, *J* = 9.1, 2.1 Hz, 1H), 7.47 (d, *J* = 2.5 Hz, 1H), 7.42 (dd, *J* = 9.3, 2.5 Hz, 1H), 4.02 (s, 3H), 2.69 (s, 3H).

^{13}C NMR (126 MHz, Chloroform-*d*) δ 161.4 (6-C), 140.8 (11-C), 131.0 (2-C), 129.3 (8-CH), 126.0 (12-C), 125.3 (10-C), 125.3 (4-CH), 124.7 (3-CH), 122.7 (1-CH), 117.0 (7-CH), 115.3 (9-C), 110.0 (14-C), 106.0 (5-CH), 55.8 (16-CH_3), 15.1 (15-CH_3).

HRMS (ESI): Calculated for $C_{16}H_{13}N_2OS$:281.0743. Found 281.0743 Error -0.O5 ppm.

IR (diamond, cm^{-1}): 3075.55 (aromatic H), 2918.39 (saturated CH) 2218.66 (CN), 1288.21(C-O).

6-fluoro-2-(methylthio)acridine-9-carbonitrile 25

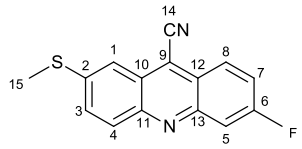

Yellow solid. (129.8 mg, 82 %).

MP: 190.2-193.2^{0}C.

^{1}H NMR (500 MHz, Chloroform-*d*) δ 8.34 (dd, *J* = 9.4, 5.8 Hz, 1H), 8.11 (d, *J* = 9.2 Hz, 1H), 7.88 (dd, *J* = 9.7, 2.5 Hz, 1H), 7.83 (d, *J* = 2.0 Hz, 1H), 7.70 (dt, *J* = 9.2, 1.4 Hz, 1H), 7.53 – 7.62 (m, 1H), 2.71 (s, 3H).

^{13}C NMR (126 MHz, Chloroform-*d*) δ 163.2 (d, *J* = 254.4 Hz,) (6-C), 147.7 (13-C), 142.6 (11-C), 131.5 (2-C), 129.7 (8-CH), 127.3 (12-C), 126.2 (10-C), 123.5 (4-CH), 121.1 (1-CH), 120.9 (7-CH), 116.3 (9-C), 115.0 (14-C), 112.8 (5-CH), 14.9 (15-CH_3).

HRMS: (ESI) Calculated for $C_{15}H_{10}N_2FS$:269.0543. Found: 269.0546. Error -1.11 ppm.

IR (diamond, cm^{-1}): 3051.70 (aromatic H), 2218.39 (CN), 1621.78(aromatic C=C).

6-chloro-2-(methylthio)acridine-9-carbonitrile 26

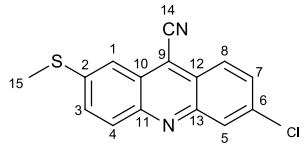

Yellow solid. (131.6 mg, 78 %).

MP: 207.9-210.9 ^{0}C.

^{1}H NMR (500 MHz, Chloroform-*d*) δ 8.23 (d, *J* = 8.4 Hz, 2H), 8.08 (d, *J* = 9.0 Hz, 1H), 7.77 (s, 1H), 7.64 – 7.71 (m, 2H), 2.70 (s, 3H).

^{13}C NMR (126 MHz, Chloroform-*d*) δ 147.7 (13-C), 147.0 (11-C), 143.2 (6-C), 136.4 (2-C) , 131.5 (8-CH), 130.5 (5-CH), 130.0 (12-C), 128.9 (7-CH), 126.6 (10-C), 126.2 (4-CH), 124.6 (3-CH), 116.2 (1-CH), 114.9 (9-C), 112.4 (14-C), 14.9 (15-C).

HRMS: (ESI) Calculated for $C_{15}H_{10}N_2ClS$:285.0248.Found:285.0250. Error -0.75 ppm.

IR (diamond, cm^{-1}): 3055.51 (aromatic H), 2221.95 (CN), 1626.19 (aromatic C=C).

2,3,4-trimethoxy-7-(methylthio)acridine-9-carbonitrile 27

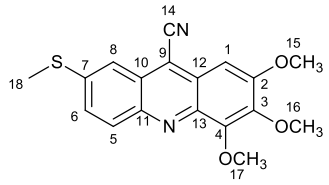

Yellow solid. (158.7 mg, 79 %).

MP: 207.5-209.5 ^{0}C.

^{1}H NMR (500 MHz, Chloroform-*d*) δ 8.18 (d, *J* = 9.1 Hz, 1H), 7.78 (d, *J* = 2.0 Hz, 1H), 7.60 (dd, *J* = 9.1, 2.1 Hz, 1H), 7.23 (s, 1H), 4.24 (s, 3H), 4.12 (s, 3H), 4.11 (s, 3H) 2.69 (s, 3H).

^{13}C NMR (126 MHz, Chloroform-*d*) δ 156.2 (2-C), 147.1 (13-C), 145.0 (4-C), 144.4 (11-C), 141.8 (7-C), 140.5 (3-C), 130.4 (12-C), 129.3 (10-C), 126.3 (5-CH), 125.3 (6-CH), 116.3 (8-CH), 115.8 (9-C), 110.0 (14-C), 96.85 (1-CH), 62.43 (17-CH_3), 61.68 (16-CH_3), 56.48 (15-CH_3), 15.03 (18-CH_3).

HRMS: (ESI) Calculated for $C_{18}H_{17}N_2O_3S$:341.0954. Found: 341.0956. Error -0.36 ppm.

IR (diamond, cm^{-1}): 2938.39 (saturated CH) 2219.42 (CN), 1600.77 (aromatic C=C).

6-fluoro-2-methoxyacridine-9-carbonitrile 28

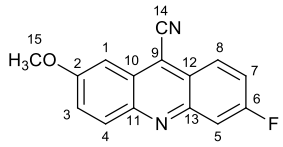

Yellow solid. (129.4 mg, 87 %).

MP: 191.8-193.8 ^{0}C.

^{1}H NMR (500 MHz, Chloroform-*d*) δ 8.30 (dd, *J* = 9.5, 5.8 Hz, 1H), 8.12 (d, *J* = 9.5 Hz, 1H), 7.86 (d, *J* = 9.7 Hz, 1H), 7.51 – 7.60 (m, 2H), 7.40 (s, 1H), 4.06 (s, 3H).

^{13}C NMR (126 MHz, Chloroform-*d*) δ162.8 (d, *J* = 254.5 Hz,) (6-C), 159.8 (2-C), 146.4 (13-C), 131.7 (11-C), 127.5 (8-CH), 127.3 (4-CH), 127.0 (12-C), 123.4 (10-C), 120.9 (3-CH), 120.7 (7-CH), 115.3 (9-C), 113.0 (14-C), 112.8 (5-CH), 100.3 (1-CH), 56.0 (15-CH_3).

HRMS: (ESI) Calculated for $C_{15}H_{10}N_2OF$:253.0772. Found: 253.0776. Error -1.56 ppm.

IR (diamond, cm^{-1}): 2224.87 (CN), 1626.23 (aromatic C=C).

6-chloro-2-methoxyacridine-9-carbonitrile 29

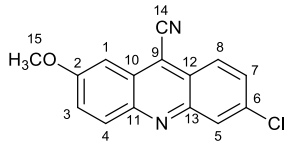

Yellow solid. (157.2 mg, 90 %).

MP: 219.2-221.2 ^{0}C.

^{1}H NMR (500 MHz, Chloroform-*d*) δ 8.23 – 8.30 (m, 2H), 8.15 (d, *J* = 9.4 Hz, 1H), 7.69 (dd, *J* = 9.1, 2.1 Hz, 1H), 7.56 (dd, *J* = 9.5, 2.7 Hz, 1H), 7.43 (d, *J* = 2.7 Hz, 1H), 4.07 (s, 3H).

^{13}C NMR (126 MHz, Chloroform-*d*) δ 160.2 (2-C), 148.7 (13-C), 146.2 (11-C), 135.6 (6-C), 131.9 (8-CH), 130.2 (4-CH), 128.8 (10-C), 127.9 (5-CH), 127.2 (7-CH), 125.8 (3-CH), 124.4 (9-C), 115.1 (14-C), 100.2 (1-CH), 56.0 (15-CH_3).

HRMS: (ESI) Calculated for $C_{15}H_{10}N_2OCl$:269.0476. Found 269.0479. Error -1.09 ppm.

IR (diamond, cm^{-1}): 3077.37 (aromatic H), 2222.69 (CN), 1630.27 (aromatic C=C).

2, 3, 7-trimethoxyacridine-9-carbonitrile 30

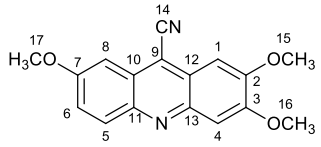

Yellow solid. (168.3 mg, 88 %).

MP: 218.6-220.6 ^{0}C.

^{1}H NMR (600 MHz, Chloroform-*d*) δ 8.35 – 8.40 (m, 1H), 7.81 (s, 1H), 7.52 (d, *J* = 9.3 Hz, 1H), 7.35 (d, *J* = 16.5 Hz, 2H), 4.11-4.13 (m, 6H), 4.04 (s, 3H).

^{13}C NMR (151 MHz, Chloroform-*d*) δ 159.7 (7-C), 155.7 (3-C), 153.7 (2-C), 127.7 (5-CH), 126.7 (12-C), 126.5 (10-C), 124.8 (6-CH), 115.0 (14-C), 103.8 (1-CH), 101.0 (4-CH), 100.8 (8-CH), 57.0 (16-CH_3), 56.7 (15-CH_3), 56.0 (17-CH_3).

HRMS: (ESI) Calculated for $C_{17}H_{15}N_2O_3$:295.1077. Found 295.1074. Error: 0.98 ppm.

IR (diamond, cm^{-1}): 3021.91 (aromatic H), 2183.38 (CN), 1618.59(aromatic C=C).

6-bromo-2-methoxyacridine-9-carbonitrile 31

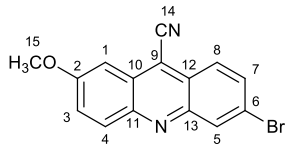

Yellow solid. (179.6 mg, 88 %).

MP: 218.7-221.7 ^{0}C

. **^{1}H NMR (500 MHz, Chloroform-*d*) δ** 8.45 (d, *J* = 1.8 Hz, 1H), 8.14 (t, *J* = 8.9 Hz, 2H), 7.79 (dt, *J* = 9.1, 1.5 Hz, 1H), 7.55 (ddd, *J* = 9.5, 2.6, 1.2 Hz, 1H), 7.39 (d, *J* = 2.6 Hz, 1H), 4.06 (d, *J* = 1.3 Hz, 3H).

^{13}C NMR (126 MHz, Chloroform-*d*) δ 160.2 (2-C), 146.4 (13-C), 146.2 (11-C), 132.5 (5-CH), 132.3 (7-CH), 132.0 (8-CH), 128.0 (4-CH), 127.3 (12-C), 125.8 (10-C), 124.6 (6-C), 123.9 (3-CH), 115.1 (9-C), 112.5 (14-C), 100.2 (1-CH), 56.1 (15-CH_3).

HRMS: (ESI) Calculated for $C_{15}H_{10}N_2OBr$:312.9971. Found 312.9976. Error -1.46 ppm.

IR (diamond, cm^{-1}): 3079.5 (aromatic H), 2937.15 (saturated CH) 2221.98 (CN), 1630.45cm (aromatic C=C).

2, 3-dimethoxy-7-(methylthio)acridine-9-carbonitrile 32

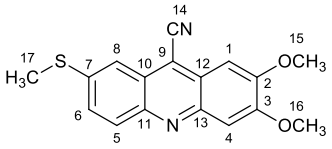

Yellow solid. (156.8 mg, 86 %)

.MP: 216.9-217. 9 ^{o}C.

^{1}H NMR (600 MHz, Chloroform-*d*) δ 8.02 (d, *J* = 9.1 Hz, 1H), 7.63 (s, 1H), 7.55 (d, *J* = 9.1 Hz, 1H), 7.46 (s, 1H), 7.23 (s, 1H), 4.12 (s, 3H), 4.07 (s, 3H), 2.66 (s, 3H).

^{13}C NMR (151 MHz, Chloroform-*d*) δ 154.7(3-C), 153.3 (2-C), 143.9 (13-C), 141.2 (11-C), 130.1 (7-C), 127.9 (12-C), 125.2 (10-C, 5-CH), 124.2 (6-CH), 116.5 (8-CH), 115.3 (9-C), 110.1 (14-C), 105.8 (1-CH), 100.9 (4-CH), 56.7 (16-CH_3), 56.6 (15-CH_3), 14.9 (17-CH_3).

HRMS: (ESI) Calculated for $C_{17}H_{15}N_2O_2S$:311.0849. Found: 311.0850. Error -0.27 ppm.

IR (diamond, cm^{-1}): 2991.17 (saturated CH) 2181.58 (CN), 1612.81 (aromatic C=C).

6-bromo-2-(methylthio)acridine-9-carbonitrile 33

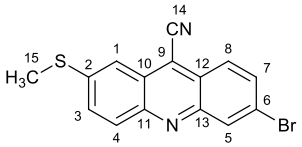

Yellow solid. (156.5 mg, 81%).

MP: 215.7-217.7^{0}C.

^{1}H NMR (500 MHz, Chloroform-*d*) δ 8.41 (d, *J* = 2.0 Hz, 1H), 8.13 (d, *J* = 9.0 Hz, 1H), 8.06 (d, *J* = 9.1 Hz, 1H), 7.71 – 7.81 (m, 2H), 7.63 – 7.69 (m, 1H), 2.69 (s, 3H).

^{13}C NMR (126 MHz, Chloroform-*d*) δ 147.5 (13-C), 147.1 (11-C), 143.3 (2-C), 132.7 (5-CH), 132.3 (7-CH), 131.4 (8-CH), 129.9 (12-C), 126.6 (10-C), 126.1 (4-CH), 125.0 (3-CH), 124.7 (6-C), 116.21-CH), 114.9 (9-C), 112.4 (14-C), 14.9 (15-CH_3).

MS (EI) m/z: 328 (100), 329 (25), 269 (25). 313 (20)

HRMS: (ESI) Calculated for $C_{15}H_{10}N_2BrS$:328.9743 Found: 328.9746. Error 1.0 ppm.

IR (diamond, cm^{-1}): 3054.61 (aromatic H), 2223.30 (CN), 1613.86 (aromatic C=C).

Acridine-9-carbonitrile 34

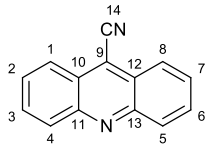

Yellow solid. . (137.8 mg, 83 %).

MP:189.8-191.8^{0}C.Lit.[242] mp: 186 ^{o}C.

^{1}H NMR (500 MHz, Chloroform-*d*) δ 9.20 (d, *J* = 8.9 Hz, 2H), 8.59 (d, *J* = 8.7 Hz, 2H), 8.25 (t, *J* = 7.8 Hz, 2H), 8.06 (t, *J* = 7.7 Hz, 2H).

^{13}C NMR (126 MHz, Chloroform-*d*) δ 141.1 (13-C, 11-C), 136.5 (3-CH, 6-CH), 131.0 (12-C, 10-C, 4-CH, 5-CH), 126.7 (2-CH, 7-CH), 125.7 (1-CH, 8-CH), 123.6 (9-C), 113.0 (14-C).

HRMS: (ESI) Calculated for $C_{14}H_9N_2$:205.0760. Found: 205.0749. Error 4.78 ppm.

IR (diamond, cm^{-1}): 3026.73 (aromatic H), 2220.72 (CN), 1629.68(aromatic C=C).

3-methoxyacridine-9-carbonitrile 35

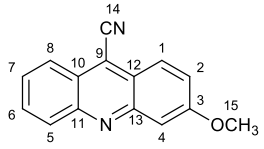

Yellow solid. (163.2 mg, 86 %).

MP: 196.7-198. 7 ^{0}C.

^{1}H NMR (500 MHz, Chloroform-*d*) δ 9.06 (d, *J* = 8.8 Hz, 1H), 8.50 (d, *J* = 8.6 Hz, 1H), 8.38 – 8.46 (m, 2H), 8.19 (ddd, *J* = 8.4, 6.9, 1.2 Hz, 1H), 7.93-8.00 (m, 1H), 7.63 (dd, *J* = 9.5, 2.3 Hz, 1H), 4.20 (s, 3H).

^{13}C NMR (126 MHz, Chloroform-*d*) δ 167.1 (3-C), 143.3 (13-C), 139.5 (11-C), 136.7 (6-CH), 129.7 (1-CH), 127.3 (12-C), 127.2 (10-C), 125.9 (5-CH), 124.2 (7-CH), 124.1 (8-CH), 123.5 (2-CH), 121.7 (9-C), 112.7 (14-C), 98.4 (4-CH), 57.5 (15-CH_3).

HRMS: (ESI) Calculated for $C_{15}H_{11}N_2O$:235.0866. Found: 235.0869. Error -1.34 ppm.

IR (diamond, cm^{-1}): 2200.81(CN), 1624.50(aromatic C=C).

3-fluoroacridine-9-carbonitrile 36

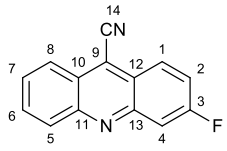

Yellow solid. (148.6 mg, 83 %)

.MP: 190.8-192.8 ^{0}C.

^{1}H NMR (500 MHz, Chloroform-*d*) δ 8.67 (d, *J* = 8.9 Hz, 1H), 8.44 – 8.54 (m, 2H), 8.34 (d, *J* = 9.2 Hz, 1H), 8.04 – 8.11 (m, 1H), 7.91 (dd, *J* = 8.5, 6.8 Hz, 1H), 7.71 (ddd, *J* = 9.9, 7.7, 2.5 Hz, 1H).

^{13}C NMR (126 MHz, Chloroform-*d*) δ 164.0 (d, *J* = 257.4 Hz,) (3-C), 148.0 (13-C), 132.3(11-C), 129.2 (1-CH), 129.1 (6-CH), 128.0 (12-C), 127.8 (10-C), 127.8 (5-CH), 125.6 (7-CH), 123.5 (8-CH), 121.5 (2-CH), 121.3 (9-C), 114.5 (14-C), 112.2 (4-CH).

HRMS: (ESI) Calculated for $C_{14}H_8N_2F$:223.0666. Found: 223.0661. Error 2.23 ppm.

IR (diamond, cm^{-1}): 3037.20 (aromatic H), 2230.18 (CN), 1628.25 (aromatic C=C).

3-chloroacridine-9-carbonitrile 37

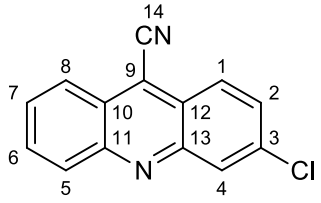

Yellow solid. (153.4 mg, 79 %).

MP: 211.7-212. 7 ^{0}C

^{1}H NMR (500 MHz, Chloroform-*d*) δ 8.63 – 8.71 (m, 2H), 8.43 (dd, *J* = 22.0, 8.9 Hz, 2H), 8.07 (t, *J* = 7.7 Hz, 1H), 7.88 – 7.95 (m, 1H), 7.79 – 7.85 (m, 1H).

^{13}C NMR (126 MHz, Chloroform-*d*) δ 152.7 (13-C), 132.5 (3-C), 130.8 (6-CH), 129.7 (1-CH), 129.4 (4-CH), 127.8 (12-C), 126.6 (2-CH), 126.1 (10-C, 5-CH, 7-CH), 125.4 (8-CH), 124.5 (9-C), 114.4 (14-C).

HRMS: (ESI) Calculated for $C_{14}H_8N_2Cl$:239. 0371. Found: 239.0376. Error -2.24 ppm.

IR (diamond, cm^{-1}): 3091.85 (aromatic H), 2223.92 (CN), 1635.21 (aromatic C=C).

IV.3. General Procedure for the Synthesis of Compounds 41-61.

$AgClO_4$ (4.2 mg, 0.020 mmol, 1 equiv.) and Ph_3PAuCl (10.0 mg, 0.020 mmol, 1 equiv.) were dissolved in methanol (0.5 mL), forming a white precipitate instantly. The mixture was stirred for 30 minutes. ^{31}P NMR of this intermediate was completed shifted at 27.5 ppm. A solution of corresponding acridine (0.020 mmol, 1 equiv) in CH_2Cl_2 (0.6 ml,) was added to the solution of cationic gold prepared previously and stirred for 30 minutes. The

mixture was filtered over a glass microfiber filter placed in a syringe and into an NMR Schlenk flask, under nitrogen. Solution was dried under reduced pressure and $CDCl_3$ (0.5 mL) was added. ^{31}P, ^{1}H and ^{13}C NMR analysis were recorded with this solution. The material was concentrated under reduced pressure to obtain the title complex as solid.

[Ph_3PAu(2-chloroacridine-9-carbonitrile)ClO_4] 41

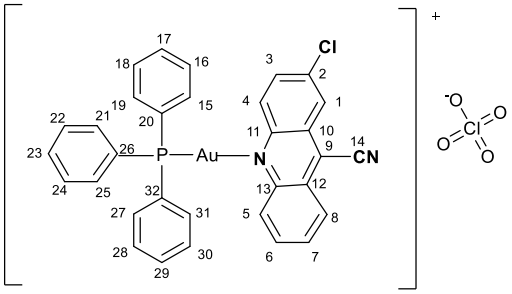

Greenish yellow solid (5.6 mg, 70 %).

MP: 149.5-150.8 ^{o}C.

^{1}H NMR (500 MHz, Chloroform-*d*) δ 9.09 (dd, *J* = 16.5, 9.1 Hz, 2H), 8.52 – 8.60 (m, 2H), 8.30 (t, *J* = 7.9 Hz, 1H), 8.15 – 8.21 (m, 1H), 7.98 (t, *J* = 7.7 Hz, 1H), 7.55 – 7.66 (m, 15H).

^{13}C NMR (126 MHz, Chloroform-*d*) δ 146.5 (13-C), 135.8 (11-C), 134.2 (20-C, 26-C, 32-C), 134.1 (2-C), 132.1 (15-CH, 19-CH,21-CH, 25-CH, 27-CH,31-CH) 131.96 (3-CH), 132.0 (12-C), 131.7 (6-CH), 130.2 (4-CH), 130.0 (16-CH, 18-CH, 22-CH, 24-CH,28-CH, 30-CH), 129.3 (17-CH, 23-CH, 29-CH), 129.2 (5-CH) 128.8 (10-C) 128.5 (8-CH) 126.6 (7-CH), 125.2 (1-CH), 123.6 (9-C), 114.6 (14-C).

^{31}P NMR (400 MHz, Chloroform-*d*) δ 33.00

HRMS: (ESI) Calculated for $C_{32}H_{22}AuClN_2P^+$:697.0869. Found: 697. 0843. Error: 3.71 ppm

IR (diamond, cm^{-1}): 2245.60 (CN), 1430.65 (PPh_3), 616.27 (C-Cl).

[Ph_3PAu(2-bromoacridine-9-carbonitrile)ClO_4] 42

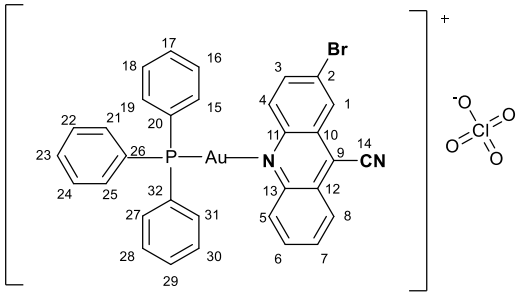

Greenish yellow solid (8.5 mg, 72 %).

MP: 156.5-157.5 ^oC.

^{1}H NMR (500 MHz, Chloroform-*d*) δ 8.97 (s, 1H), 8.86 (d, *J* = 9.3 Hz, 1H), 8.73 (d, *J* = 2.0 Hz, 1H), 8.57 (d, *J* = 8.6 Hz, 1H), 8.29 (ddd, *J* = 17.7, 8.9, 1.7 Hz, 2H), 8.01 (t, *J* = 7.8 Hz, 1H), 7.58 (ddt, *J* = 30.0, 13.7, 7.3 Hz, 15H)

^{13}C NMR (151 MHz, Chloroform-*d*) δ 148.3 (13-C), 146.6 (11-C), 134.9 (20-C, 26-C, 32-C), 134.2(3-CH), 132.3(15-CH, 19-CH,21-CH, 25-CH, 27-CH,31-CH), 131.8 (6-CH), 131.5 (12-C), 130.4 (4-CH), 129.9 (16-CH, 18-CH, 22-CH, 24-CH,28-CH, 30-CH), 129.5 (17-CH, 23-CH, 29-CH), 127.1 (5-CH), 126.9 (8-CH), 126.7 (7-CH), 126.3 (10-C), 125.2 (1-CH), 124.2 (2-C), 114.7 (9-C), 114.4 (14-C).

^{31}P NMR (162 MHz, Chloroform-*d*) δ 29.96

HRMS: (ESI) Calculated for $C_{32}H_{22}AuBrN_2P^+$:741.0364. Found: 741.0397.Error: -4.42 ppm

IR (diamond, cm^{-1}): 2243.80 (CN), 1431.54 (PPh_3), 537.94 (C-Br).

[Ph_3PAu(2-chloro-6-methoxyacridine-9-carbonitrile)ClO_4] 43

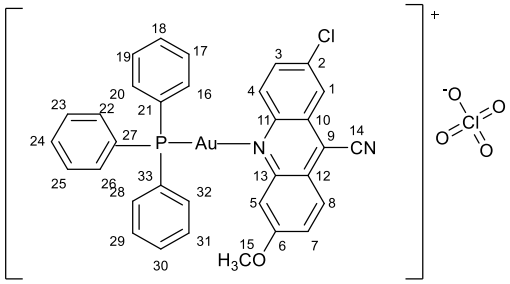

Yellow solid (7.9 mg, 68 %).

MP: 150.3-152.3 ^oC.

^{1}H NMR (600 MHz, Chloroform-*d*) δ 8.32 (d, *J* = 2.1 Hz, 1H), 8.23 (d, *J* = 9.3 Hz, 1H), 8.17 (d, *J* = 9.2 Hz, 1H), 7.79 (dd, *J* = 9.2, 2.2 Hz, 1H), 7.44 – 7.56 (m, 17H), 4.04 (s, 3H).

^{13}C NMR (151 MHz, Chloroform-*d*) δ 150.2 (6-C), 134.2 (13-C), 134.1 (11-C), 134.0 (21-C, 27-C, 33-C), 132.4 (2-C), 132.0 (16-CH, 20-CH,22-CH, 26-CH, 28-CH,32-CH), 131.9 (3-CH), 131.24 (12-C), 129.25 (8-CH), 129.17 (4-CH), 128.92(17-CH, 19-CH, 23-CH, 25-CH,29-CH, 31-CH) , 128.5 (18-CH, 24-CH, 30-CH), 126.18 (10-C) , 123.7 (1-CH), 123.0 (7-CH), 114.7 (9-C), 114.3 (14-C), 105.9 (5-CH), 55.9 (15-CH_3).

^{31}P NMR (162 MHz, Chloroform-*d*) δ 31.29

HRMS: (ESI) Calculated for $C_{33}H_{24}AuClN_2OP^+$:727.0975. Found: 727.1044.Error: -9.54 ppm

IR (diamond, cm^{-1}): 2927.40 (saturated C-H) 2224.30 (CN), 1627.64 (aromatic C=C) 1467.00 (PPh_3).

[Ph_3PAu(2-bromo-6-methoxyacridine-9-carbonitrile)ClO_4] 44

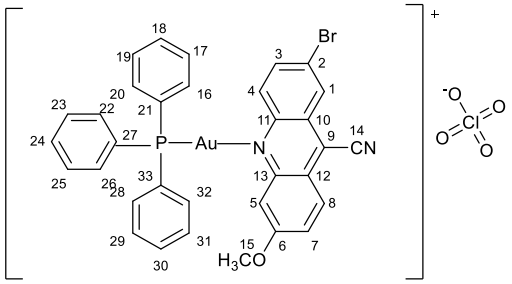

Orange solid (8.0 mg, 66 %).

MP: 133.7-135.7 ^{o}C.

^{1}H NMR (600 MHz, Chloroform-*d*) δ 8.50 (d, *J* = 2.0 Hz, 1H), 8.23 (d, *J* = 9.3 Hz, 1H), 8.11 (d, *J* = 9.1 Hz, 1H), 7.91 (dd, *J* = 9.2, 2.0 Hz, 1H), 7.44 – 7.56 (m, 17H), 4.04 (s, 3H).

^{13}C NMR (151 MHz, Chloroform-*d*) δ 162.3 (6-C), 135.0 (13-C), 134.2 (11-C), 134.1 (21-C, 27-C, 33-C), 132.0 (3-C), 131.9 (16-CH, 20-CH,22-CH, 26-CH, 28-CH,32-CH), 130.9 (8-CH), 129.2 (12-C), 129.1 (4-CH), 129.0(17-CH, 19-CH, 23-CH, 25-CH,29-CH, 31-CH), 128.5 (18-CH, 24-CH, 30-CH), 126.2 (10-C), 125.6 (1-C), 125.3 (2-C), 123.0 (7-CH), 122.4 (9-C), 114.7 (14-C), 105.7 (5-CH), 55.9 (15-CH_3).

HRMS: (ESI) Calculated for $C_{33}H_{24}AuBrN_2OP^{+}$:771.0470. Found: 771.0453.Error: 4.23 ppm

IR (diamond, cm^{-1}): 2923.75 (saturated C-H) 2188.00 (CN), 1623.74 (aromatic C=C) 1477.16 (PPh_3).

[Ph_3PAu(2-bromo-6-fluoroacridie-9-carbonitrile)ClO_4] 45

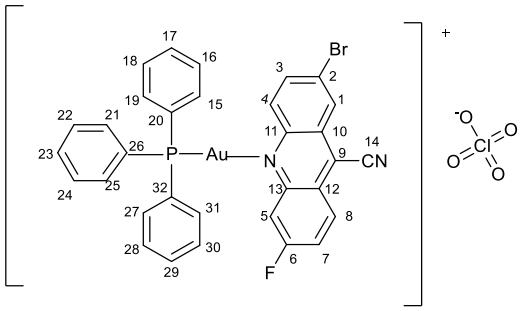

Light orange solid (8.4 mg, 70 %)

.**MP:**191.8-192.8 ºC.

^{1}H NMR (600 MHz, Chloroform-*d*) δ 8.07 – 8.13 (m, 3H), 7.83 (d, *J* = 9.4 Hz, 1H), 7.74 (d, *J* = 9.4 Hz, 1H), 7.56 – 7.68 (m, 13H), 7.32 (d, *J* = 16.6 Hz, 2H), 7.26 (s, 1H).

^{13}C NMR (151 MHz, Chloroform-*d*) δ 164.9 (d, *J* = 196.3 Hz,) (6-C), 155.9 (13-C), 139.1 (11-C), 134.3 (20-C, 26-C, 32-C), 134.2 (3-CH), 132.7 (15-CH, 19-CH,21-CH, 25-CH, 27-CH,31-CH), 130.3 (8-CH), 130.2 (12-C), 129.8 (4-CH), 129.7 (16-CH, 18-CH, 22-CH, 24-CH,28-CH, 30-CH), 127.0 (17-CH, 23-CH, 39-CH), 126.5 (10-C), 122.5 (1-CH), 122.3 (2-C), 117.4 (7-CH), 117.3 (9-C), 115.6 (14-C), 115.5 (5-CH).

^{31}P NMR (400 MHz, Chloroform-*d*) δ 31.29

HRMS: (ESI) Calculated for $C_{32}H_{21}AuBrFN_2P^+$:759.0270. Found: 761.0287.Error: -5.69 ppm.

IR (diamond, cm^{-1}): 2168.00 (CN), 1631.30 (aromatic C=C) 1436.56 (PPh_3).

[Ph_3PAu(2, 6-dichloroacridine-9-carbonitrile)ClO_4] 46

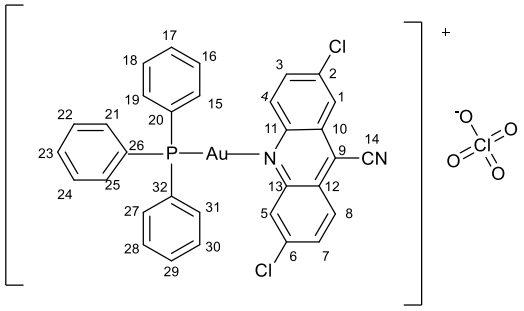

Orange solid (8.4 mg, 72 %).

MP: 207.1-209.1 ºC.

^{1}H NMR (500 MHz, Chloroform-*d*) δ 8.59 (d, *J* = 9.3 Hz, 1H), 8.26 (d, *J* = 9.5 Hz, 1H), 7.83 – 7.70 (m, 1H), 7.58 – 7.68 (m, 4H), 7.41 – 7.58 (m, 14H).

^{13}C NMR (151 MHz, Chloroform-*d*) δ 163.2 (13-C), 156.3 (11-C), 136.9 (6-C), 134.2 (20-C, 26-C, 32-C), 134.1 (2-C), 132.9 (3-CH), 132.6 (15-CH, 19-CH, 21-CH, 25-CH, 27-CH, 31-CH), 132.5 (12-C), 130. 9 (8-CH), 129.9 (4-CH), 129.8 (16-CH, 18-CH, 22-CH, 24-CH,28-CH, 30-CH), 129.7 (5-CH), 129.5 (17-CH, 23-CH, 29-CH), 127.7 (10-C), 126.1 (7-CH), 118.6 2 (1-CH), 117.2 (9-C), 114.6 (14-C).

^{31}P NMR (400 MHz, Chloroform-*d*) δ31.92

HRMS: (ESI) Calculated for $C_{32}H_{21}AuCl_2N_2P^+$:731.0479. Found: 731.0492.Error: -1.74 ppm.

IR (diamond, cm^{-1}): 3061.30 (aromatic C-H) 2231.70 (CN), 1619.20 (aromatic C=C) 1436.50 (PPh_3).

[Ph_3PAu(2-iodoacridine-9-carbonitrile)ClO_4] 47

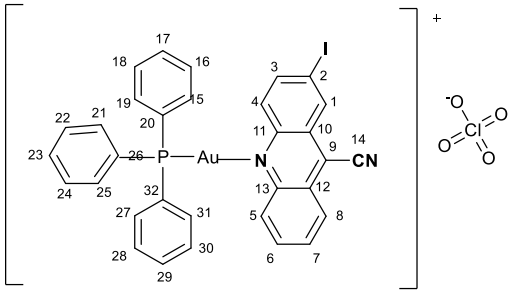

Deep orange solid (8.6 mg, 69 %).

MP: 133.0-134.0 ^oC.

^{1}H NMR (600 MHz, Chloroform-*d*) δ 8.73 (d, *J* = 2.0 Hz, 2H), 8.33 (d, *J* = 8.7 Hz, 2H), 8.27 (d, *J* = 8.8 Hz, 2H), 8.07 (dt, *J* = 9.3, 2.0 Hz, 2H), 7.99 (d, *J* = 9.3 Hz, 4H), 7.90 (t, *J* = 7.8 Hz, 3H), 7.78 (t, *J* = 7.5 Hz, 2H), 7.39 – 7.70 (m, 5H).

^{13}C NMR (151 MHz, Chloroform-*d*) δ 148.4 (13-C), 146.8 (11-C), 139.9 (3-CH), 134.2 (20-C, 26-C, 32-C), 134.1 (1-CH), 133.8 (15-CH, 19-CH,21-CH, 25-CH, 27-CH,31-CH), 131.5 (12-C), 131.5 (10-C), 130.4 (6-CH), 129.7 (16-CH, 18-CH, 22-CH, 24-CH,27-CH, 30-CH), 129.5 (17-CH, 23-CH, 29-CH), 127.16 (5-CH), 126.1 (8-CH), 125.2 (7-CH), 114.7 (9-C), 114.0 (14-C), 96.2 (2-C).

^{31}P NMR (400 MHz, Chloroform-*d*) δ 31.76

HRMS: (ESI) Calculated for $C_{32}H_{22}AuIN_2P^+$:789.0225. Found: 789.0298.Error: -9.23 ppm

IR (diamond, cm^{-1}): 3069.70 (aromatic C-H) 2236.10 (CN), 1635.60 (aromatic C=C) 1439.09 (PPh_3).

[Ph_3PAu(7-chloro-2, 3, 4-trimethoxyacridine-9-carbonitrile)ClO_4] 48

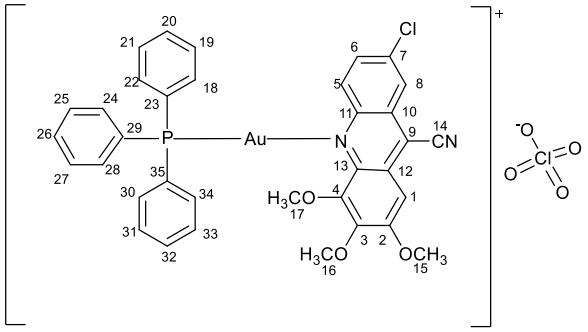

Orange solid (8.9 mg, 72 %).

MP: 126.4-128.4 ^{o}C.

^{1}H NMR (500 MHz, Chloroform-*d*) δ 9.06 (s, 1H), 8.39 (d, *J* = 2.3 Hz, 1H), 7.85 – 7.91 (m, 1H), 7.50 – 7.68 (m, 15H), 7.40 (s, 1H), 4.15 – 4.22 (m, 6H), 4.06 (s, 3H).

^{13}C NMR (151 MHz, Chloroform-*d*) δ 156.6 (2-C), 146.7 (13-C), 145.9 (4-C), 144.0 (11-C), 141.8 (7-C), 135.0 (6-CH), 134.2 (23-C, 29-C, 35-C) , 132.4 (3-C), 132.2 (18-CH, 22-CH,24-CH, 28-CH, 30-CH,34-CH), 130.9 (12-C), 129.5(19-CH, 21-CH, 25-CH, 27-CH,31-CH, 33-CH), 125.8(20-CH, 26-CH, 32-CH), 125.4 (5-CH), 123.0 (10-C), 122.9 (8-CH), 115.2 (9-C), 111.1 (14-C), 96.7 (1-CH), 62.5 (17-CH_3), 61.7 (16-CH_3), 56.5 (15-CH_3).

^{31}P NMR (400 MHz, Chloroform-*d*) δ 31.29

HRMS: (ESI) Calculated for $C_{35}H_{28}AuClN_2O_3P^+$:787.1186. Found: 787.1177.Error: 1.18 ppm

IR (diamond, cm^{-1}): 3077.60 (aromatic C-H) 2927.4 (saturated C-H) 2169.00 (CN), 1633.16 (aromatic C=C) 1436.91 ($^{(}PPh_3$).

[Ph_3PAu(7-iodo-2, 3, 4-trimethoxyacridine-9-carbonitrile)ClO_4] 49

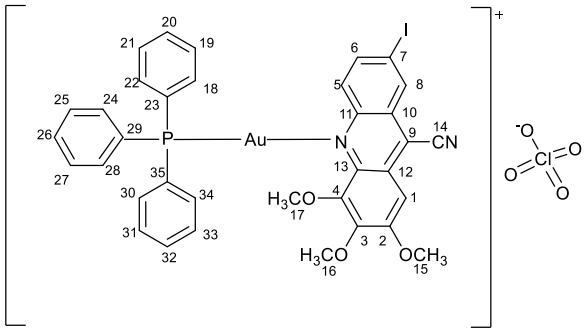

Brownish yellow solid (10.2 mg, 75 %).

MP: 120.9-121.9 ^oC.

^{1}H NMR (600 MHz, Chloroform-*d*) δ 8.78 (d, *J* = 1.8 Hz, 1H), 8.13 (dd, *J* = 9.3, 1.9 Hz, 1H), 7.55 – 7.69 (m, 15H), 7.52 (d, *J* = 8.7 Hz, 1H), 7.40 (s, 1H), 4.15-4.18 (m, 6H), 4.08 (s, 3H).

^{13}C NMR (151 MHz, Chloroform-*d*) δ 156.7(2-C), 144.2 (4-C), 141.6 (11-C), 139.2 (6-CH), 134.1 (23-C, 29-C, 35-C), 134.0 (8-CH), 133.4 (3-C), 132.5 (18-CH, 22-CH,24-CH, 28-CH, 30-CH,34-CH), 131.5 (5-CH), 129.7 (12-C), 129.6 (19-CH, 21-CH, 25-CH, 27-CH,31-CH, 33-CH), 127.5 (20-CH, 26-CH, 32-CH), 127.1 (10-C), 125.7 (9-C), 115.0 (14-C), 97.2 (7-C), 96.0 (1-CH), 62.9 (17-CH_3), 61.8 (16-CH_3), 56.7 (15-CH_3).

^{31}P NMR (162 MHz, Chloroform-*d*) δ 31.53

HRMS: (ESI) Calculated for $C_{35}H_{28}AuIN_2O_3P^+$:879.0542. Found: 879.0517.Error: 2.83 ppm

IR (diamond, cm^{-1}): 2930.13 (saturated C-H) 2258.62 (CN), 1614.85 (aromatic C=C) 1437.45 (PPh_3).

[Ph_3PAu(2-iodo-6-methoxyacridine-9-carbonitrile)ClO_4] 50

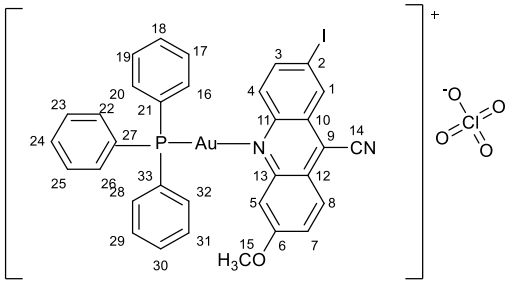

Deep orange solid (9.1mg, 71 %).

MP: 156.7-157.7 ^{o}C.

^{1}H NMR (600 MHz, Chloroform-*d*) δ 8.72 (s, 1H), 8.23 (d, *J* = 9.3 Hz, 1H), 8.07 (d, *J* = 9.1 Hz, 1H), 7.95 (d, *J* = 9.1 Hz, 1H), 7.66 (d, *J* = 9.3 Hz, 1H), 7.36 – 7.51 (m, 16H), 4.04 (s, 3H).

^{13}C NMR (151 MHz, Chloroform-*d*) δ 162.2 (13-C), 150.2 (6-C), 147.0 (11-C), 139.8 (3-CH), 134.2 (21-C, 27-C, 33-C), 131.97 (1-CH), 131.9 (16-CH, 20-CH,22-CH, 26-CH, 28-CH,32-CH), 130.9 (4-CH), 129.3 (12-C), 129.2 (17-CH, 19-CH, 23-CH, 25-CH,29-CH, 31-CH), 128.9(18-CH, 24-CH, 30-CH), 128.5 (10-C) 125.5 (8-CH), 122.7 (7-CH), 114.7 (9-C), 113.8 (14-C), 105.8 (5-CH), 94.1 (2-C), 55.9 (15-CH_3).

^{31}P NMR (162 MHz, Chloroform-*d*) δ 33.10

HRMS (ESI) Calculated for $C_{33}H_{24}AuIN_2OP^{+}$:819.0331. Found: 819.0361.Error: -3.65 ppm

IR (diamond, cm^{-1}): 2923.50 (saturated C-H) 2228.20 (CN), 1628.48 (aromatic C=C) 1427.61 ($^{(}PPh_3$).

[Ph_3PAu(7-bromo-2, 3, 4-trimethoxyacridine-9-carbonitrile)ClO_4] 51

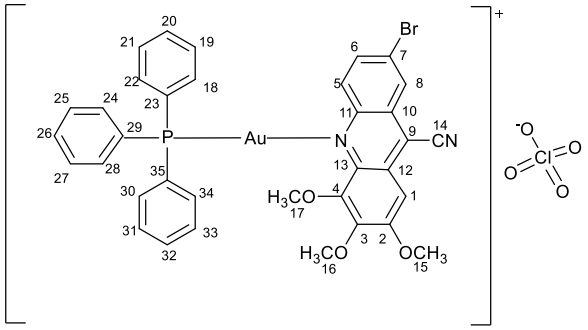

Orange solid (9.7 mg, 74 %).

MP: 137.8-138.8 ºC.

^{1}H NMR (600 MHz, Chloroform-*d*) δ 8.96 (s, 1H), 8.58 (d, *J* = 2.1 Hz, 1H), 8.00 (d, *J* = 9.1 Hz, 1H), 7.68 – 7.50 (m, 15H), 7.41 (s, 1H), 4.15-4.18 (m, 6H), 4.09 (s, 3H).

^{13}C NMR (151 MHz, Chloroform-*d*) δ 156.8 (2-C), 146.0 (13-C), 144.0 (11-C), 141.5 (4-C), 134.2 (23-C, 29-C, 35-C) , 134.1 (6-CH), 134.0 (3-C), 132.5 (18-CH, 22-CH,24-CH, 28-CH, 30-CH,34-CH) , 131.7 (12-C), 129.7 (5-CH), 129.6(19-CH, 21-CH, 25-CH, 27-CH,31-CH, 33-CH), 128.0 (20-CH, 26-CH, 32-CH) 127.6 (10-C), 126.6 (8-CH), 125.9 (7-C), 123.8 (9-C), 114.9 (14-C), 97.2 (1-CH), 62.8 (17-CH_3), 61.8 (16-CH_3), 56.6 (15-CH_3).

^{31}P NMR (162 MHz, Chloroform-*d*) δ 31.76

HRMS (ESI) Calculated for $C_{35}H_{28}AuBrN_2O_3P^+$:831.0681. Found: 833.0591.Error: 3.58 ppm

IR (diamond, cm^{-1}): 3069.70 (aromatic C-H) 2936.75 (saturated C-H) 2220.78 (CN), 1619.74 (aromatic C=C) 1437.32 (PPh_3).

[Ph_3PAu(7-iodo-2,3-dimethoxyacridine-9-carbonitrile)ClO_4] 52

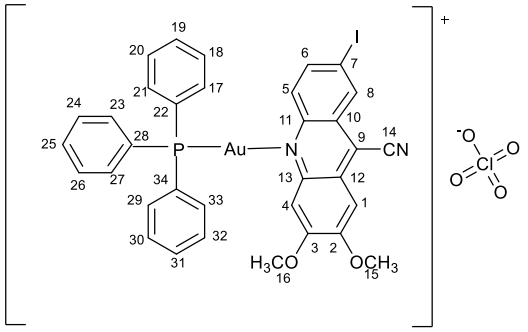

Pale yellow solid (10.3 mg, 78 %).

MP: 161.1-163.1 ^oC.

^{1}H NMR (600 MHz, Chloroform-*d*) δ 8.27 (s, 1H), 7.80 (d, *J* = 9.3 Hz, 1H), 6.99-7.87 (m, 17H), 7.06 (d, *J* = 8.4 Hz, 1H), 4.03 (s, 3H), 3.97 (s, 3H).

^{13}C NMR (151 MHz, Chloroform-*d*) δ 164.5 (3-C) , 156.0 (2-C), 151.9 (13-C), 149.7 (11-C), 140.4 (6-CH), 134.2 (22-C, 28-C, 34-C), 132.8 (8-CH), 132.7 (17-CH, 21-CH,23-CH, 27-CH, 29-CH,33-CH), 129.9 (5-CH), 129.8 (12-C), 129.7 (18-CH, 20-CH, 24-CH, 26-CH,30-CH, 32-CH), 127.0 (19-CH, 25-CH, 31-CH), 126.6 (10-C), 116.2 (9-C), 115.7 (14-C), 111.5 (1-CH), 109.6 (4-CH), 89.0 (7-C) , 56.3 (16-CH_3), 56.1 (15-CH_3).

^{31}P NMR (162 MHz, Chloroform-*d*) δ 31.50

HRMS (ESI) Calculated for $C_{34}H_{26}AuIN_2O_2P^+$:849.0437. Found: 849.0392.Error: 5.23 ppm

IR (diamond, cm^{-1}): 3053.90 (aromatic C-H) 2924.00 (saturated C-H) 2226.48 (CN), 1626.42 (aromatic C=C) 1428.89 ($^(PPh_3$).

[Ph_3PAu(7-chloro-2, 3-dimethoxyacridine-9-carbonitrile)ClO_4] 53

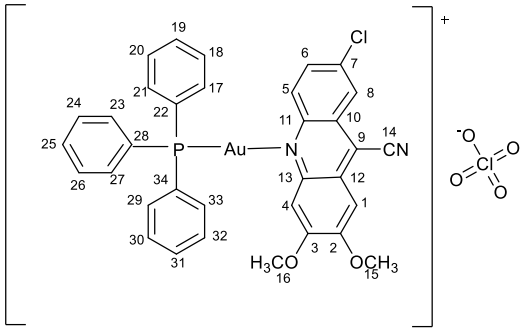

Pale yellow solid (9.3 mg, 78 %).

MP: 126.6-128.6 ºC.

^{1}H NMR (600 MHz, Chloroform-*d*) δ 8.31 (s, 3H), 7.81 (s, 2H), 7.71 (s, 3H), 7.59 (d, *J* = 18.3 Hz, 8H), 7.43 (s, 4H), 4.16 (s, 3H), 4.08 (s, 3H).

^{13}C NMR (151 MHz, Chloroform-*d*) δ155.1 (3-C) 153.7 (2-C), 146.4 (13-C), 144.3 (11-C), 134.2(22-C, 28-C, 34-C), 134.2 (7-C), 134.1 (6-CH), 131.2 (17-CH, 21-CH,23-CH, 27-CH, 29-CH,33-CH), 130.7 (18-CH, 20-CH, 24-CH, 26-CH,30-CH, 32-CH), 129.3(19-CH, 25-CH, 31-CH) 125.0 (5-CH), 124.6 (8-CH), 123.2 (9-C), 115.0 (14-C), 106.7 (1-CH), 100.8 (4-CH), 56.7 (16-CH_3), 56.6 (15-CH_3).

^{31}P NMR (162 MHz, Chloroform-*d*) δ 30.82

HRMS (ESI) Calculated for $C_{34}H_{26}AuClN_2O_2P^+$:757.1080. Found: 757.1097.Error: -2.14 ppm

IR (diamond, cm^{-1}): 3062.62 (aromatic C-H) 2926.43 (saturated C-H) 2161.54 (CN), 1623.57 (aromatic C=C) 1429.76 (PPh_3).

[Ph_3PAu(7-chloro-2, 3-dimethoxyacridine-9-carbonitrile)ClO_4] 54

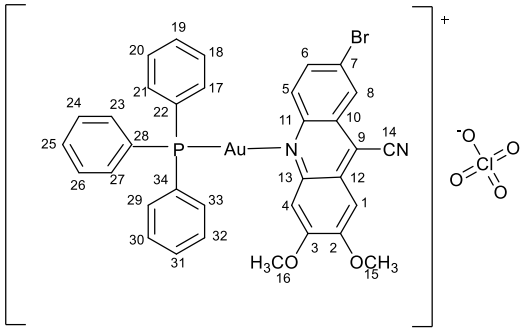

Orange solid (10.1 mg, 80 %).

MP: 121.3-123.3ºC.

^{1}H NMR (600 MHz, Chloroform-*d*) δ 8.47 (s, *J* = 30.0 Hz, 1H), 8.32 (s, *J* = 2.2 Hz, 1H), 8.22 (dd, *J* = 15.2, 9.1 Hz, 2H), 8.08 (d, *J* = 9.1 Hz, 1H), 7.77 – 7.94 (m, 3H), 7.29 – 7.74 (m, 12H), 4.16 (s, 3H), 4.12 (s, 3H).

^{13}C NMR (151 MHz, Chloroform-*d*) δ 153.9 (3-C), 148.4 (2-C), 147.2 (13-C), 136.1 (11-C), 134.2(22-C, 28-C, 34-C), 133.4 (6-CH), 132.1 (12-C), 132.0 (5-C), 132.0(17-CH, 21-CH,23-CH, 27-CH, 29-CH,33-CH), 129.3 (18-CH, 20-CH, 24-CH, 26-CH,30-CH, 32-CH), 128.9 (19-CH, 25-CH, 31-CH), 126.3 (10-C), 125.6(8-CH), 124.8 (7-C), 123.6 (9-C), 115.0 (14-C), 114.2 (1-CH), 100.9 (4-CH), 56.8 (16-CH_3), 56.7 (15-CH_3).

^{31}P NMR (162 MHz, Chloroform-*d*) δ 31.06

HRMS (ESI) Calculated for $C_{34}H_{26}AuBrN_2O_2P^+$:801.0575. Found: 801.0543.Error: 3.40 ppm.

IR (diamond, cm^{-1}): 3076.80 (aromatic C-H) 2229.31 (CN), 1617.96 (aromatic C=C) 1433.54 (PPh_3).

[Ph_3PAu(6-methoxy-2-(methylthio)acridine-9-carbonitrile)ClO_4] 55

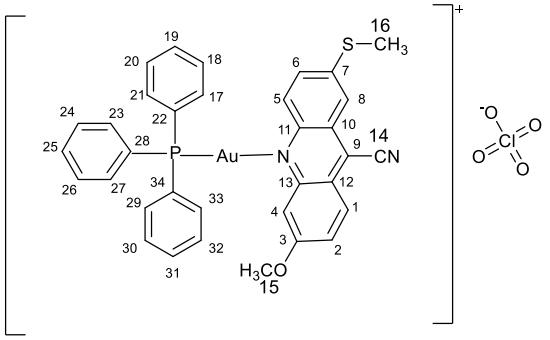

Pale orange solid (13.1 mg, 78 %).

MP: 120.3-122.3^{o}C.

^{1}H NMR (600 MHz, Chloroform-*d*) δ 8.09 (dd, *J* = 9.2, 3.6 Hz, 3H), 7.98 (d, *J* = 8.8 Hz, 3H), 7.86 (s, *J* = 8.1 Hz, 1H), 7.68 – 7.77 (m, 3H), 7.61 (d, *J* = 9.1 Hz, 3H), 7.39 – 7.58 (m, 6H), 7.34 – 7.38 (m, 2H), 3.99 (s, 3H), 2.66 (s, 3H).

^{13}C NMR (151 MHz, Chloroform-*d*) δ 161.4 (6-C), 146.8 (13-C), 140.8 (11-C), 134.2 (2-C), 134.1(22-C, 28-C, 34-C) 132.5(17-CH, 21-CH,23-CH, 27-CH, 29-CH,33-CH), 129.7 (8-CH), 129.2 (18-CH, 20-CH, 24-CH, 26-CH,30-CH, 32-CH), 129.2 (19-CH, 25-CH, 31-CH), 127.6 (12-C), 126.0 (10-C), 125.9 (4-CH), 125.2 (3-CH), 122.6 (1-CH), 118.56, 117.2 (7-CH), 116.9 (9-C), 115.1 (14-C), 105.9 (5-CH), 55.8 (15-CH_3), 15.1 (16-CH_3).

^{31}P NMR (162 MHz, Chloroform-*d*) δ 30.00.

HRMS (ESI) Calculated for $C_{34}H_{27}AuN_2OPS^{+}$:739.1242. Found: 739.1211.Error: 4.21 ppm.

IR (diamond, cm^{-1}): 3056.90 (aromatic C-H), 2924.63 (saturated CH), 2162.16 (CN), 1622.05 (aromatic C=C) 1435.60 (PPh_3).

[Ph_3PAu(6-fluoro-2-(methylthio)acridine-9-carbonitrile)ClO_4] 56

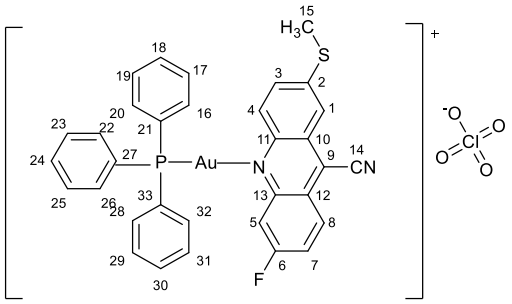

Greenish yellow solid (12.4 mg, 75 %).

MP: 137.4-138.4 ^{o}C.

^{1}H NMR (600 MHz, Chloroform-*d*) δ 8.39 (dd, *J* = 9.4, 5.8 Hz, 2H), 8.33 (s, 1H), 8.06 (d, *J* = 9.5 Hz, 1H), 7.87 (d, *J* = 1.9 Hz, 2H), 7.83 (d, *J* = 9.2 Hz, 2H), 7.32 – 7.74 (m, 13H), 2.72 (s, 3H).

^{13}C NMR (151 MHz, Chloroform-*d*) δ 163.3 (d, *J* = 255.0 Hz,) (6-C), 147.8 (13-C), 147.6 (11-C), 142.73 (2-C), 134.2 (21-C, 27-C, 33-C), 132.4(16-CH, 20-CH,22-CH, 26-CH, 28-CH,32-CH), 131.6 (8-CH), 129.5 (17-CH, 19-CH, 23-CH, 25-CH,29-CH, 31-CH), 127.4(18-CH, 24-CH, 30-CH), 127.4 (12-C), 126.3 (10-C), 123.6 (4-CH), 121.2 (1-CH), 121.0 (7-CH), 116.4 (9-C), 114.9 (14-C), 112.90, 112.8 (5-CH), 15.0 (15-CH_3).

^{31}P NMR (162 MHz, Chloroform-*d*) δ 32.86.

HRMS (ESI) Calculated for $C_{33}H_{24}AuFN_2PS^{+}$:727.1042. Found: 727.1070.Error: -3.81 ppm.

IR (diamond, cm^{-1}): 2921.94 (saturated CH), 2219.99 (CN), 1628.91 (aromatic C=C) 1436.04 (PPh_3).

[Ph_3PAu(2,3,4-trimethoxy-7-(methylthio)acridine-9-carbonitrile)ClO_4] 57

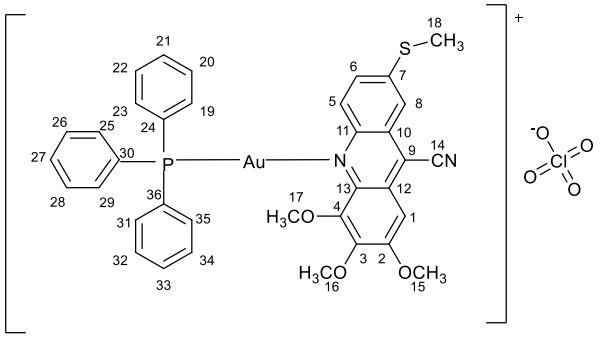

Greenish yellow solid (12.8 mg, 71 %).

MP: 140.7-142.7^{o}C.

^{1}H NMR (600 MHz, Chloroform-*d*) δ 8.16 (s, 1H), 7.84 (d, *J* = 1.9 Hz, 1H), 7.71 (d, *J* = 8.9 Hz, 1H), 7.65 (d, *J* = 8.9 Hz, 1H), 7.54 (m, *J* = 8.6 Hz, 8H), 7.49 (m, 3H), 7.44 - 7.48 (m, *J* = 31.2 Hz, 4H), 4.16 (s, 6H), 4.11 (s, 3H), 2.70 (s, 3H).

^{13}C NMR (151 MHz, Chloroform-*d*) δ 155.0 (2-C), 153.4 (13-C), 141.4 (4-C), 134.2 (7-C), 134.1(24-C, 30-C, 36-C), 132.0 (19-CH, 23-CH,25-CH, 29-CH, 31-CH,35-CH), 130.3 (3-C), 129.2 (20-CH, 22-CH, 26-CH, 28-CH,32-CH, 34-CH), 129.1 (12-C), 128.9 (21-CH, 27-CH, 33-CH), 127.5 (10-C), 127.5 (5-CH) 125.2 (6-CH), 124.3 (8-CH), 116.4 (9-C), 115.1 (14-C) , 100.9 (1-CH), 80.4 (17-CH_3), 56.7 (16-CH_3), 56.6 (15-CH_3), 15.0 (18-CH_3).

^{31}P NMR (162 MHz, Chloroform-*d*) δ 30.58.

HRMS (ESI) Calculated for $C_{36}H_{31}AuN_2O_3PS^{+}$:799.1453. Found: 799.1516.Error: -7.85 ppm

IR (diamond, cm^{-1}): 2924.57 (saturated CH), 2227.16 (CN), 1614.65 (aromatic C=C) 1436.52 (PPh_3).

[Ph_3PAu(2, 3, 7-trimethoxyacridine-9-carbonitrile)ClO_4] 58

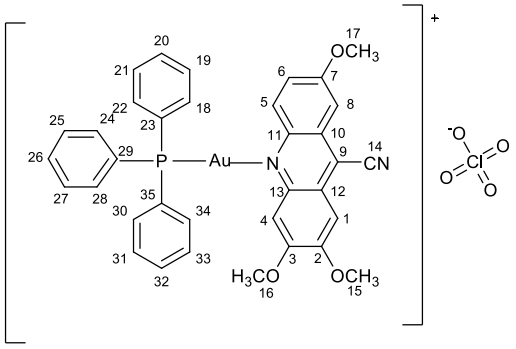

Orange solid (14.2 mg, 83 %).

MP: 140.5-142.5 ^{o}C.

^{1}H NMR (600 MHz, Chloroform-*d*) δ 8.33 (m, *J* = 9.3 Hz, 4H), 7.76 (m, 3H), 7.51 (dt, *J* = 12.9, 6.2 Hz, 5H), 7.46 (s, *J* = 7.3, 2.8 Hz, 1H), 7.18 – 7.39 (m, 7H), 4.14 (s, 6H), 4.04 (s, 3H).

^{13}C NMR (151 MHz, Chloroform-*d*) δ 159.7 (7-C) 155.8 (3-C), 153.66 (2-C), 134.2 (23-C, 29-C, 35-C), 134.0 (5-CH), 131.2 (18-CH, 22-CH,24-CH, 28-CH, 30-CH,34-CH), 129.2(19-CH, 21-CH, 25-CH, 27-CH,31-CH, 33-CH), 129.1 (20-CH, 26-CH, 32-CH), 127.5 (12-C) , 126.8 (10-C), 126.47 (6-CH), 124.7 (9-C), 114.91 (14-C), 103.7 (1-CH), 100.8 (4-CH), 100.7 (8-CH), 57.0 (16-CH_3), 56.7 (15-CH_3), 56.0 (17-CH_3),

^{31}P NMR (162 MHz, Chloroform-*d*) δ 32.08

HRMS (ESI) Calculated for $C_{35}H_{29}AuN_2O_3P^+$:753.1576. Found: 753.1619.Error: -5.68 ppm.

IR (diamond, cm^{-1}): 3065.70 (aromatic C-H) 2959.00 (saturated CH), 2192.70 (CN), 1622.66 (aromatic C=C) 1429.52 (PPh_3).

[Ph_3PAu(2, 3-dimethoxy-7-(methylthio)acridine-9-carbonitrile)ClO_4] 59

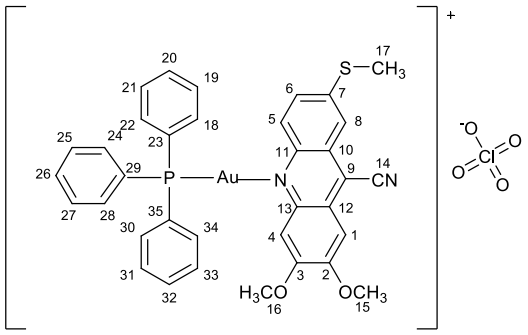

Orange solid (12.5 mg, 72 %).

MP: 120.5-122.5 ^{o}C.

^{1}H NMR (600 MHz, Chloroform-*d*) δ 8.16 (s, 1H), 7.84 (d, *J* = 1.9 Hz, 1H), 7.71 (d, *J* = 8.9 Hz, 1H), 7.65 (d, *J* = 8.9 Hz, 1H), 7.54 (m, *J* = 8.6 Hz, 8H), 7.49 (m, 3H), 7.45 (m, *J* = 39.5 Hz, 5H), 4.16 (s, 3H), 4.11 (s, 3H), 2.70 (s, 3H).

^{13}C NMR (151 MHz, Chloroform-*d*) δ 155.0 (3-C), 153.4 (2-C), 141.4 (11-C), 134.2 (23-C, 29-C, 35-C), 134.0 (7-C), 132.0 (18-CH, 22-CH,24-CH, 28-CH, 30-CH,34-CH), 130.3 (12-C), 129.2 (19-CH, 21-CH, 25-CH, 27-CH,31-CH, 33-CH), 129.2 (10-C), 128.9 (20-CH, 26-CH, 32-CH), 127.5 (5-CH), 125.2 (6-CH), 124.3 (8-CH), 116.4 (9-C), 115.1 (14-C), 105.4 (1-CH), 100.9 (4-CH),56.7 (16-CH_3), 56.6 (15-CH_3), 15.0 (17-CH_3).

^{31}P NMR (162 MHz, Chloroform-*d*) δ 32.39

HRMS (ESI) Calculated for $C_{35}H_{29}AuN_2O_2PS^+$:769.1347. Found: 769.1329.Error: 2.39 ppm

IR (diamond, cm^{-1}): 3073.20 (aromatic C-H), 2978.00 (saturated C-H), 2163.15 (CN), 1623.37 (aromatic C=C) 1428.07 (PPh_3).

[Ph_3PAu(3-methoxyacridine-9-carbonitrile)ClO_4] 60

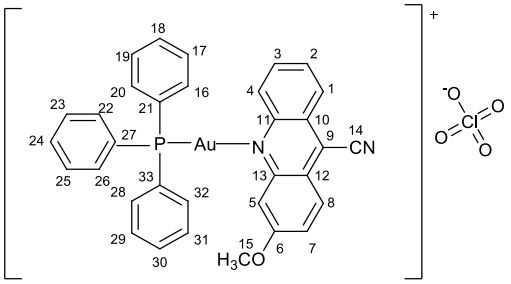

Greenish yellow solid (11.3 mg, 71 %).

MP: 120.9-122.9^{o}C.

^{1}H NMR (600 MHz, Chloroform-*d*) δ 9.01 (d, *J* = 7.0 Hz, 2H), 8.49 (d, *J* = 8.2 Hz, 3H), 8.40 (d, *J* = 9.8 Hz, 4H), 8.18 (s, 2H), 7.95 (m, *J* = 7.1 Hz, 3H), 7.62 (d, *J* = 9.1 Hz, 3H), 7.42 – 7.54 (m, 5H), 4.07 (s, 3H).

^{13}C NMR (151 MHz, Chloroform-*d*) δ 166.9 (3-C), 143.7 (13-C), 136.6 (11-C), 134. 2(21-C, 27-C, 33-C), 132.0(16-CH, 20-CH,22-CH, 26-CH, 28-CH,32-CH), 131.9 (6-CH), 129.7 (1-CH), 129.3 (17-CH, 19-CH, 23-CH, 25-CH,29-CH, 31-CH), 129.1 (12-C), 128.9 (18-CH, 24-CH, 30-CH), 128.46 (10-C), 127.3 (5-CH), 127.0 (7-CH), 125.9 (8-CH), 124.2 (2-CH), 124.1 (9-C), 112.8 (14-C), 98.9 (4-CH), 57.7 (15-CH_3).

^{31}P NMR (162 MHz, Chloroform-*d*) δ 30.11

HRMS (ESI) Calculated for $C_{33}H_{25}AuN_2OP^{+}$:693.1365 Found: 693.1391.Error: -3.79 ppm

IR (diamond, cm^{-1}): 3073.08 (aromatic C-H), 2165.13 (CN), 1633.80 (aromatic C=C) 1435.85 (PPh_3).

[Ph_3PAu(3-fluoroacridine-9-carbonitrile)ClO_4] 61

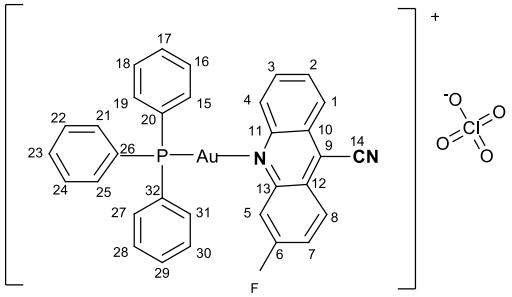

Yellow solid (11.6 mg, 74 %).

MP: 124.0-126.0 ^{o}C

^{1}H NMR (600 MHz, Chloroform-*d*) δ 8.42 – 8.51 (m, 2H), 8.01 – 8.10 (m, 2H), 7.87 (t, *J* = 7.7 Hz, 1H), 7.67 (s, 1H), 7.44 – 7.57 (m, 15H), 7.26 (s, 1H).

^{13}C NMR (151 MHz, Chloroform-*d*) δ 134.2 (20-C, 26-C, 32-C), 134.1 (11-C), 132.1 (1-CH), 132.0 (15-CH, 19-CH,21-CH, 25-CH, 27-CH,31-CH), 129.6 (6-CH), 129.3 (16-CH, 18-CH, 22-CH, 24-CH,28-CH, 30-CH), 129.2 (12-C), 128.8 (17-CH, 23-CH, 29-CH), 128.4 (10-C), 128.2 (5-CH), 128.1 (7-CH), 125.6 (8-CH), 123.69 (2-CH), 121.8 (9-C), 121.6 (14-C), 114.2 (4-CH).

^{31}PNMR (162 MHz, Chloroform-*d*) δ 29.72 (ESI) calculated for $C_{32}H_{22}AuFN_2P^{+}$:681.1165. Found: 681.1225.Error: -8.84 ppm

IR (diamond, cm^{-1}): 3056.99 (aromatic C-H), 2224.67 (CN), 1633.95 (aromatic C=C) 1437.28 (PPh_3).

IV.4. General Procedure for the Synthesis of Compounds 62, 63a, 64a, 65b and 66b.

$AgClO_4$ (4.2 mg, 0.020 mmol, 1 eq.) and Ph_3PAuCl (10.0 mg, 0.020 mmol, 1 eq.) were dissolved in methanol (0.5 mL) yielding a white precipitate instantly. The mixture was stirred for 30 minutes. The completion of the reaction was monitored by ^{31}P NMR (162

MHz, Chloroform-*d*) δ 27.5 ppm. A solution of corresponding pyrazole (0.020 mmol, 1 eq.) in CH_2Cl_2 (0.5 ml) was added to the previous solution and stirred for a further 30 minutes. The mixture was filtered over a glass microfiber filter placed in a syringe and into an NMR Schlenk flask, under nitrogen. The solution was dried under reduced pressure and $CDCl_3$ (0.5 mL) was added. ^{31}P, ^{1}H and ^{13}C NMR analyses were recorded. The material was concentrated under reduced pressure to obtain the title complex as a solid.

Triphenylphosphine(5-amino-4-(pyridin-2-yl)-1H-pyrazole)gold(I) perchlorate 62

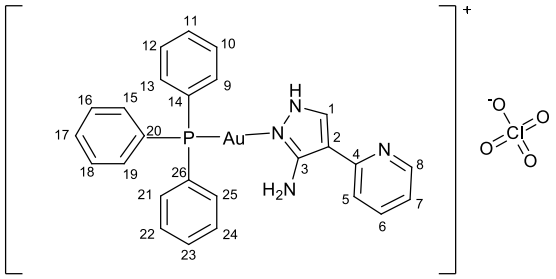

Brown solid (11.9 mg, 83 %).

MP: 165.6-168.2 ºC

^{1}H NMR (600 MHz, Chloroform-*d*) δ 8.49 (d, *J* = 4.7 Hz, 1H), 7.85 (s, 1H), 7.64 (td, *J* = 7.8, 1.9 Hz, 2H), 7.42-7.62 (m, 14H), 7.39 (d, *J* = 7.8 Hz, 2H), 7.06 (dd, *J* = 7.5, 4.9Hz, 1H), 6.39 (s, 2H).

^{13}C NMR (151 MHz, Chloroform-*d*) δ 154.7 (4-C), 148.6 (3-C), 136.5 (8-CH), 134.3 (6-CH), 134.2 (14-C, 20-C, 26-C), 132.5 (1-CH), 132.4(9-CH, 13-CH, 15-CH, 19-CH, 21-CH, 25-CH), 129.6(10-CH 12-CH, 16-CH, 18-CH, 22-CH,24-CH), 128.0(11-CH, 17-CH,23-CH), 127.1 (7-CH), 120.1 (5-CH), 118.4 (2-C).

^{31}P NMR (162 MHz, Chloroform-*d*) δ 30.0

HRMS (ESI) Calculated for $C_8H_8N_4AuPh_3P^+$: 619.1320. Found 619.1320. Error: 0.12 ppm.

IR (diamond, cm^{-1}): 3073.97 (NH_2), 2923.29 (CH), 1621.74 (C=C), 1514.68 (benzene ring).

Triphenylphosphine(5-Amino-4-(4-bromophenyl)-pyrazole) gold(I) perchlorate 63a

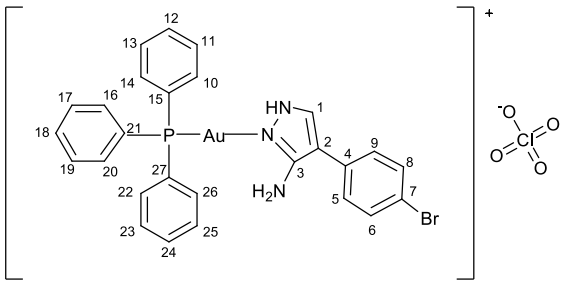

Light brown solid (15.0 mg, 94 %).

MP: 142.4-144.6^{o}C.

^{1}H NMR (600 MHz, Chloroform-*d*) δ 12.21 (broad s, 1H), 7.52–7.62 (m, 21H), 7.24 (s, 1H).

^{13}C NMR (151 MHz, Chloroform-*d*) δ 134.3 (3-C), 134.2(15-C, 21-C, 27-C), 132.5 (1-CH), 132.5 (4-CH), 132.4 ((10-CH, 14-CH, 16-CH, 20-CH, 22-CH, 26-CH), 129.8 (5-CH), 129.8 (9-CH), 129.6 (11-CH, 13-CH, 17-CH, 19-CH, 23-CH,25-CH), 128.3 (12-CH, 18-CH,24-CH), 127.4 (7-C), 127.0 (6-CH, 8-CH), 120.9(2-C).

^{31}P NMR (162 MHz, Chloroform-*d*) δ 31.0.

HRMS (ESI) calculated for $C_9H_8BrN_3AuPh_3P^+$:696.0473. Found: 696.0469. Error: -5.22 ppm.

IR (diamond, cm^{-1}): 3356.99 (NH_2), 2921.62 (CH), 1621.58 (C=C), 1598.78 (benzene ring).

Triphenylphosphine(5-Amino-4-(4-bromophenyl)-3-methylpyrazole) gold(I) perchlorate 64a

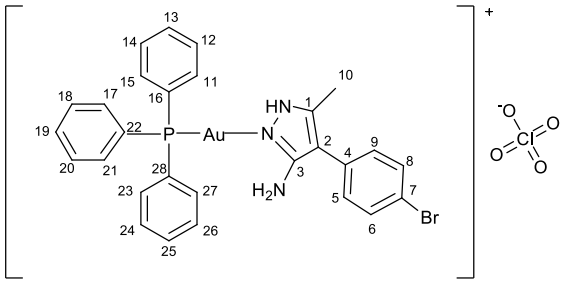

Grey solid (14.3 mg, 88 %).

MP: 148.0-149.6ºC.

^{1}H NMR (600 MHz, Chloroform-*d*) δ 11.86 (broad s, 2H), 7.51–7.62 (m, 16H), 7.45 (d, *J* = 8.7 Hz, 1H), 7.16 (d, *J* = 8.3 Hz, 2H), 3.72 (q, *J* = 7.0 Hz, 1H), 2.32 (s, 3H).

^{13}C NMR (151 MHz, Chloroform-*d*) δ 134.4 (1-C), 134.2(16-C, 22-C, 28-C), 132.5 (4-C), 132.4(11-CH, 15-CH, 17-CH, 21-CH, 23-CH, 27-CH), 130.5 (5-CH, 9-CH), 130.4 (7-C), 129.7 (6-CH, 8-CH), 129.6(12-CH 14-CH, 18-CH, 20-CH, 24-CH,26-CH), 127.6(13-CH, 19-CH, 25-CH),121.2 (2-C), 13.8 (10-CH_3)

. **^{31}P NMR (162 MHz, Chloroform-*d*) δ** 31.50

HRMS (ESI) Calculated for $C_{10}H_{10}BrN_3AuPh_3P^+$:710.0630. Found: 710. 0634. Error: -2.01 ppm

IR (diamond, cm^{-1}): 3316.13 (NH_2), 2924.07 (CH), 1598.28 (benzene ring).

Triphenylphosphine(5-Amino-4-cyano-1-(2-hydroxyethyl)-pyrazole gold(I) perchlorate 65b

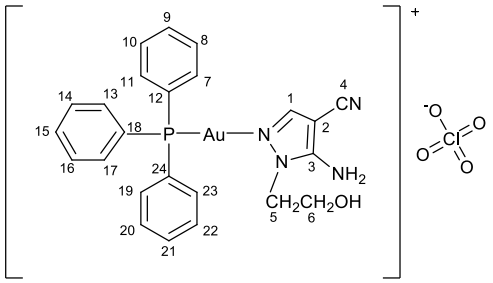

Yellow solid. (13.5 mg, 95%).

MP: 126.3-127.4 ºC.

^{1}H NMR (600 MHz, Chloroform-*d*) δ 7.82 (s, 1H), 7.45 – 7.63 (m, 16H), 5.86 (s, 2H), 4.44 (t, *J* = 5.0 Hz, 2H), 4.10 (t, *J* = 5.1 Hz, 2H).

^{13}C NMR (151 MHz, Chloroform-*d*) δ 152.9 (3-C), 134.1(1-CH), 134.0 (12-C, 18-C, 24-C), 132.8(7-CH, 11-CH, 13-CH, 17-CH, 19-CH, 23-CH), 129.9 (8-CH 10-CH, 14-CH, 16-CH, 20-CH,22-CH) , 129.8(9-CH, 15-CH, 21-CH), 109.9 (4-C), 78.0 (2-C), 60.5 (5-CH_2), 52.7 (6-CH_2)

^{31}P NMR (162 MHz, Chloroform-*d*) δ 29.70

HRMS (ESI) Calculated for $C_6H_8N_4OAuPh_3P^+$:611.1270. Found: 611.1253. Error: 2.76 ppm.

IR (diamond, cm^{-1}): 3339.28 (NH_2), 3214.86 (OH) 2924.76 (CH), 2224.58 (CN), 1645.18 (C=C), 1583.90 (benzene ring).

Triphenylphosphine(3-Amino-4-bromo-2-methylpyrazol) gold(I) perchlorate 66b

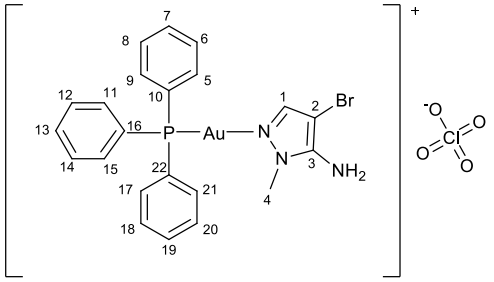

Dark brown solid (12.8 mg, 87%).

MP: 172.2-174.3 ^{o}C.

^{1}H NMR (600 MHz, Chloroform-*d*) δ 7.60 – 7.66 (m, 3H), 7.47 – 7.60 (m, 12H), 7.35 (s, 1H), 4.97 (s, 2H), 3.98 (s, 3H)

^{13}C NMR (151 MHz, Chloroform-*d*) δ 157.2 (3-C), 134.0 (10-C, 16-C, 22-C), 133.9 (1-CH), 132.9 (5-CH, 9-CH, 11-CH, 15-CH, 17-CH, 21-CH), 129.8(6-CH 8-CH, 12-CH, 14-CH, 18-CH,20-CH), 127.0(7-CH, 13-CH, 19-CH) , 78.5 (2-C), 36.8 (4-CH_3).

^{31}P NMR (162 MHz, Chloroform-*d*) δ 30.0.

HRMS (ESI) Calculated for $C_4H_6BrN_3AuPh_3P^+$:634.0317. Found: 634.0310 Error: 0.95 ppm

IR (diamond, cm^{-1}): 3337.43 (NH_2), 2925.08 (CH), 1645.83 (C=C), 1579.65 (benzene ring)

IV.5. General Procedure for the Synthesis of Compounds 67-75

$AgClO_4$ (4.2 mg, 0.020 mmol, 1 eq.) were dissolved in methanol (0.5 mL) yielding a white precipitate. A solution of corresponding acridine/pyrazole (0.020 mmol, 1 eq.) in CH_2Cl_2 (0.5 ml) was added to the solution and stirred for 30 minutes. The mixture was filtered over a glass microfiber filter placed in a syringe and into an NMR Schlenk flask,

under nitrogen. The solution was dried under reduced pressure and $CDCl_3$ (0.5 mL) was added. ^1H and ^{13}C NMR analyses were recorded. The material was concentrated under reduced pressure to obtain the title complex as a solid.

[Ag(2-chloroacridine-9-carbonitrile)ClO_4] 67

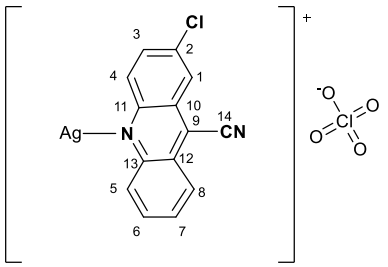

Yellowish green solid (5.4 mg 78 %)

MP: 221.3-223.3 ^oC

^{1}H NMR (600 MHz, Chloroform-*d*) δ 8.30 – 8.35 (m, 2H), 8.28 (d, *J* = 8.7 Hz, 1H), 8.23 (d, *J* = 9.2 Hz, 1H), 7.89 (t, *J* = 7.7 Hz, 1H), 7.76 – 7.82 (m, 2H).

^{13}C NMR (151 MHz, Chloroform-*d*) δ 148.3 (13-C), 146.5 (11-C), 135.6 (2-C), 132.4 (3-CH), 132.0(12-C), 131.2 (6-CH), 130.5 (4-CH), 129.7 (5-CH), 126.3 (10-C), 126.2 (8-CH), 125.1 (7-CH), 123.5 (1-CH), 114.7 (9-C), 114.2 (14-C).

HRMS (ESI) Calculated for $C_{14}H_7AgClN_2$:344.9343. Found: 344.9338.Error: 1.59 ppm

IR (diamond, cm^{-1}): 3073.26 (aromatic C-H), 2231.85 (CN), 1622.64 (C=C) 1516.54 (benzene ring)

[Ag(2-bromoacridine-9-carbonitrile)ClO_4] 68

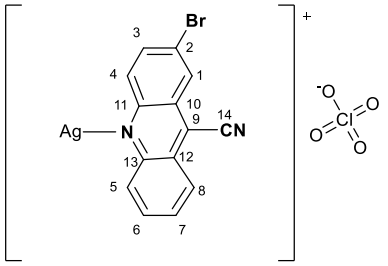

Yellowish green solid (5.9 mg, 75 %)

MP: 166.1-168.1 ^oC

^{1}H NMR (600 MHz, Chloroform-*d*) δ 8.42 (s, 1H), 8.27 (d, *J* = 8.6 Hz, 1H), 8.21 (d, *J* = 8.7 Hz, 1H), 8.08 (d, *J* = 9.1 Hz, 1H), 7.86 (d, *J* = 8.7 Hz, 2H), 7.75 (t, *J* = 7.6 Hz, 1H).

^{13}C NMR (151 MHz, Chloroform-*d*) δ 148.3 (13-C), 146.5 (11-C), 134.7 (3-CH), 131.8 (6-CH), 131.2 (12-C), 130.4 (4-CH), 129.7 (5-CH), 126.9 (8-CH), 126.6 (7-CH), 126.1 (10-C), 125.1 (1-CH), 124.0 (2-C), 114.6 (9-C), 114.0 (14-C).

HRMS (ESI) Calculated for $C_{14}H_7AgBrN_2$:388.8838. Found: 388.8826.Error: 0.38 ppm

IR (diamond, cm^{-1}): 3195.80 (aromatic C-H), 2171.97 (CN), 1619.40 (aromatic C=C).

[Ag(2-chloro-6-methoxyacridine-9-carbonitrile)ClO_4] 69

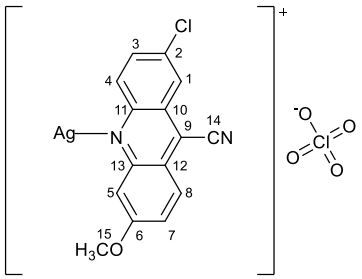

Yellowish brown solid (5.4 mg, 72 %)

MP: 224.7-226.7 ^oC

^{1}H NMR (600 MHz, Chloroform-*d*) δ 7.90 (d, *J* = 8.5 Hz, 2H), 7.77 (s, 1H), 7.54 (d, *J* = 9.4 Hz, 1H), 7.34 – 7.16 (m, 1H), 7.05 (s, 1H), 3.89 (s, 3H).

^{13}C NMR (151 MHz, Chloroform-*d*) δ 162.0 (6-C), 150.2 (13-C), 146.7 (11-C), 134.1 (2-C), 132.4 (3-CH), 131.2 (12-C), 126.1 (8-CH), 125.5 (4-CH), 124.9 (10-C), 123.7 (1-CH), 122.9 (7-CH), 114.7 (9-C), 114.2 (14-C), 105.8 (5-CH), 55.9 (15-CH_3).

HRMS (ESI) Calculated for $C_{15}H_9AgClON_2$:376.5700. Found: 374.9449.Error:-3.67 ppm

IR (diamond, cm^{-1}): 2930.50 (CH sat), 2228.50 (CN), 1627.74 (aromatic C=C), 1295.94 (C-O).

[Ag(7-chloro-2, 3, 4-trimethoxyacridine-9-carbonitrile)ClO_4] 70

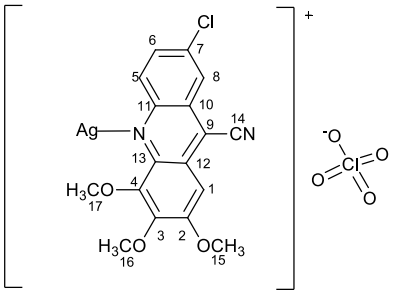

Brown solid (7.5 mg, 86 %)

MP: 210.2-212.2 ^{o}C

^{1}H NMR (600 MHz, Chloroform-*d*) δ 8.30 (d, *J* = 9.1 Hz, 1H), 8.25 (s, 1H), 7.74 – 7.69 (m, 1H), 7.25 (s, 1H), 4.24 (s, 3H), 4.13 (d, *J* = 13.1 Hz, 6H).

^{13}C NMR (151 MHz, Chloroform-*d*) δ 156.6 (2-C), 146.8 (13-C), 145.8 (4-C), 144.0 (11-C), 141.8 (7-C), 135.1 (6-CH), 132.2 (3-C), 131.0 (12-C), 125.9 (5-CH), 125.4 (10-C), 123.0 (8-CH), 115.2 (9-C)7, 111.1 (14-C), 96.7 (1-CH), 62.5 (17-CH_3), 61.7 (16-CH_3), 56.6 (15-CH_3).

HRMS (ESI) Calculated for $C_{17}H_{13}AgClO_3N_2$:434.9660. Found: 434.9677.Error:-6.40 ppm

IR (diamond, cm^{-1}): 2942.90 (saturated CH) 2243.60 (CN), 1608.60 (aromatic C=C).

[Ag(7-bromo-2, 3, 4-trimethoxyacridine-9-carbonitrile)ClO_4] 71

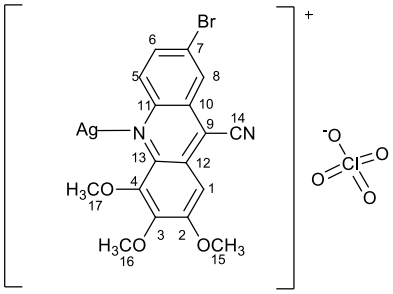

Brown solid (8.0 mg, 83 %)

MP: 217.8-219.8 ^{o}C

^{1}H NMR (600 MHz, Chloroform-*d*) δ

8.45 (d, *J* = 2.0 Hz, 1H), 8.22 (d, *J* = 9.1 Hz, 1H), 7.85 (dd, *J* = 9.0, 2.1 Hz, 1H), 7.26 (s, 1H), 4.24 (s, 3H), 4.14 (d, *J* = 13.6 Hz, 6H).

^{13}C NMR (151 MHz, Chloroform-*d*) δ 156.6 (2-C), 146.7 (13-C), 144.2 (4-C), 142.0 (6-CH), 133.4 (3-C), 132.2 (12-C), 126.4 (5-CH), 126.3 (10-C), 125.4 (8-CH), 123.5 (7-C), 115.3 (9-C), 111.0 (14-C), 96.7 (1-CH), 62.5 (17-CH_3), 61.6 (16-CH_3), 56.5 (15-CH_3).

HRMS (ESI) Calculated for $C_{17}H_{13}AgBrO_3N_2$:478.9155. Found: 478.9183.Error:-8.81 ppm

IR (diamond, cm^{-1}):

2916.70 (aromatic H), 2247.50 (CN), 1627.30 (aromatic C=C),

[Ag(5-amino-4-(pyridin-2-yl)-1H-pyrazole)ClO_4] 72

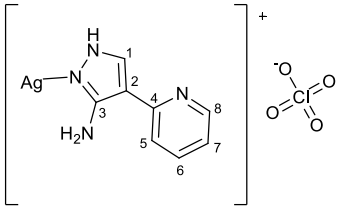

Greenish brown solid (4.7 mg 88 %)

MP: 142.2-144.2 ^oC

^{1}H NMR (600 MHz, Chloroform-*d*) δ 8.50 (s, 1H), 7.76 (d, *J* = 4.9 Hz, 2H), 7.61 (m, *J* = 7.8, 1.9 Hz, 1H), 7.41 (d, *J* = 8.1 Hz, 2H), 7.01 (dd, *J* = 7.4, 5.1 Hz, 2H).

^{13}C NMR (151 MHz, Chloroform-*d*) δ 168.7(4-C), 148.6 (8-CH), 144.5 (6-CH), 136.2 (1-CH), 119.4 (7-CH), 118.7 (5-CH), 73.6 (2-C).

HRMS (ESI) Calculated for $C_8H_8AgN_4$:266.9794. Found: 266.9799.Error: -1.81 ppm

IR (diamond, cm^{-1}): 3264.05 (NH_2), 2922.54 (CH), 1597.62 (C=C), 1549.44 (benzene ring).

[Ag(5-Amino-4-(4-bromophenyl)-pyrazole)ClO_4] 73

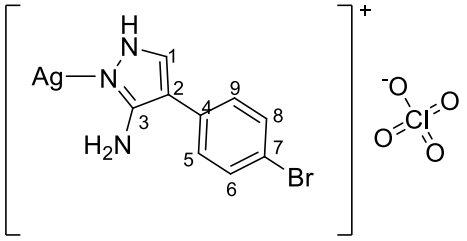

Dark green solid (6.4 mg, 93 %)

MP: 156.8-157-8 ^oC

^{1}H NMR (600 MHz, Chloroform-*d*) δ 7.47-7.53 (m, 4H), 7.34 (d, *J* = 8.1 Hz, 3H), 7.26(s, 1H).

^{13}C NMR (151 MHz, Chloroform-*d*) δ 132.0 (3-C), 131.8 (1-CH), 128.3 (4-C), 128.3 (5-CH, 9-CH), 119.9 (7-C), 108.1 (6-CH, 8-CH), 103.6 (2-C).

HRMS (ESI) Calculated for $C_9H_8AgBrN_3$:343.8947. Found: 343.8948.Error: -0.40 ppm

IR (diamond, cm^{-1}): 3316.69 (NH_2), 2926.96 (CH), 1644.30 (C=C), 1502.30 (benzene ring).

[Ag(5-Amino-4-(4-bromophenyl)-3-methylpyrazole)ClO4] 74

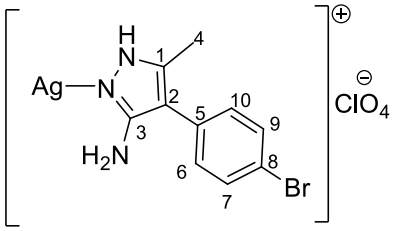

Dark green solid (6.5 mg, 91 %)

MP: 154.9-156.9 ºC

^{1}H NMR (600 MHz, Chloroform-*d*) δ 7.50 – 7.55 (m, 2H), 7.19 – 7.23 (m, *J* = 1.3 Hz, 4H).4.28 (broad s, 1H) 2.25 (s, 3H)

^{13}C NMR (151 MHz, Chloroform-*d*) δ 151.9 (3-C), 137.9 (1-C), 131.9 (5-C), 131.9 (6-CH, 10-CH), 130.1 (8-C), 120.0 (7-CH, 9-CH), 105.5 (2-C), 10.8 (4-CH_3).

HRMS (ESI) Calculated for $C_{10}H_{10}AgBrN_3$:357.9104. Found: 359.9098.Error: -4.47 ppm

IR (diamond, cm^{-1}): 3290.19 (NH_2), 2997.00 (CH), 1670.00 (C=C), 1579.20 (benzene ring).

[Ag (3-Amino-4-bromo-2-methylpyrazol)ClO_4] 75

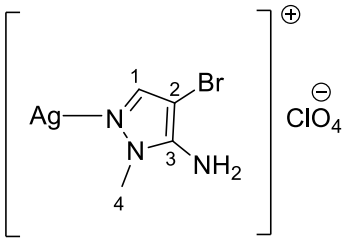

Dark green solid (5.1 mg, 90 %)

MP: 130.2-132.2 ^oC

^{1}H NMR (600 MHz, Chloroform-*d*) δ 7.23 (s, 3H), 3.52 – 3.60 (s, 3H)

^{13}C NMR (151 MHz, Chloroform-*d*) δ 142.4 (3-C), 137.6 (1-CH), 77.9(2-C), 35.4 (4-CH_3).

HRMS (ESI) Calculated for $C_4H_6AgBrN_3$:281.8791 Found: 283.8783.Error: -0.64 ppm

IR (diamond, cm^{-1}): 3340.25 (NH_2), 2923.52 (CH), 1626.60 (C=C), 1570.27 (benzene ring).

IV.6. Uv-Vis and fluorescence

$1X10^{-3}$ M stock solution of acridine ligand, acridine gold complexes and the standard were prepared with absolute ethanol (99 %) in 50 mL volumetric flasks and placed in the sonic bath for 5 minutes in other to obtain a homogeneous solution. Then, $1X10^{-4}$ M, $1X10^{-5}$ M, $1X10^{-6}$ M, $1X10^{-7}$ M, $1X10^{-8}$ M, $1X10^{-9}$ M of each solution were prepared in 10 mL volumetric flask from the stock solutions by serial dilution. The UV-vis specra of the solutions were measured by Thermo Spectronic UV 300 UV-visible spectrometer to find the concentration of each sample that gave a maximum absorption closed to 0.5 Absorbance at 365nm. The linear mode of each sample were taken in other to ensure that Beer Lambert law was obeyed. The fluorescence data of each sample were taken by a Perkin Elmer LS 45 Fluorescence spectrometer. The quantum yield of each sample were calculated.

IV.7. Cell viability assays

The biological activity of the complexes were assessed after dilution in DMSO/H_2O (10% v/v) and addition to HepG2 cells. Assays were performed in 96-well plates using the Promega CellTiter-Blue assay as an endpoint method with a 2-hour incubation with the assay reagent. This assay measures cell viability and is based upon the ability of living cells to convert a redox dye (resazurin) into a fluorescent product (resorufin). Each well received 90 µL of cell suspension at a density of 22,500 cells per well and was cultured overnight (at 37 °C/5% CO_2 humidified air) before 10 µL of the test sample was added. The experiments were set up in triplicate. The mock control wells received 90 µL of cell suspension and 10 µL of the appropriate buffer (DMSO/H_2O). Wells that contained just 100 µL of cell culture medium served as background fluorescence controls. Fluorescent measurements were taken using the GloMax-Multi Detection System (Promega).

References

(1) Saad, B.; Azaizeh, H.; Said, O. Tradition and Perspectives of Arab Herbal Medicine: A Review. *Evidence-based Complement. Altern. Med.* **2005**, *2* (4), 475–479.

(2) Pan, S. Y.; Litscher, G.; Gao, S. H.; Zhou, S. F.; Yu, Z. L.; Chen, H. Q.; Zhang, S. F.; Tang, M. K.; Sun, J. N.; Ko, K. M. Historical Perspective of Traditional Indigenous Medical Practices: The Current Renaissance and Conservation of Herbal Resources. *Evidence-based Complement. Altern. Med.* **2014**, *2014*, 1–21.

(3) Zhang, P.; Sadler, P. J. Advances in the Design of Organometallic Anticancer Complexes. *J. Organomet. Chem.* **2017**, *839*, 5–14.

(4) Gasser, G.; Metzler-Nolte, N. The Potential of Organometallic Complexes in Medicinal Chemistry. *Curr. Opin. Chem. Biol.* **2012**, *16* (1–2), 84–91.

(5) Wai-Yin Sun, R.; Ma, D.-L.; Wong, E. L.-M.; Che, C.-M. Some Uses of Transition Metal Complexes as Anti-Cancer and Anti-HIV Agents. *Dalt. Trans.* **2007**, 43, 4884-4892.

(6) Zou, T.; Lum, C. T.; Chui, S. S. Y.; Che, C. M. Gold(III) Complexes Containing N-Heterocyclic Carbene Ligands: Thiol “Switch-on” Fluorescent Probes and Anti-Cancer Agents. *Angew. Chemie - Int. Ed.* **2013**, *52* (10), 2930–2933.

(7) Desoize, B. Metals and Metal Compounds in Cancer Treatment. *Anticancer Res.* **2004**, *24* (3 A), 1529–1544.

(8) Chen, P.; Xu, R.; Yan, L.; Wu, Z.; Wei, Y.; Zhao, W.; Wang, X.; Xie, Q.; Li, H. Properties of Realgar Bioleaching Using an Extremely Acidophilic Bacterium

and Its Antitumor Mechanism as an Anticancer Agent. *Biol. Res.* **2017**, *50*, (17) 1-11.

(9) Mayorga, J.; Richardson-Hardin, C.; Dicke, K. A. Arsenic Trioxide as Effective Therapy for Relapsed Acute Promyelocytic Leukemia. *Clin. J. Oncol. Nurs.* **2002**, *6* (6), 341–346.

(10) Leoni, F.; Gianfaldoni, G.; Annunziata, M.; Fanci, R.; Ciolli, S.; Nozzoli, C.; Ferrara, F. Arsenic Trioxide Therapy for Relapsed Acute Promyelocytic Leukemia: A Bridge to Transplantation. *Haematologica* **2002**, *87* (5), 485–489.

(11) Mejia, C.; Ortega-Rosales, S.; Ruiz-Azuara, L. *Biomedical Applications of Metals*; Rai, M., Ingle, A. P., Medici, S., Eds.; Springer International Publishing: Cham, **2018**, 213-234.

(12) Muller, S.; Miller Jr., W. H.; Dejean, A. Trivalent Antimonials Induce Degradation of the PML-RAR Oncoprotein and Reorganization of the Promyelocytic Leukemia Nuclear Bodies in Acute Promyelocytic Leukemia NB4 Cells. *Blood* **1998**, *92* (11), 4308–4316.

(13) Haldar, A. K.; Sen, P.; Roy, S. Use of Antimony in the Treatment of Leishmaniasis: Current Status and Future Directions. *Mol. Biol. Int.* **2011**, *2011*, 1–23.

(14) Goldbeck-Wood, S. Antimony as a Symbol in Medicine. *Lancet* **2000**, *355* (9214), 1565.

(15) Keogan, D. M.; Griffith, D. M. Current and Potential Applications of Bismuth-Based Drugs. *Molecules* **2014**, *19* (9), 15258–15297.

(16) Beatrix Bialek, F. T. Medical Use of Bismuth: The Two Sides of the Coin. *J. Clin. Toxicol.* **2011**, *s3* (01), 1–5.

(17) Andrews, P. C.; Blair, V. L.; Ferrero, R. L.; Junk, P. C.; Kedzierski, L.; Peiris, R. M. Bismuth(III) β-Thioxoketonates as Antibiotics against Helicobacter Pylori and as Anti-Leishmanial Agents. *Dalt. Trans.* **2014**, *43* (3), 1279–1291.

(18) Yang, Y.; Ouyang, R.; Xu, L.; Guo, N.; Li, W.; Feng, K.; Ouyang, L.; Yang, Z.; Zhou, S.; Miao, Y. Review: Bismuth Complexes: Synthesis and Applications in Biomedicine. *J. Coord. Chem.* **2015**, *68* (3), 379–397.

(19) Melnikov, P.; Malzac, A.; Coelho, M. de B. Gallium and Bone Pathology. *Acta Ortopédica Bras.* **2008**, *16* (1), 54–57.

(20) Chitambar, C. R. Medical Applications and Toxicities of Gallium Compounds. *Int. J. Environ. Res. Public Health* **2010**, *7* (5), 2337–2361.

(21) Hart, M. M.; Adamson, R. H. Antitumor Activity and Toxicity of Salts of Inorganic Group IIIa Metals: Aluminum, Gallium, Indium, and Thallium. *Proc. Natl. Acad. Sci. U. S. A.* **1971**, *68* (7), 1623–1626.

(22) Kheiri, R.; Koohi, M. K.; Sadeghi-Hashjin, G.; Nouri, H.; Khezli, N.; Hassan, M. A.; Hoomani, F.; Shams, G.; Rasouli, A.; Motaghinejad, M. Comparison of the Effects of Iron Oxide, as a New Form of Iron Supplement, and Ferrous Sulfate on the Blood Levels of Iron and Total Iron-Binding Globulin in the Rabbit. *Iran. J. Med. Sci.* **2017**, *42* (1), 79–84.

(23) Ferrari, P.; Nicolini, A.; Manca, M. L.; Rossi, G.; Anselmi, L.; Conte, M.; Carpi, A.; Bonino, F. Treatment of Mild Non-Chemotherapy-Induced Iron Deficiency Anemia in Cancer Patients: Comparison between Oral Ferrous Bisglycinate

Chelate and Ferrous Sulfate. *Biomed. Pharmacother.* **2012**, *66* (6), 414–418.

(24) Oexle, H.; Gnaiger, E.; Weiss, G. Iron-Dependent Changes in Cellular Energy Metabolism: Influence on Citric Acid Cycle and Oxidative Phosphorylation. *Biochim. Biophys. Acta - Bioenerg.* **1999**, *1413* (3), 99–107.

(25) Cowley, A.; Woodward, B. A Healthy Future: Platinum in Medical Applications Platinum Group Metals Enhance the Quality of Life of the Global Population. *Platin. Met. Rev.* **2011**, *55* (2), 98–107.

(26) Agnew, W. F.; Yuen, T. G. H.; McCreery, D. B.; Bullara, L. A. Histopathologic Evaluation of Prolonged Intracortical Electrical Stimulation. *Exp. Neurol.* **1986**, *92* (1), 162–185.

(27) Desoize, B.; Madoulet, C. Particular Aspects of Platinum Compounds Used at Present in Cancer Treatment. *Crit. Rev. Oncol. Hematol.* **2002**, *42* (3), 317–325.

(28) Shaloam Dasari and Paul Bernard Tchounwou. Cisplatin in Cancer Therapy : Molecular Mechanisms of Action. *Eur J Pharmacol* **2015**, *5* (0), 364–378.

(29) Casini, A.; Reedijk, J. Interactions of Anticancer Pt Compounds with Proteins: An Overlooked Topic in Medicinal Inorganic Chemistry? *Chem. Sci.* **2012**, *3* (11), 3135–3144.

(30) Shimada, M.; Itamochi, H.; Kigawa, J. Nedaplatin: A Cisplatin Derivative in Cancer Chemotherapy. *Cancer Manag. Res.* **2013**, *5* (1), 67–76.

(31) Lu, X.; Wu, Y.-M.; Yang, J.-M.; Ma, F.-E.; Li, L.-P.; Chen, S.; Zhang, Y.; Ni, Q.-L.; Pan, Y.-M.; Hong, X.; et al. Preparation of Rhodium(III) Complexes with 2(1H)-Quinolinone Derivatives and Evaluation of Their in Vitro and in Vivo

Antitumor Activity. *Eur. J. Med. Chem.* **2018**, *151*, 226–236.

(32) Gras, M.; Therrien, B.; Süss-Fink, G.; Casini, A.; Edafe, F.; Dyson, P. J. Anticancer Activity of New Organo-Ruthenium, Rhodium and Iridium Complexes Containing the 2-(Pyridine-2-Yl)Thiazole N,N-Chelating Ligand. *J. Organomet. Chem.* **2010**, *695* (8), 1119–1125.

(33) Katsaros, N.; Anagnostopoulou, A. Rhodium and Its Compounds as Potential Agents in Cancer Treatment. **2002**, *42*, 297–308.

(34) Zhong, H. J.; Wang, W.; Kang, T. S.; Yan, H.; Yang, Y.; Xu, L.; Wang, Y.; Ma, D. L.; Leung, C. H. A Rhodium(III) Complex as an Inhibitor of Neural Precursor Cell Expressed, Developmentally Down-Regulated 8-Activating Enzyme with in Vivo Activity against Inflammatory Bowel Disease. *J. Med. Chem.* **2017**, *60* (1), 497–503.

(35) Yang, C.; Wang, W.; Liang, J. X.; Li, G.; Vellaisamy, K.; Wong, C. Y.; Ma, D. L.; Leung, C. H. A Rhodium(III)-Based Inhibitor of Lysine-Specific Histone Demethylase 1 as an Epigenetic Modulator in Prostate Cancer Cells. *J. Med. Chem.* **2017**, *60* (6), 2597–2603.

(36) Elias, C. N.; Lima, J. H. C.; Valiev, R.; Meyers, M. A. Biomedical Applications of Titanium and Its Alloys. *Jom* **2008**, *60* (3), 46–49.

(37) Clarke, M. J.; Zhu, F.; Frasca, D. R. Non-Platinum Chemotherapeutic Metallopharmaceuticals. *Chem. Rev.* **1999**, *99* (9), 2511–2534.

(38) Kopf, H.; Kopfmaier, P. Titanocene Dichloride - 1St Metallocene With Cancerostatic Activity. *Angew. Chemie-International Ed. English* **1979**, *18* (6), 477–478.

(39) Tsiani, E.; Fantus, I. G. Vanadium Compounds Biological Actions and Potential as Pharmacological Agents. *Trends Endocrinol. Metab.* **1997**, *8* (2), 51–58.

(40) Goldwaser, I.; Gefel, D.; Gershonov, E.; Fridkin, M.; Shechter, Y. Insulin-like Effects of Vanadium: Basic and Clinical Implications. *J. Inorg. Biochem.* **2000**, *80* (1–2), 21–25.

(41) Thompson, H. J.; Chasteen, N. D.; David, L. Dietary Vanadyl(IV) Sulfate Inhibits Chemically-Induced Mammary Carcinogenesis Henry. *Carcinogenesis* **1984**, *5* (6), 849–851.

(42) Sadler, P. J.; Guo, Z. Metal Complexes in Medicine: Design and Mechanism of Action. *Pure Appl. Chem.* **1998**, *70* (4), 863–871.

(43) Sekhon, B. S.; Gandhi, L. Medicinal Uses of Inorganic Compounds - 1. *Resonance* **2006**, *11* (4), 75–89.

(44) Anilanmert, B. Therapeutic Organometallic Compounds. *Pharmacology* **2012**, 651–680.

(45) Warra, A. A. Transition Metal Complexes and Their Application in Drugs and Cosmetics. *J. Chem. Pharm. Res.* **2011**, *3* (4), 951–958.

(46) Monney, A.; Albrecht, M. Transition Metal Bioconjugates with an Organometallic Link between the Metal and the Biomolecular Scaffold. *Coord. Chem. Rev.* **2013**, *257* (17–18), 2420–2433.

(47) Farrell, N. *Transition Metal Complexes as Drugs and Chemotherapeutic Agents*; Catalysis by Metal Complexes; Springer Netherlands: Dordrecht, **1989**, 11, 1-40.

(48) Albada, B.; Metzler-Nolte, N. Organometallic-Peptide Bioconjugates: Synthetic

Strategies and Medicinal Applications. *Chem. Rev.* **2016**, *116* (19), 11797–11839.

(49) Jain, P. K.; Huang, X.; El-Sayed, I. H.; El-Sayed, M. A. ChemInform Abstract: Noble Metals on the Nanoscale: Optical and Photothermal Properties and Some Applications in Imaging, Sensing, Biology, and Medicine. *ChemInform* **2009**, *40* (14), 7–9.

(50) Mjos, K. D.; Orvig, C. Metallodrugs in Medicinal Inorganic Chemistry. *Chem. Rev.* **2014**, *114* (8), 4540–4563.

(51) Guo, Z.; Sadler, P. J. Metals in Medicine. *Angew. Chemie Int. Ed.* **1999**, *38* (11), 1512–1531.

(52) Witt, M.; Roesky, H. W. Transition and Main Group Metals in Cyclic Phosphazanes and Phosphazenes. *Chem. Rev.* **1994**, *94* (5), 1163–1181.

(53) Green, M. L. H.; Ng, D. K. P. Cycloheptatriene and -Enyl Complexes of the Early Transition Metals. *Chem. Rev.* **1995**, *95* (2), 439–473.

(54) McRae, R.; Bagchi, P.; Sumalekshmy, S.; Fahrni, C. J. In Situ Imaging of Metals in Cells and Tissues. *Chem. Rev.* **2009**, *109* (10), 4780–4827.

(55) Scott, L. E.; Orvig, C. Medicinal Inorganic Chemistry Approaches to Passivation and Removal of Aberrant Metal Ions in Disease. *Chem. Rev.* **2009**, *109* (10), 4885–4910.

(56) Schwerdtfeger, P. Relativistic Effects in Properties of Gold. *Heteroat. Chem.* **2002**, *13* (6), 578–584.

(57) Nardon, C.; Boscutti, G.; Fregona, D. Beyond Platinums: Gold Complexes as

Anticancer Agents. *Anticancer Res.* **2014**, *34* (1), 487–492.

(58) Kostova, I.; Bentham Science Publishers, B. S. P. Gold Coordination Complexes as Anticancer Agents. *Anticancer. Agents Med. Chem.* **2006**, *6* (1), 19–32.

(59) Negom Kouodom, M.; Ronconi, L.; Celegato, M.; Nardon, C.; Marchi??, L.; Dou, Q. P.; Aldinucci, D.; Formaggio, F.; Fregona, D. Toward the Selective Delivery of Chemotherapeutics into Tumor Cells by Targeting Peptide Transporters: Tailored Gold-Based Anticancer Peptidomimetics. *J. Med. Chem.* **2012**, *55* (5), 2212–2226.

(60) Sivaram, H.; Tan, J.; Huynh, H. V. Syntheses, Characterizations, and a Preliminary Comparative Cytotoxicity Study of Gold(I) and Gold(III) Complexes Bearing Benzimidazole- and Pyrazole-Derived N-Heterocyclic Carbenes. *Organometallics* **2012**, *31* (16), 5875–5883.

(61) Papaiconomou, N.; Vite, G.; Goujon, N.; Lévêque, J.-M.; Billard, I. Efficient Removal of Gold Complexes from Water by Precipitation or Liquid–liquid Extraction Using Ionic Liquids. *Green Chem.* **2012**, *14* (7), 2050.

(62) Laguna, A. *Modern Supramolecular Gold Chemistry: Gold-Metal Interactions and Applications*; John Wiley & Sons, **2008,** 65-129.

(63) Fonteh, P. N.; Keter, F. K.; Meyer, D. New Bis (Thiosemicarbazonate) Gold (III) Complexes Inhibit HIV Replication at Cytostatic Concentrations : Potential for Incorporation into Virostatic Cocktails. *J. Inorg. Biochem.* **2011**, *105* (9), 1173–1180.

(64) Gogvadze, V.; Orrenius, S.; Zhivotovsky, B. Mitochondria as Targets for Cancer Chemotherapy. *Semin. Cancer Biol.* **2009**, *19* (1), 57–66.

(65) Nomiya, K.; Noguchi, R.; Ohsawa, K.; Tsuda, K. Synthesis and Crystal Structure of Gold(I) Complexes with Triazole and Triphenylphosphine Ligands: Monomeric Complex [Au(1,2,3-L)(PPh3)] and Dimeric Complex [Au(1,2,4-L)(PPh3)]2 (HL = Triazole) through an Au–Au Bond in the Solid State. *J. Chem. Soc. Dalt. Trans.* **1998**, *2* (24), 4101–4108.

(66) Gurunanjappa, P.; Kariyappa, A. K. Design, Synthesis and Biological Evaluation of 1,3,4-Oxadiazoles/Thiadiazoles Bearing Pyrazole Scaffold as Antimicrobial and Antioxidant Candidates. *Curr. Chem. Lett.* **2016**, *5*, 109–122.

(67) Sutton, B. M. Gold Compounds for Rheumatoid Arthritis. *Gold Bull.* **1986**, *19* (1), 15–16.

(68) Finkelstein, A. E.; Walz, D. T.; Batista, V.; Mizraji, M.; Roisman, F.; Misher, A. Auranofin. New Oral Gold Compound for Treatment of Rheumatoid Arthritis. *Ann. Rheum. Dis.* **1976**, *35* (3), 251–257.

(69) Mirabelli, C. K.; Johnson, R. K.; Hill, D. T.; Faucette, L. F.; Girard, G. R.; Kuo, G. Y.; Sung, C. M.; Crooke, S. T. Correlation of the in Vitro Cytotoxic and in Vivo Antitumor Activities of Gold(I) Coordination Complexes. *J. Med. Chem.* **1986**, *29* (2), 218–223.

(70) Tiekink, E. R. T. Gold Derivatives for the Treatment of Cancer. *Crit. Rev. Oncol. Hematol.* **2002**, *42* (3), 225–248.

(71) Newcombe, S.; Bobin, M.; Shrikhande, A.; Gallop, C.; Pace, Y.; Yong, H.; Gates, R.; Chaudhuri, S.; Roe, M.; Hoffmann, E.; et al. Gold Amides as Anticancer Drugs: Synthesis and Activity Studies. *Org. Biomol. Chem.* **2013**, *11* (19), 3255-3260.

(72) Gandin, V.; Fernandes, A. P.; Rigobello, M. P.; Dani, B.; Sorrentino, F.; Tisato, F.; Björnstedt, M.; Bindoli, A.; Sturaro, A.; Rella, R.; et al. Cancer Cell Death Induced by Phosphine Gold(I) Compounds Targeting Thioredoxin Reductase. *Biochem. Pharmacol.* **2010**, *79* (2), 90–101.

(73) Hickey, J. L.; Ruhayel, R. A.; Barnard, P. J.; Baker, M. V; Berners-Price, S. J.; Filipovska, A. Mitochondria-Targeted Chemotherapeutics: The Rational Design of Gold(I) N-Heterocyclic Carbene Complexes That Are Selectively Toxic to Cancer Cells and Target Protein Selenols in Preference to Thiols. *J. Am. Chem. Soc.* **2008**, *130* (38), 12570–12571.

(74) Barnard, P. J.; Berners-Price, S. J. Targeting the Mitochondrial Cell Death Pathway with Gold Compounds. *Coord. Chem. Rev.* **2007**, *251* (13–14), 1889–1902.

(75) Bindoli, A.; Rigobello, M. P.; Scutari, G.; Gabbiani, C.; Casini, A.; Messori, L. Thioredoxin Reductase: A Target for Gold Compounds Acting as Potential Anticancer Drugs. *Coord. Chem. Rev.* **2009**, *253* (11–12), 1692–1707.

(76) Gómez-Suárez, A.; Nelson, D. J.; Thompson, D. G.; Cordes, D. B.; Graham, D.; Slawin, A. M. Z.; Nolan, S. P. Synthesis, Characterization and Luminescence Studies of Gold(I)-NHC Amide Complexes. *Beilstein J. Org. Chem.* **2013**, *9* (I), 2216–2223.

(77) Dong, B.; Su, Y.; Ye, X.; Petersen, J. L.; Shi, X. Synthesis and Characterization of Fluorescent-Active Triazole-Gold Complexes. *Sci. China Chem.* **2015**, *58* (7), 1235–1238.

(78) Rackham, O.; Nichols, S. J.; Leedman, P. J.; Berners-Price, S. J.; Filipovska, A.

A Gold(I) Phosphine Complex Selectively Induces Apoptosis in Breast Cancer Cells: Implications for Anticancer Therapeutics Targeted to Mitochondria. *Biochem. Pharmacol.* **2007**, *74* (7), 992–1002.

(79) Newcombe, S.; Bobin, M.; Shrikhande, A.; Gallop, C.; Pace, Y.; Yong, H.; Gates, R.; Chaudhuri, S.; Roe, M.; Hoffmann, E.; et al. Gold Amides as Anticancer Drugs: Synthesis and Activity Studies. *Org. Biomol. Chem.* **2013**, *11* (19), 3255–3260.

(80) Duan, H.; Sengupta, S.; Petersen, J. L.; Akhmedov, N. G.; Shi, X. Triazole−Au(I) Complexes: A New Class of Catalysts with Improved Thermal Stability and Reactivity for Intermolecular Alkyne Hydroamination. *J. Am. Chem. Soc.* **2009**, *131* (34), 12100–12102.

(81) Zhdanko, A.; Maier, M. E. The Mechanism of Gold(I)-Catalyzed Hydroalkoxylation of Alkynes: An Extensive Experimental Study. *Chem. – A Eur. J.* **2014**, *20* (7), 1918–1930.

(82) Widenhoefer, R. A. Recent Developments in Enantioselective Gold(I) Catalysis. *Chem. - A Eur. J.* **2008**, *14* (18), 5382–5391.

(83) Widenhoefer, R. A.; Han, X. Gold-Catalyzed Hydroamination of C-C Multiple Bonds. *European J. Org. Chem.* **2006**, 4555–4563.

(84) Nieto-Oberhuber, C.; López, S.; Echavarren, A. M. Intramolecular [4 + 2] Cycloadditions of 1,3-Enynes or Arylalkynes with Alkenes with Highly Reactive Cationic Phosphine Au(I) Complexes. *J. Am. Chem. Soc.* **2005**, *127* (17), 6178–6179.

(85) Wang, Y.; Wang, Z.; Li, Y.; Wu, G.; Cao, Z.; Zhang, L. A General Ligand

Design for Gold Catalysis Allowing Ligand-Directed Anti-Nucleophilic Attack of Alkynes. *Nat. Commun.* **2014**, *5* (1), 3470-3488.

(86) Hancock, N. P. F. and R. D. A New Approach to the Study of Gold Putting. *Gold Bull.* **1974**, *7* (3), 72–77.

(87) Westland, A. D. A Study of Complexing of Au(I) with Tertiary Phosphines and Arsines and Stilbenes. *Can. J. Chem.* **1969**, *47*, 4135–4140.

(88) Gammons, C. H.; Yu, Y.; Williams-Jones, A. E. The Disproportionation of Gold(I) Chloride Complexes at 25 to 200°C. *Geochim. Cosmochim. Acta* **1997**, *61* (10), 1971–1983.

(89) Elder, R. C.; Zeiher, E. H. K.; Onady, M.; Whittle, R. R. Nearly Regular Tetrahedral Geometry in a Gold(I)-Phosphine Complex. X-Ray Crystal Structure of Tetrakis(Methyldiphenylphosphine)Gold(I) Hexafluorophosphate. *J. Chem. Soc. Chem. Commun.* **1981**, 900–901.

(90) Johnson, G. E.; Olivares, A.; Hill, D.; Laskin, J. Cationic Gold Clusters Ligated with Differently Substituted Phosphines: Effect of Substitution on Ligand Reactivity and Binding. *Phys. Chem. Chem. Phys.* **2015**, *17* (22), 14636–14646.

(91) Bauer, A.; Gabbaï, F.; Schier, A.; Schmidbaur, H.; Bauer, B. A.; Gabbai, F.; Schier, A. Gold (I) Clustering at the Triphenylphosphinimine Nitrogen Atom. *Philos. Trans. Math. Phys. Eng. Sci.* **1996**, *354* (1706), 381–394.

(92) Ahmad, S.; Isab, A. A.; Perzanowski, H. P.; Hussain, M. S.; Akhtar, M. N. Gold(I) Complexes with Tertiary Phosphine Sulfide Ligands. *Transit. Met. Chem.* **2002**, *27* (2), 177–183.

(93) Jones, P. G. I s Regular Tetrahedral Geometry Possible in Gold (I) -Phosphine Complexes ? X-Ray Crystal Structures of Three Modifications of (PPh,),Au+BPh,. *J.C.S. CHEM. COMM* **1980**, 1031–1033.

(94) Co, R.; Pn, P.; Ch, M.; Me, C. H.; Balakrishna, M. S.; Walawalker, M. G. Transition Metal Chemistry of Phosphorus Based Ligands : Synthesis and Transition Metal Chemistry of N , N % -Dimethyl , -Bis (Diphenylphosphino) Ethylenediamine . The Crystal and Molecular Structure Of. *J. Organomet. Chem.* **2001**, *628*, 76–80.

(95) Wingerter, S.; Pfeiffer, M.; Murso, A.; Lustig, C.; Stey, T.; Chandrasekhar, V.; Stalke, D. Phosphorus-Based Ambidentate Chelating Ligands : Pyridyl- N - and Imido- N - Metal Coordination in the Py 2 P (NSiMe 3) 2 Anion. *J. Am. Chem. Soc.* **2001**, *123* (c), 1381–1388.

(96) Pregosin, P. S. 31P And13C NMR Studies on Metal Complexes of Phosphorus-Donors: Recognizing Surprises. *Coord. Chem. Rev.* **2008**, *252* (21–22), 2156–2170.

(97) Gimeno, M. C.; Laguna, A. Three- and Four-Coordinate Gold(I) Complexes. *Chem. Rev.* **1997**, *97* (3), 511–522.

(98) Colburn, B. C. B.; Hill, W. E. ^{31}P N.M.R. Study of Tertiary Phosphine Complexes of Gold(I). *J.C.S. CHEM. COMM* **1979**, 218–219.

(99) Brown, T. J.; Widenhoefer, R. A. Synthesis and Equilibrium Binding Studies of Cationic, Two-Coordinate Gold(I) π-Alkyne Complexes. *J. Organomet. Chem.* **2011**, *696* (6), 1216–1220.

(100) Bobin, M.; Day, I. J.; Roe, S. M.; Viseux, E. M. E. Insights into the Mechanism

for Gold Catalysis: Behaviour of Gold(i) Amide Complexes in Solution. *Dalt. Trans.* **2013**, *42* (18), 6592–6602.

(101) Marx, D. E.; Barillo, D. J. Silver in Medicine: The Basic Science. *Burns* **2014**, *40* (S1), S9–S18.

(102) Barillo, D. J.; Marx, D. E. Silver in Medicine: A Brief History BC 335 to Present. *Burns* **2014**, *40* (S1), S3–S8.

(103) Lansdown, A. B. G. Silver in Health and Disease. *Issues Toxicol.* **2010**, *6*, 261–268.

(104) Gallego, M. L.; Ovejero, P.; Cano, M.; Heras, J. V.; Campo, J. A.; Pinilla, E.; Torres, M. R. (Pyrazole)Silver(I) and -Gold(I) Complexes with Strong and Weak Hydrogen-Bonding Interactions as the Basis of One- or Two-Dimensional Structures. *Eur. J. Inorg. Chem.* **2004**, 3089–3098.

(105) Li, H.; Siu, K. W. M.; Guevremint, R.; Yves Le Blanc, J. C. Complezes of Silver(I) With Peptides and Proteins as Produced in Electrospray Mass Spectrometry. *J Am Soc Mass Spectrom.* **1997**, 781–792.

(106) J. O. Edwards and R. G. Pearson. Hard and Soft Acids and Bases. *J. Am. Chem. Soc.* **1963**, *85* (22), 3533–3539.

(107) Alexander, J. W. History of the Medical Use of Silver. *Surg. Infect. (Larchmt).* **2009**, *10* (3), 289–292.

(108) Rigo, C.; Roman, M.; Munivrana, I.; Vindigni, V.; Azzena, B.; Barbante, C.; Cairns, W. R. L. Characterization and Evaluation of Silver Release from Four Different Dressings Used in Burns Care. *Burns* **2012**, *38* (8), 1131–1142.

(109) Shukla, S.; Mishra, A. P. Synthesis, Structure, and Anticancerous Properties of Silver Complexes. *J. Chem.* **2013**, *2013*, 1–6.

(110) Bassetti, S.; Hu, J.; D'Agostino, J.; Sherertz, R. J. Prolonged Antimicrobial Activity of a Catheter Containing Chlorhexidine-Silver Sulfadiazine Extends Protection against Catheter Infections in Vivo. *Antimicrob. Agents Chemother.* **2001**, *45* (5), 1535–1538.

(111) Rusu, A.; Hancu, G.; Tóth, G.; Toma, F.; Mare, A. D.; Man, A.; Velescu, B. Ş.; Uivarоși, V. Synthesis, Characterization and Microbiological Activity Evaluation of Two Silver Complexes with Norfloxacin. *Farmacia* **2016**, *64* (6), 922–932.

(112) Aziz, Z.; Abu, S. F.; Chong, N. J. A Systematic Review of Silver-Containing Dressings and Topical Silver Agents (Used with Dressings) for Burn Wounds. *Burns* **2012**, *38* (3), 307–318.

(113) Slouf, I. S. and M. Metal-Organic Compounds. *Acta Cryst* **2000**, *C56*, 1312–1313.

(114) Yang, P.; Cui, F.; Yang, X. J.; Wu, B. Syntheses and Structures of Mononuclear, Dinuclear and Polynuclear Silver(I) Complexes of 2-Pyrazole-Substituted 1,10-Phenanthroline Ligands. *Cryst. Growth Des.* **2013**, *13* (1), 186–194.

(115) Kaeser, A.; Delavaux-Nicot, B.; Duhayon, C.; Coppel, Y.; Nierengarten, J. F. Heteroleptic Silver(I) Complexes Prepared from Phenanthroline and Bis-Phosphine Ligands. *Inorg. Chem.* **2013**, *52* (24), 14343–14354.

(116) Medici, S.; Peana, M.; Crisponi, G.; Nurchi, V. M.; Lachowicz, J. I.; Remelli, M.; Zoroddu, M. A. Silver Coordination Compounds: A New Horizon in Medicine. *Coord. Chem. Rev.* **2016**, 8, 349-359.

(117) Khlobystov, A. N.; Blake, A. J.; Champness, N. R.; Lemenovskii, D. A.; Majouga, A. G.; Zyk, N. V.; Schröder, M. Supramolecular Design of One-Dimensional Coordination Polymers Based on Silver(I) Complexes of Aromatic Nitrogen-Donor Ligands. *Coord. Chem. Rev.* **2001**, *222* (1), 155–192.

(118) Meijboom, R.; Bowen, R. J.; Berners-Price, S. J. Coordination Complexes of Silver(I) with Tertiary Phosphine and Related Ligands. *Coord. Chem. Rev.* **2009**, *253* (3–4), 325–342.

(119) Seliger, P.; Gutowska, N.; Stefaniak, M.; Romanski, J. Investigation on Silver Complexes of Novel 1,2,3-Triazole Linked Crown Ethers by NMR Analysis. *J. Chem. Sci.* **2015**, *127* (10), 1811–1817.

(120) Politano, A. D.; Campbell, K. T.; Rosenberger, L. H.; Sawyer, R. G. Use of Silver in the Prevention and Treatment of Infections: Silver Review. *Surg. Infect. (Larchmt).* **2013**, *14* (1), 8–20.

(121) Martínez-Gutierrez, F.; Thi, E. P.; Silverman, J. M.; de Oliveira, C. C.; Svensson, S. L.; Hoek, A. Vanden; Sánchez, E. M.; Reiner, N. E.; Gaynor, E. C.; Pryzdial, E. L. G.; et al. Antibacterial Activity, Inflammatory Response, Coagulation and Cytotoxicity Effects of Silver Nanoparticles. *Nanomedicine Nanotechnology, Biol. Med.* **2012**, *8* (3), 328–336.

(122) Li, W. R.; Sun, T. L.; Zhou, S. L.; Ma, Y. K.; Shi, Q. S.; Xie, X. B.; Huang, X. M. A Comparative Analysis of Antibacterial Activity, Dynamics, and Effects of Silver Ions and Silver Nanoparticles against Four Bacterial Strains. *Int. Biodeterior. Biodegrad.* **2017**, *123*, 304–310.

(123) Ali, K. A.; Abd-Elzaher, M. M.; Mahmoud, K. Synthesis and Anticancer

Properties of Silver(I) Complexes Containing 2,6-Bis(Substituted)Pyridine Derivatives. *Int. J. Med. Chem.* **2013**, 1–7.

(124) Azócar, M. I.; Gómez, G.; Levín, P.; Paez, M.; Muñoz, H.; Dinamarca, N. Review: Antibacterial Behavior of Carboxylate Silver(I) Complexes. *J. Coord. Chem.* **2014**, *67* (23–24), 3840–3853.

(125) Youngs, W. J.; Knapp, A. R.; Wagers, P. O.; Tessier, C. A. Nanoparticle Encapsulated Silver Carbene Complexes and Their Antimicrobial and Anticancer Properties: A Perspective. *Dalt. Trans.* **2012**, *41* (2), 327–336.

(126) Nomiya, K.; Yokoyama, H. Syntheses, Crystal Structures and Antimicrobial Activities of Polymeric Silver(i) Complexes with Three Amino-Acids [Aspartic Acid (H2asp), Glycine (Hgly) and Asparagine (Hasn)]Note: For Ease of Reference during Discussion of Their Anions, H2asp, Hgly And . *J. Chem. Soc. Dalt. Trans.* **2002**, 2483–2490.

(127) Marzano, C.; Trevisan, A.; Giovagnini, L.; Fregona, D. Synthesis of a New Platinum (II) Complex : Anticancer Activity and Nephrotoxicity in Vitro. *Toxicoloty Vitr.* **2002**, *16*, 413–419.

(128) Russell, A. D.; Hugo, W. B. Antimicrobial Activity and Action of Silver. *Prog. Med. Chem.* **1994**, *31* (C), 351–370.

(129) Tsyba, I.; Mui, B. B. K.; Bau, R.; Noguchi, R.; Nomiya, K. Synthesis and Structure of a Water-Soluble Hexanuclear Silver(I) Nicotinate Cluster Comprised of a “Cyclohexane-Chair”-Type of Framework, Showing Effective Antibacterial and Antifungal Activities: Use of “Sparse Matrix” Techniques for Growing Crystals of Water-Soluble Inorganic Complexes. *Inorg. Chem.* **2003**, *42* (24),

8028–8032.

(130) Sun, C.; Li, X.; Xu, C.; Zhang, S.; Chen, K.; Chen, Q.; Liu, C. Determination of 9(10H)-Acridone by HPLC with Fluorescence Detection. *J. Liq. Chromatogr. Relat. Technol.* **2007**, *30* (2), 245–254.

(131) Martine Demeunynck, B. S. P.; Franck Charmantray, B. S. P.; Alain Martelli, B. S. P. Interest of Acridine Derivatives in the Anticancer Chemotherapy. *Curr. Pharm. Des.* **2001**, *7* (17), 1703–1724.

(132) Cholewiñski, G.; Dzierzbicka, K.; Koodziejczyk, A. M. Natural and Synthetic Acridines / Acridones as Antitumor Agents : Their Biological Activities and Methods of Synthesis. *Pharmacol. Reports* **2011**, 7–12.

(133) Kenneth F. Bastow, a Masataka Itoigawa, $5 .Hiroshi Furukawa,§ Yoshiki Kashiwada, B.; Ibrahim D. Bori, a Lawrence M. Ballas, c and K.-H. L. Antiproliferative Actions of 7-Substituted L$Dihydroxyacridones; Possible Involvement of DNA Topoisomerase II and Protein Kinase C as Biochemical Targets. *Bioorg. Med. Chem.* **1994**, *2* (12), 1403–1411.

(134) Dong, B.; Su, Y.; Ye, X.; Petersen, J. L.; Shi, X. Synthesis and Characterization of Fluorescent-Active Triazole-Gold Complexes. *Sci. China Chem.* **2015**, *58* (7), 1235–1238.

(135) Akanitapichat, P.; Bastow, K. F. The Antiviral Agent 5-Chloro-1,3-Dihydroxyacridone Interferes with Assembly and Maturation of Herpes Simplex Virus. *Antiviral Res.* **2002**, *53* (2), 113–126.

(136) Denny. Acridine Derivatives as Chemotherapeutic Agents. *Curr. Med. Chem.* **2002**, *9* (18), 1655–1665.

(137) Belmont, P.; Dorange, I. Acridine/Acridone: A Simple Scaffold with a Wide Range of Application in Oncology. *Expert Opin. Ther. Pat.* **2008**, *18* (11), 1211–1224.

(138) Belmont, P.; Bosson, J.; Godet, T.; Tiano, M. Acridine and Acridone Derivatives, Anticancer Properties and Synthetic Methods: Where Are We Now? *Anticancer. Agents Med. Chem.* **2007**, *7* (2), 139–169.

(139) Belmont, P.; Constant, J. F.; Demeunynck, M. Nucleic Acid Conformation Diversity: From Structure to Function and Regulation. *Chem. Soc. Rev.* **2001**, *30* (1), 70–81.

(140) Zhang, B.; Li, X.; Li, B.; Gao, C.; Jiang, Y. Acridine and Its Derivatives: A Patent Review (2009 – 2013). *Expert Opin. Ther. Pat.* **2014**, *24* (6), 647–664.

(141) Pereira, E.; Do Quental, L.; Palma, E.; Oliveira, M. C.; Mendes, F.; Raposinho, P.; Correia, I.; Lavrado, J.; Di Maria, S.; Belchior, A.; et al. Evaluation of Acridine Orange Derivatives as DNA-Targeted Radiopharmaceuticals for Auger Therapy: Influence of the Radionuclide and Distance to DNA. *Sci. Rep.* **2017**, *7*, 1–16.

(142) Wang, W.; Ho, W. C.; Dicker, D. T.; MacKinnon, C.; Winkler, J. D.; Marmorstein, R.; El-Deiry, W. S. Acridine Derivatives Activate P53 and Induce Tumor Cell Death through Bax. *Cancer Biol. Ther.* **2005**, *4* (8), 893–898.

(143) Sondhi, S. M.; Singh, J.; Rani, R.; Gupta, P. P.; Agrawal, S. K.; Saxena, A. K. Synthesis, Anti-Inflammatory and Anticancer Activity Evaluation of Some Novel Acridine Derivatives. *Eur. J. Med. Chem.* **2010**, *45* (2), 555–563.

(144) Elomri, A.; Mitaku, S.; Michel, S.; Skaltsounis, A. L.; Tillequin, F.; Koch, M.;

Pierre, A.; Guilbaud, N.; Leonce, S.; Kraus-Berthier, L.; et al. Synthesis and Cytotoxic and Antitumor Activity of Esters in the 1,2- Dihydroxy-1,2-Dihydroacronycine Series. *J. Med. Chem.* **1996**, *39* (24), 4762–4766.

(145) J. Schneider, E. L. Evans, E. Grunberg, and R. I. F. Synthesis and Biological Activity of Acronycine Analogs. *J. Med. Chem.* **1972**, *15* (3), 266–270.

(146) Tsann-Long Su,* Ting-Chao Chou, Joong Young Kim, Jai-Tung Huang, Grazyna Ciszewska, W.-Y. R.; Grenys M. Otter, Francis M. Sirotnak, and K. A. W. 9-Substituted Acridine Derivatives with Long Half-Life and Potent Antitumor Activity: Synthesis and Structure-Activity Relationships. *J. Med. Chem.* **1995**, *38*, 3226–3235.

(147) G. J. Atwell, B. F. Cain, and R. N. S. Potential Antitumor Agents. 12, 9-Anilinoacridines. *J. Med. Chem.* **1972**, *15* (6), 611–615.

(148) Rajendra Prasad, V. V. S.; Peters, G. J.; Lemos, C.; Kathmann, I.; Mayur, Y. C. Cytotoxicity Studies of Some Novel Fluoro Acridone Derivatives against Sensitive and Resistant Cancer Cell Lines and Their Mechanistic Studies. *Eur. J. Pharm. Sci.* **2011**, *43* (4), 217–224.

(149) Szymański, P.; Olszewska, P.; Mikiciuk-Olasik, E.; Różalski, A.; Maszewska, A.; Markiewicz, Ł.; Cuchra, M.; Majsterek, I. Novel Tetrahydroacridine and Cyclopentaquinoline Derivatives with Fluorobenzoic Acid Moiety Induce Cell Cycle Arrest and Apoptosis in Lung Cancer Cells by Activation of DNA Damage Signaling. *Tumor Biol.* **2017**, *39* (3), 1–13.

(150) Yang, N.; Weinfeld, M.; Lemieux, H.; Montpetit, B.; Goping, I. S. Photo-Activation of the Delocalized Lipophilic Cation D112 Potentiates Cancer

Selective ROS Production and Apoptosis. *Cell Death Dis.* **2017**, *8* (2), 1–13.

(151) Percivalle, C.; Mahmood, T.; Ladame, S. Two-in-One: A PH-Sensitive, Acridine-Based, Fluorescent Probe Binds G-Quadruplexes in Oncogene Promoters. *Medchemcomm* **2013**, *4* (1), 211–215.

(152) Frances Mary Hamer, Isidor Morris Heilbron, Joseph Henry Reade, and H. N. W. Cyanine Dyes and Related Compounds. *A. Weissberger, Interscience, London, UK,* **1964**, *100*, 251–260.

(153) Mishra, A.; Behera, R. K.; Behera, P. K.; Mishra, B. K.; Behera, G. B. Cyanines during the 1990s:A Review. *Chem. Rev.* **2000**, *100* (6), 1973–2012.

(154) Maftah, A.; Petit, J. M.; Ratinaud, M. H.; Julien, R. 10-N Nonyl-Acridine Orange: A Fluorescent Probe Which Stains Mitochondria Independently of Their Energetic State. *Biochem. Biophys. Res. Commun.* **1989**, *164* (1), 185–190.

(155) Moriyama, Y, Takano, T. and Ohkuma, S. Acridine Orange as a Fluorescent probe for lysosomal proton pump. *J. Biochem*. **1982,** 92, 1333-1336.

(156) Jiang, X.; Fu, Y.; Xu, L.; Lu, H.; Zang, S.; Tang, M.; Mak, T. C. W. A Novel Acridine-Based Fluorescent Probe for the Cascade Recognition of Cr3+ and PO4 3−. *Sensors Actuators B* **2014**, *202*, 388–394.

(157) Yunjing, L.; Hanxi, S. Study on Acridine Orange Dimer as a New Fluorescent Probe for the Determination of Protein. *Anal. Commun.* **1999**, *36* (4), 135–137.

(158) Halliday, G. M.; Nairn, R. C.; Rolland, J. M. Lymphocyte Stimulation by Concanavalin A Studied by the Fluorescent Probe Acridine Orange. *Cell Tissue Res* **1981**, *217*, 117–126.

(159) Thomé, M. P.; Filippi-Chiela, E. C.; Villodre, E. S.; Migliavaca, C. B.; Onzi, G. R.; Felipe, K. B.; Lenz, G. Ratiometric Analysis of Acridine Orange Staining in the Study of Acidic Organelles and Autophagy. *J. Cell Sci.* **2016**, 4622–4632.

(160) Jacobson, J.; Duchen, M. R.; Heales, S. J. R. Intracellular Distribution of the Fluorescent Dye Nonyl Acridine Orange Responds to the Mitochondrial Membrane Potential: Implications for Assays of Cardiolipin and Mitochondrial Mass. *J. Neurochem.* **2002**, *82* (2), 224–233.

(161) Naim, M. J.; Alam, O.; Nawaz, F.; Alam, M. J.; Alam, P. Current Status of Pyrazole and Its Biological Activities. *J. Pharm. Bioallied Sci.* **2016**, *8* (1), 2–17.

(162) Kumar, K. A.; Jayaroopa, P. Pyrazoles : Synthetic Strategies and Their Pharmaceutical Applications - An Overview. *Int. J. PharmTech Res.* **2015**, *5* (4), 1473–1486.

(163) Jena, N. P. and A. K. Fe-Catalyzed One-Pot Synthesis of 1,3-Di- and 1,3,5-Trisubstituted Pyrazoles from Hydrazones and Vicinal Diols. *J. Org. Chem.* **2012**, *77*, 9401–9406.

(164) Pal, D.; Saha, S.; Singh, S. Importance of Pyrazole Moiety in the field of Cancer. *Int J Pharm Pharm Sci* **2012**, *4* (2), 98–104.

(165) Kumar, K. A.; Govindaraju, M. Pyrazolines : Versatile Molecules of Synthetic and Pharmaceutical Applications-A Review. *Int.J. ChemTech Res* **2015**, *8* (1), 313–322.

(166) Reddy, T. S.; Kulhari, H.; Reddy, V. G.; Bansal, V. European Journal of Medicinal Chemistry Design , Synthesis and Biological Evaluation of 1 , 3-Diphenyl-1 H - Pyrazole Derivatives Containing Benzimidazole Skeleton as

Potential Anticancer and Apoptosis Inducing Agents. *Eur. J. Med. Chem.* **2015**, *101*, 790–805.

(167) Hamada, N.; Abdo, N. Synthesis, Characterization, Antimicrobial Screening and Free-Radical Scavenging Activity of Some Novel Substituted Pyrazoles. *Molecules* **2015**, *20* (12), 10468–10486.

(168) Shaw, A. Y.; Liau, H.; Lu, P.; Yang, C.; Lee, C.; Chen, J.; Xu, Z.; Flynn, G. Bioorganic & Medicinal Chemistry 3 , 5-Diaryl-1 H -Pyrazole as a Molecular Scaffold for the Synthesis of Apoptosis-Inducing Agents. *Bioorg. Med. Chem.* **2010**, *18* (9), 3270–3278.

(169) Kumar, H.; Saini, D.; Jain, S.; Jain, N. European Journal of Medicinal Chemistry Pyrazole Scaffold : A Remarkable Tool in the Development of Anticancer Agents. *Eur. J. Med. Chem.* **2013**, *70*, 248–258.

(170) Kasiotis, K. M.; Tzanetou, E. N.; Haroutounian, S. A. Pyrazoles as Potential Anti-Angiogenesis Agents: A Contemporary Overview. *Front. Chem.* **2014**, *2*, 1–7.

(171) Fa´tima Churruca, Susana Herna´ndez, Marı´a Perea, R. S. and E. D. Direct Access to Pyrazolo(Benzo)Thienoquinolines. Highly Effective Palladium Catalysts for the Intramolecular C–H Heteroarylation of Arenes†. *Chem. Commun.*, **2013**, *49*, 1413–1415.

(172) Welsch, M. E.; Snyder, S. A.; Stockwell, B. R. Privileged Scaffolds for Library Design and Drug Discovery. *Curr. Opin. Chem. Biol.* **2010**, *14* (3), 347–361.

(173) Nitulescu, G. M.; Draghici, C.; Olaru, O. T.; Matei, L.; Ioana, A.; Dragu, L. D.; Bleotu, C. Synthesis and Apoptotic Activity of New Pyrazole Derivatives in

Cancer Cell Lines. *Bioorg. Med. Chem.* **2015**, *23* (17), 5799–5808.

(174) Liu, X.; Wilcken, R.; Joerger, A. C.; Chuckowree, I. S.; Amin, J.; Spencer, J.; Fersht, A. R. Small Molecule Induced Reactivation of Mutant P53 in Cancer Cells. *Nucleic Acids Res.* **2013**, *41* (12), 6034–6044.

(175) Galassi, R.; Burini, A.; Ricci, S.; Pellei, M.; Rigobello, M. P.; Citta, A.; Dolmella, A.; Gandin, V.; Marzano, C. Synthesis and Characterization of Azolate Gold(i) Phosphane Complexes as Thioredoxin Reductase Inhibiting Antitumor Agents. *Dalt. Trans.* **2012**, *41* (17), 5307.

(176) Galassi, R.; Oumarou, C. S.; Burini, A.; Dolmella, A.; Micozzi, D.; Vincenzetti, S.; Pucciarelli, S. A Study on the Inhibition of Dihydrofolate Reductase (DHFR) from Escherichia Coli by Gold(i) Phosphane Compounds. X-Ray Crystal Structures of (4,5-Dichloro-1H-Imidazolate-1-Yl)-Triphenylphosphane-Gold(i) and (4,5-Dicyano-1H-Imidazolate-1-Yl)-Triphenylphos. *Dalt. Trans.* **2015**, *44* (7), 3043–3056.

(177) Stana, A.; Tiperciuc, B.; Duma, M.; Vlase, L.; Crişan, O.; Pîrnău, A.; Oniga, O. Synthesis and Antimicrobial Activity of Some New N-Substituted-5-Arylidene-Thiazolidine-2,4-Diones. *J. Heterocycl. Chem.* **2014**, *51* (2), 411–417.

(178) Surendra Kumar, R.; Arif, I. A.; Ahamed, A.; Idhayadhulla, A. Anti-Inflammatory and Antimicrobial Activities of Novel Pyrazole Analogues. *Saudi J. Biol. Sci.* **2016**, *23* (5), 614–620.

(179) Rai, R.; Shrivastava, S. P. Antitubercular, Antibacterial and Antifungal Activity of Some Pyridoquinazolones Derivatives. *Der Pharma Chem.* **2012**, *4* (3), 1186–1190.

(180) Hassan, A. A.; Abdel-Latif, F. F.; El-Din, A. M. N.; Abdel-Aziz, M.; Mostafa, S. M.; Bräse, S. Synthesis of Novel Spiro(Indolone-3,2′-[1,3,4]Thiadiazol)-2-Ones and Evaluation of Their Antidepressant and Anticonvulsant Activities. *J. Heterocycl. Chem.* **2011**, *48* (5), 1050–1055.

(181) Anandarajagopal, K.; Sunilson, J. A. J.; Illavarasu, A.; Kalirajan, R. Antiepileptic and Antimicrobial Activities of Novel Pyrazole Derivatives. *Int.J. ChemTech Res.* **2010**, *2* (1), 45–49.

(182) Souza, F. R.; Souza, V. T.; Ratzlaff, V.; Borges, L. P.; Oliveira, M. R.; Bonacorso, H. G.; Zanatta, N.; Martins, M. A. P.; Mello, C. F. Hypothermic and Antipyretic Effects of 3-Methyl- and 3-Phenyl-5-Hydroxy-5-Trichloromethyl-4,5-Dihydro-1H-Pyrazole-1-Carboxyamides in Mice. *Eur. J. Pharmacol.* **2002**, *451* (2), 141–147.

(183) Soliman, R. Preparation and Antidiabetic Activity of Some Sulfonylurea Derivatives of 3, 5-Disubstituted Pyrazoles. *J. Med. Chem.* **1979**, *22* (3), 321–325.

(184) Nitulescu, G. M.; Draghici, C.; Missir, A. V. Synthesis of New Pyrazole Derivatives and Their Anticancer Evaluation. *Eur. J. Med. Chem.* **2010**, *45* (11), 4914–4919.

(185) El-sabbagh, O. I.; Baraka, M. M.; Ibrahim, S. M.; Pannecouque, C.; Andrei, G.; Snoeck, R.; Balzarini, J.; Rashad, A. A. Synthesis and Antiviral Activity of New Pyrazole and Thiazole Derivatives. *Eur. J. Med. Chem.* **2009**, *44* (9), 3746–3753.

(186) Keter, F. K.; Darkwa, J. Perspective : The Potential of Pyrazole-Based Compounds in Medicine. *Biometals* **2012**, *25*, 9–21.

(187) Nyamato, G. S.; Alam, M. G.; Ojwach, S. O.; Akerman, M. P. (Pyrazolyl) - (Phosphinoyl) Pyridine Iron (II), Cobalt (II) and Nickel (II) Complexes : Synthesis , Characterization and Ethylene Oligomerization Studies. **2015**, *783*, 64–72.

(188) Dresch, L. C.; Junges, C. H.; Casagrande, O. de L.; Stieler, R. Nickel Complexes Supported by Selenium-Based Tridentate Ligands and Their Use as Effective Catalyst Systems for Ethylene Dimerisation. *J. Organomet. Chem.* **2018**, *856*, 34–40.

(189) Wang, T.; Dong, B.; Chen, Y. H.; Mao, G. L.; Jiang, T. Nickel Complexes Incorporating Pyrazole-Based Ligands for Ethylene Dimerization to 1-Butylene. *J. Organomet. Chem.* **2015**, *798*, 388–392.

(190) Ainooson, M. K.; Ojwach, S. O.; Guzei, I. A.; Spencer, L. C.; Darkwa, J. Pyrazolyl Iron, Cobalt, Nickel, and Palladium Complexes: Synthesis, Molecular Structures, and Evaluation as Ethylene Oligomerization Catalysts. *J. Organomet. Chem.* **2011**, *696* (8), 1528–1535.

(191) Matos, K.; de Oliveira, L. L.; Favero, C.; Monteiro, A. L.; Hörner, M.; Carpentier, J. F.; Gil, M. P.; Casagrande, O. L. Palladium Complexes Based on Tridentate Pyrazolyl-Ligands: Synthesis, Structures and Use in Suzuki Cross-Coupling Reactions. *Inorganica Chim. Acta* **2009**, *362* (12), 4396–4402.

(192) Kang, Y. K.; Jeong, J. H.; Lee, N. Y.; Lee, Y. T.; Lee, H. Synthesis, Characterization, and Catalytic Application of a Zinc(II) Complex Bearing a Pyrazole-Based Ligand. *Polyhedron* **2010**, *29* (12), 2404–2408.

(193) Schachner, J. A.; Traar, P.; Sala, C.; Melcher, M.; Harum, B. N.; Sax, A. F.;

Volpe, M.; Belaj, F.; Mösch-Zanetti, N. C. Dioxomolybdenum(VI) Complexes with Pyrazole Based Aryloxide Ligands: Synthesis, Characterization and Application in Epoxidation of Olefins. *Inorg. Chem.* **2012**, *51* (14), 7642–7649.

(194) Fantin, V. R.; Leder, P. Mitochondriotoxic Compounds for Cancer Therapy. *Oncogene* **2006**, *25*, 4787–4797.

(195) Robertson, D. E.; Rottenberg, H. Membrane Potential and Surface Potential in Mitochondria. Flurescence and Binding of 1-Anilinonaphtalene-8-Sulfonate. *J. Biol. Chem.* **1983**, *25*, 11039–11048.

(196) Hockenbery, D. M. Targeting Mitochondria for Cancer Therapy. *Environ. Mol. Mutagen.* **2010**, *51* (5), 476–489.

(197) Ngen, E. J.; Rajaputra, P.; You, Y. Evaluation of Delocalized Lipophilic Cationic Dyes as Delivery Vehicles for Photosensitizers to Mitochondria. *Bioorganic Med. Chem.* **2009**, *17* (18), 6631–6640.

(198) Kelley, S. O.; Stewart, K. M.; Mourtada, R. Development of Novel Peptides for Mitochondrial Drug Delivery : Amino Acids Featuring Delocalized Lipophilic Cations. *Pharm Res* **2011**, *28*, 2808–2819.

(199) Koya, K.; Li, Y.; Wang, H.; Ukai, T.; Tatsuta, N.; Kawakami, M.; Shishido, T.; Chen, L. B. MKT-077, a Novel Rhodacyanine Dye in Clinical Trials, Exhibits Anticarcinoma Activity in Preclinical Studies Based on Selective Mitochondrial Accumulation. *Cancer Res.* **1996**, *56*, 538–543.

(200) Sun, X.; Wong, J. R.; Song, K.; Hu, J.; Garlid, K. D.; Chen, L. B. AA1 , A Newly Synthesized Monovalent Lipophilic Cation , Expresses Potent in Vivo Antitumor Activity. *Cancer Res.* **1994**, *54*, 1465–1471.

(201) Powers, S. K.; Pribil, S.; Gillespie, G. Y. 3rd; Watkins, P. J. Laser Photochemotherapy of Rhodamine-123 Sensitized Human Glioma Cells in Vitro. *J. Neurosurg.* **1986**, *64* (6), 918–923.

(202) Oseroff, A. R.; Ohuoha, D.; Ara, G.; McAuliffe, D.; Foley, J.; Cincotta, L. Intramitochondrial Dyes Allow Selective in Vitro Photolysis of Carcinoma Cells. *Proc. Natl. Acad. Sci. U. S. A.* **1986**, *83* (24), 9729–9733.

(203) Zinkewich-Peotti, K.; Andrews, P. A. Loss of Cis-Diamminedichloroplatinum(II) Resistance in Human Ovarian Carcinoma Cells Selected for Rhodamine 123 Resistance. *Cancer Res.* **1992**, *52* (Ii), 1902–1906.

(204) Weiss, M. J.; Wong, J. R.; Ha, C. S.; Bledaytt, R.; Salemt, R. R.; Steele, G. D.; Chen, L. A. N. B. Dequalinium, a Topical Antimicrobial Agent, Displays Anticarcinoma Activity Based on Selective Mitochondrial Accumulation. *Proc. Natl. Acad. Sci. USA* **1987**, *84*, 5444–5448.

(205) Kandela, I.; Lee, W.; Indig, G. L. Effect of the Lipophilic/Hydrophilic Character of Cationic Triarylmethane Dyes on Their Selective Phototoxicity toward Tumor Cells. *Biotech. Histochem.* **2003**, *78* (3–4), 157–169.

(206) Trapp, S.; Horobin, R. W. A Predictive Model for the Selective Accumulation of Chemicals in Tumor Cells. *Eur. Biophys. J.* **2005**, *34* (7), 959–966.

(207) Li, D.; Qi, Z.; Ding, X.; Li, J.; Jiang, F.; Liu, Y.; Kwong, D. W. J.; Wong, W. Photophysics of Three Delocalized Lipophilic Cations in Reverse Micelles : A Fluorescence Spectroscopy Study. **2013**, *134*, 830–836.

(208) Chen, L. B. Mitochondrial Membrane Potential in Living cells. *Ann. Rev. Cell BioI* **1988**, *4*, 155–181.

(209) Fantin, V. R.; Leder, P. F16 , a Mitochondriotoxic Compound , Triggers Apoptosis or Necrosis Depending on the Genetic Background of the Target Carcinoma Cell F16 , a Mitochondriotoxic Compound , Triggers Apoptosis or Necrosis Depending on the Genetic Background of the Target Carc. *Cancer Res.* **2004**, *64* (617), 329–336.

(210) Modica-napolitano, J. S.; Aprille, J. R. Delocalized Lipophilic Cations Selectively Target the Mitochondria of Carcinoma Cells. **2001**, *49*, 63–70.

(211) Lampidis, M. K. and T. J. From Delocalized Lipophilic Cations to Hypoxia: Blocking Tumor Cell Mitochondrial Function Leads to Therapeutic Gain with Glycolytic Inhibitors. *Mol Nutr Food Res* **2009**, *53* (1), 68–75.

(212) So, P. T.; Dong, C. Y. Fluorescence Spectrophotometry. *Encycl. Life Sci.* **2001**, 1–4.

(213) Peter Atkins and J. D. P. *Physical Chemistry*, Ninth Edit.; Oxford University Press, **2010**, 503-508.

(214) Lichtman, J. W.; Conchello, J. A. Fluorescence Microscopy. *Nat. Methods* **2005**, *2* (12), 910–919.

(215) Lavis, L. D.; Raines, R. T. Bright Building Blocks for Chemical Biology. *ACS Chem. Biol.* **2014**, *9* (4), 855–866.

(216) Sauer, M.; Hofkens, J.; Enderlein, J. *Basic Principles of Fluorescence Spectroscopy*; Wiley, **2011**, 1-30.

(217) Lakowicz, J. R. *Principles of Fluorescence Spectroscopy Third Edit; SPringer* **2006**, 1-26.

(218) Goryacheva, I. Y.; Mel'nikov, G. V.; Shtykov, S. N. Acridine Dyes in the Triplet State as Reagents for the Selective Luminescence Determination of Polycyclic Aromatic Hydrocarbons. *J. Anal. Chem.* **2000**, *55* (9), 874–878.

(219) Yamaguchi, Y.; Matsubara, Y.; Ochi, T.; Wakamiya, T.; Yoshida, Z.-I. How the π Conjugation Length Affects the Fluorescence Emission Efficiency. *J. AM. CHEM. SOC.* **2008**, 130, 13867–13869

(220) Williams, R. T.; Bridges, J. W. Fluorescence of Solutions: A Review. *J. Clin. Pathol.* **1964**, *17*, 371–394.

(221) Dasgupta, B. R. S. and D. [50] Simple Fluorescence Assays Probing Conformational Changes of Escherichia Coli RNA Polymerase During Transcription Initiation. *METHODS Enzymol.* **2003**, *370* (1998), 598–605.

(222) Manivannan, C.; Renganathan, R. Spectroscopic Investigation on the Interaction of 9-Aminoacridine with Certain Dyes. *Spectrochim. Acta - Part A Mol. Biomol. Spectrosc.* **2012**, *95*, 685–692.

(223) Barnard, P. J.; Wedlock, L. E.; Baker, M. V; Berners-price, S. J.; Joyce, D. A.; Skelton, B. W.; Steer, J. H. Luminescence Studies of the Intracellular Distribution of a Dinuclear Gold(I) N-Heterocyclic Carbene Complex.*Angew. Chemical. Int. Ed*. **2006**, 45, 5966–5970.

(224) Floor, L.; Dumont, J. E.; Maenhaut, C.; Raspe, E. Hallmarks of Cancer : Of All Cancer Cells , All the Time ? *Trends Mol Med* **2012**, *18* (9), 509–515.

(225) Hanahan, D.; Weinberg, R. A. The Hallmarks of Cancer. *Cell* **2000**, *100*, 57–70.

(226) Hanahan, D.; A., W. and R.; Hallmarks of Cancer: The Next Generation. *Cell*

2011, *144*, 646–674.

(227) Jones, M. J. K.; Jallepalli, P. V. Chromothripsis: Chromosomes in Crisis. *Dev. Cell* **2012**, *23* (5), 908–917.

(228) Vogelstein, B.; Kinzler, K. W. Cancer Genes and the Pathways They Control. *Nat. Med.* **2004**, *10* (8), 789–799.

(229) Hausen, H. Z. U. R. Viruses in Human Cancers. *Science.* **1991**, *254*, 1167–1173.

(230) Siegel, R. L.; Miller, K. D.; Jemal, A. Cancer Statistics , 2018. *CA CANCER J CLIN* **2018**, *68* (01), 7–30.

(231) Haines, I. The War on Cancer: Time for a New Terminology. *Lancet* **2014**, *383*, 1883.

(232) Raoul, J. L. Natural History of Hepatocellular Carcinoma and Current Treatment Options. *Semin. Nucl. Med.* **2008**, *38* (2).S13-S18

(233) Zhu, A. X. Systemic Therapy of Advanced Hepatocellular Carcinoma: How Hopeful Should We Be? *Oncologist* **2006**, *11* (7), 790–800.

(234) Huang, M.; Liu, G. The Study of Innate Drug Resistance of Human Hepatocellular Carcinoma Bel7402 Cell Line. *Cancer Lett.* **1999**, *135* (1), 97–105.

(235) Tu, J.; Chen, Y.; Cai, L.; Xu, C.; Zhang, Y.; Chen, Y.; Zhang, C.; Zhao, J.; Cheng, J.; Xie, H.; et al. Functional Proteomics Study Reveals SUMOylation of TFII-I Is Involved in Liver Cancer Cell Proliferation. *J. Proteome Res.* **2015**, *14* (6), 2385–2397.

(236) Gan, N.; Sun, X.; Song, L. Activation of Nrf2 by Microcystin-LR Provides

Advantages for Liver Cancer Cell Growth. *Chem. Res. Toxicol.* **2010**, *23* (9), 1477–1484.

(237) Shangguan, D.; Meng, L.; Cao, Z. C.; Xiao, Z.; Fang, X.; Li, Y.; Cardona, D.; Witek, R. P.; Liu, C.; Tan, W. Identification of Liver Cancer-Specific Aptamers Using Whole Live Cells Identification of Liver Cancer-Specific Aptamers Using Whole Live Cells. *Anal. Chem.* **2008**, *80* (3), 721–728.

(238) Lin, C.-C.; Huang, C.-Y.; Mong, M.-C.; Chan, C.-Y.; Yin, M.-C. Antiangiogenic Potential of Three Triterpenic Acids in Human Liver Cancer Cells. *J. Agric. Food Chem.* **2011**, *59* (2), 755–762.

(239) Galmiche, A.; Chauffert, B.; Barbare, J. C. New Biological Perspectives for the Improvement of the Efficacy of Sorafenib in Hepatocellular Carcinoma. *Cancer Lett.* **2014**, *346* (2), 159–162.

(240) Hsieh, Y. C.; Rao, Y. K.; Wu, C. C.; Huang, C. Y. F.; Geethangili, M.; Hsu, S. L.; Tzeng, Y. M. Methyl Antcinate a from Antrodia Camphorata Induces Apoptosis in Human Liver Cancer Cells through Oxidant-Mediated Cofilin- and Bax-Triggered Mitochondrial Pathway. *Chem. Res. Toxicol.* **2010**, *23* (7), 1256–1267.

(241) Davis, R. B.; Carlos, D. D.; Mattingly, G. S. Condensation of Aromatic Nitro Compounds with Arylacetonitriles. VII. Some Studies Concerning the Reduction of Phenylcy Anomethylenequinone Oximes. *J. Org. Chem.* **1965**, *30* (8), 2607–2610.

(242) Bobin, M.; Kwast, A.; Wróbel, Z. Efficient Formation of ΣH-Adducts as a Key Step in the Synthesis of Acridines via Lewis Acid-Promoted Transformations of

the Nitro Group. *Tetrahedron* **2007**, *63* (45), 11048–11054.

(243) Więcław, M.; Bobin, M.; Kwast, A.; Bujok, R.; Wróbel, Z.; Wojciechowski, K. General Synthesis of 2,1-Benzisoxazoles (Anthranils) from Nitroarenes and Benzylic C–H Acids in Aprotic Media Promoted by Combination of Strong Bases and Silylating Agents. *Mol. Divers.* **2015**, *19* (4), 807–816.

(244) Ma, M.; Wojciechowski, K.; Ma, M. Nucleophilic Substitution of Hydrogen in Heterocyclic Chemistry Nucleophilic Substitution of Hydrogen in Heterocyclic Chemistry. *Chem. Rev.* **2004**, *104* (5), 2631–2666.

(245) Rahimizadeh, M.; Pordel, M.; Bakavoli, M.; Eshghi, H.; Shiri, A. Vicarious Nucleophilic Substitution in Nitro Derivatives of Imidazo[1,2-a]Pyridine. *Mendeleev Commun.* **2009**, *19* (3), 161–162.

(246) Fowler, P. W.; Steiner, E. Ring Currents and Aromaticity of Monocyclic π - Electron Systems. *J. Phys. Chem. A* **1997**, *5639* (96), 1409–1413.

(247) Baguley, B.; Wakelin, L.; Jacintho, J.; Kovacic, P. Mechanisms of Action of DNA Intercalating Acridine-Based Drugs: How Important Are Contributions from Electron Transfer and Oxidative Stress? *Curr. Med. Chem.* **2003**, *10* (24), 2643–2649.

(248) Ulitzur, S.; Weiser, I. Acridine Dyes and Other DNA-Intercalating Agents Induce the Luminescence System of Luminous Bacteria and Their Dark Variants. *Proc. Natl. Acad. Sci. U. S. A.* **1981**, *78* (6), 3338–3342.

(249) DeRuiter, J. Principles of Drug Action 1: Resonace and Induction Tutorial. *Princ. Drug Action 1* **2005**, 1–19.

(250) Rahimizadeh, M.; Pordel, M.; Bakavoli, M.; Rezaeian, Sh.; Eshghi, H. B-N as a C-C substitute in aromatic systems. *Can. J. Chem.* **2009**, 87 (1), 8-29.

(251) Rahimizadeh, M.; Pordel, M.; Bakavoli, M.; Eshghi, H. The Synthesis of Highly Fluorescent Heterocyclic Compounds: Pyrido[2',1':2,3]Imidazo[4,5-b]Quinoline-12-Yl Cyanides. *Dye. Pigment.* **2010**, *86* (3), 266–270.

(252) Pakjoo, V.; Roshani, M.; Pordel, M.; Hoseini, T. Synthesis of New Fluorescent Compounds from 5-Nitro-1H-Indazole. *Arkivoc* **2012**, *2012* (9), 195–203.

(253) Elliott, E.; Bowkett, E. R.; Maggs, J. L.; Bacsa, J.; Park, B. K.; Regan, S. L.; Neill, P. M. O.; Stachulski, A. V. Convenient Syntheses of Benzo-Fluorinated Dibenz [b , f] Azepines : Rearrangements Of. *Org. Lett.* **2011**, 9–12.

(254) Stopka, T.; Marzo, L.; Zurro, M.; Janich, S.; Würthwein, E. U.; Daniliuc, C. G.; Alemán, J.; Mancheño, O. G. Oxidative C-H Bond Functionalization and Ring Expansion with TMSCHN2: A Copper(I)-Catalyzed Approach to Dibenzoxepines and Dibenzoazepines. *Angew. Chemie - Int. Ed.* **2015**, *54* (17), 5049–5053.

(255) Adamczyk, M.; Mattingly, P. G.; Moore, J. A.; Pan, Y. Regiodependent Luminescence Quenching of Biotinylated N-Sulfonyl-Acridinium-9-Carboxamides by Avidin. *Org. Lett.* **2003**, *5* (21), 3779–3782.

(256) Razavi, Z.; McCapra, F. Stable and Versatile Active Acridinium Esters II. *Luminescence* **2000**, *15* (4), 245–249.

(257) Yu, Q.; Zhang, A. S.; Hu, T. L.; Bu, X. H. Silver(I) Complexes with (1-Pyrazolyl)Pyridazine Ligands: Synthesis, Crystal Structures and Luminescent Properties. *Solid State Sci.* **2010**, *12* (8), 1484–1489.

(258) Colburn, B. C. B.; Hill, W. E. ^{31}PN.M.R. Study of Tertiary Phosphine Complexes of Gold(I). **1979**, 218-219.

(259) Colton, R.; Harrison, K. L.; Mah, Y. A.; Traeger, J. C. Cationic Phosphine Complexes of Gold(I) and Electrospray Mass Spectrometric Study. *Inorg. Chim. Acta* **1995**, *231*, 65–71.

(260). Muetterties, E.L. and Alegranti C. W. Solution Structure of Coinage Metal-Phosphine Complexes. *Journal of the American Chemical Society*. **1970**, 4114–4115.

(261) McAuliffe, C. A.; Parish, R. V. (Dick); Randall, P. D. Studies in Mössbauer Spectroscopy. Part 9. Gold-197 Spectra of Gold Compounds. *J. Chem. Soc., Dalt. Trans.* **1977**, *32* (15), 1426–1430.

(262) Clegg, W. Bis(Dimethylphenylphosphine)Triehlorostanniogold. *Acta Cryst.* **1978**, *B34*, 278–281.

(263) Brooner, R. E. M.; Brown, T. J.; Widenhoefer, R. A. Synthesis and Study of Cationic, Two-Coordinate Triphenylphosphine- Gold-π Complexes. *Chem. - A Eur. J.* **2013**, *19* (25), 8276–8284.

(264) López-De-Luzuriaga, J. M.; Schier, A.; Schmidbaur, H. Gold Coordination by 2-(Diphenylphosphanyl) Aniline. *Chem. Ber.* **1997**, *130* (5), 647–650.

(265) Zhdanko, A.; Ströbele, M.; Maier, M. E. Coordination Chemistry of Gold Catalysts in Solution: A Detailed NMR Study. *Chem. - A Eur. J.* **2012**, *18* (46), 14732–14744.

(266) Parish R. V. and Rush, J. D. 197Au MÖSSBAUER SPECTRA OF TWO-,

THREE-, AND FOUR-COORDINATE GOLD(I) COMPLEXES. *Phys. Lett.* **1979**, *63* (1), 37–39.

(267) Brown, G. M.; Gu, B. The Chemistry of Perchlorate in the Environment. *Perchlorate Environ. Occur. Interact. Treat.* **2006**, 17–47.

(268) Vargeese, A. a; Joshi, S. S.; Krishnamurthy, V. N. Role of Poly (Vinyl Alcohol) in the Crystal Growth of Ammonium Perchlorate. *Cryst. Growth Des.* **2008**, *8* (3), 1060–1066.

(269) Munakata, M.; Yan, S.-G.; Maekawa, M.; Akiyama, M.; Kitagawa, S. Solid and Solution Structures of Ternary Gold(I) Complexes with Triphenylphosphine and Nitrogen-Containing Ligands. *J. Chem. Soc. Dalt. Trans* **1997**, 4257–4262.

(270) Keter, F. K.; Guzei, I. A.; Nell, M.; Zyl, W. E. V.; Darkwa, J. Phosphinogold(I) Dithiocarbamate Complexes: Effect of the Nature of Phosphine Ligand on Anticancer Properties. *Inorg. Chem.* **2014**, *53* (4), 2058–2067.

(271) Galassi, R.; Oumarou, C. S.; Burini, A.; Dolmella, A.; Micozzi, D.; Vincenzetti, S.; Pucciarelli, S. A Study on the Inhibition of Dihydrofolate Reductase (DHFR) from Escherichia Coli by Gold(i) Phosphane Compounds. X-Ray Crystal Structures of (4,5-Dichloro-1H-Imidazolate-1-Yl)-Triphenylphosphane-Gold(i) and (4,5-Dicyano-1H-Imidazolate-1-Yl)-Triphenylphos. *Dalt. Trans.* **2015**, *44* (7), 3043–3056.

(272) Nomiya, K.; Noguchi, R.; Ohsawa, K.; Tsuda, K. Synthesis and Crystal Structure of Gold(I) Complexes with Triazole and Triphenylphosphine Ligands: Monomeric Complex [Au(1,2,3-L)(PPh3)] and Dimeric Complex [Au(1,2,4-L)(PPh3)]2 (HL = Triazole) through an Au-Au Bond in the Solid State. *J. Chem.*

Soc., Dalt. Trans. **1998**, 4101–4108.

(273) Nomiya, K. Transformation of Polymeric Silver (I) Imidazolate to Monomeric Imidazolatotris (Triphenylphosphine) Silver (I) Complex . Synthesis of [Ag (Imd)(PPh 3) 3] (Himd ˆ Imidazole) and Its Characterization in the Solid-State and in Solution. *J. Inorg. Biochem.* **1998**, *69* (1998), 9–14.

(274) Afolabi, F.; Souissi, W.; Rivière, G.; Lemaitre, C.; Roe, S. M.; Crickmore, N.; Viseux, E. M. E. Synthesis of Novel Heteroleptic Delocalised Cationic Pyrazole Gold Complexes as Potent HepG2 Cytotoxic Agents. *Dalt. Trans.* **2018,** 15338-15343.

(275) Liu, X.; Wilcken, R.; Joerger, A. C.; Chuckowree, I. S.; Amin, J.; Spencer, J.; Fersht, A. R. Small Molecule Induced Reactivation of Mutant P53 in Cancer Cells. *Nucleic Acids Res.* **2013**, *41* (12), 6034–6044.

(276) Sheldrick, G. M. SHELXT - Integrated Space-Group and Crystal-Structure Determination. *Acta Crystallogr. Sect. A Found. Crystallogr.* **2015**, *71* (1), 3–8.

(277) Sheldrick, G. M. Crystal Structure Refinement with SHELXL. *Acta Crystallogr. Sect. C Struct. Chem.* **2015**, *71*, 3–8.

(278) Dolomanov, O. V.; Bourhis, L. J.; Gildea, R. J.; Howard, J. A. K.; Puschmann, H. OLEX2: A Complete Structure Solution, Refinement and Analysis Program. *J. Appl. Crystallogr.* **2009**, *42* (2), 339–341.

(279) Bobin, M.; Day, I. J.; Roe, S. M.; Viseux, E. M. E. Insights into the Mechanism for Gold Catalysis: Behaviour of Gold(I) Amide Complexes in Solution. *Dalton Trans.* **2013**, *42* (18), 6592–6602.

(280) Messori, L.; Abbate, F.; Marcon, G.; Orioli, P.; Fontani, M.; Mini, E.; Mazzei, T.; Carotti, S.; O'Connell, T.; Zanello, P. Gold(III) Complexes as Potential Antitumor Agents: Solution Chemistry and Cytotoxic Properties of Some Selected Gold(III) Compounds. *J. Med. Chem.* **2000**, *43* (19), 3541–3548.

(281) Schwerdtfeger, P.; Boyd, P.; Burrell, A. Relativistic Effects in Gold Chemistry. 3. Gold (I) Complexes. *Chemistry (Easton).* **1990**, 3593–3607.

(282) Keter, F. K.; Guzei, I. A.; Nell, M.; Zyl, W. E. Van; Darkwa, J. Phosphinogold(I) Dithiocarbamate Complexes: Effect of the Nature of Phosphine Ligand on Anticancer Properties. *Inorg. Chem.* **2014**, *53* (4), 2058–2067.

(283) Valeur, B. *Molecular Fluorescence: Principles and Applications.*; Valeur, B., Ed.; Wiley-VCH: Weinheim (Federal Republic of Germany)., **2001**, 3-70.

(284) Fery-forgues, S.; Lavabre, D. Are Fluorescence Quantum Yields So Tricky to Measure ? A Demonstration Using Familiar Stationery Products. **1999**, *76* (9), 1260–1264.

(285) Swinehart, D. F. The Beer-Lambert Law. *J. Chem. Educ.* **1962**, *39* (7), 333.

(286) Furuuchi, H.; Arai, T.; Sakuragi, H.; Tokumaru, K.; Nishimura, Y.; Yamazaki, I. Novel Rotational Isomerization of Anthracene Nucleus around Its Bond Connecting to C=N Bond in the Excited Singlet State of (E)-N-Methoxy-1-(2-Anthryl)Ethanimine; *J. Phys. Chem*.**1991**; 95 10322-10325.

(287) Flom, S. R.; Nagarajan, V.; Barbara, P. F. Dynamic Solvent Effects on Large-Amplitude Isomerization Rates. 1. 2-Vinylanthracene; *J Phys. Chem*. **1986**, 90, 2085-2092.

(288) Albrecht, M.; Bohne, C.; Granzhan, A.; Ihmels, H.; Pace, T. C. S.; Schnurpfeil, A.; Waidelich, M.; Yihwa, C. Dual Fluorescence of 2-Methoxyanthracene Derivatives. *J Phys. Chem* **2007,** 111**,** 1036-1044.

(289) Becker, H., Hammarberg E., Brian W. S, and Allan. H. W. Formation and Photochemical Rearrangement of Carbon-Oxygen-Linked Anthracenes. *Tetrahedron Lett.* **1989**, *30* (16), 2137–2140.

(290) Becker, H. D. Unimolecular Photochemistry of Anthracenes. *Chem. Rev.* **1993**, *93* (1), 145–172.

(291) Tripathi, D. D. P. C. J. B. Photophysics of 9-Aminoacridinium Hydrochloride D. *Pramana* **1986**, *27* (August), 161–170.

(292) Mitra, P.; Chakraborty, B.; Bhattacharyya, D.; Basu, S. Excimer of 9 - Aminoacridine Hydrochloride Hydrate in Con Fi Ned Medium : An Integrated Experimental and Theoretical Study. *J. Phys. Chem. A* **2013,** 117, 1428-1438.

(293) Exner, O.; Krygowski, T. M. The Nitro Group as Substituent. *Chemical Society Reviews*. **1996**, 71-75.

(294) Muller, P. Glossary of Terms Used in Physical Organic Chemistry. *Pure Appl. Chem.* **1994**, *66* (5), 1077–1184.

(295) Krygowski, T. M.; Stępień, B. T. Sigma- and Pi-Electron Delocalization: Focus on Substituent Effects. *Chem. Rev.* **2005**, *105* (10), 3482–3512.

(296) Berlman, I. B. Empirical Study of Heavy-Atom Collisional Quenching of the Fluorescence State of Aromatic Compounds in Solution1. *J. Phys. Chem.* **1973**, *77* (4), 562–567.

(297) Medinger, T.; Wilkinson, F. Mechanism of Fluorescence Quenching in Solution Part 1 .-Quenching by Bromobenzene *Trans Faraday Soc*. **1965**, 61, 620-630.

(298) Rae, M.; Perez-Balderas, F.; Baleizão, C.; Fedorov, A.; Cavaleiro, J. A. S.; Tomé, A. C.; Berberan-Santos, M. N. Intra-and Intermolecular Heavy-Atom Effects on the Fluorescence Properties of Brominated C 60 Polyads. *J. Phys. Chem. B* **2006,** 110, 12809-12814.

(299) Katrib, A.; Rabalais, J. W. *Electronic* Interaction between the Vinyl Group and Its Substituents.*J. Phys Chem*.**1973.** 77, (19), 2358-2363.

(300) Yamaguchi, E.; Shibahara, F.; Murai, T. 1-Alkynyl-and 1-Alkenyl-3-Arylimidazo[1,5-a]Pyridines: Synthesis, Photophysical Properties, and Observation of a Linear Correlation between the Fluorescent Wavelength and Hammett Substituent Constants. *J. Org. Chem.* **2011**, *76*, 6146-6158.

(301) Pang, S.; Jang, D.; Lee, W. S.; Kang, H. M.; Hong, S. J.; Hwang, S. K.; Ahn, K. H. The Effect of a "Push-Pull" Structure on the Turn-on Fluorescence of Photochromic Thio-Ketone Type Diarylethenes. *Photochem. Photobiol. Sci.* **2015**, *14* (4), 765–774.

(302) Thooft, A. M.; Cassaidy, K.; Vanveller, B. A Small Push-Pull Fluorophore for Turn-on Fluorescence. *J. Org. Chem.* **2017**, *82* (17), 8842–8847.

(303) Nano, A.; Ziessel, R.; Stachelek, P.; Harriman, A. Charge-Recombination Fluorescence from Push-Pull Electronic Systems Constructed around Amino-Substituted Styryl-BODIPY Dyes. *Chem. - A Eur. J.* **2013**, *19* (40), 13528–13537.

(304) Bello, K. A.; Griffiths, J. Azo Dyes with Absorption Bands in the Near Infrared.

J Chem. Soc., Chem. Commun.,**1986,** 1639-1640.

(305) Sager, W. F.; Filipescu, N.; Serafin, F. A. Substituent Effects on Intramolecular Energy Transfer. I. Absorption and Phosphorescence Spectra of Rare Earth β-Diketone Chelates. *J. Phys. Chem.* **1965**, *69* (4), 1092–1100.

(306) Pu, S.; Wang, R.; Liu, G.; Liu, W.; Cui, S.; Yan, P. Photochromism of New Unsymmetrical Diarylethene Derivatives Bearing Both Benzofuran and Thiophene Moieties. *Dye. Pigment.* **2012**, *94* (2), 195–206.

(307) Noomnarm, U.; Clegg, R. M. Fluorescence Lifetimes: Fundamentals and Interpretations. *Photosynth. Res.* **2009**, *101* (2–3), 181–194.

(308) Abbyad, P.; Childs, W.; Shi, X.; Boxer, S. G. Dynamic Stokes Shift in Green Fluorescent Protein Variants. *Proc. Natl. Acad. Sci.* **2007**, *104* (51), 20189–20194.

(309) Gao, Z.; Hao, Y.; Zheng, M.; Chen, Y. A Fluorescent Dye with Large Stokes Shift and High Stability: Synthesis and Application to Live Cell Imaging. *RSC Adv.* **2017**, *7* (13), 7604–7609.

(310) Zhang, X. F.; Zhang, J.; Lu, X. The Fluorescence Properties of Three Rhodamine Dye Analogues: Acridine Red, Pyronin Y and Pyronin B. *J. Fluoresc.* **2015**, *25* (4), 1151–1158.

(311) Kubota, Y. Fluorescence Lifetimes and Quantum Yields ofAcridine Dyes Bound to DNA. *Chem. Lett.* **1973**, *2* (3), 299–304.

(312) Morris, J. V; Mahaney, M. A.; Huber, J. R. Fluorescence Quantum Yield Determinations - 9,10-Diphenylanthracene as a Reference-standard in Different

Solvents. *J. Phys. Chem.* **1976**, *80* (9), 969–974.

(313) Heinrich, G.; Schoof, S.; Gusten, H. 9,10-Diphenylanthracene as a Fluorescence Quantum Yield Standard. *J. Photochem.* **1974**, *3* (2), 315–320.

(314) Soep, B.; Kellmann, A.; Martin, M.; Lindqvist, L. Study of Triplet Quantum Yields Using a Tunable Dye Laser. *Chem. Phys. Lett.* **1972**, *13* (3), 241–244.

(315) Strickler, S. J.; Berg, R. A. Relationship between Absorption Intensity and Fluorescence Lifetime of Molecules. *J. Chem. Phys.* **1962**, *37* (4), 814–822.

(316) Birks, J. B. Fluorescence Quantum Yield Measurements. *J. Res. Natl. Bur. Stand. Sect. A Phys. Chem.* **1976**, *80A* (3), 389-399.

(317) Maulding, D. R.; and Robert B. G. Electronic Absorption and Fluorescence of Phenylethynyl- Substituted Acenes. *J. Org. Chem. contents* **1969**, *34* (6), 1734–1736.

(318) Pascale, F.; Bedouet, L.; Baylatry, M.; Namur, J.; Laurent, A. Comparative Chemosensitivity of VX2 and HCC Cell Lines to Drugs Used in TACE. *Anticancer Res.* **2015**, *35* (12), 6497–6504.